

**Bio-functionalized Polymeric Nanocarrier
System for Targeting Inflamed Intestinal
Mucosa**



PhD Thesis

By

MAHIRA ZEESHAN

**Department of Pharmacy
Faculty of Biological Sciences
Quaid-i-Azam University
Islamabad, Pakistan**

2022

**Bio-functionalized Polymeric Nanocarrier
System for Targeting Inflamed Intestinal
Mucosa**

Thesis Submitted by

MAHIRA ZEESHAN

Registration No: 03331711004

Session: Spring 2017-Fall 2021

to

Department of Pharmacy,

In partial fulfillment of the requirements for degree of

Doctor of Philosophy

in

Pharmacy (Pharmaceutics)

Department of Pharmacy
Faculty of Biological Sciences
Quaid-i-Azam University
Islamabad, Pakistan
2017-2022

AUTHOR'S DECLARATION

I hereby declare that the thesis entitled "**Bio-functionalized polymeric nanocarrier System for targeting inflamed intestinal mucosa**" submitted at Department of Pharmacy, Faculty of Biological Sciences, Quaid-i-Azam University Islamabad for the award of degree of Doctor of Philosophy in Pharmacy (Pharmaceutics) is the result of research work carried out by me under the supervision of supervisor Dr. Hussain Ali during the period Spring 2017- Fall 2021. I further declare that the results present in this thesis have not been submitted for the award of any other degree or fellowship, I am aware of the terms copyright and plagiarism, and I will be responsible for any copyright violation found in this work.



MAHIRA ZEESHAN

Date: 24-08-2022

PLAGIARISM UNDERTAKING

I, Mahira Zeeshan, solemnly declare that research work presented in the thesis titled **“Bio-functionalized polymeric nanocarrier System for targeting inflamed intestinal mucosa”** is solely my research work with no significant contribution from any other person. Small contribution/help wherever taken has been duly acknowledged and that complete thesis has been written by me.

I understand zero tolerance policy of Quaid-i-Azam University, Islamabad and HEC towards plagiarism. Therefore, I as an author of the above titled dissertation declare that no portion of my thesis is plagiarized, and every material used as reference is properly referred/cited.

I undertake that if I am found guilty of committing any formal plagiarism in the above titled thesis even after award of PhD degree, the University reserves the right to withdraw/revoke my PhD degree and that HEC and University has the right to publish my name on the HEC/University Website on which names of those students are placed who submitted plagiarized thesis.




MAHIRA ZEESHAN

APPROVAL CERTIFICATE


This is certified that the dissertation titled “**Bio-functionalized polymeric nanocarrier System for targeting inflamed intestinal mucosa**” submitted by Mahira Zeeshan to the Department of Pharmacy, Faculty of Biological Sciences, Quaid-i-Azam University Islamabad, Pakistan is accepted in its present form as it is satisfying the dissertation requirements for the Degree of Doctor of Philosophy in **Pharmacy (Pharmaceutics)**.

Supervisor:




Dr. Hussain Ali
Associate Professor
Department of Pharmacy,
Quaid-i-Azam University, Islamabad

External Examiner I:




Dr. Fawad Ali Shah
Associate Professor
Riphah Institute of Pharmaceutical
Sciences, Riphah International University,
Islamabad.

External Examiner II:



Dr. Muzaffar Abbas
Associate Professor
Department of Pharmacy,
Capital University of Science &
Technology, Islamabad.

Chairperson:



Dr. Gul Shahnaz
Associate Professor
Department of Pharmacy,
Quaid-i-Azam University, Islamabad.

Dated:

August 24, 2022

Verily with every hardship, there is an ease.

No work can attain success but only with

ALLAH's will

I dedicate my work to my

Mother and Father,

Whose prayers, love and encouragement

supports me to achieve success in fulfillment of

my task.

Table of Contents

| Title | Page No. |
|---|----------|
| Acknowledgments..... | i |
| List of Tables | iii |
| List of Figures | vi |
| List of Abbreviations | xi |
| Abstract..... | xvi-xvii |
| 1. INTRODUCTION | 1 |
| 1.1. Background | 1 |
| 1.2. IBD Physiological and Pathophysiological Considerations..... | 3 |
| 1.2.1. pH..... | 3 |
| 1.2.2. Transit time | 4 |
| 1.2.3. Luminal contents..... | 5 |
| 1.2.4. Colonic microbiome..... | 5 |
| 1.3. pH-Dependent DDS for IBD..... | 7 |
| 1.3.1. pH-sensitive polymers | 7 |
| 1.3.2. Conventional pH-sensitive dosage forms | 7 |
| 1.4. Novel pH-Dependent DDS for IBD | 10 |
| 1.4.1. pH-dependent macro-DDS for IBD | 10 |
| 1.4.2. pH-dependent micro/nanoparticulate-mediated DDS for IBD | 12 |
| 1.5. Dual microbial enzyme sensitive and pH sensitive nanocarriers for IBD | 27 |
| 1.5.1. Pullulan-a new versatile microbial sensitive polymer | 28 |
| 1.6. Second generation of ligand anchored nanocarriers for IBD..... | 28 |
| 1.6.1. MGL..... | 29 |
| 1.6.2. Transferrin receptor (TFR) | 30 |
| 1.7. Patents For pH-Dependent Micro/Nanoparticulate DDS for IBD | 31 |
| 1.8. Present Advancements & Directions..... | 32 |

| | |
|--|-----------|
| 1.9. Safety and Challenges | 32 |
| 1.10. Study Rationale | 33 |
| 1.11. Aims and Objectives | 36 |
| 2. MATERIALS AND METHODS..... | 38 |
| 2.1. Materials..... | 38 |
| 2.1.1. Chemicals and reagents..... | 38 |
| 2.1.2. Animals | 38 |
| 2.1.3. Preparation of solutions | 39 |
| 2.2. Methods..... | 40 |
| PART-I (Section A)..... | 40 |
| 2.2.1. HPLC instrumentation and analytical procedure..... | 40 |
| 2.2.2. Molecular docking | 40 |
| 2.2.3. Polymer synthesis: Conjugation reaction between D-galactose and PLGA | 42 |
| 2.2.4. Preparation of dye/drug-loaded GAL-PLGA nanoparticles | 44 |
| 2.2.5. Physicochemical characterization..... | 50 |
| 2.2.6. Thermogravimetric (TGA) analysis..... | 50 |
| 2.2.7. X-ray powder diffraction (XPRD) analysis | 51 |
| 2.2.8. Fourier-transformed Infrared Spectroscopic (FTIR) of excipients and formulation | 51 |
| 2.2.9. In vitro drug release | 51 |
| 2.2.10. In vitro hemocompatibility studies | 52 |
| 2.2.11. In vitro cell-based studies | 53 |
| 2.2.12. In vivo preliminary studies to understand nanoparticles behavior in the inflammation..... | 54 |
| 2.2.13. Harvesting of inflammation led macrophages for flow cytometry analysis | 54 |

| | |
|---|----|
| 2.2.14. Accumulation of nano-formulation in the visceral organs and colon under inflammation..... | 55 |
| PART-I (SECTION-B) | 55 |
| 2.2.15. Preparation and characterization of GP/ES100, GP/Pu Nanoparticles (NPs), and G-PLGA/ES/Pu NCs | 55 |
| 2.2.16. Physicochemical Characterization | 56 |
| 2.2.17. Drug Release and Kinetics of GP/ES100, GP/Pu and GP/ES/Pu NCs.. | 56 |
| 2.2.18. Mucin Binding Study | 57 |
| 2.2.19. In vitro Biocompatibility Studies | 57 |
| 2.2.20. In vitro Permeability Assay | 57 |
| 2.3. Animal Studies | 58 |
| 2.3.1. Development of DSS induced colitis model for in vivo studies..... | 58 |
| 2.3.2. NCs Targeting Index and Localization Capacity in the Inflamed Colon | 58 |
| 2.3.3. Flow cytometry | 59 |
| 2.3.4. Therapeutic intervention of DSS induced colitis mice | 59 |
| 2.3.5. Assessment of progression and intervention of colitis thorough morphological parameters and mortality rate | 60 |
| 2.3.6. Evaluation of colonic vascular integrity | 60 |
| 2.3.7. Histopathological assessment | 61 |
| 2.3.8. Immunohistochemistry | 61 |
| 2.3.9. ATR-FTIR analysis of the colon tissues | 61 |
| 2.3.10. Evaluation of colon microbial content..... | 61 |
| 2.3.11. Real time-polymerase chain reaction (RT-PCR) analysis for the expression of regulatory, inflammatory, and mechanistic proteins..... | 62 |
| 2.3.12. Pro-Inflammatory cytokines detection through ELISA..... | 62 |
| 2.3.13. Biochemical antioxidant assays | 62 |
| 2.3.14. Assessment of hematological parameters | 63 |

| | |
|--|----|
| 2.3.15. In vivo biocompatibility and toxicity investigations of Dexa-GP/ES100/Pu NCs..... | 63 |
| PART-II (SECTION A)..... | 64 |
| 2.4. HPLC Method for Tofa | 64 |
| 2.5. Preparation of Tofa Loaded PLGA/tfr Nanocarriers (Tofa-P/tfr NCs)..... | 65 |
| 2.6. Physicochemical Characterization | 69 |
| 2.6.1. Protein quantification..... | 69 |
| 2.6.2. TGA, ATR-FTIR and XPRD..... | 70 |
| 2.6.3. DSC..... | 70 |
| 2.7. Drug Release and Kinetics | 70 |
| 2.8. Mucin Binding Study | 71 |
| 2.9. In Vitro Biocompatibility and Toxicity Studies..... | 71 |
| 2.9.1. Hemolysis assay..... | 71 |
| 2.9.2. Cellular biocompatibility on murine derived colon cells and macrophages | 71 |
| 2.9.3. Cellular uptake study | 71 |
| 2.10. Stability Studies..... | 72 |
| 2.11. Animal Studies | 72 |
| 2.11.1. Induction of ulcerative colitis (UC)..... | 72 |
| 2.11.2. Nanocarrier targeting ability and biodistribution..... | 72 |
| 2.11.3. Evaluation of therapeutic efficacy in the DSS induced colitis mice..... | 73 |
| 2.11.4. Assessment of progression and intervention of colitis thorough morphological parameters and mortality rate | 74 |
| 2.11.5. Histological investigations..... | 74 |
| 2.11.6. Assessment of vascular integrity | 74 |
| 2.11.7. RT-PCR analysis of expression of inflammatory and regulatory proteins | 74 |
| 2.11.8. Pro-inflammatory cytokines analysis (ELISA)..... | 75 |

| | |
|---|----|
| 2.11.9. Assessment of antioxidant protection level | 75 |
| 2.11.10. Biochemical hematological parameters | 76 |
| 2.11.11. Evaluation of colon microbiome..... | 76 |
| PART-II (SECTION B) | 76 |
| 2.12. Preparation of Tofa-LP/tfr NSh and Tofa-LP/tfr/ES NSh | 76 |
| 2.13. Physicochemical Characterization | 77 |
| 2.14. Drug Release and Kinetics | 77 |
| 2.15. Mucin Binding Study | 77 |
| 2.16. In Vitro Cell-Based Assays | 77 |
| 2.16.1. Hemo-toxicity assay..... | 77 |
| 2.16.2. Cellular biocompatibility assay..... | 78 |
| 2.16.3. Colon uptake study | 78 |
| 2.16.4. Macrophage assays | 78 |
| 2.17. Stability Studies..... | 80 |
| 2.18. Animal Studies | 80 |
| 2.19. Preliminary In Vivo Studies..... | 80 |
| 2.19.1. Nanoshells localization and colon targeting ability | 80 |
| 2.19.2. Flow cytometry uptake study..... | 80 |
| 2.19.3. In vivo biodistribution and visualization study..... | 80 |
| 2.20. In Vivo Therapeutic Efficacy in DSS-Induced Colitis Mice | 81 |
| 2.20.1. Evaluation of therapeutic efficacy in the DSS-induced colitis mice | 81 |
| 2.20.2. Morphological assessment for colitis severity and treatment efficacy, histopathology, and vascular membrane integrity..... | 81 |
| 2.20.3. RT-PCR analysis for the expression of the epithelial membrane (E- cadherin), inflammatory (iNOS), mechanistic (STAT-1), and receptor-oriented proteins (TFR-1)..... | 82 |
| 2.20.4. Assessment of pro-inflammatory cytokines..... | 82 |
| 2.20.5. Antioxidant protection by the nano-formulations..... | 82 |

| | | |
|--------------------|--|-----------|
| 2.20.6. | Biochemical hematological parameters | 83 |
| 2.20.7. | Colon microbiome growth evaluation | 83 |
| 2.20.8. | In vivo biocompatibility of nanoshells in the healthy mice | 83 |
| PART-III | | 84 |
| 2.21. | HPLC Analysis of TAC | 84 |
| 2.22. | Preparation and Optimization of TAC-P/Lys NCs and TAC- PLGA/Lys/ES-L100 NCs | 84 |
| 2.23. | Physicochemical properties | 85 |
| 2.24. | Drug Release Studies and Kinetics | 85 |
| 2.25. | In Vitro Cell-Based Studies..... | 86 |
| 2.25.1. | Caco-2 viability assay with 7-AAD and PI staining..... | 86 |
| 2.25.2. | Caco-2 uptake studies | 86 |
| 2.25.3. | Macrophage uptake studies..... | 86 |
| 2.26. | Animal Studies | 87 |
| 2.26.1. | Instillation of oxazolone (OXA) to induce UC..... | 87 |
| 2.27. | Therapeutic Evaluation of Nanocarriers | 87 |
| 2.27.1. | Assessment of therapeutic efficacy through morphological indices..... | 88 |
| 2.27.2. | Histopathological analysis | 88 |
| 2.27.3. | IVIS imaging to assess myeloperoxidase (MPO) activity | 88 |
| 2.27.4. | Immunohistochemistry for the pITK expression in the CD3 ⁺ T cells of the colon tissue | 89 |
| 2.27.5. | RT-PCR analysis of inflammation markers and ELISA for pro-Inflammatory mediators' analysis | 90 |
| 2.27.6. | Flowcytometry | 90 |
| 2.28. | Statistical Analysis | 91 |
| 3. RESULTS | | 92 |
| PART-I (SECTION A) | | 92 |
| 3.1. | HPLC Calibration Curve of Dexa | 92 |

| | | |
|--------|--|-----|
| 3.2. | Molecular Docking..... | 92 |
| 3.3. | GAL-PLGA Polymer Synthesis..... | 95 |
| 3.3.1. | Confirmation of synthesized polymer through ATR-FTIR, NMR, and TGA | 98 |
| 3.3. | Preparation of Drug-Loaded GAL-PLGA Nanoparticles & Optimization . | 101 |
| 3.3.1. | QbD process for Dexa-GAL-PLGA nanoparticles..... | 101 |
| 3.3.2. | DOE: Box-Behnken design..... | 101 |
| 3.3.3. | Experimental design validation and optimization..... | 106 |
| 3.3.4. | Physicochemical characterization..... | 107 |
| 3.3.5. | TGA | 110 |
| 3.3.6. | X-ray powder diffraction (XPRD) analysis..... | 110 |
| 3.3.7. | FTIR of excipients and formulation..... | 111 |
| 3.4. | <i>In Vitro</i> Drug Release Study | 112 |
| 3.4.1. | Drug release kinetic modeling | 113 |
| 3.5. | <i>In Vitro</i> Biocompatibility Studies | 115 |
| 3.5.1. | Hemolysis assay..... | 115 |
| 3.5.2. | <i>In vitro</i> cell-based cytotoxicity assay on derived macrophages and colon cells | 116 |
| 3.5.3. | Cellular uptake studies..... | 116 |
| 3.5.4. | Elucidation of galactose mediated cell uptake by murine macrophages | 117 |
| 3.6. | <i>In Vivo</i> Preliminary Studies to Understand Nanoparticles Behavior in the Inflammation..... | 118 |
| 3.6.1. | Flow cytometric analysis | 118 |
| 3.6.2. | Accumulation of nano-formulation in the visceral organs and colon under inflammation..... | 119 |
| | PART-I (SECTION B) | 120 |
| 3.7. | Synthesis of Nanocargoes and Characterization | 120 |

| | | |
|--------------------------|---|-----|
| 3.8. | Drug Release and Kinetics | 124 |
| 3.9. | Mucin Binding Study | 129 |
| 3.10. | In vitro Biocompatibility Studies | 130 |
| 3.10.1. | Hemolysis assay | 130 |
| 3.10.2. | Cellular biocompatibility (MTT) | 130 |
| 3.10.3. | Cell uptake studies | 132 |
| 3.11. | In vitro Permeation and Retention Assay | 132 |
| 3.12. | Animal Studies | 134 |
| 3.12.1. | Nanocargoes targeting ability | 134 |
| 3.12.2. | Oral Delivery of Dexamethasone-Gelatin/Polyurethane Nanoparticles for Therapeutic Intervention of DSS Induced Colitis | 135 |
| PART-II (SECTION A)..... | | 147 |
| 3.13. | Preparation of Tofacitinib-Poly(tetrafluoroethylene) Nanoparticles | 147 |
| 3.14. | Preparation of Tofacitinib-Poly(tetrafluoroethylene) Nanoparticles | 148 |
| 3.14.1. | DOE: Box-Behnken design (3 ³)..... | 151 |
| 3.14.2. | 3 ³ Box-Behnken design validation..... | 156 |
| 3.15. | Physicochemical Characteristics and tetracycline Adsorption | 156 |
| 3.15.1. | TGA | 157 |
| 3.15.2. | DSC..... | 157 |
| 3.15.3. | ATR-FTIR..... | 158 |
| 3.15.4. | XPRD..... | 160 |
| 3.16. | In Vitro Drug Release Studies..... | 160 |
| 3.17. | Mucin Binding Study | 160 |
| 3.18. | In Vitro Biocompatibility and Toxicity Studies..... | 162 |
| 3.18.1. | Hemolysis assay | 162 |
| 3.18.2. | Cellular biocompatibility (MTT assay) | 162 |
| 3.18.3. | Cellular uptake study-colon and macrophages | 164 |

| | |
|--|-----|
| 3.19. Stability Studies..... | 166 |
| 3.20. Animal Studies | 166 |
| 3.21. In Vivo Nanocarrier Targeting Ability..... | 166 |
| 3.22. Therapeutic Evaluation of Tofa-P/tfr NCs in DSS-Induced Colitis..... | 167 |
| 3.22.1. Morphological parameters assessment to determine colitis severity and the treatment efficacy | 167 |
| 3.22.2. Histopathological investigations..... | 169 |
| 3.22.3. Vascular function test | 170 |
| 3.22.4. RT-PCR analysis to determine mechanistic and therapeutic effects on ameliorating inflammation and recovering barrier function..... | 170 |
| 3.22.5. Evaluation of pro-inflammatory cytokines | 171 |
| 3.22.6. Assessment of colon antioxidant protection | 172 |
| 3.22.7. Evaluation of blood indices and RFTs..... | 173 |
| 3.22.8. Investigation of colon microbiome | 174 |
| PART-II (SECTION B)..... | 175 |
| Graphical Abstract: | 175 |
| 3.23. Preparation and Physicochemical Characterization of Tofa-LP/tfr NSh and Tofa-LP/tfr/ES NSh..... | 175 |
| 3.23.1. TGA | 176 |
| 3.23.2. DSC..... | 178 |
| 3.23.3. ATR-FTIR..... | 178 |
| 3.24. In Vitro Drug Release Studies..... | 179 |
| 3.25. Mucin Binding Study | 180 |
| 3.26. In Vitro Biocompatibility and Toxicity Studies..... | 183 |
| 3.26.1. Hemolysis assay..... | 183 |
| 3.27. Cellular biocompatibility | 183 |
| 3.28. Caco-2 Uptake Studies | 185 |
| 3.29. Macrophage Assays..... | 186 |

| | |
|--|-----|
| 3.29.1. Macrophage uptake | 186 |
| 3.29.2. Macrophage JAK/STAT inhibition assay | 187 |
| 3.30. Stability Studies..... | 189 |
| 3.31. Animal Studies | 189 |
| 3.32. Preliminary In Vivo Studies..... | 189 |
| 3.32.1. Nanoshell's colon targeting ability and localization..... | 189 |
| 3.32.2. Flow cytometry uptake study..... | 190 |
| 3.32.3. In vivo visualization of biodistribution of nanoshells..... | 191 |
| 3.33. In Vivo Therapeutic Efficacy Investigations | 193 |
| 3.33.1. Morphological assessment of colitis severity and treatment efficacy . | 193 |
| 3.33.2. Histopathological reversal of colitis | 194 |
| 3.33.3. Assessment of vascular integrity | 196 |
| 3.33.4. RT-PCR analysis for the expression of inflammatory (iNOS), mechanistic (STAT-1), epithelial membrane (E-cadherin), and receptor-oriented proteins (TFR-1)..... | 196 |
| 3.33.5. Pro-inflammatory cytokines assessment..... | 197 |
| 3.33.6. Antioxidant protection by the nanoshell delivered drug to the colon.. | 198 |
| 3.33.7. Evaluation of bloodborne indices | 201 |
| 3.33.8. Assessment of feces microbial growth | 201 |
| 3.33.9. In vivo biocompatibility evaluation of Tofa-LP/tfr/ES NSh | 202 |
| PART-III..... | 204 |
| 3.34. Preparation and Optimization of TAC-P/Lys NCs and TAC- P/Lys/ES-L100 NCs | 204 |
| 3.35. Drug Release Studies and Kinetics | 207 |
| 3.36. In Vitro Cell-Based Studies..... | 208 |
| 3.36.1. Caco-2 viability assay with 7-AAD and PI staining..... | 208 |
| 3.36.2. Caco-2 uptake | 210 |
| 3.36.3. Macrophage uptake studies..... | 210 |

| | |
|--|------------|
| 3.37. Animal Studies | 211 |
| 3.37.1. Development of OXA-induced colitis and Therapeutic evaluation of nanocarriers through morphological indices | 211 |
| 3.37.2. Histopathological analysis | 214 |
| 3.37.3. IVIS imaging to assess myeloperoxidase (MPO) activity | 215 |
| 3.37.4. Evaluation of treatment mediated pITK suppression to mediate protection against OXA-colitis by Immunohistochemistry and flowcytometry..... | 216 |
| 3.37.5. Investigation of RT-PCR expression of inflammatory proteins and epithelial barrier proteins and ELISA for pro-Inflammatory mediator analysis | 219 |
| 3.37.6. Assessment of pro-inflammatory M1-macrophages by flowcytometry | 222 |
| 4. DISCUSSION..... | 224 |
| 5. CONCLUSIONS..... | 231 |
| 6. FUTURE PROSPECTIVE | 233 |
| REFERENCES..... | 234 |
| Annexure I: List of Publications | 261-265 |
| Annexure II: Similarity Index Report | 266 |

Acknowledgments

Foremost thanks and praises to the ONE who created this universe, world, mankind and each and everything that happens in this universe. Nothing is possible without **ALLAH**'s will and mercy. The entire phenomenon in this world is dependent upon HIS words '**Kun**' '**Fayakun**' to happens. My research and findings are only due to HIS utmost blessings. I would also like to thank Prophet Muhammad ﷺ who enlightened mankind with knowledge and encourage his preachers to seek knowledge.

My special gratitude and regards to my supervisor Dr. Hussain Ali, Associate Professor, Department of Pharmacy, QAU, for the support and guidance during my whole research journey. I am also grateful to the Dean of Faculty of Biological Sciences, QAU, and Dr. Gul Shahnaz, Chairperson, Department of Pharmacy, QAU for their motivation to the research students and providing lab facilities and resources to conduct research.

I am especially grateful to Prof. Benno Weigmann, Chair, Medical clinic 1, University Clinic Hospital, Erlangen, Germany for his support and assistance through the research journey and specially facilitating me in his lab during IRSIP fellowship abroad. I am also thankful to Prof. Dagmar Fischer, Chair of Pharmaceutics, Friedrich-Alexander University Erlangen-Nürnberg, for providing me lab space and facilities during IRSIP visit.

The research cannot be completed without the support of Higher Education Commission (HEC) of Pakistan that granted HEC Indigenous scholarship (PIN No. 315-12214-2BS3-132), and NRPU grant (No. 9272/Federal/NRPU/R&D/HEC/2017) to peruse research activities. Further, and HEC had awarded IRSIP fellowship (1-8/HEC/HRD/2021/10951) for the period of six months to conduct advanced research studies at University Clinic Hospital, FAU, Germany. The kind gestures and awards are highly appreciable especially in the current situation of country.

I obliged all faculty members at Department of Pharmacy, QAU, especially Dr. Ihsan, Dr. Asim, and Dr. Salman for the provision of facilities at the department. And Dr. Naseem to allow me to synthesize polymer in his lab. I would like to acknowledge my lab colleagues and friends especially Qurat Ul Ain, Iqra Afzal, Mahwash Mukhtar,

Rabia Gul, Samra Farooq, Rabia Arshad and Danish for the generous help and support in the whole journey. I sincerely recognize PhD seniors Amna, Maria Mir and Imran Asad and some helpful juniors for their kind support and encouragement.

Very big thanks to my family, parents, and siblings. From the beginning till the end of my work, my parents' loyalty, motivation, and support assisted me to complete my task. Their prayers always worked for me.

At the end, I pray that this research will be fruitful to the humanity and provide relief to the sufferings of the whole mankind.

Mahira Zeeshan

List of Tables

| Table | Title | Page No. |
|-------|---|----------|
| 1.1 | Physiological and pathophysiological considerations in IBD | 6 |
| 1.2 | pH-sensitive polymers for colon | 8 |
| 1.3 | Commercial products based on pH-dependent DDS for IBD | 10 |
| 1.4 | Novel pH-dependent macro drug delivery systems for IBD | 12 |
| 1.5 | pH-dependent microparticles and nanoparticles for the drug targeting in IBD | 25-26 |
| 1.6 | Patents for a pH-sensitive micro-/nanoparticulate system for the treatment of IBD | 31 |
| 2.1 | (A) The studied independent variables and their variation level in 2 ^{IV} (4-1) fractional factorial design (B) The constant variables with constant reaction conditions during GAL-PLGA polymer synthesis | 43 |
| 2.2 | The selected QTPP elements, CQAs, and CPPs/CMAs with targets and justifications for dexamethasone loaded GAL-PLGA nanoparticles | 47-48 |
| 2.3 | Studied independent variables at three different levels (-1, 0, +1) in 33 Box-Behnken DOE to prepare GAL-PLGA nanoparticles of the desirable criteria | 50 |
| 2.4 | Sequence of primers for the gene of interest | 62 |
| 2.5 | QTPP for Tofa-P/tfr NCs | 67 |
| 2.6 | Studied independent variables at three different levels (-1, 0, +1) in 33 Box-Behnken DOE to prepare Tofa-P/tfr NCs of desired characteristics | 68 |
| 2.7 | Forward and reverse primer sequence of the targeted genes | 75 |
| 2.8 | Inflammation indices determining the MEICS | 88 |
| 3.1 | Two-level 2 ^{IV} (4-1) fractional factorial design to study the effect of reaction variables on % yield and powder consistency of the synthesized GAL-PLGA polymer | 97 |
| 3.2 | ANOVA analysis to study the influence of independent variables on % Yield (Y1) of GAL-PLGA polymer under 2 ^{IV} (4-1) fractional factorial design | 97 |

| | | |
|------|--|-----|
| 3.3 | ANOVA analysis to study influence of independent variables on powder consistency (Y2) of GAL-PLGA polymer under 2IV ⁽⁴⁻¹⁾ fractional factorial design | 98 |
| 3.4 | 3-level, 3-factor Box-Behnken DOE to explore the effect of independent variables (A1-A3) on experimental and predicted values of response variables (particle size (Z1), zeta potential (Z2) and PDI (Z3)) to control GAL-PLGA nanoparticles quality | 102 |
| 3.5 | ANOVA analysis to study effect of independent variables (A1-A3) on particle size (Z1) of GAL-PLGA nanoparticles under 33 Box-Behnken DOE | 105 |
| 3.6 | ANOVA analysis to study effect of independent variables (A1-A3) on zeta potential (Z2) of GAL-PLGA nanoparticles under 33 Box-Behnken DOE | 106 |
| 3.7 | ANOVA analysis to study effect of independent variables (A1-A3) on PDI (Z3) of GAL-PLGA nanoparticles under 33 Box-Behnken DOE | 106 |
| 3.8 | Effect of storage conditions on physicochemical characteristics of Dexamethasone loaded GAL-PLGA nanoparticles | 110 |
| 3.9 | Mathematical models describing drug release kinetics from GAL-PLGA and PLGA nanoparticles at pH 1.2 (SGF) and pH 7.4 (SIF) | 114 |
| 3.10 | Physicochemical characteristics of Dexa loaded nanocargoes | 121 |
| 3.11 | Effect of storage conditions on physicochemical characteristics of Dexa-GP/ES/Pu NCs (ICH guidelines) | 122 |
| 3.12 | Evaluation of Dexa-GP/ES/Pu NCs in physiological buffers (pH 7.4) | 122 |
| 3.13 | Drug release from Dexa-GP/ES/Pu NCs at acidic pH and pH 7.4, without or with cecal content | 126 |
| 3.14 | Drug release from Dexa-GP/ES NPs at acidic pH and pH 7.4, without or with cecal content | 127 |
| 3.15 | Drug release from Dexa-GP/Pu NPs at acidic pH and pH 7.4, without or with cecal content | 128 |

| | | |
|------|--|-----|
| 3.16 | QbD-risk assessment of the impact of QTPPs on CQAs for Tofa-P/tfr NCs | 151 |
| 3.17 | QbD-risk assessment of the impact of CPPs/CMAAs on CQAs for Tofa-P/tfr NCs | 151 |
| 3.18 | 33 Box-Behnken Experimental design generating different runs to produce desired values of the dependent variables (output) | 153 |
| 3.19 | Physicochemical characteristics of Tofa-PLGA NCs and Tofa-P/tfr NCs (mean \pm SD, n=3) | 157 |
| 3.20 | Drug release kinetics of Tofa-P/tfr NCs in SGF at pH 1.2 (stomach) and SIF at pH 7.4 (colon) | 162 |
| 3.21 | Effect of storage conditions on freeze-dried Tofa-P/tfr NCs (mean \pm SD, n=3) | 166 |
| 3.22 | Physicochemical characteristics of drug-loaded nanoshells (mean \pm SD, n=3) | 176 |
| 3.23 | Drug release kinetics of Tofa-LP/tfr NSh at pH 1.2 and 7.4 | 182 |
| 3.24 | Drug release kinetics of Tofa-LP/tfr/ES NSh at pH 1.2 and 7.4 | 182 |
| 3.25 | Effect of storage conditions on physicochemical properties of Tofa-LP/tfr/ES NSh (mean \pm SD, n=3) | 189 |
| 3.26 | Drug release kinetic modeling of TAC-P/Lys NCs and TAC-P/Lys/ES-L100 NCs at pH 1.2 and 7.4 | 208 |

List of Figures

| Figure | Title | Page No. |
|---------------|--|-----------------|
| 1.1 | Common types and characteristics of IBD | 2 |
| 1.2 | pH dependent colon-specific targeting at organ and tissue levels | 13-14 |
| 1.3 | Classification of pH-sensitive nanostructures for IBD | 23 |
| 1.4 | Advantages and disadvantages of conventional and novel pH-dependent drug delivery systems | 24 |
| 1.5 | pH sensitive ligand anchored polymeric nanocarriers and proposed strategies for IBD | 35 |
| 2.1 | Molecular structures of MGL-2 homologous receptor (5JPV) (a); D-galactose ligand (b); GAL-PLGA polymer (monomer unit) (c) as a ligand | 42 |
| 2.2 | Synthesis of GAL-PLGA polymer and nanoparticles under QbD and DOE approach | 45 |
| 3.1 | HPLC standard curve of Dexamethasone (Dexa) | 92 |
| 3.2 | Evaluation of quality of MGL-2 homologous model through Ramachandran plot (a) and, Z-score plot (b) | 93 |
| 3.3 | Molecular docking: simulated ligand interaction with MGL-2 homologous receptor (model/coordinates A and B) with binding energies, H-bonds, and binding amino acid residues | 94 |
| 3.4 | Effect of reaction variables on quality of GAL-PLGA powder and physicochemical characterization of GAL-PLGA polymer | 100 |
| 3.5 | QbD risk assessment and 3 ³ Box-Behnken DOE to investigate effect of independent variables on nanoparticles outcomes | 104-105 |
| 3.6 | Prediction and desirability profiling of the optimum values of independent variables to produced GAL-PLGA nanoparticles with desired characteristics | 107 |
| 3.7 | Physicochemical and In vitro characteristics of Dexa-GAL-PLGA nanoparticles | 109 |
| 3.8 | In vitro hemolysis and cellular biocompatibility assessment of GAL-PLGA nanoparticles | 115 |

| | | |
|------|--|---------|
| 3.9 | Cell uptake assays and in vivo biodistribution studies of GAL-PLGA nanoparticles | 118 |
| 3.10 | Physicochemical characterization of Dexa-GP/ES/Pu NCs (A-E) | 123 |
| 3.11 | Drug release study of GP/ES/Pu NCs and mucin-nanocargoes binding investigations | 129 |
| 3.12 | Cellular biocompatibility and uptake assay of Dexa-GP/ES/Pu NCs and galactose-based nano-formulations | 131 |
| 3.13 | Ex vivo permeation and retention assay of Rho-GP/ES/Pu NCs, in vivo biodistribution studies and vascular integrity assessment | 133 |
| 3.14 | Therapeutic evaluation of Dexa-GP/ES/Pu NCs through morphologic and physical parameters | 137 |
| 3.15 | Histopathology, immunoreactivity, ATR-FTIR, colon feces microbial count and blood glucose evaluation to determine therapeutic efficiency of Dexa-GP/ES/Pu NCs | 141 |
| 3.16 | RT-PCR, ELISA, antioxidant assays and blood indices to determine inflammation severity and Dexa-GP/ES/Pu NCs treatment effects | 143 |
| 3.17 | Assessment of in vivo biocompatibility and toxicology during and after 7 days of administration Dexa-GP/ES/Pu to the healthy mice (n=3) | 146 |
| 3.18 | Tofacitinib citrate (Tofa) calibration curves with various solvents using UV spectrophotometer (A-C) and HPLC calibration curves (I-II) | 147-148 |
| 3.19 | QbD analysis: Cause and effect Ishikawa diagram for Tofa-P/tfr NCs (A); Screening of critical process parameters (B), and critical quality attributes (C) through risk-based assessment of severity scores | 150 |
| 3.20 | Surface-response plots for the study of effects of independent variables on dependent variables (outcomes) under 3 ³ Box-Behnken DOE | 154 |

| | | |
|------|---|-----|
| 3.21 | Pareto charts of standardized effects on dependent variables (X, Y, Z); D-F: Difference between the predicted and experimental values of dependent variables using 3 ³ Box-Behnken design | 155 |
| 3.22 | Desirability profile to obtain the desired values of dependent variables (outcomes) from an appropriate combination of independent variables | 156 |
| 3.23 | Physicochemical characterization of Tofa-P/tfr NCs | 159 |
| 3.24 | Tofa-P/tfr NCs drug release studies and mucin interaction studies | 161 |
| 3.25 | In vitro hemolysis and cellular biocompatibility assays of Tofa-P/tfr NCs | 163 |
| 3.26 | Cellular uptake of dye-loaded P/tfr NCs by murine-macrophages (I) and colon cells (II) | 164 |
| 3.27 | Uptake of dye loaded PLGA NCs and P/tfr NCs in the absence and presence of anti-TFR-1 antibody (a-f) and the emitted fluorescence intensity (g) | 165 |
| 3.28 | Tofa-P/tfr NCs in vivo biodistribution, colon-macrophages uptake and therapeutic assessment through morphological and physical parameters | 168 |
| 3.29 | Histological and vascular integrity evaluation of the colon excised from normal, DSS-colitis, Tofa and Tofa-P/tfr NCs treated groups | 169 |
| 3.30 | RT-PCR expression of STAT-1 (A), TFR-1 (B), E-cadherin (C) and iNOS (D); And levels of proinflammatory cytokines, IL-6 (E) and TNF- α (F) from the colon tissue excised from normal, DSS-colitis, Tofa and Tofa-P/tfr NCs groups (n=5) | 171 |
| 3.31 | Antioxidant protection evaluated through quantification of antioxidants in the colon tissue excised from normal, DSS-colitis, Tofa and Tofa-P/tfr NCs groups (n=5) | 173 |
| 3.32 | Elucidation of the effect of therapy on blood parameters, renal function, inflammatory blood marker, and colon feces microbial content | 174 |

| | | |
|------|---|-----|
| 3.33 | pH sensitive nanoshells (Tofa-LP/tfr/ES NSh) target colon tissues to mitigate inflammation | 175 |
| 3.34 | Physicochemical properties of Tofa-LP/tfr NSh and Tofa-LP/tfr/ES NSh | 177 |
| 3.35 | ATR-FTIR spectra of drug, excipients and nanoshells | 179 |
| 3.36 | Tofa-LP/tfr NSh and of Tofa-LP/tfr/ES NSh drug release and mucin binding studies | 181 |
| 3.37 | In vitro hemolysis and cellular biocompatibility studies of Tofa-LP/tfr NSh and Tofa-LP/tfr/ES NSh | 184 |
| 3.38 | Evaluation of Caco-2 apoptosis by the Tofa-LP/tfr NSh and Tofa-LP/tfr/ES NSh, as indicated by 7-AAD (I) and PI (II) viability dyes | 185 |
| 3.39 | Caco-2 uptake investigations of nanoshells by dye fluorescence and FACS analysis | 186 |
| 3.40 | In vitro THP-1 derived macrophages uptake assay and JAK/STAT inhibition assay | 188 |
| 3.41 | Preliminary in vivo nanoshells localization and retention studies and colon-macrophages uptake | 190 |
| 3.42 | Nanoshells in vivo biodistribution imaging studies | 192 |
| 3.43 | Therapeutic evaluation of Tofa loaded nanoshells' treatment efficacy through morphological, physical, histological and vascular integrity assessment | 195 |
| 3.44 | RT-PCR expression of STAT-1 (A), TFR-1 (B), E-cadherin (C) and iNOS (D); And levels of proinflammatory cytokines, IL-6 (E) and TNF- α (F) from the colon tissue excised from normal, DSS-colitis, Tofa and Tofa-LP/tfr NSh and Tofa-LP/tfr/ES NSh groups (n=5) | 198 |
| 3.45 | Tofa-LP/tfr NSh and Tofa-LP/tfr/ES NSh mediated in vivo antioxidant protection analysis through immunohistochemistry and biochemical antioxidant assays | 200 |
| 3.46 | Elucidation of the effect of therapy on the blood cells count (A), renal function (B), C-reactive proteins (CRP) (C), and | 202 |

| | | |
|------|---|-----|
| | colony-forming units from the feces of Normal control, DSS-colitis, Tofa, and Tofa-P/tfr NCs groups (D) | |
| 3.47 | In vivo biocompatibility evaluation of Tofa-LP/tfr/ES NSh through morphological, microbial, and apoptotic parameters | 203 |
| 3.48 | HPLC Calibration Curve of TAC | 204 |
| 3.49 | Physicochemical properties of TAC-P/Lys NCs and TAC-P/Lys/ES-L100 NCs (mean \pm SD, n=3) | 206 |
| 3.50 | In vitro drug release of TAC-P/Lys NCs and TAC-P/Lys/ES-L100 NCs in SGF at pH 1.2 and SIF at pH 7.4 | 207 |
| 3.51 | Effect of TAC loaded nanocarriers on caco-2 viability after 6 and 24 hours of incubation using 7-AAD (I) and PI (II) dyes | 209 |
| 3.52 | TAC based nanocarriers uptake by Caco-2 cells (I) and THP-1 derived macrophages (II) | 211 |
| 3.53 | Therapeutic evaluation of TAC nanocarriers in the OXA-colitis mice through endoscopic and morphological parameters | 213 |
| 3.54 | Histopathological investigation of OXA-colitis group and the treatment groups; I. Colon, II. Colon histoscore, III. Small intestine, IV. Stomach | 215 |
| 3.55 | Effect of TAC based nanocarriers on the MPO activity in the OXA-colitis, assessed by IVIS system | 216 |
| 3.56 | Evaluation of inflammatory mediator pITK in the T-cells through immunoreactivity and flowcytometry | 218 |
| 3.57 | RT-PCR analysis of inflammation mediator proteins (pITK, NFATc-1, NF- κ B, TGF- β), tight junction protein (Oc1n-1), angiogenesis factor (VEGF-A), and ELISA analysis of pro-inflammatory IL-6 expression | 221 |
| 3.58 | Assessment of pro-inflammatory M1- macrophages expressing CD38 surface marker in the treatment and disease groups through flowcytometer (n=3) | 223 |

List of Abbreviations

| Abbreviations | Description |
|----------------------|--|
| 7-AAD | 7-Aminoactinomycin D |
| adj-R ² | Adjusted coefficient of determination |
| AIC | Akaike information criterion |
| ANOVA | Analysis of variance |
| ATR-FTIR | Attenuated total reflectance- Fourier transform infrared spectroscopy |
| Caco | Adenocarcinoma of the colon (cell line) |
| CAMs | Cell adhesion molecules |
| CBC | Complete blood count |
| CDNB | 1-Chloro-2,4-dinitrobenzene |
| CFU | Colony forming unit |
| CMA | Critical material attribute |
| Co-6 | Coumarin-6 |
| COX-2 | Cyclooxygenase-2 |
| CPP | Critical process parameter |
| CQA | Critical quality attribute |
| CrD | Crohn's disease |
| CRP | C-Reactive Protein |
| CTAB | Cetyltrimethylammonium bromide |
| CTT | Colonic transit time |
| DAB | 3,3'-Diaminobenzidine |
| DAI | Disease activity index |
| DAPI | 4',6-diamidino-2-phenylindole |
| DDS | Drug delivery system |
| Dexa-GAL-PLGA NPs | Dexamethasone loaded galactosylated-PLGA nanoparticles |
| Dexa-GP/ES NCs | Dexamethasone loaded galactose-PLGA/ES100 nanocargoes |
| Dexa-GP/ES/Pu NCs | Dexamethasone loaded ES100/pullulan coated galactose-PLGA (GP) nanocargoes |

| | |
|----------------|--|
| Dexa-GP/Pu NCs | Dexamethasone loaded galactose-PLGA/Pullulan nanocargoes |
| DLS | Dynamic light scattering |
| DOE | Design of experiment |
| DSC | Differential scanning calorimetry |
| DSS | Dextran sulphate sodium |
| E. coli | Escherichia coli |
| EDTA | Ethylenediaminetetraacetic acid |
| EE | Encapsulation efficiency |
| eEPR | Enhanced epithelial permeation and retention effect |
| EFS30D | Eudragit® FS 30D |
| EL100 | Eudragit® L100 |
| EL100-55 | Eudragit® L10055 |
| EL30D-55 | Eudragit® L30D55 |
| ELISA | Enzyme-linked immunosorbent assay |
| EP4135F | Eudragit® P4135F |
| ES100, ES | Eudragit® S100 |
| ES-RL/RS | Eudragit® RL/RS |
| FACS, FCS | Flowcytometer |
| FBS | Fetal bovine serum |
| GAL-PLGA | Galactosylated-PLGA |
| GI | Gastrointestinal |
| GIT | Gastrointestinal tract |
| GSH | Glutathione |
| GST | Glutathione S-transferases |
| Hb | Hemoglobin |
| HEPES | N-2-Hydroxyethylpiperazine-N'-2-Ethanesulfonic Acid |
| HO-1 | heme oxygenase 1 |
| IBD | Inflammatory bowel disease |

| | |
|----------------|---|
| ICAM | Intercellular adhesion molecule |
| ICH | International Council for Harmonisation |
| IF- γ | Interferon-gamma |
| IG | Immunoglobulin |
| IL | Interleukin |
| iNOS | Inducible nitric oxide synthase |
| IVIS | In Vivo Imaging System |
| JAK/STAT | Janus kinase-signal transducer and activator of transcription |
| LMWH | Lower molecular weight heparin |
| LPO | Lipid peroxidation |
| MAPK | Mitogen-activated protein kinase |
| MCH | Mean corpuscular hemoglobin |
| MCHC | Mean corpuscular hemoglobin concentration |
| MCV | Mean corpuscular volume |
| MDA | Malondialdehyde |
| MEICS | Murine Endoscopic Index of Colitis Severity |
| MGL | Macrophage galactose type lectin C |
| MPO | Myeloperoxidase |
| MPs | Microparticles |
| MSC | Model selection criteria |
| MTT | 3-(4,5-dimethylthiazol-2-yl)-2,5-diphenyltetrazolium bromide |
| NFATc | Nuclear factor of activated T-cells |
| NF- κ B | Nuclear Factor Kappa B |
| NIH | National Institute of Health |
| NiMOS | Nanoparticles-in-microspheres |
| NOD 2 | Nucleotide binding oligomerization domain 2 |
| NP-MC | NPs-in-microcomposites |
| NP-MS | NP-in-pH-sensitive microsphere |
| NPs | Nanoparticles |

| | |
|----------------|---|
| Nrf2 | Nuclear factor-erythroid factor 2-related factor 2 |
| O/W | Oil-in-water |
| OROS-CT | Osmotically controlled drug delivery System |
| OTT | Orocecal transit time |
| OXA | Oxazolone |
| PBS | Phosphate buffered saline |
| PCL | Poly caprolactone |
| PCV/HCT | Packed cell volume/hematocrit |
| PDI | Poly dispersity index |
| PEI | Polyethyleneimine |
| PI | Propidium iodide |
| pITK | Phosphorylated IL-2–inducible kinase |
| PLA | Poly lactic acid |
| PLGA | Poly lactic co-glycolic acid |
| PMA | Phorbol myristate acetate |
| PMAA | Polymethacrylic acid |
| Pu | Pullulan |
| PVA | Polyvinyl alcohol |
| QbD | Quality by design |
| QTPP | Quality target product profile |
| R ² | Coefficient of determination |
| RBC | Red blood cell |
| RFT | Renal function test |
| Rho | Rhodamine-b |
| ROS | Reactive oxygen species |
| RP-HPLC | Reversed phase high-performance liquid chromatography |
| RT-PCR | Reverse transcription polymerase chain reaction |
| SEM | Scanning electron microscopy |
| SGF | Simulated gastric fluid |
| SIF | Simulated intestinal fluid |

| | |
|-----------------------|---|
| siRNA | Small interfering Ribonucleic acid |
| STEM | Scanning transmission electron microscopy |
| TAC | Tacrolimus |
| TAC-P/Lys NCs | Tacrolimus loaded PLGA/L-Lysine nanocarrier |
| TAC-P/Lys/ES-L100 NCs | Tacrolimus loaded ES100/EL100 coated PLGA/L-Lysine nanocarriers |
| TEM | Transmission electron microscope |
| tfr | Transferrin |
| TFR | Transferrin receptor |
| TGA | Thermogravimetric analysis |
| TGF- β | Transforming growth factor beta |
| T _H | T-helper cell |
| TLC | Total leukocytes count |
| TNBS | 2,4,6-Trinitrobenzenesulphonic acid |
| TNF | Tumor necrosis factor |
| Tofa | Tofacitinib citrate |
| Tofa-LP/tfr NSh | Tofacitinib citrate loaded Lipid-PLGA/tfr nanoshells |
| Tofa-LP/tfr NSh | Tofacitinib citrate loaded transferrin-lipid/PLGA nanoshell |
| Tofa-LP/tfr/ES NSh | Tofacitinib citrate loaded ES100 coated Lipid-PLGA/tfr nanoshells |
| Tofa-P/tfr NCs | Tofacitinib citrate loaded transferrin-PLGA nanocarrier |
| TT | Transit time |
| UC | Ulcerative colitis |
| UV-Vis | Ultraviolet-Visible |
| VEGF | Vascular endothelial growth factor |
| W/O | Water-in-oil |
| W/O/W | Water-in-oil-in-water |
| XPRD | X-ray Powder Diffraction |

Abstract

Inflammatory bowel disease (IBD) is the chronic inflammation of the Gastrointestinal tract (GIT). Ulcerative colitis (UC) is one of the major types of IBD that confines to the colon. The available conventional therapies for the treatment of IBD are less promising because of pathophysiological, and cellular barriers. In this context, nanocarrier-based drug delivery system specifically delivers various therapeutic agents to the target area. Nanocarriers made up of pH-sensitive polymers protect against drug degradation and absorption in the upper GIT. The combination of pH-sensitive polymer with a sustained-release polymer like PLGA release and concentrate the drug at the target area for a prolonged time. Further, to overcome inter and intra-cellular barriers at the colon, ligand-based strategy enables specific targeting of colon cells and recruited immune cells like macrophages via specific surface receptors overexpressed under inflammation. Based on the altered immunological condition of the colon in UC, various surface receptors like macrophage galactose type lectin-C (MGL-2) and transferrin receptor (TFR-1) are exploited for colon drug delivery purpose. We aimed to develop stimuli sensitive-ligand anchored sustained release polymeric nanocarriers to target the colon for prolonged duration and bypass obstacles via the oral route. The outer stimuli sensitive coat dissolves at the colon microenvironment and exposes underneath drug-containing ligand anchored PLGA nanocores that target the overexpressed surface receptors and releases the drug for a prolonged duration. Under stimuli sensitive-ligand anchored polymeric nanocarriers based rationale, we have developed three strategies to target inflamed colon through the oral route. In the first one, we have prepared Dexamethasone (Dexa) loaded D-galactose-PLGA nanoparticles (GAL-PLGA NPs) and stimuli sensitive Dexa loaded D-galactose/Eudragit S100/Pullulan nanocargoes (Dexa-GP/ES/Pu NCs). The later have all attributes to target colon because of dual stimuli sensitive coat of Eudragit S100 (ES) and Pullulan (Pu) that dissolved under pH and microbial enzymes of the colon. Further, ligand anchored galactose-PLGA (GAL-PLGA or GP) core has a high affinity towards MGL-2, that is overexpressed on the surface of macrophages at the colon. The Dexa-GAL-PLGA NPs were developed under systemic quality by design (QbD) approach and Box-Behnken design. Further, coating with ES/Pu generated Dexa-GP/ES/Pu NCs that have appropriate physicochemical properties, thermal stability, negligible interactions between excipients, and retardation of drug release at pH 1.2 and sustained

drug release at pH 7.4, biocompatible and good uptake by the colon and macrophage cells. The Dexa-GP/ES/Pu NCs demonstrated efficient targeting and amelioration of Dextran sulfate sodium (DSS) induced colitis. Under the second approach, we have developed Tofacitinib citrate (Tofa) loaded PLGA/transferrin nanocarriers (Tofa-P/tfr NCs) using QbD and Box-Behnken design. Furthermore, Tofa-P/tfr NCs were modified to formulate nanoshells (NSh) i.e., Tofa-LP/tfr NSh and Tofa-LP/tfr/ES NSh with enhanced properties because of lipidic content (L) in the core that facilitates more drug content to be encapsulated, controlled drug release and have some protective effects on intestine mucosa. The pH-sensitive nature of Tofa-LP/tfr/ES NSh enabled more colon-specific action. Tofa-P/tfr NCs, Tofa-LP/tfr NSh and Tofa-LP/tfr/ES NSh have an adsorbed tfr ligand that facilitated direct binding with TFR-1 receptors. The minimal drug release at pH 1.2 was observed with Tofa-LP/tfr/ES NSh. These three nanoformulations have extensive uptake potential. Tofa-LP/tfr NSh and Tofa-LP/tfr/ES NSh were more biocompatible than Tofa-P/tfr NCs. All Tofa-P/tfr NCs, Tofa-LP/tfr NSh and Tofa-LP/tfr/ES NSh proved to be efficacious in restoring inflammation in the DSS-colitis model as manifested from restored clinical and inflammatory indices. However, Tofa-LP/tfr/ES NSh had the superior action because of multiple characteristics. Under the third strategy, tacrolimus (TAC) loaded nanocarriers (NCs) were developed with adhered L-Lysine content on PLGA (P/Lys), coated with dual ES100 and EL100 (ES-L100) pH-sensitive coat. The combined rationale is developed to counter the inter- and intra-individual variations and have more control over drug release at colon. TAC-P/Lys NCs and TAC-P/Lys/ES-L100 NCs were developed with optimal characteristics. ES-L100 coated formulation have more retardation of drug release at pH 1.2 than uncoated nano-formulation. Both TAC-P/Lys NCs and TAC-P/Lys/ES-L100 have good biocompatibility and uptake potential into the caco-2 cells and macrophages. TAC-P/Lys NCs and TAC-P/Lys/ES-L100 have promising therapeutic effects in the oxazolone (OXA) induced colitis model, as manifested through the endoscopy, morphological parameters, histology, inflammatory proteins, and mediators' levels. Further, TAC loaded nanocarriers inhibited inflammatory pITK levels in the T-cells, as indicated through immunohistochemistry, flowcytometry, and RT-PCR. In short, TAC-P/Lys/ES-L100 NCs have superior therapeutic efficacy in the OXA-colitis model as compared to uncoated TAC-P/Lys NCs. However, further investigations are required to check the therapeutic efficiency of all these nano-formulations on a relevant bigger animal model and to translate this concept into clinical studies.

CHAPTER 1

INTRODUCTION

1. INTRODUCTION

1.1. Background

Inflammatory bowel disease (IBD) is a chronic, episodic mucosal inflammation of the gastrointestinal tract (GIT) mainly affecting the colon and ileum. Ulcerative colitis (UC) and Crohn's disease (CrD) are the two most prevalent types of IBD (Abraham and Cho, 2009); the major point of differentiation between the two is the location and the depth to which the intestine is inflamed. In UC, inflammation afflicts the innermost mucosal layer and proceeds continuously from the rectum to the proximal colon (Figure 1. 1). On the contrary, in CrD, inflammation penetrates to the deeper tissues instead of being confined to the mucosal layer and can appear in any GI section, often the colon and terminal ileum in a discontinuous manner (Figure 1. 1) (Abraham and Cho, 2009; Hua *et al.*, 2015). The worldwide growing prevalence of IBD affected about 412–505/100,000 persons in Europe and 286/100,000 in North America and led to 51,000 deaths worldwide in 2013 (Kaplan, 2015; Naghavi *et al.*, 2015; Ng *et al.*, 2017). Although patients belong to any age group, the main target group is those aged 15–30 years (Hanauer, 2006). The etiology of IBD is still under investigation. Genes, immune system dysfunction, environmental factors, and microbiome might contribute to it (Sartor, 2010). The underlying pathogenesis involves one of the following: autoimmune response against a mucosal antigen, immune system dysfunction that attacks commensal microbes, or infection caused by pathogens, leading to a chronic inflammatory process (Hendrickson *et al.*, 2002). Investigations have suggested that chromosomes 1, 3, 6, 7, 12, 14, 16, and 19 play a role in the inflammatory process (Hanauer, 2006; Hendrickson *et al.*, 2002). Genetic mutations in nucleotide-binding oligomerization domain 2 (NOD-2) probably provoke the innate immune response and susceptibility to CrD (Hugot *et al.*, 2001).

Patients with IBD alternate between two stages. One is the active disease period, where symptoms are obvious, and is termed the flare-up/relapse state. This is followed by a silent period with negligible symptoms, known as the remission state. The general symptoms are abdominal pain, severe diarrhea, bloody stool, weight loss, fatigue, and fever. Other complications internal and external to the intestine, such as skin problems, liver inflammation, bone thinning, and anemia, might develop.

Multifarious etiology and disease complexity are the challenges for IBD therapeutics. Unfortunately, a permanent cure for IBD is not available to date, and patients have to rely on lifelong drug treatment. IBD therapy focuses on inducing and maintaining the remission state and providing symptomatic relief during the active disease state. Currently, the newer therapeutic agents focus on the underlying mucosal healing of the bowel. Conventional therapies including aminosalicylates, corticosteroids, immunosuppressants, and biological agents have deleterious consequences following long-term consumption, which is required for IBD treatment. The conventional drugs are associated with adverse effects, and the development of resistance and tolerance, as patients become refractory to the therapy and ultimately relapse to the active disease state upon withdrawal (Buchman, 2001). Most of the drugs are administered in a higher dose to counter the first-pass metabolism in the intestine and liver for the desired therapeutic efficacy (Prantera and Marconi, 2013). Moreover, safety is the foremost concern with the advanced therapeutic classes, immunosuppressants, and biologicals, as immune system suppression renders the patient vulnerable to infections, bone marrow suppression, malignancy, reactivation of latent hepatitis B, and tuberculosis (Bernstein *et al.*, 2010; Dassopoulos *et al.*, 2013).

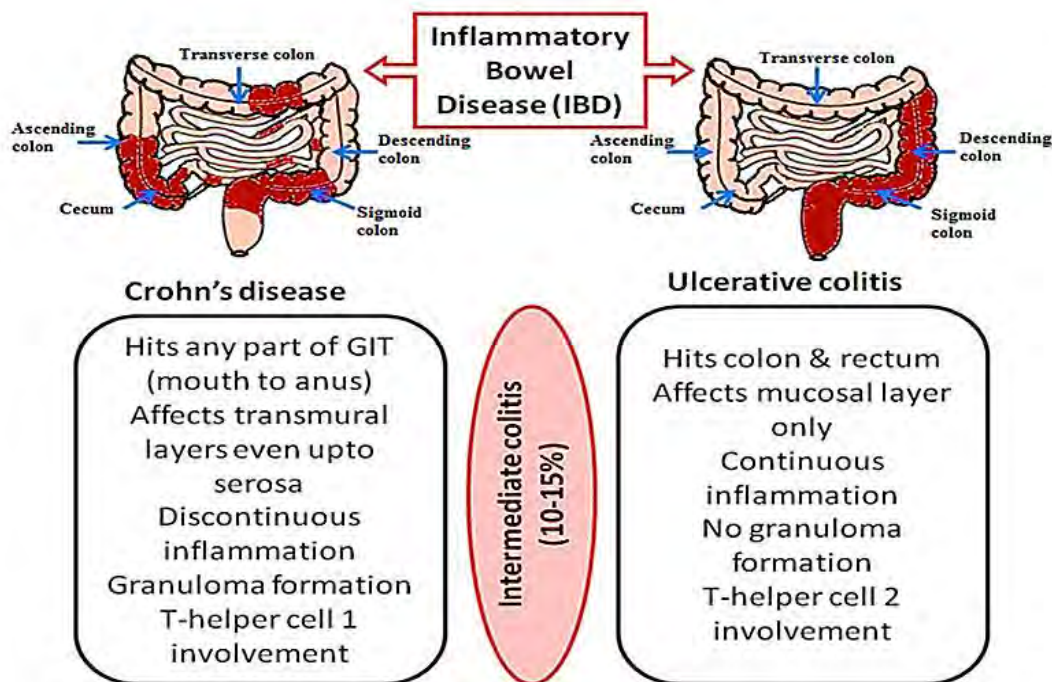


Figure 1. 1: Common types and characteristics of IBD

Furthermore, unique location, and anatomical and disease state variations render colon targeting potentially difficult. Rectal formulations are successful to a limited extent in UC; however, their coverage includes areas of the distal colon only (Collnot *et al.*, 2012). In this regard, oral formulations have an advantage, as the normal passage includes the whole GIT and covers the entire colon. Despite their advantages, oral dosage forms have not achieved expected success in IBD due to obstacles such as acidic and enzymatic degradation, reduced stability, first-pass metabolism, and earlier systemic absorption from the stomach or small intestine. This results in a diminished localized concentration of the drug at the inflamed tissues of the colon. In addition, heavy diarrhea, which is common in IBD, leads to rapid clearance and short-term residence time of conventional dosage forms such as tablets, granules, and capsules. Higher doses or repeated administration further aggravates the problem and leads to severe adverse effects. Therefore, the current area of focus is the development of novel drug delivery systems (DDS) such as micro- and nanoparticles that specifically target and localize the drug at the inflamed colon tissues with minimal systemic absorption and adverse effects and enhanced therapeutic efficacy. One step further, the development of pH-sensitive micro- and nanoparticles facilitate colon targeting and overcome the drawbacks associated with simple micro- and nanoparticles.

1.2. IBD Physiological and Pathophysiological Considerations

In IBD, underlying inflammation of mucosa causes epithelial intestinal membrane disintegration, increase mucus production, immune cell (macrophages, lymphocytes, neutrophils) recruitment, fluid, and electrolyte loss, ulcer, bleeding and edema (Thoreson and Cullen, 2007; Antoni *et al.*, 2014). The recruited macrophages produce cytokines at the inflamed tissues and are responsible for exacerbating inflammation and for the differentiation of T-lymphocytes; type 1 helper T-cells are predominant in CrD, whereas type 2 helper T-cells play a role in UC (Brand, 2009). These immune responses destroy mucosal integrity and give rise to chronic inflammation. These pathophysiological alterations mediate changes in gut motility, microbiome, pH, transit time, and intestinal volume and hence affecting the performance of drug-carrying dosage forms approaching the colon.

1.2.1. pH

From the drug delivery point of view, pH is a major aspect, as the GIT has pH variations across its different regions. The stomach has an acidic pH range, whereas the small intestine has a slightly acidic to neutral pH; and the pH ranges 6.1–7.5 in the colon and rectum (Nugent *et al.*, 2001; Chowdary Vadlamudi *et al.*, 2012), as mentioned in Table 1. 1. The pH gradient enables the development of colon-targeting DDS that respond to a specific pH of the colon only. However, possible colonic pH alterations in IBD compromise the efficiency of the DDS. pH variations are the consequence of multiple processes, including mucosal bicarbonate discharge; microbial lactate production; altered short-chain fatty acid absorption; and changes in intestinal fluid volume, carbohydrate metabolism, and transit time (Nugent *et al.*, 2001). Some studies have reported decreased colon pH; however, in light of the limited studies performed so far, pH reduction in UC cannot be concluded (Nugent *et al.*, 2001). The small intestine pH remains unchanged in IBD. Likewise, most of the time, in CrD, the luminal pH value is within the normal range. However, Sasaki *et al.* (Sasaki *et al.*, 1997) reported a decline in the luminal pH value. The range of pH values in UC and CrD, based on some reported studies, are listed in Table 1. 1. To date, investigations of pH changes in UC and CrD are insufficient and outdated; and the topic is still debatable. The possible reasons for pH fluctuations in some studies were signal loss during pH recording or intra- and inter-individual variations (Ewe *et al.*, 1999). Furthermore, pH values are quietly different in the active and remission states. To obtain more convincing evidence, extensive studies on a larger number of IBD patients must be performed. As pH values have a major impact on pH-sensitive polymer erosion and subsequent drug release; variations in colonic pH may affect such strategies and impede the drug release and action.

1.2.2. Transit time

Transit time (TT) is another important feature of GIT. In normal conditions, TT across the small intestine is 4 hours, with 2–6 hours variability among individuals (Hu *et al.*, 2000; Hua *et al.*, 2015). Pathophysiological alterations shorten colon TT in IBD patients. Mainly, diarrhea accelerates GI peristaltic movement which affects TT in IBD. In UC, the colonic TT is 9.5–39.1 hours as compared to 41.1–62.3 hours in healthy

individuals, as mentioned in Table 1.1. While the orocecal TT, the time taken by a substance to reach the cecum from the mouth, is prolonged in both UC and CrD (Rana *et al.*, 2013; Fischer *et al.*, 2017). In dysbiosis, where small intestinal bacteria have been overgrown, orocecal TT is shortened (Kashyap *et al.*, 2013). Mostly, dosage forms based on TT such as time-dependent bilayer tablets or capsules face obstacles because of the variable gastric emptying time, which depends upon the patient's fed state, disease stage, and dosage form size (Podczeczek *et al.*, 2007). TT must be considered while developing orally-delivered colon targeting DDS for IBD because it influences their retention and clearance across the bowel (Hebden *et al.*, 2000). Even in the remission state of CrD, altered GI motility and contractions compromise their effectiveness (Annese *et al.*, 2009).

1.2.3. Luminal contents

The colonic luminal contents are diluted in IBD due to the large fluid secretion and defective reabsorption of water, which culminates in heavy diarrhea (Van Citters and Lin, 2006). The large fluid volume dilutes the enzymes and affects nutrient absorption (Hua *et al.*, 2015; Van Citters and Lin, 2006) and carbohydrate metabolism by the intestinal microbes (Yang, 2008). For polymeric drug delivery, this is an important fact to be considered while developing any formulation. In CrD, inflammation or terminal ileum resection leads to defective absorption of fats and bile salts (Uchiyama *et al.*, 2018). Therefore, it could impair the absorption of lipophilic drugs and carriers.

1.2.4. Colonic microbiome

About 10^{11} - 10^{12} CFU (colony-forming units)/mL microbes are present in the colon (Zhang and Li, 2014). The natural microbiome of the colon involved in the metabolism, degradation, and activation of many dosage forms rely on the microbiome. A large population of anaerobic bacteria secrete enzymes to degrade and metabolize organic substances such as carbohydrates and proteins (Chourasia and Jain, 2004). Therefore, dosage forms based on polymeric carriers such as chitosan, dextran, guar gum, and chondroitin are used for colon targeting. In IBD, microbiome alterations direct colon epithelial layer disturbance, enhance mucosal permeability and stimulate the immune system that influences TT, pH, and the metabolism of endogenous and exogenous substances across the GIT (Sartor, 2008). Meanwhile, these are the important driving

forces that augment the inflammatory processes, as the immune system attacks commensal microbes as antigens and drives the inflammatory cascade (Matricon *et al.*, 2010). In UC, there is an overgrowth of facultative anaerobes and *Escherichia coli* (*E. coli*), while *Clostridium* species are decreased (Zhang and Li, 2014; Rhodes, 2007). Likewise, eubacteria, *E. coli*, and *Peptostreptococcus* are overgrown in CrD, whereas bifidobacteria and *Bacteroides* are reduced (Rhodes, 2007; Zhang and Li, 2014; Zhou and Zhi, 2016) (Table 1. 1.). Therefore, the microbial alterations affect formulations based on microbial/enzymatic metabolism, such as polysaccharides-based dosage forms and pro-drugs. It affects the extent of drug release from such carriers and the amount of released drug available for local therapeutic effect cannot be predicted.

Table 1. 1: Physiological and pathophysiological considerations in IBD

| Gastrointestinal Region | Healthy State | UC | CrD | References |
|---------------------------|---|---|--|--|
| pH | | | | |
| Stomach | 1.2-2 (fasted), 2-6 (fed) | ~2 | ~2 | (Nugent <i>et al.</i> , 2001) |
| Small Intestine | Duodenum | 5.5-7 | 6.1-7.4 | |
| | Jejunum | 5.5-7 | 6.8-8 | |
| | Ileum | 6.5-7.5 | 6.8-8 | |
| Large Intestine (colon) | Cecum | 5.5-7.5 | 3-7.4 | |
| | Right colon | 6.1-7.5 | 3-7.4 | |
| | Left colon | 6.5-7.5 | 6.5-7.5 | |
| TRANSIT TIME | | | | |
| Stomach | 2-3 hours | N/A | N/A | -- |
| Small intestine | 4-6 hours | Prolonged | Prolonged | (Fischer <i>et al.</i> , 2017) |
| Large intestine (colon) | 41.1- 62.3 hours | 9.5-39.1 hours | N/A | (Hebden <i>et al.</i> , 2000) |
| MICROBIOME | | | | |
| Colon Microbes | 10 ¹¹ -10 ¹² CFU/mL microbes, 1000-1150 specie, Bacteroides and Firmicutes made 90% of microbiome | E. coli increased/ Clostridium sp., Bacteroides decreased | Peptostreptococcus, Enterobacteria, E.coli exceeded/ Bifidobacteria , Bacteroides Reduced | (Zhang and Li, 2014; Zhou and Zhi, 2016) |
| MUCUS PRODUCTION | | | | |
| Colon mucus | N/A | Decreased mucus, Goblet cells depletion | Increased mucus, Goblet cells hypertrophy | (McGuckin <i>et al.</i> , 2008; Vindigni <i>et al.</i> , 2016) |
| INTESTINAL BARRIER | | | | |
| Colon Tight junctions | Tight junctions' integrity and barrier function maintained | Tight junctions widened, loss of barrier function, | Tight Junctions widened, loss of barrier function, | (Sasaki <i>et al.</i> , 1997) |

| | | | | |
|--|--|---|---|--|
| | | Increase permeability across the epithelium | Increase permeability across the epithelium | |
|--|--|---|---|--|

1.3. pH-Dependent DDS for IBD

GIT natural conditions such as pH differences among the GI organs facilitate scientists' targeting of the colon. Currently, several pH-sensitive dosage forms (tablets, capsules) are commercially available for IBD; however, certain limitations hinder their anticipated success.

1.3.1. pH-sensitive polymers

pH-sensitive polymers are used for stimuli-based DDS. When exposed to a specific pH stimulus, the polymers undergo structural changes. The main purpose is to target the colon and to prevent earlier drug release and absorption in the upper GIT region (stomach, small intestine) with additional protection against hostile GI conditions such as microbes, gastric juices, and enzymes (proteases, lipases, trypsin, chymotrypsin, amylases) (Hua *et al.*, 2015). Polymers used for the colon are methacrylic acid, polymethacrylic acid, polyacrylic acid, and their derivatives with an anionic, acidic functional group, which respond to the higher pH of the colon (≥ 6.8) (Maroni *et al.*, 2017; Yoshida *et al.*, 2013), enlisted in Table 1. 2. The most commonly used polymer for colonic drug delivery is Eudragit[®] by Evonik Industries. Chemically, the Eudragit[®] series includes polymethacrylic acid-co-methyl methacrylate copolymers. The ester to carboxylic acid functional group ratio of different Eudragit[®] derivatives vary, which dictates their solubility at the corresponding pH values. The mechanism of drug release from the pH-sensitive polymers involves deprotonation of the carboxylic acid group when exposed to the respective pH threshold (6.8–7.4) and subsequent swelling, followed by polymeric erosion, dissolution, or a combination thereof. It results in the immediate burst release of the drug in the surrounding fluid (Wang and Zhang, 2012).

1.3.2. Conventional pH-sensitive dosage forms

pH-sensitive polymers are incorporated or coated on conventional dosage forms such as tablets, capsules, granules, and pellets to be degraded at the higher pH of the colon while remaining intact at the lower pH of the upper GIT. Dew *et al.* (Dew *et al.*, 1982)

used Eudragit[®] S100 (ES100) for the first time to coat hard gelatin capsules for drug delivery to the colon.

Table 1. 2: pH-sensitive polymers for colon

| Polymer | pH Threshold | References |
|---|--------------|--|
| Eudragit [®] S100 (ES100) | 7 | (Wang and Zhang, 2012; Yoshida <i>et al.</i> , 2013) |
| Eudragit [®] L100 (EL100) | 6 | |
| Eudragit [®] FS 30D (EFS30D) | 6.8 | |
| Eudragit [®] L10055 (EL100-55) | ≥5.5 | |
| Eudragit [®] L30D55 (EL30D-55) | ≥5.5 | |
| Eudragit [®] P4135F (EP4135F) | ≥7.2 | |
| Hydroxy propyl methyl cellulose phthalate (HPMC) 50 | 5 | |
| Hydroxy propyl methyl cellulose phthalate (HPMC) 55 | 5.5 | |
| Shellac | 7.2-7.6 | |
| Hydroxyl propyl methyl cellulose acetate succinate | >6 | |
| Cellulose acetate phthalate | 6 | |

Later, he developed ES100 coated tablets using 5-aminosalicylic acid (5-ASA) as a drug (Dew *et al.*, 1983). Afterward, several other pH-sensitive products entered the market, as listed in Table 1. 3. Although enteric coated dosage forms are used commercially, they are unable to overcome many hurdles in the route to the colon. One issue that reduces the efficiency of pH-sensitive dosage forms is the inter- and intra-individual variability in the pH values of the colon; differences of about 2 pH units have been noted among different people (Fallingborg *et al.*, 1998). Further, the disease severity sometimes determines the extent of pH fall, consequently governing disintegration failure of enteric-coated tablets and capsules, with poor drug release and therapeutic effect (Nugent *et al.*, 2001). Several other factors might influence the disintegration failure of the dosage forms. For example, Ibekwe *et al.* (Ibekwe *et al.*, 2006; Ibekwe *et al.*, 2008) reported intact doses in the feces, indicating the absence of disintegration when administered to healthy volunteers in fasted and fed states. The possible factors for this might be the variable GI fluid volume and composition, ileocecal TT, or feeding status of the person (Ibekwe *et al.*, 2008). The same problems are also associated with the ES100 coated pellets (McConnell *et al.*, 2008).

Furthermore, pH-sensitive conventional dosage forms encounter stability issues of the coating material against bile salts; and the altered mucus viscosity in IBD reduces their cellular uptake (Keely *et al.*, 2011). Most of the time, variable GI conditions direct burst release of the drug from the conventional dosage forms even before it reaches the colon. Moreover, in IBD, heavy diarrhea can cause rapid clearance of the conventional dosage forms before the drug executes its therapeutic action. These factors not only influence the efficacy of macro-sized pH-dependent DDS but also create obstacles for other macro-sized colon DDS such as pro-drugs, time-dependent and microbially triggered systems. To resolve these associated concerns, a combination of ES100 and Eudragit[®] L100 (EL100) has been used to deliver indomethacin in a pellet dosage form that releases the drug only above pH 6.8 (Akhgari *et al.*, 2005). The same Eudragit[®] S/L (ES-L) combination in a mesalamine tablet (Asamax), releases the drug at the ileocecal junction and the colon (Brunner *et al.*, 2006). Similarly, Eudragit[®] L100-55 (EL100-55) has been mixed with ES100 to release the drug at pH 5.5–7 (Khan *et al.*, 1999). Apart from the dual pH-sensitive polymeric combinations, coupling a sustained-release or enzyme-dependent polymer with a pH-sensitive polymer can reduce such issues and aid colon-directed therapy. Furthermore, other novel strategies such as size-reduced pH-sensitive carriers have been used to achieve fruitful results.

Table 1. 3: Commercial products based on pH-dependent DDS for IBD

| Drug | Polymer | pH Threshold | Site of Drug Release | Dosage Form | Brand | Manufacturer |
|-----------------------------|---|--------------|--|---------------------|--|---|
| 5-Aminosalicylic Acid | ES100 | ≥ 7 | Distal part of small intestine & colon | Tablets | Asacol [®] Ipocal [®] Lialda [®] (USA) Mesavant [®] (Europe) | Warner Chilcott Sandoz Cosmo-Pharmaceuticals Cosmo-Pharmaceuticals |
| | EL100 | > 6 | Mid and distal small intestine & colon | Tablets | Claversal [®] Mesasal [®] Calitoflak [®] Rowasa [®] Salofac [®] Mesren [®] Apriso [®] | GSK GSK Dr. Falk Pharma Meda Pharmaceuticals Aspen Pharmacare Teva Pharmaceuticals Salix Pharmaceuticals |
| | Outer coat: combined Eudragit [®] L100 & Eudragit [®] S100 and inner coat: Eudragit [®] S100 | ≥ 7 | Distal part of small intestine & colon | Tablets | Asacol HD [®] | Allergan, Inc., Warner Chilcott (US), LLC |
| Budesonide | EL100-55 | > 5.5 | Proximal intestine & colon | Capsules & granules | Entocort [®] | Prometheus Lab |
| | EL100 & ES100 | 6-7 | Mid-distal colon & intestine | Capsules & granules | Budenofalk [®] | Dr. Falk Pharma |
| Beclomethasone dipropionate | EL100-55 | > 5.5 | Proximal intestine & colon | Tablets | Clipper [®] | Chiesi Pharmaceuticals |
| Sulfasalazine | EL100-55 | > 5.5 | Proximal intestine & colon | Tablets | Colopleon [®] | Sanofi-Aventis |
| | Cellulose acetate phthalate | 6 | Mid and distal small intestine & colon | Tablets | Azulfidine [®] | Pfizer |

1.4. Novel pH-Dependent DDS for IBD

1.4.1. pH-dependent macro-DDS for IBD

Certain modifications to the pH-dependent system can resolve drug delivery issues and render it more workable. The modifications produce a multifunctional system comprising layers of polymers with different properties like pH-sensitive, sustained-

release, or microbially triggered polymers. One initiative was to formulate an *osmotically controlled DDS (OROS-CT)*, by ALZA Corporation, for delivering drugs to the colon. The OROS-CT comprises 5–6 push-pull units inside a hard gelatin capsule. Each unit contains the drug layer and the osmotic push layer, covered by a semi-permeable membrane with an orifice drilled on it. The semi-permeable membrane is further coated with the pH-sensitive enteric polymer. After administration, the gelatin capsule dissolves upon being swallowed, but the enteric coat dissolves only at the higher pH of 7. For UC, the push-pull unit must be designed with a 3–4-hour lag time to prevent earlier release in the small intestine and to target the colon. However, more efforts are required to introduce this dual pH- and time-dependent approach for further use in IBD (Talaie *et al.*, 2013).

Likewise, pH- and time-dependent systems have been combined in a multi-unit system. This scheme involves using a pH-sensitive polymer such as Eudragit[®] FS (EFS) as the outer layer and a delayed-release polymer such as ethyl cellulose, Eudragit[®] RL/RS (ES-RL/RS), or hydroxypropyl methylcellulose as the inner part. It releases the drug at a higher pH gradually (Gupta *et al.*, 2001). In another multi-matrix (MMX) system, the core is composed of the drug-containing lipophilic matrix, which is covered by the hydrophilic matrix. Then, the entire matrix is protected under a pH-sensitive film, which dissolves upon reaching the colon; the fluid moves inside the core and forms a viscous gel that diffuses the drug outside. 5-ASA and budesonide are used in the MMX system (McConnell *et al.*, 2009).

Although the novel pH-dependent macro-DDS for IBD provide better strategies for targeting the colon, further investigations are still required to prove their effectiveness over the conventional dosage forms. Second, the diarrhea-mediated clearance of the macro-dosage forms in IBD should be addressed. All these strategies are summarized in Table 1.4.

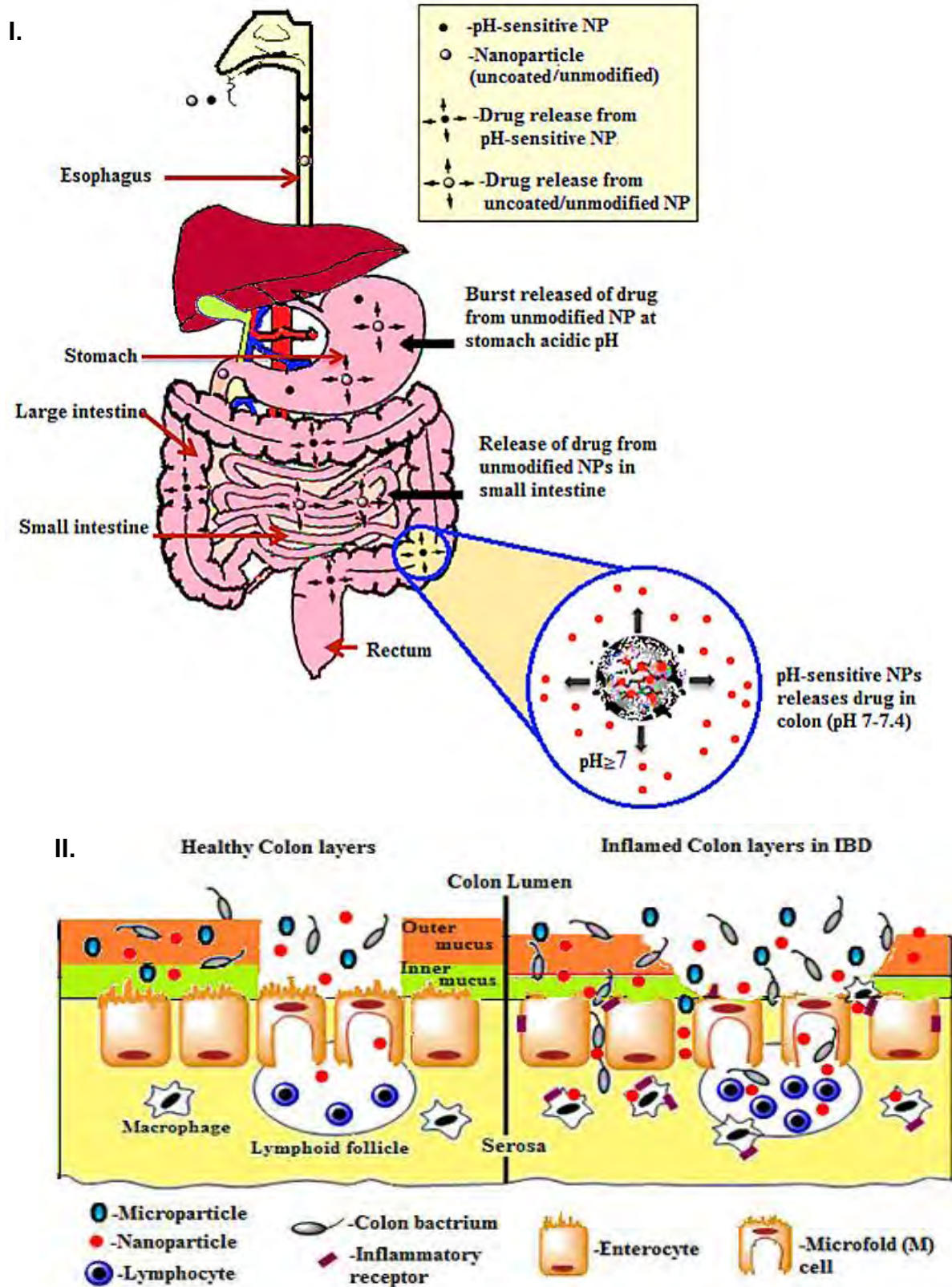
Table 1. 4: Novel pH-dependent macro drug delivery systems for IBD

| Main Strategy | Additional strategy | Novel DDS for IBD | Drug(s) | Inventor/ References |
|---------------------|------------------------------|---|-------------------------------------|---|
| pH-dependent system | ----- | Muti-matrix system TM (Lialda) | 5-ASA Budesonide | Shire Pharmaceuticals Inc., Wayne, Pennsylvania, USA |
| pH-dependent system | Microbially triggered system | TARGIT | Budesonide | West Pharmaceutical Services Drug Delivery & Clinical Research Centre Ltd., Nottingham, UK (Watts and Smith, 2005) |
| | Microbially triggered system | CODES TM | 5-ASA Budesonide | Yamanouchi Pharmaceuticals Co. Ltd., Japan (Masataka Katsuma <i>et al.</i> , 2004; Katsuma <i>et al.</i> , 2002; Varshosaz <i>et al.</i> , 2011) |
| pH-dependent system | Time dependent system | OROS-CT | Aminosalicylates Corticosteroids | Alza Corp., Palo Alto, California, USA |
| | Time dependent system | Entocort EC | Budesonide | AstraZeneca, Sodertalje, Sweden |
| | Time dependent system | Multi-unit system | 5-ASA | (Gupta <i>et al.</i> , 2001) |

1.4.2. pH-dependent micro/nanoparticulate-mediated DDS for IBD

As mentioned earlier, macro-dosage forms for colon-directed therapy face many obstacles; one such issue is reduced retention at the inflamed site. Recently, nanotechnology applied to the field of drug delivery, discovery, and development yielded *nanopharmaceuticals* or *nanoparticle-mediated DDS* (Jain, 2012). The concerns associated with macro-DDS can be resolved by reducing the size of the drug molecules and their *carriers to the particulate level*. Due to their particular nature and properties, the size reduction enhances the residence time and local action of the drug in the colon (Collnot *et al.*, 2012). To acquire the benefits of both pH-dependent and particulate-mediated DDS and to overcome the problems faced by the application of either strategy alone, the pH-dependent approach has been applied to micro- and nanoparticulate-mediated DDS (nanopharmaceuticals) for delivering drugs to the colon. pH-sensitive nanoparticles can deliver the drug to the colon under specific colon

pH stimuli and localized under the enhanced epithelial permeation and retention effect (eEPR), which overcomes colon drug delivery issues Figure 1. 2.



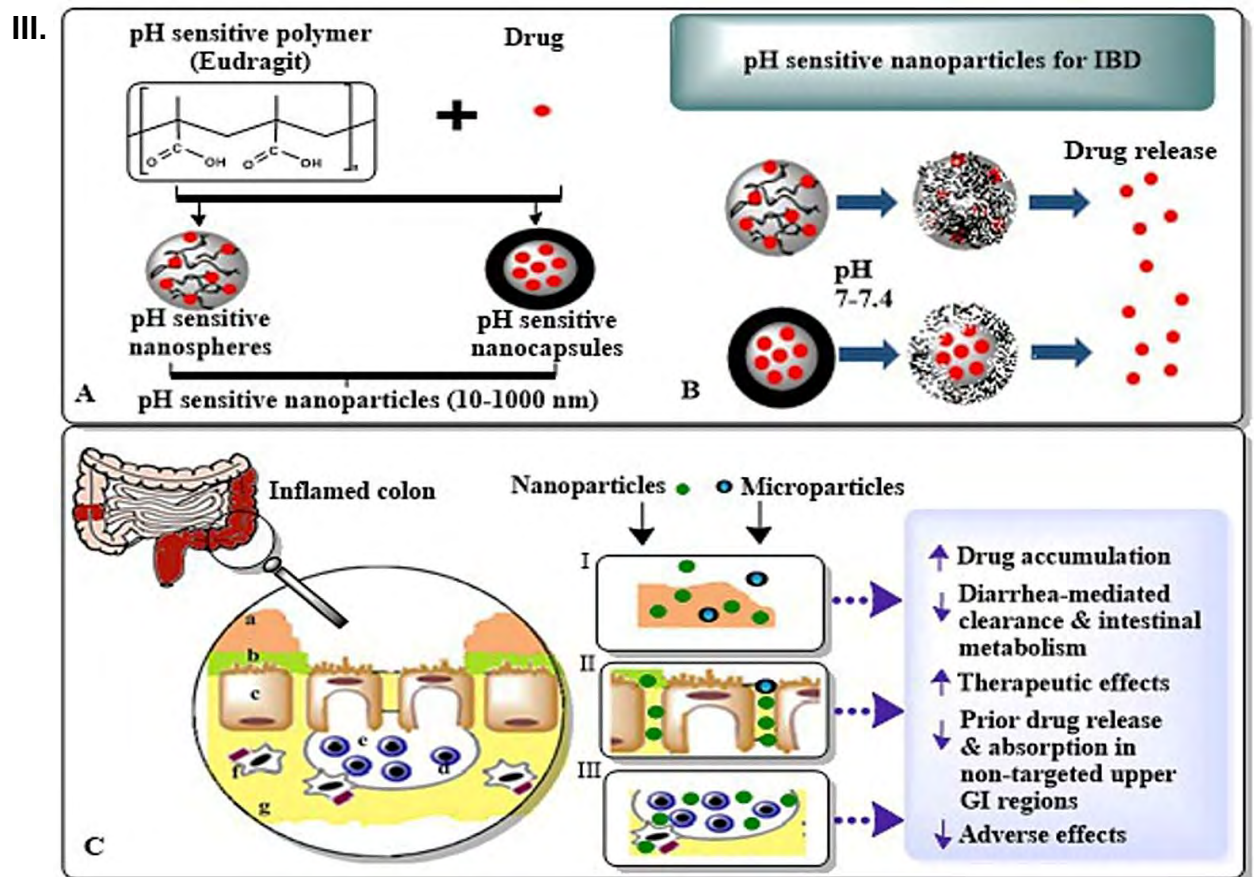


Figure 1. 2: pH dependent colon-specific targeting at organ and tissue levels; I. pH-sensitive nanoparticles have colon-specific drug release, while unmodified nanoparticles have burst release of drug at stomach pH; II. Pathophysiological alterations in IBD include heavy mucus, epithelial membrane disruptions, and immune cells infiltration. Resultant eEPR effect facilitates nanoparticles accumulation; III: A. pH-sensitive nanocarriers for IBD, B. Different types of pH-sensitive nanocarriers disintegrated at the colon pH of 7, C. Pathological state in inflammation favors nanoparticle-mediated drug delivery system with enhanced mucoadhesion, penetration, and uptake by immune cells (a: Outer mucus layer, b: inner mucus layer, c: enterocytes, d: lymphocyte, e: lymphocyte follicle, f: macrophage, g: serosa) (Zeeshan *et al.*, 2019a)

1.4.2.1. pH-dependent microparticles

Microparticles are of micron size range, mostly 10–300 μm in diameter, and consist of the drug and the polymeric carriers. In IBD, particles $> 200 \mu\text{m}$ are influenced by diarrhea and are rapidly cleared off (Viscido *et al.*, 2014), and internalization by the immune cells becomes difficult. The reasons behind the efficacy of particles $> 200 \mu\text{m}$ are reduced small intestinal absorption and slower movement across the colon, which allows the drug to act for a sufficient period (Collnot *et al.*, 2012). Microparticles

synthesized with a lower size range show better targeting and accumulation, as particles < 5 μm are taken up by microfold cells (M-cells) of Peyer's patch in the colon (Nidhi *et al.*, 2016). Dexamethasone-loaded polylactic acid (PLA) microspheres, which are <4 μm , have been found in the lymphoid tissue of the colon with significant tissue accumulation after 12 hours. The results have indicated mucosal healing with no elevation of serum dexamethasone levels (Nakase *et al.*, 2000). Microparticles provide a localized concentration of the drug in the colon while minimizing systemic absorption.

Microparticles comprising pH-sensitive polymers have been investigated for more specific targeting in IBD. Badhana *et al.* (Badhana *et al.*, 2013) prepared ES100 coated chitosan microspheres with 61–90 μm particle size for treating UC; the microparticles showed pH-dependent drug release, with maximum release at pH 7.4, which corresponds to the colon pH (Badhana *et al.*, 2013). Another study supported ES100 coated chitosan microspheres loaded with 5-ASA and camylofin dihydrochloride separately to treat UC. In vitro experiments showed that a larger amount of drug was released in the presence of rat cecal matter, and in vivo studies showed enhanced mucoadhesion and that a major portion of the drug was released after 9 hours at the colon site (Dubey *et al.*, 2010).

Occasionally, a pH-sensitive coating reduces the size of the particles. In this regard, Crcarevska *et al.* (Crcarevska *et al.*, (2008)) prepared chitosan-calcium-alginate (Ch-Ca-Al) microspheres containing budesonide, and coated them with the pH-sensitive ES100 polymer. The pH-sensitive polymer coating reduced the particle size to 4 μm as compared to the 5.3 μm of the uncoated microspheres. The reason for this was the rapid evaporation of the organic solvent and the simultaneous contraction of chitosan chains during the coating process. The pH-sensitive Ch-Ca-Al microspheres released the appropriate amount of drug at pH 7.4, whereas minimal drug was released at pH 2 and 6.8. For in vivo studies, the microspheres were administered to a 2,4,6-trinitrobenzenesulfonic acid (TNBS)-induced rat colitis model at a dose of 167 $\mu\text{g}/\text{kg}$ once daily for 5 consecutive days; inflammation severity was markedly diminished, with promising outcomes for clinical activity score and colon body weight, and the treatment proved to be more effective in comparison to the uncoated microspheres and budesonide alone (Crcarevska *et al.*, 2009; Crcarevska *et al.*, (2008)).

Contrary to this finding, the coating might increase the particle size. Microspheres formed by chitosan-succinyl-prednisolone conjugate was 1.3 μm in size; coating them with EL100 increased their diameter up to $31.8 \pm 11 \mu\text{m}$. Additionally, the drug loading rate was lowered, possibly due to ester hydrolysis during synthesis. On administration to TNBS-induced rat colitis models, the EL100-coated chitosan-succinyl microspheres had the greatest efficacy and the least toxicity in comparison to the uncoated microspheres and prednisolone alone (Onishi *et al.*, 2008).

The pH-sensitive approach also facilitates the delivery of herbal remedies, which have multiple therapeutic advantages but face pharmacokinetics issues. Curcumin is an herbal anti-inflammatory agent and can cure IBD. Curcumin-loaded ES100 coated chitosan microspheres have been developed for IBD. Release studies demonstrated a controlled release pattern at pH 7.4 and the absence of burst release of the drug in different buffer media. In vivo administration to acetic acid-induced rat colitis model showed increased localization in the colon, whereas a negligible drug amount was present in the stomach and small intestine, along with effective suppression of inflammation (Sareen *et al.*, 2016). Similarly, the development of ES100 coated thiolated chitosan-alginate microparticles co-loaded with 5-ASA, and curcumin for treating IBD further improved colon site retention, as the thiolation of chitosan improved its mucoadhesive properties (Roldo *et al.*, 2004). In vitro drug release studies indicated drug release only above pH 7 in a controlled manner. Ex vivo studies confirmed mucoadhesion to the mucosal layer of the colon, and in vivo administration to a TNBS-induced rat colitis model showed therapeutic effectiveness. This investigation elucidated that the mucoadhesive thiolated chitosan and pH-sensitive ES100 are compatible and that their combination proved advantageous in colon-specific targeting of drugs for IBD (Duan *et al.*, 2016).

Lamprecht *et al.* prepared 5-fluorouracil (5-FU) (Lamprecht *et al.*, 2003) and tacrolimus (Lamprecht *et al.*, 2004) microparticles by using the newer pH-sensitive Eudragit[®] P4135F (EP4135F) polymer. EP4135F prevented the release of the drug in the terminal ileum and achieved more specificity in colon targeting. Drug leakage was reduced to <10% at pH 6.8, while a greater amount of the drug was released at pH 7.4 within 30 min (Lamprecht *et al.*, 2004).

Furthermore, lower-molecular weight heparin (LMWH) has been proven efficacious in IBD when administered parentally (Dotan *et al.*, 2001). However, the use of heparin is limited due to the severe adverse effects (Papa *et al.*, 2000). To circumvent the issue, a pH-sensitive local targeting strategy through oral administration was adopted. Enoxaparin, an LMWH, was loaded in pH-sensitive microspheres using EP4135F. Assessment of inflammation through the colon to body weight ratio, myeloperoxidase activity, and alkaline phosphatase showed promising results. Its activity was parallel to the rectally administered LMWH and better than that of subcutaneous injection. The enteric coating prevented LMWH absorption in the small intestine and showed low systemic bioavailability (<5%), which diminished the chances of adverse effects (Pellequer. Yann *et al.*, 2007).

Recently, dexamethasone-loaded pH-sensitive microcrystals were prepared using a layer-by-layer technique comprising multiple layers of chitosan and alginate and finally coated with ES100. The pH-sensitive microcrystals exhibited colon-targeting properties with pH-mediated sustained drug release and considerable amelioration of inflammation in a dextran sodium sulfate (DSS)-induced mouse colitis model (Oshi *et al.*, 2018).

Apart from the polymeric blend, proteinaceous elements have been assimilated in pH-dependent micro-DDS. One such innovation was the synthesis of ES100 coated egg albumin microspheres to deliver mesalamine (5-ASA) to the colon. Egg albumin contributes sustained-release properties to the system. An In vitro release study showed negligible amounts of drug released at pH 1.2, up to 26% at pH 6.8, and a large amount at pH 7.4. Thus, pH-sensitive egg albumin microparticles can achieve colon targeting in IBD (Namdev and Patidar, 2016). All these research findings are mentioned in Table 1. 5.

1.4.2.2. pH-dependent nanoparticles (NPs)

With one-step-further advancements in technology, the development of NPs, (10–1000 nm) have shown remarkable achievement in targeted drug delivery. As mentioned earlier, NPs specifically target colon inflamed tissue with increased drug localization and reduced systemic adverse effects at a much lower dose compared to conventional therapy (Xiao and Merlin, 2012; Collnot *et al.*, 2012). NPs can effectively target and

reside at the inflamed colon tissues through multiple ways. The NPs can passively accumulate at the inflamed tissues through eEPR effect (Xiao and Merlin, 2012). The eEPR is observed in inflamed colon tissues due to disrupted epithelial layer integrity because of inflammation, leading to epithelial tight junction re-arrangement and broadening, which forms gaps between the enterocytes. It leads to the loss of epithelial barrier function and increased permeability of small-sized particles across the epithelial membrane (Chen *et al.*, 2017). Moreover, particles < 500 nm are readily taken up by enterocytes and immune cells such as neutrophils, macrophages, and M-cells through transcytosis (Meissner *et al.*, 2006). The immunopathological changes in IBD and NP retention through the eEPR are diagrammatically illustrated in Figure 1. 2. The enhanced colonic localization of NPs reduced diarrhea-mediated clearance, improved the therapeutic effects of the drug, minimized the required drug dose, and decreased the systemic adverse effects. In addition, the micro- and nanoparticles ruled out the need for frequent dosing rules, which increased patient compliance.

Furthermore, the induction of surface charge through charged polymers or ligand attachment on the surface can improve NP-mediated drug delivery for receptor-mediated active targeting. Surface charge facilitated NP bioadhesion and mucus penetration in IBD. In this regard, NPs comprising pH-sensitive polymers have an anionic surface charge, which promotes electrostatic interaction and adhesion to positively charged proteins such as eosinophils and transferrin, and facilitates internalization at the inflamed site (Tirosh *et al.*, 2009; Hua *et al.*, 2015). Furthermore, anionic NPs can cross a thick mucus barrier at the inflamed colon tissues through less interference with mucosal content and reach the internal epithelial layer of the colon (Hua *et al.*, 2015). By contrast, cationic and neutral particles cannot cross the mucus barrier in inflamed conditions (Jubeh *et al.*, 2004). Furthermore, NPs tailored with a pH-sensitive strategy protect the drug against harsh GIT conditions and prevent earlier drug release at acidic pH while discharging the drug only at the colon or ileocecal junction, where the pH corresponds to 6.8–7 as illustrated in Figure 1. 2. In this scenario, researchers developed ES100 coated prednisolone NPs to investigate the benefits of pH-sensitive polymers at the nanoparticulate level. In vitro analysis showed pH-dependent drug release after a lag time of 4.5 hours, which corresponds to the time required to reach the colon (Kshirsagar *et al.*, 2012). Subsequently, a combination of

drugs including celecoxib, a non-steroidal anti-inflammatory drug, and curcumin, an anti-inflammatory agent, was used for their synergistic effects and contained within a pH-sensitive nanocarrier, ES100. The celecoxib–curcumin-loaded pH-sensitive NPs had superior therapeutic effects in the rat colitis model compared to the single drug–NPs and drug suspensions (Gugulothu *et al.*, 2014).

Many forms of pH-sensitive nanostructures have been developed, including simple spherical polymeric matrix (simple nanospheres), hybrid nanospheres, nanocapsules, hybrid nanocapsules enclosing cores of other material, nanofibers, and nanolipids, as depicted in Figure 1. 3.

Likewise, Makholf *et al.* (Makhlof *et al.*, 2009) developed pH-sensitive hybrid nanospheres by incorporating a sustained-release polymer, poly lactic-co-glycolic acid (PLGA). The loaded drug, budesonide, had good entrapment efficiency of >85% and was released only at pH 7.4 with minimal release at pH 6.8 and 1.2 (20% and 28%, respectively). pH-sensitive NPs face the prospect of burst release of a drug due to a larger surface area, which was overcome through the integration of PLGA, which exhibited a sustained-release pattern. In vivo studies in the TNBS-induced rat colitis model demonstrated that pH-sensitive nanospheres exhibited higher drug localization in the colon and reduced systemic levels when compared to the unmodified nanospheres. Further, strong adhesion of pH-sensitive nanospheres at the inflamed tissues clarified the role of particulate-mediated targeting, with increased retention time and elevated therapeutic efficacy; the effects persisted even after 7 days of the last administered dose (Makhlof *et al.*, 2009). Similarly, curcumin loaded ES100/PLGA nanospheres were developed to resolve curcumin pharmacokinetic issues and to achieve local drug accumulation in the colon for IBD therapy. These nanospheres showed better permeation across colorectal adenocarcinoma (Caco-2) cell monolayers as compared to the free curcumin suspension. In vivo administration to a DSS-induced rat colitis model yielded promising results in terms of suppression of inflammation by decreasing tumor necrosis factor- α (TNF- α) levels and neutrophil infiltration (Beloqui *et al.*, 2014). Therefore, a matrix combination of PLGA and ES100 proved suitable while designing pH-sensitive sustained-release nanospheres. Likewise, cyclosporin A was loaded in dual-function EFS30D/PLGA nanospheres, which released the drug at pH 7.4 in a sustained manner. The improved morphological scores, histopathological

scores, and cytokine profiles in the murine model suggested the potential for use in UC therapy (Naeem *et al.*, 2018a).

Another approach is combining pH-sensitive and time-dependent systems at the nanoscale level for treating colitis. Budesonide was loaded in polymeric nanocarriers comprising EFS30D (pH-sensitive polymer) and Eudragit® RS100 (a time-dependent, controlled-release polymer). These hybrid nanospheres prevented burst release of budesonide in acidic pH while releasing it in a sustained manner at colonic pH. In vivo administration to a DSS-induced rat colitis model showed therapeutic efficacy in the inflamed colon tissues when measured through different clinical indices. The dual strategy had better outcomes than the single pH-sensitive nanospheres (Naeem *et al.*, 2015b).

Further investigations have described the effect of a pH-sensitive polymeric coating on NP cores (nanocapsule) to achieve specific targeting in IBD. One such effort involved the development of budesonide loaded PLGA NPs with an ES100 outer coating. The ES100 coat dissolves when encountering the threshold pH, while the inner PLGA core releases the drug in a sustained manner for a prolonged duration. The ES100 coated PLGA NPs showed maximum drug release at pH 7.4, with minimal release at acidic pH. In comparison, uncoated PLGA NPs failed to withstand the acidic pH. The In vivo effects of the coated PLGA NPs proved much better in reducing colitis severity when compared to the uncoated PLGA NPs and free drug solution in the mouse colitis model (Ali *et al.*, 2014). Similarly, hydrophilic Glycyrrhizic acid drug was encapsulated in the PLGA core, coated with ES100 coat. The formed nanoparticles had sustained release of the drug, with retardation of drug dumping at pH 1.2; and proved to be efficacious in mitigating DSS induced colitis (Zeeshan *et al.*, 2019b).

In another attempt, chitosan was incorporated in the core of pH-sensitive NPs. 5-ASA-loaded chitosan NPs were prepared and then coated with pH-sensitive ES100 for treating UC. In vitro studies revealed drug release at colon pH values only (Mongia *et al.*, 2014).

An innovation to the system is the use of a newly derived, pH-sensitive polymer from the Eudragit® series that can target the drug to the colon effectively. Under this approach, Meissner *et al.* (Meissner *et al.*, 2006) developed tacrolimus-loaded NPs by

using two polymers separately, namely, PLGA and a newer pH-sensitive EP4135F polymer, to investigate the effect of particle-mediated targeting versus pH-mediated targeting, respectively. On administration to a DSS-induced mouse colitis model, both types of NPs exhibited the same effects in terms of induction and maintenance of remission in IBD. Both reduced the nephrotoxic adverse effects when compared to the oral-free drug solution. There was greater PLGA NP accumulation in the inflamed tissues; however, there was disassociation at lower pH in the upper GIT. However, the pH-sensitive NPs released the drug only at the higher pH of the colon, which might be the reason behind the slightly less nephrotoxic effects compared to PLGA NPs.

In another experiment, a natural product, silybin, was loaded in ES-RL PO polymer (a rate-controlling polymer) to formulate NPs. Subsequently, the new pH sensitive ES-FS30D polymer was used to coat the inside of the NPs to target the colon for treating UC. In vitro analysis showed major drug release at pH 7.4. The macroscopic and histopathological evaluation indicated improvement in the disease condition, but overall these effects could not surpass the effects of Dexamethasone (Dexa) (Varshosaz *et al.*, 2015).

Furthermore, pH-sensitive nanofibers proved effective in targeting the inflamed tissues of the colon. In this regard, Xu *et al.* (Xu *et al.*, 2013) prepared budesonide-loaded ES100/ethyl cellulose nanofibers. The in vitro drug release profile of the nanofibers was parallel to that of spherical NPs, with the maximum amount of drug released at pH 7.4.

Moreover, pH-sensitive liposomes were designed by coating cationic lipids with anionic ES100, which exhibited significant drug release at pH 7.8 while retarding release at pH 1.4 and 6.3. However, the inclusion of bile salts in the release media reduced the integrity of the pH-sensitive coating, which served as a challenge for the pH-dependent liposomal system and needs to be addressed (Barea *et al.*, 2010).

Recently, surface charge-reversal pH-sensitive lipid NPs were fabricated, where cationic polyethyleneimine (PEI) lipid-core NPs were covered under an anionic ES100 coating. The pH-sensitive lipid NPs had -30 mV zeta potential, which released a major portion of the drug, budesonide, at pH 7.4. The in vivo experiments demonstrated charge reversal characteristics after reaching the colon and enhanced mucoadhesion by

the uncovered cationic PEI–lipid core NPs (zeta potential: +23 mV), and significantly ameliorated DSS-induced colitis in mice (Naeem *et al.*, 2018b).

Another novel advancement in the pH-responsive approach was the formation of NaYF₄:Yb³⁺/Er³⁺ silicon dioxide (SiO₂) nanocomposites that were further engraved with a pH-sensitive polymethacrylic acid polymer (PMAA) to yield NaYF₄:Yb³⁺/Er³⁺-SiO₂-PMAA nanocomposites. 5-ASA was the loaded drug for treating IBD. In vitro drug release studies demonstrated that the major portion of the drug was released at pH 7.4 in the simulated colonic fluid, along with a smaller portion of drug releases at pH 1.2 (Tian *et al.*, 2016).

In the search to obtain better colon-specific DDS, Lamprecht *et al.* (Lamprecht *et al.*, 2005) innovated the particulate systems by fabricating *NP-in-pH-sensitive microsphere (NP-MS)* formulation; tacrolimus-loaded PLGA NPs were entrapped inside EP4135F microspheres. The structure is illustrated in Figure 1. 3. The NP-MS strictly followed pH-dependent drug release at pH 7.4 only. In vivo studies on an animal colitis model indicated that the NP-MS had statistically significant therapeutic effects in comparison to the free drug solution, tacrolimus NPs, and tacrolimus microspheres when measured through the colon–body weight ratio and myeloperoxidase activity. The low systemic absorption of the fluorescent dye coumarin-6 demonstrated the lower systemic bioavailability of tacrolimus (Lamprecht *et al.*, 2005).

Likewise, rifaximin was loaded in dual pH- and redox-sensitive NPs-in-microcomposites (NP-MC). With this approach, redox-sensitive, mucoadhesive chitosan NPs were formulated first. Then, the NPs were encapsulated inside pH-sensitive microcomposites using hydroxypropyl methylcellulose acetate succinate as a pH-sensitive polymer. The NP-MC were resistant to drug release at acidic pH and released the drug at pH 6.8 and in response to the oxidative radicals, hydrogen peroxide (H₂O₂). H₂O₂ is an oxidative species; its levels are significantly elevated in inflammation. In comparison to pH-sensitive microcomposite alone, the addition of the redox-sensitive polymer in the NP-MC provided better control over the burst release of the drug. The NP-MC could serve as a better alternative to colon-specific drug delivery in IBD but requires further in vivo investigations (Bertoni *et al.*, 2018). All the research findings are summarized in Table 1. 5.

pH-sensitive polymeric combinations or hybrid combinations reduce problems such as burst release of the drug and stability issues of the coating material. However, inter- and intra-individual variability in pH, microbiome, TT, immune regulation, and colon fluids still threaten the efficiency of pH-dependent systems and require detailed human investigations. The sum-up of advantages and drawbacks of the pH-dependent strategies is illustrated in Figure 1. 4.

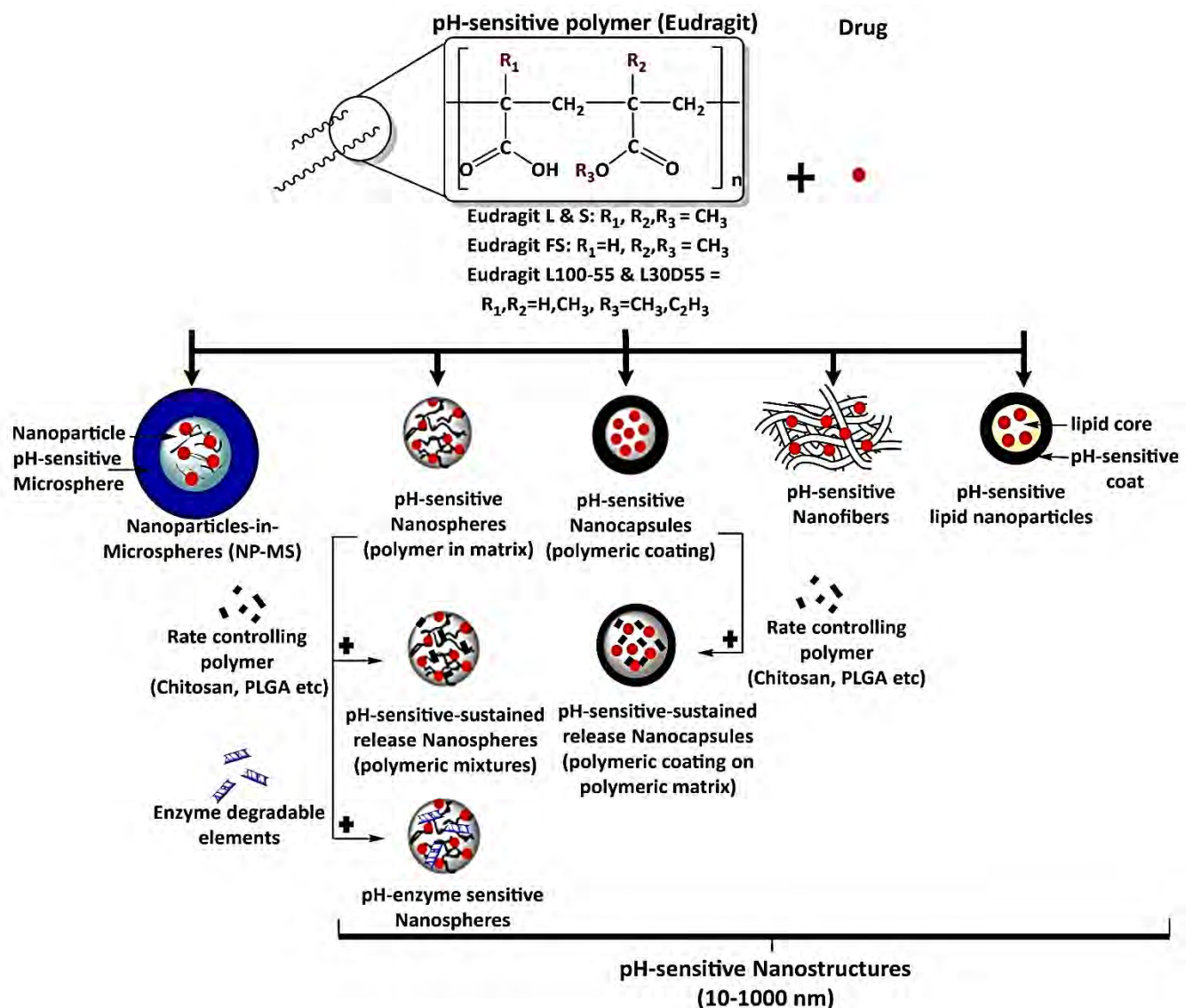


Figure 1. 3: Classification of pH-sensitive nanostructures for IBD (Zeeshan *et al.*, 2019a)

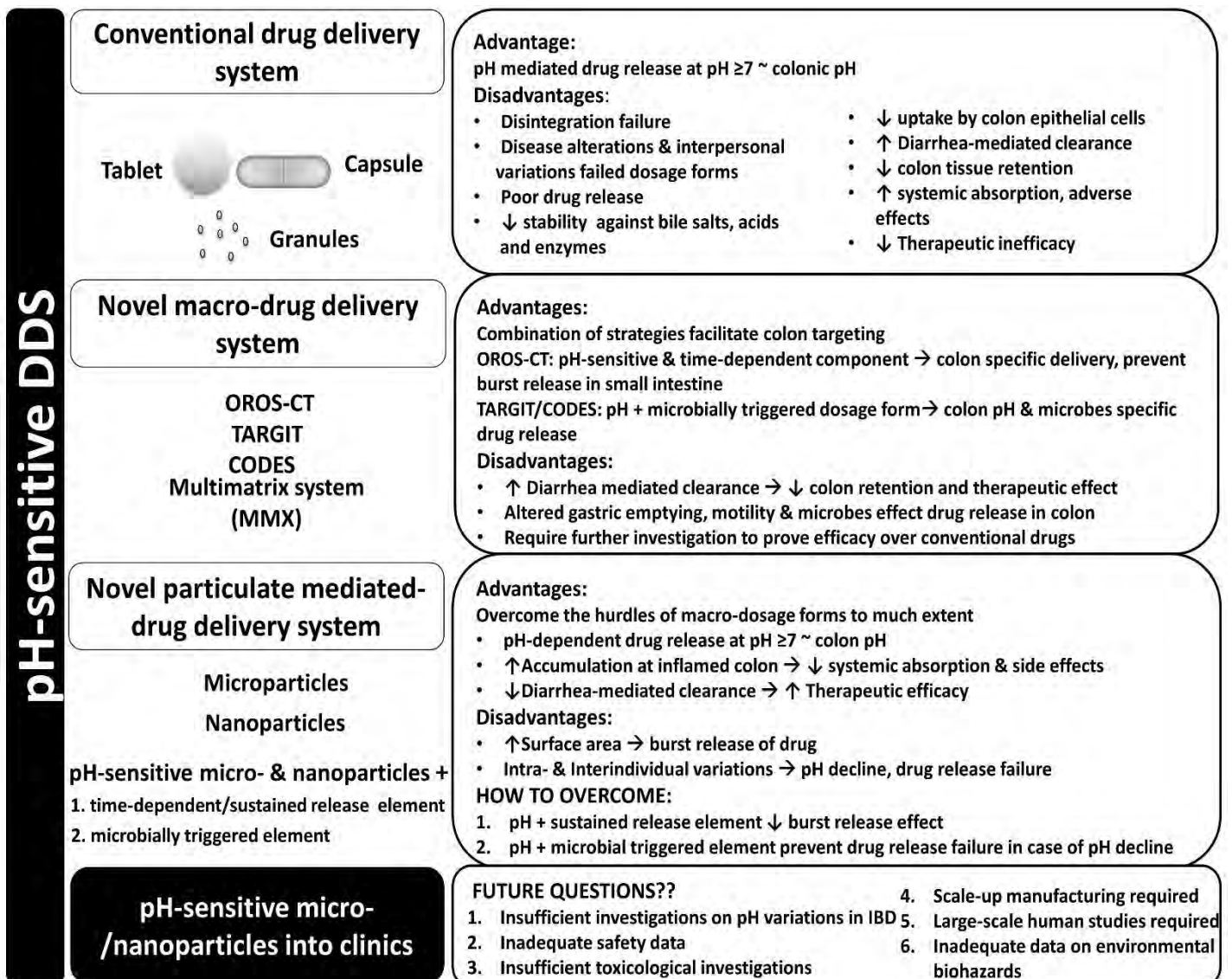


Figure 1. 4: Advantages and disadvantages of conventional and novel pH-dependent drug delivery systems (Zeeshan *et al.*, 2019a)

Table 1. 5: pH-dependent microparticles and nanoparticles for the drug targeting in IBD

| DRUG | pH-SENSITIVE POLYMER | ADJACENT POLYMER/MATERIAL | SIZE | RAT COLITIS MODEL/EFFECT | REFERENCES |
|------------------------------------|----------------------|---|------------------------------|------------------------------|--|
| pH-DEPENDENT MICROPARTICLES | | | | | |
| 5-Aminosalicylic acid (5-ASA) | ES100 | Chitosan | 61-90 μm | Only In vitro | (Badhana <i>et al.</i> , 2013) |
| | ES100 | Egg albumin | 75- 107 μm | In vitro only | (Namdev and Patidar, 2016) |
| 5-ASA + Curcumin | ES100 | Thiolated chitosan-alginate | 35.3 \pm 3.6 μm | TNBS | (Duan <i>et al.</i> , 2016) |
| 5-ASA + Camylofine | ES100 | Chitosan | 21-27 μm | TNBS | (Dubey <i>et al.</i> , 2010) |
| Budesonide | ES100 | Chitosan | 4 μm | TNBS | (Crcarevska <i>et al.</i> , (2008); Crcarevska <i>et al.</i> , 2009) |
| | -- | Chitosan | 5.3 μm | TNBS | (Crcarevska <i>et al.</i> , (2008); Crcarevska <i>et al.</i> , 2009) |
| Curcumin | ES100 | Chitosan | 36-129 μm | Acetic acid | (Sareen <i>et al.</i> , 2016) |
| Enoxaparin (LMWH) | EP4135F | -- | 120-133 μm | TNBS, OXA | (Pellequer. Yann <i>et al.</i> , 2007) |
| 5-Fluorouracil | EP4135F | ES-RS100 | 123-135 μm | In vitro (at pH 6.8 and 7.4) | (Lamprecht <i>et al.</i> , 2003) |
| Prednisolone | EL100 | Chitosan | 31.8 \pm 11 μm | TNBS | (Onishi <i>et al.</i> , 2008) |
| | -- | Chitosan | 1.3 μm | TNBS | (Onishi <i>et al.</i> , 2008) |
| Tacrolimus | EP4135F | -- | 113-157 μm | In vitro (at pH 6.8 and 7.4) | (Lamprecht <i>et al.</i> , 2004) |
| pH-DEPENDENT MICROCRYSTALS | | | | | |
| Dexamethasone | ES100/alginate | Chitosan | 2-2.5 μm | DSS | (Oshi <i>et al.</i> , 2018) |
| pH-DEPENDENT NANOPARTICLES | | | | | |
| 5-ASA | ES100 | Chitosan | 501nm | In vitro only | (Mongia <i>et al.</i> , 2014) |
| | Polymethacrylic acid | NaYF ₄ :Yb ³⁺ /Er ³⁺ -SiO ₂ | 324 nm | In vitro only | (Tian <i>et al.</i> , 2016) |
| Budesonide | ES100 (mixture) | PLGA | 260-290 nm | TNBS | (Makhlof <i>et al.</i> , 2009) |
| | ES100 (coating) | PLGA | 240 nm | TNBS, DSS, OXA | (Ali <i>et al.</i> , 2014) |
| | ES100 | -- | 191 nm | TNBS | (Nacem <i>et al.</i> , 2015a) |
| | ES100 | Azo-polyurethane | 195 nm | TNBS | (Nacem <i>et al.</i> , 2015a) |
| | ES100 | Ethylcellulose | 190 nm | In vitro only | (Xu <i>et al.</i> , 2013) |
| | ES-FS30D | ES-RS100 | 251 nm | DSS | (Nacem <i>et al.</i> , 2015b) |
| Curcumin | ES100 | PLGA | 166 nm | Caco-2 cells, DSS | (Beloqui <i>et al.</i> , 2014) |
| Curcumin + Celecoxib | ES100 | -- | 111 nm | TNBS | (Gugulothu <i>et al.</i> , 2014) |
| Coumarin-6 (model drug) | ES100 | -- | 214 nm | TNBS | (Nacem <i>et al.</i> , 2014) |
| | ES100 | Azo-polyurethane | 244 nm | TNBS | (Nacem <i>et al.</i> , 2014) |

| | | | | | |
|---|---|--|--|---|------------------------------------|
| Cyclosporin A | EFS30D | PLGA | 200-260 nm | DSS | (Naeem <i>et al.</i> , 2018a) |
| Prednisolone | ES100 | -- | 567.87 nm | Rat plasma study | (Kshirsagar <i>et al.</i> , 2012) |
| Silybin | ES-FS30D | ES-RL PO | 109±6 nm | Acetic acid | (Varshosaz <i>et al.</i> , 2015) |
| Tacrolimus | EP4135F | -- | 469 nm | DSS | (Meissner <i>et al.</i> , 2006) |
| Glycyrrhizic Acid | ES100 | PLGA | 203.57 ± 11.5 nm | DSS | (Zeeshan <i>et al.</i> , 2019b) |
| NANOPARTICLE-in-pH-SENSITIVE MICROSPHERE (NP-MS) | | | | | |
| Tacrolimus | EP4135F (microsphere) | PLGA (nanoparticle) | 238-256 nm (NP) 30-60 µm (MS) | TNBS | (Lamprecht <i>et al.</i> , 2005) |
| Rifaximin | Hydroxypropyl methylcellulose acetate succinate (microcomposite) | Oxidation-sensitive dextran/chitosan (nanoparticle) | 50-200 nm (NP) 53±3 µm (MS) | C2BBe1/HT29-MTX. Cell monolayer | (Bertoni <i>et al.</i> , 2018) |
| pH-SENSITIVE NANOMICELLES | | | | | |
| Celecoxib | Succinic anhydride | Inulin-Vitamin E (INVITE) | 13-22 nm | Caco-2 cells Cross cellular monolayer | (Mandracchia <i>et al.</i> , 2018) |
| pH-SENSITIVE LIPIDIC NANOPARTICLES | | | | | |
| Budesonide | ES100 | Phospholipon 90 G, Polyethyleneimine | 302 nm | DSS | (Naeem <i>et al.</i> , 2018b) |
| pH-SENSITIVE MICROENCAPSULATED NANOGELS | | | | | |
| TNF-α siRNA | Trypsin- Poly(methacrylic acid-co-vinyl- pyrrolidone) (P[MAA-co-NVP]) hydrogel | polycationic 2- (diethylamino)ethyl methacrylate (DEAEMA) nanogel | 110-122 nm (nanogel) <30 µm (microgel) | Gene knockdown of TNF-α in macrophages | (Knipe <i>et al.</i> , 2016) |

1.5. Dual microbial enzyme sensitive and pH sensitive nanocarriers for IBD

Colon microenvironment is suitable for the growth of microorganisms that constitutes the natural microbiome. The microbiome has various beneficial bacteria that secrete numerous enzymes and peptidases to carry out multiple metabolic reactions. Therefore, the biomaterial degraded by microbiome enzymes had been exploited for colon drug delivery purpose. Coupling of pH sensitive and microbial enzyme sensitive approach is a better choice to override the obstacles faced by either strategy alone.

TARGIT technology is a novel approach that combined pH-dependent and microbially triggered systems. It was comprised of a pH sensitive EL/S (3:1) coating on injection-molded starch capsules. Upon administration, 73 of 84 *TARGIT* capsules were found in the colon and terminal ileum (Table 1.4). It is currently under phase II clinical trials for delivering budesonide in IBD (Watts and Smith, 2005). The potential threats are the versatile colonic environment and pathophysiology of IBD. Likewise, CODES™ was developed using pH-dependent and microbially triggered polymers. CODES™ have an inner core containing an active site for lactulose, surrounded by an acid-sensitive layer of Eudragit® E and further encapsulated by Eudragit® L. Eudragit® L dissociates upon contact with the higher pH colonic fluid. Subsequently, the colon microbes degrade the lactulose into organic acid, which decreases the surrounding pH, disintegrating Eudragit® E and releasing the encapsulated drug (Masataka Katsuma *et al.*, 2004). CODES™ is used to deliver 5-ASA (Katsuma *et al.*, 2002) and budesonide (Varshosaz *et al.*, 2011) for colon-specific delivery and can be further refined for use in IBD (Table 1.4).

A combination of approaches facilitates targeted drug delivery to the colon; a hybrid pH- and enzyme-sensitive approach at a nanoparticulate system had been developed, using the pH-sensitive ES100 and enzyme-sensitive azo-polyurethane polymers. Coumarin-6 was loaded as a model drug into plain ES100 and ES100-azo-polyurethane (ES100-azopu) nanospheres. The plain ES100 nanospheres exhibited burst release of the drug at pH 7.4 in a rat colitis model. In comparison, the ES100-azopu nanospheres had more controlled drug release and showed a sustained-release pattern with 5.5 times greater accumulation in the inflamed colon tissues as compared to the plain ES100 nanospheres (Naeem *et al.*, 2014) (Table 1.5). Likewise, budesonide was delivered to inflamed colon tissues through ES100-azopu nanospheres. In vivo investigations

revealed a greater accumulation of the combined nanospheres in the inflamed tissues as compared to simple ES100 nanospheres. It clarifies the role of the enzyme-sensitive polymer in achieving a controlled release rate of the drug and improving selective targeting to the inflamed colon tissues. Moreover, ES100-azopu nanospheres were more efficacious in reducing signs of inflammation in the colon, along with decreased plasma levels (Naeem *et al.*, 2015a) (Table 1. 5.).

Furthermore, dual pH- and enzyme-sensitive microencapsulated nanogels have been fabricated for the specific targeting of TNF- α -siRNA (small interfering RNA) to murine macrophages. The findings showed significant uptake and internalization by the macrophages and the ability to withstand lower gastric pH, whereby polymeric swelling was observed at pH 6–7.5. This novel strategy can be considered for treating IBD in the future (Knipe *et al.*, 2016).

1.5.1. Pullulan-a new versatile microbial sensitive polymer

Researchers attempted to utilize new natural polymers degradable by colonic resident bacteria (microbiome) for nanoparticle-oriented drug delivery to the colon (Sohail *et al.*, 2019). In this quest, pullulan (Pu) is a neutral polysaccharide with widespread biomedical applications because of its biodegradability, adhesiveness, film-forming nature, mechanical strength, and can be used as a binder, stabilizer, emulsifier, and prone to degradation by colonic bacteria by the pullulanase enzyme (Singh *et al.*, 2017; Singh and Saini, 2014). Additionally, Pu can serve as a probiotic that improves colon health. Recently, Pu had been employed for colon targeting purpose with good in vitro outcomes (Lima *et al.*, 2017; de Arce Velasquez *et al.*, 2014), however, Pu based nano-formulations are not yet explored in animal models of IBD.

1.6. Second generation of ligand anchored nanocarriers for IBD

Though nanocarriers can passively deliver the drug to the inflamed colon tissue under eEPR effect, still drug effective concentrations may be lost because of inter-and intra-cellular barriers and rapid clearance.

Colon inflammation is governed by several pathophysiological changes. Under inflammation, some receptors and cell adhesion molecules are overexpressed onto the surface of colon epithelial cells and the recruited immune cells like macrophage

galactose type lectin-C (MGL/CD301), mannose receptor (CD206), hyaluronic receptor (CD44), transferrin receptor, Folate receptor, CD98, PepT1, etc. (Liu *et al.*, 2021). Active targeting of the overexpressed receptors in IBD through ligand anchored nanocarriers can facilitate in delivering the drug moieties to the destined inflamed colon cells in effective concentrations and avoid off-site drug delivery and its rapid clearance.

Moreover, cell adhesion molecules (CAMs) are overexpressed on the luminal side of mucosal endothelium to recruit leukocytes that triggered inflammatory cascade in IBD. Such CAMs can be targeted by specific antibodies and proteins anchored nanocarriers in IBD. In this regard, an anti-intercellular adhesion molecule (ICAM) functionalized bacterial nanocarriers targeted ICAM-1 receptor in the inflamed tissues (Anselmo *et al.*, 2016).

1.6.1. MGL

MGL or CD301 is a transmembrane type-II C-lectin protein with N-terminal cytoplasmic domains, transmembrane domains, extracellular domains, and C-type carbohydrate recognition domain that binds to the N-acetylgalactosamine and D-galactose (Zizzari *et al.*, 2015; Pirro *et al.*, 2020). MGL-2 receptors are heavily expressed on macrophages and dendritic cells (van Kooyk *et al.*, 2015). Therefore, nanocarriers with galactose moiety can efficiently interact with MGL-2 receptor and mediate specific targeting of macrophages, recruited at the inflamed site. This ligand-receptor oriented drug delivery approach have been opted by some researchers for targeting inflamed colon via rectal and oral routes. However, the intravenous or systemic route is not desirable for colitis therapy because the asialoglycoprotein receptor preferably binds to the galactose residues and is abundantly expressed on the liver. Therefore, systemic delivery of galactose anchored nanocarriers may have larger accumulation in the liver instead of the colon (D'souza and Devarajan, 2015).

For oral drug delivery, galactosylated low molecular weight chitosan nanocarriers were developed to deliver anti-sense TNF- α oligonucleotide to the macrophages of the inflamed colon. Colon TNF- α and other pro-inflammatory cytokines were prominently decreased with significant improvement in the severity of TNBS induced and CD4⁺ CD45RB^{hi} T cell transfer colitis (Zuo *et al.*, 2010). Further, TNF- α -siRNA loaded PLGA nanoparticles were coated with galactosylated chitosan (GPNs) for macrophage

targeting in UC via the oral route. GPNs have marked internalization by RAW 264.7 macrophages and delivered stable TNF- α -siRNA to the inflamed colon with superb anti-inflammatory action against the colitis (Huang *et al.*, 2018).

Galactose-trimethyl chitosan-cysteine (GTC) nanoparticles delivered ‘mitogen-activated protein kinase 4-siRNA (Map4k4-siRNA)’ to the activated macrophages of the inflamed colon in the murine colitis model through oral administration. The GTC nanoparticles protected Map4k4-siRNA against GIT harsh environment and accumulated it at the colon with significant alleviation of TNF- α and colitis clinical symptoms (Zhang *et al.*, 2013).

Galactosylated polymeric nanoparticles encapsulating siTNF- α were co-delivered with IL-22 embedded into a chitosan/alginate hydrogel via the oral route. The combined rationale had efficient colon targeting ability and proved to be synergistic in mucosal healing with superior therapeutic efficacy in UC (Xiao *et al.*, 2018).

1.6.2. Transferrin receptor (TFR)

TFR is a glycoprotein transmembrane receptor that is present on the normal cells surface at a lower concentration. TFR efficiently binds and uptake transferrin (tfr) through receptor-mediated endocytosis to maintain the normal supply of iron in the cells (Gammella *et al.*, 2017). In special circumstances like inflammation, cancer, and on rapidly proliferating cells including macrophages, the TFR especially TFR-1 is overexpressed on the cell surface (Shen *et al.*, 2018; Tacchini *et al.*, 2008). Therefore, the overexpressed receptor can be exploited to mediate specific targeting of immune cells, inflamed and cancerous cells. Tfr modified nanocarriers have been developed for drug delivery purpose in cancer and inflammation (Zhou *et al.*, 2018; Tirosh *et al.*, 2009). In IBD, TFR-1 is upregulated not only on macrophages but also on colon epithelial cells on the apical and basolateral sides (Harel *et al.*, 2011; Tirosh *et al.*, 2009). Therefore, tfr anchored nanocarriers can extensively target the TFR-1 on the macrophages and epithelial cells and specifically deliver the drug to the inflamed colon. In an experiment, tfr-antibody modified liposomes have better internalization by the caco-2 cells than plain liposomes, because cytokines treated caco-2 cells have higher expression of TFR (Harel *et al.*, 2011). However, the efficacy of tfr-anchored nanocarriers must be elucidated in the IBD animal models because the current strategies

are focused on in vitro and ex vivo models. Further, the question of the stability of such nanocarriers across GIT is unresolved. Drug delivery strategy should be designed in a way that avoids degradation by the stomach acidic pH, enzymes, etc. in the upper GIT.

1.7. Patents For pH-Dependent Micro/Nanoparticulate DDS for IBD

Patents concerning pH-sensitive micro/nanoparticulate systems for the oral delivery of drugs to the colon are listed in Table 1. 6. ES100 coated mesalamine NPs for oral drug delivery to the colon for treating IBD with the desired characteristics have been invented, which protect the drug from GI juices and release the drug at $\text{pH} > 7$ (Hu and Liu, 2015). Several other pH-sensitive particulate systems have been developed for the colon with the potential to be used in IBD, such as the nanospheres-in-pH-sensitive microspheres system for delivering several moieties including steroids and antibiotics (Shefer and Shefer, 2010), and DNA, vaccines, and genes (Shefer and Shefer, 2004).

Table 1. 6: Patents for a pH-sensitive micro-/nanoparticulate system for the treatment of IBD

| Patent No. | Title | Encapsulating Moiety | Particulate System | Publication Date | References |
|--------------------------|---|---|-----------------------------|------------------|---------------------------|
| CN1033159 59B | Orally taken colon-targeted preparation for treatment of inflammatory bowel diseases and preparation method thereof | Eudragit S100 5-ASA | Nanoparticles 70-400 nm | May 6, 2015 | (Hu and Liu, 2015) |
| US7670627 B2 | pH triggered targeted controlled release systems for the delivery of pharmaceutical active ingredients | Various therapeutic agents including steroids, analgesics, and antibiotics | Nanospheres-in-microspheres | Mar 2, 2010 | (Shefer and Shefer, 2010) |
| US2004022 4019 A1 | Oral controlled release system for targeted drug delivery into the cell and its nucleus for gene therapy, DNA vaccination, and administration of gene-based drugs | Sense, antisense nucleotide sequences, antigens, antibodies, ribozymes, oligonucleotides and polynucleotide viruses, vectors, proteins, peptides, and nucleic acids, DNA or RNA fragments | Nanosphere-in-microsphere | Nov 11, 2004 | (Shefer and Shefer, 2004) |

1.8. Present Advancements & Directions

The advancements in oral DDS have significantly improved the selective targeting of active agents to the inflammation site. In this context, pH-sensitive NPs serve as a platform to deliver the drug to the colon, accompanied by multiple anatomical and pathophysiological challenges and opportunities. Inflammation targeting can be improved with targeting modalities or ligand attachment to the pH-sensitive polymeric surface to target overexpressed macrophages, proteins, and receptors at the colon site. Currently, the focus is on developing nanovesicles derived from living cell origins, such as macrophages, leukocytes, platelets, and red blood cells, to constitute biomimetic nanovesicles that are not only biocompatible but also resemble endogenous inflammatory mediators and suppressors. In this regard, leukocyte-derived nanovesicles were effective in a mouse model of IBD (Corbo *et al.*, 2017). Coupling biomimetic nanovesicles with pH-sensitive moieties could facilitate oral colon-specific delivery to the inflamed tissues.

1.9. Safety and Challenges

Some key issues are associated with the translational use of NPs in clinics for IBD. The foremost concern is the limited investigations on the toxicity of NPs/pH-dependent NPs for human usage, particularly in the GIT. Second, data on biodistribution studies still need to be elucidated. Human investigations have revealed the accumulation of microparticles in ulcerated tissues; however, contrary to animal findings, only traces of NPs were found at the mucosal surfaces (Schmidt *et al.*, 2013), highlighting the prerequisite of evaluating pH-dependent micro- and nanocarriers in humans. Third, it should be kept in mind that NPs have unique physicochemical properties that pose a greater threat to biological systems and demand assessment of their environmental impact (Pichai and Ferguson, 2012). Fourth, polymeric carriers must be carefully selected; most of the time, non-biological carriers cause cellular-level toxicity by derangement of the membranes, disturbance of the cytoskeleton, and exploitation of phagocytic cells (Pichai and Ferguson, 2012). ES100 is a non-biodegradable and non-absorbable pH-sensitive synthetic polymer but is least associated with toxicity (Thakral *et al.*, 2013). Thus, it overcomes the issues of synthetic polymer toxicity, but further investigations are required at the nanoscale level. A daily intake of 2 mg/kg (150 mg

for an adult) of ES100 is safe for human consumption (Rowe *et al.*, 2009), and usually, NPs require smaller amounts of polymers as compared to the macro-dosage forms. However, the allocated occupational exposure limits in the United Kingdom for methyl methacrylate polymers is 208 mg/m³ (50 ppm) for long-term exposure and 416 mg/m³ (100 ppm) for short-term exposure, which should be kept in mind when fabricating pH-sensitive NPs (Executive., 2002).

pH-dependent nanoparticulate DDS have shown promising and encouraging results in treating IBD, especially through the oral route. Based on the results to date, we may postulate that the future of IBD therapy would be much more significant and effective by designing them the right way. This approach enables a wide array of small-drug substances and even proteinaceous drugs to be delivered successfully to the colon, with improved retention and therapeutic effects. The combination of the pH-dependent nanoparticulate strategy with other approaches facilitates the targeting potential and drug release characteristics of the drug delivery system. However, the successful translation of this novel concept into clinical practice depends on the associated issues that need to be addressed, such as the safety of the polymers or other materials; the nanocarrier surface chemistry, followed by the uptake or binding mechanism and stability during GI transit would need to be explored exclusively. Finally, with respect to the commercialization of these nanocarriers, simplification and stability of the preparation method are essentially desirable for large-scale manufacturing.

1.10. Study Rationale

The rationale is to develop stimuli-sensitive ligand anchored nanocarriers that have multi-level targeting properties. The stimuli sensitive dissolves at the pH of the colon, while the underneath ligand anchored core binds specifically to the targeted receptors overexpressed at the immune cells or epithelial colon cells in the inflammation (Figure 1. 5 A). To achieve targeted drug delivery to the inflamed tissues of the colon and to avoid oral-route related obstacles in the colonic drug delivery; we hypothesized to develop stimuli sensitive, bio-functionalized nanocarrier system, which adopts a two-level targeting approach. At first, pH-sensitive or microbial-sensitive polymeric coat on the nanocarrier system enables the nanocarriers to breach the anatomical and pathophysiological barriers and to reach the colon, At the colon, stimuli sensitive coat

dissolves under the influence of colon pH or microbes. Afterward, the attached bio-moiety, either the galactose or transferrin, on the drug-containing PLGA core would specifically target the immune cells or epithelial cells or both to achieve intracellular targeting and stay there for a prolonged duration (Corbo *et al.*, 2017). The entrapped drug releases in a sustained fashion and mechanistically interferes with the inflammatory cascade and pathways to inhibit the pro-inflammatory mediators. The drugs dexamethasone (Dexa), a corticosteroid and tofacitinib citrate (Tofa), a Janus kinase inhibitor (immunosuppressant) are used for two different types of bio-functionalized nano-formulations separately. Dexa possesses anti-inflammatory properties through mediating intracellular glucocorticoid activity (Nunes *et al.*, 2013). On the other hand, Tofa inhibits the activation and phosphorylation of the JAK-STAT pathway intracellularly, preventing cytokines production which ultimately suppresses inflammation. Whereby, intestinal degradation, dose-related adverse events, and systemic absorption of dexamethasone and tofacitinib will be reduced through entrapment in the bio-functionalized nanocarrier. Further, tacrolimus, an immunosuppressant, is a drug used for severe IBD cases and we load it in the third strategy. Tacrolimus (TAC) worked by suppressing T-cells, however, associated with systemic adverse effects. Its entrapment within biofunctionalized nanocarrier not only reducing its systemic absorption and adverse effects but also enhance local therapeutic effects at the colon.

PLGA, a versatile biocompatible biodegradable polymer (Makadia and Siegel, 2011; Danhier *et al.*, 2012) and approved safer for human use, is selected as a main polymeric nanocarrier for bio-functionalization. It serves as a platform for a wide range of bio-molecular attachment and modifications. Afterward, the bio-functionalized PLGA nanocarrier is coated with pH-sensitive/microbially triggered polymers to exploit pathophysiological conditions for colon-specific targeting.

Overall, the combined rationale of stimuli sensitive and ligand-mediated colon targeting overcome the pathophysiological barriers at the organ level plus mucus and inter-and intra-cellular barriers at a ground level. Therefore, nanocarriers localized at inflamed colon for a prolonged duration, concentrating more drug at colon with lesser chances of diarrhea mediated clearance or degradation and enhanced therapeutic

efficacy of the drug. We have hypothesized three strategies under this approach (Figure 1.5 B).

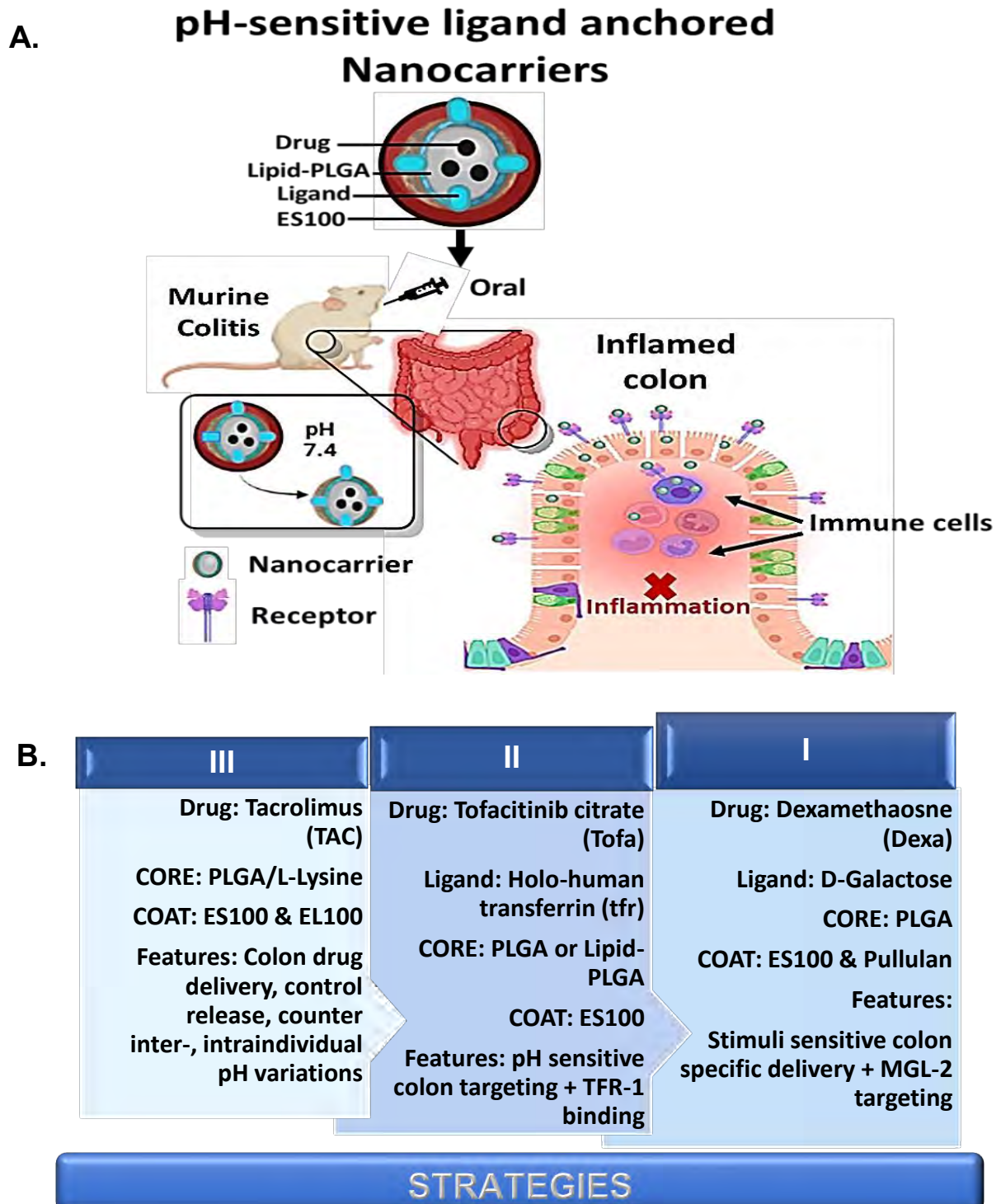


Figure 1.5: pH sensitive ligand anchored polymeric nanocarriers and proposed strategies for IBD; **A.** Dual pH-sensitive ligand anchored nanocarriers evade the anatomic and pathophysiological barriers at organs and cellular levels to target inflamed colon, **B.** Three strategies for stimuli sensitive biofunctionalized nanocarriers to target inflamed colon (I-III)

1.11. Aims and Objectives

The study aims to fabricate stimuli-sensitive, biofunctionalized PLGA nanocarriers incorporating surface attached biomolecules for more specific targeting of colon inflamed tissues through active and passive mechanisms. Stimuli sensitive coat facilitates colon targeting and exposes underneath biofunctionalized PLGA core only at the colon, where it binds to specific receptors and releases the drug in a sustained fashion for long-term therapeutic effects.

The objectives to achieve the goals are:

1. Development of analytical methods (HPLC, UV) for the drugs

2. Preparation and optimization of nanocarriers

A. Bio-functionalized PLGA nanoparticles/nanocarriers/nanoshells

- Synthesis and Characterization of galactosylated-PLGA (GAL-PLGA) polymer and dexamethasone loaded galactosylated-PLGA nanocarrier (Dexa-GAL-PLGA NPs) under quality by design (QbD) approach
- Preparation and characterization of transferrin-PLGA nanocarrier under QbD approach and fabrication of tofacitinib citrate loaded transferrin-PLGA nanocarrier (Tofa-P/tfr NCs) and tofacitinib citrate loaded transferrin-lipid/PLGA nanoshells (Tofa-LP/tfr NSh)
- Preparation and characterization of tacrolimus loaded PLGA/L-Lysine nanocarrier (TAC-P/Lys NCs)

B. Stimuli sensitive, biofunctionalized PLGA nanocarriers/ nanocargoes/ nanoshells

- Preparation of suitable enteric coatings; ES100 and pullulan mixture
- Preparation and characterization of dual pH+ microbial enzyme sensitive ES100/ pullulan coated bio-functional GAL-PLGA (GP) nanocargoes (Dexa-GP/ES/Pu NCs)
- Coating of Tofa-LP/tfr NSh with pH-sensitive ES100 coat to prepare pH sensitive Tofa-LP/tfr/ES NSh
- Coating of TAC-P/Lys NCs with the dual pH-sensitive coat (ES100 + EL100) to prepare TAC-P/Lys/ES-L100 NCs

3. Evaluation of physicochemical characteristics of nano-formulations

- Particle size, morphology, zeta potential, drug entrapment, interactions and compatibility, surface coating analysis, thermal stability, physical state analysis, etc.
- 4. In vitro drug release profiling and kinetics at GIT pH values (1.2 and 7.4)**
 - 5. Cell-based studies to explore nanocarriers biocompatibility and cell-uptake potential**
 - 6. Establishment of murine colitis models for in vivo animal studies**
 - Development of chemically induced (DSS or OXA) colitis model
 - Preliminary investigations to determine colon targeting potential of nanocarriers
 - Evaluation of therapeutic effects of drug-loaded DEXA-GP/ES/Pu NCs, in the DSS induced colitis mice
 - Evaluation of therapeutic effects of Tofa-P/tfr NCs, Tofa-LP/tfr NSH, and Tofa-LP/tfr/ES NSH in the DSS induced animal colitis model
 - Evaluation of therapeutic effects of TAC-P/Lys NCs and TAC-P/Lys/ES-L100 NCs in Oxazolone induced colitis model
 - In vivo toxicity evaluation of nanocarriers

CHAPTER 2

MATERIALS AND METHODS

2. MATERIALS AND METHODS

2.1. Materials

2.1.1. Chemicals and reagents

PLGA (Resomer[®] 502, 50:50, MW 7000-17000) and ES100 were obtained from Evonik Industries (Darmstadt, Germany). Pullulan (Pu) (CAS: 9057-02-7, MW 500-700 kDa) was gifted from Xi'an Sgonek Biological Technology Co., Ltd (China). Dexa (MW 392.46), polyvinyl alcohol (PVA; Mowiol[®], MW 31000), D-galactose (MW 180.68), DSS (MW 40000), organic solvents (methanol, ethyl acetate, chloroform, acetonitrile, etc.), Evans blue, sodium phosphate buffer and NaCl had been taken from Sigma Aldrich (Germany). HCl, potassium di-hydrogen phosphate (KH₂PO₄), and di-sodium hydrogen phosphate (Na₂HPO₄·2H₂O) were purchased from BDH Laboratory Supplies (Poole, UK). Cetyltrimethylammonium bromide (CTAB), rhodamine-B, thioglycolate, Glutathione (GSH), Glutathione S-transferases (GST), catalase, thiobarbituric acid, 3-(4,5-dimethylthiazol-2-yl)-2,5-diphenyltetrazolium bromide (MTT), cRPMI-1640, fetal bovine serum (FBS), penicillin/ streptomycin, methane sulfonic acid, and N, N-dimethylformamide (DMF) were purchased from Millipore Sigma Aldrich (St Louis, MO, USA). Propidium iodide (PI) and annexin-V from BD Biosciences (San Diego, CA, USA), TAC (FK506) were purchased from Abcam. EL100 was the gift samples from Evonik Industries. The organic reagents were obtained from Millipore Sigma Aldrich, Germany. Coumarin-6 was obtained from Sigma Aldrich, Germany, L-Lysine monohydrochloride (L5626, Sigma Aldrich)

2.1.2. Animals

Part I and II: Male BALB/c mice, 3-4 weeks old (25-30 g), were purchased from the National Institute of Health (NIH), Islamabad, Pakistan. Mice were kept under protocols prescribed for care and use of laboratory animals under QAU, Islamabad bioethical committee, and NIH. The protocol for animal studies of the project was approved under protocol no. BEC-FBS-QAU2020-238. The mice were housed at standard laboratory conditions of temperature and humidity and fed with standard diet and distilled tap water under 12 hours light-dark cycle.

Part III: C57BL/6J mice (weighing 20-22 g) were housed and acclimatized to a pathogen-free hygienic environment under standard environmental conditions. The study was planned according to the ethical guidelines of NIH care and handling of lab animals. The protocol was approved under RUF-55.2.2-2532-2-1152-18 for the conductance of animal studies at University Hospital Clinic, Erlangen by the government of Middle Franconia, Germany.

2.1.3. Preparation of solutions

2.1.3.1. HEPES buffer

HEPES solution is prepared by mixing 1.8mmol of CaCl₂ (199.764 mg), 0.8 mmol of MgSO₄ (96.288 mg), 5.6 mmol of KCl (417.48 mg), 0.8 mmol of NaH₂PO₄ (95.984 mg), 5.5 mmol of D-glucose (990.825 mg), 116 mmol of NaCl (6779 mg) and 25 mmol of HEPES (5957.5 mg) in 1L of distilled water. CaCl₂ was added in the last step after dissolving other ingredients, otherwise, it forms precipitates.

2.1.3.2. 0.1 N NaOH solution

0.4g of NaOH pellets were added to a small amount of distilled water and mix well. Then make up the volume up to 100 mL with distilled water.

2.1.3.3. PVA solutions

Add either 1, 2 or 3 g of PVA to 100 mL of distilled water. Stir overnight to make 1, 2, or 3% PVA solution, respectively.

2.1.3.4. Brewer thioglycollate solution (3%)

Dissolve 3g of thioglycollate medium, brewer (Millipore Sigma Aldrich, Germany) in 100 mL distilled water and boil it to dissolve the solid. Then sterilize it through autoclave and store it in the dark.

2.1.3.5. FACS buffer

Take Phosphate buffer saline (PBS, 1x) and add 2% of FBS to it. Dissolve well to prepare FACS buffer.

2.2. Methods

Synthesis and characterization of the first two parts were executed at the Department of Pharmacy, QAU, Islamabad, and the last part at the University Clinic Hospital, Erlangen, Germany. In vitro cell-based studies and In vivo experiments have been done at QAU and Medical Clinic 1, University Hospital Clinic, Erlangen, Germany. Allied pharmacy institutes in Islamabad were considered for some in vitro characterization techniques.

PART-I (Section A)

Note: Part-I has two sections, A and B. Section A describes the synthesis, optimization, characterization, and preliminary in vivo testing of D-galactose-PLGA nanoparticles (Dexa-GAL-PLGA NPs). Section B describes further modifications and coating of dual stimuli sensitive coat, ES100 and Pullulan (ES/Pu), on GAL-PLGA nanocore (GP). The formed Dexa-GP/ES/Pu nanocargoes (NCs) have been characterized through in vitro, ex vivo, and animal studies in the murine colitis model.

2.2.1. HPLC instrumentation and analytical procedure

Dexa quantification was conducted through RP-HPLC system (Agilent technologies 1200 series), assisted with UV detector and C18 column (250 mm x 4.6 mm, 5 μ m pore size; supelcosil LC-1, Supelco). For isocratic chromatographic separation, the mobile phase consisting of acetonitrile (32%) and 10 mM sodium phosphate buffer (68%, pH 5) eluted the column at a flow rate of 1 mL/min and ambient column temperature. The UV detector was operated at 240 nm wavelength and the injection volume for the samples was 20 μ L. A stock solution of Dexa (1 mg/mL) was prepared in the mobile phase and a standard calibration curve was obtained over a concentration of 6.25-100 μ g/mL with suitable linearity ($R^2 = 0.998$).

2.2.2. Molecular docking

The sequence of Human macrophage galactose type lectin-2 (MGL, isoform-2) was obtained from the NCBI database, accession no. NP_006335. The homologous structure Q8IUN9, C-type lectin domain family 10 member A (CLC10_HUMAN), was considered the best template, which was based on the protein template, mammalian asialoglycoprotein receptor 1 (PDB code: 5JPV, sequence identity 71.22%), (). The two

ligands recognized by the MGL-2 receptor were prepared by ChemBioDraw Ultra 14.0 (Cambridge Soft interface, PerkinElmer, Cambridge, USA). The studied ligands were D-galactose and galactose conjugated PLGA polymer (GAL-PLGA), for simplicity monomer was considered (). Macromolecule (MGL-2 protein homolog) and ligands were loaded in the PyRx 0.8, a virtual screening program. Docking studies were performed using AutoDock Vina 4.2 tool (Scripps Research, La Jolla, CA, USA), integrated with the PyRx 0.8 program. It is an automated docking software to study ligand-receptor binding in the 3D dimensions. Docking calculations were interpreted in the form of binding energy scores. The best ligand binding pose was further evaluated for molecular orientation and amino acid interactions using BIOVIA Discovery Studio Visualizer v16.1.0.15350.

2.2.2.1. Homology modeling for MGL-2 receptor

The MGL-2 (accession no. NP_006335) sequences were investigated using Research Collaboratory for Structural Bioinformatics (RCSB) Protein data bank to find suitable templates. Further, the SWISS-MODEL repository server was accessed to find the best template for homology modeling. The homologous structure Q8IUN9, C-type lectin domain family 10 member A (CLC10_HUMAN), was considered which was based on the protein template, mammalian asialoglycoprotein receptor 1 (PDB code: 5JPV, sequence identity 71.22%). The MGL-2 homology model (a) was saved in PDB format for docking. Furthermore, the constructed homology model was accessed for quality and structural stability with the verified programs like PROCHECK and ProSA which generate Ramachandran and quality score plots, respectively for the protein model.

2.2.2.2. Ligands Preparation

Since D-galactose residue is known to target the MGL-2 receptor, thus two ligands were prepared. One with a simple galactose unit (b) which is used as a control to be recognized by MGL-2 proteins. Another prepared ligand to interact MGL-2 receptor is galactose conjugated PLGA polymer (GAL-PLGA), for simplicity monomer unit is considered (c). The ligand structures were investigated and drawn using ChemBioDraw Ultra 14.0 (Cambridge Soft interface, PerkinElmer, Cambridge, USA) and converted to 3D models were using ChemBio3D Ultra 14.0. The structures were submitted to energy minimization using the Merck Molecular Force Field 94

(MMFF94) method built in the ChemBio3D Ultra 14.0 program. The ligand structures were saved in MOL2 format for docking purposes.

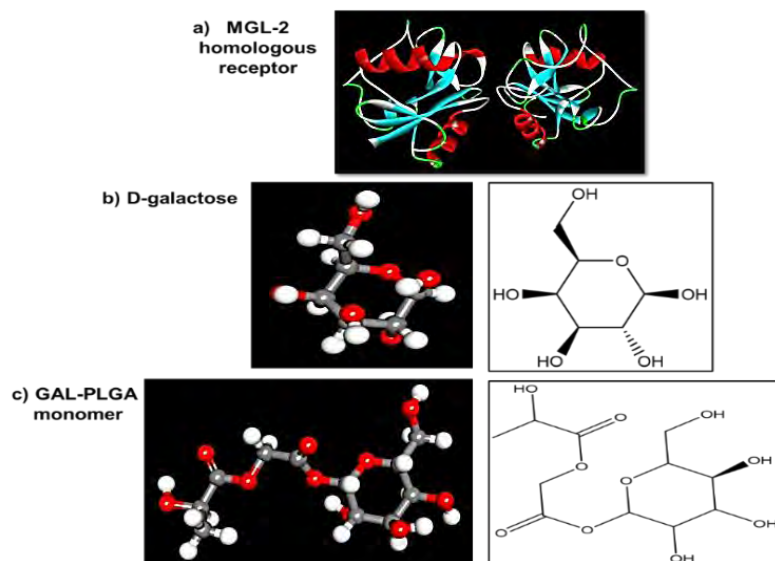


Figure 2. 1: Molecular structures of MGL-2 homologous receptor (5JPV) (a); D-galactose ligand (b); GAL-PLGA polymer (monomer unit) (c) as a ligand (Zeeshan *et al.*, 2021)

2.2.3. Polymer synthesis: Conjugation reaction between D-galactose and PLGA

GAL-PLGA conjugated polymer was synthesized through an esterification reaction. In brief, 10 mg of D-galactose was solubilized in 10 mL DMF; followed by the addition of methane sulfonic acid (0.004 mL, 0.056 mmol) and 200 mg of PLGA in the round bottom flask. The flask was clamped with the distillation assembly and the process was continued for 24 hours (Figure 2. 2 I) (Peça *et al.*, 2012). Afterward, the flask solution was immersed in ice-cold distilled water to get white precipitates. The precipitates were washed and filtered under vacuum and dried to obtain a white powder of GAL-PLGA conjugated polymer. Conjugation of galactose moiety to the PLGA backbone was confirmed through spectroscopic and thermal analysis techniques. A two-level fractional factorial design $2^{IV}(4-1)$ was applied to study the reaction variables controlling the outcomes of the synthesized polymer using STATISTICA[®] 10.0 software (Statsoft. Inc., USA). The independent reaction variables (X) optimized through fractional factorial design (Table 2. 1) and the measured outcomes or responses (Y) are % yield and powder consistency.

Controlling parameters for better yield and powder consistency:

A two-level fractional factorial design $2^{IV}(4-1)$ was applied to study the reaction variables controlling the outcomes of the synthesized polymer using STATISTICA[®] 10.0

software (Statsoft. Inc., USA). The independent reaction variables optimized through fractional factorial design and their two-level variations are presented in Table 2. 1, while some factors are kept constant during the reaction. The studied variables are temperature (X_1), heating conditions (X_2), drying conditions (X_3), and atmospheric conditions (X_4). In a 2-level fractional factorial design, some variables and their interactions have the same effect, aliases, or confounded variables, and thus have a negligible role to be computed individually. Therefore, this type of design omits unnecessary runs and facilitates the cost-effective optimization of experimental procedures (Djuris *et al.*, 2013). To find the effect estimate of variables on each response, the following mathematical equation (1) is computed:

$$Y = I_0 + I_1X_1 + I_2X_2 + I_3X_3 + I_4X_4 + I_{12}X_1X_2 + I_{13}X_1X_3 + I_{14}X_1X_4 + \dots \quad 1$$

Where Y is the response factor, I_0 is a constant, I_A represents the effect of variables and I_{AB} their interactions.

Under these conditions, the $2_{IV}^{(4-1)}$ fractional factorial design for the synthesis of GAL-PLGA polymer is referred to in Table 3. 1. The measured outcomes or response factors for the synthesized GAL-PLGA polymer were %age yield (Y_1) and obtained dried powder consistency (Y_2). Powder consistency was evaluated on the basis of flow properties and moisture content. For the computational purpose, powder consistency (Y_2) was graded on a scale of 0-100 anonymously, corresponding to 0 = swollen clumps and aggregates; 25 = loose aggregates; 50 = flaky powder; 100 = fine powder. The data is utilized to estimate the effect by the above-mentioned mathematical equation.

Table 2. 1: (A) The studied independent variables and their levels in $2_{IV}^{(4-1)}$ fractional factorial design (B) The constant variables with constant reaction conditions during GAL-PLGA polymer synthesis

| (A) In-dependent variables and their levels | | | |
|---|------------------------|---------------------------------------|------------|
| Code | Independent variables | Level (-1) | Level (+1) |
| X1 | Temperature (°C) | 60 | 70 |
| X2 | Heating conditions | Sand bath | Oil bath |
| X3 | Drying conditions | Lyophilizer/ Freeze dryer | Desiccator |
| X4 | Atmospheric conditions | Air | Nitrogen |
| (B) Variables that remain constant (not optimized) | | | |
| Code | Constant variables | Value | |
| C1 | Reagent | CH ₃ SO ₃ H/DMF | |
| C2 | Duration | 24 hours | |
| C3 | Galactose: PLGA ratio | 1:20 | |

2.2.4. Preparation of dye/drug-loaded GAL-PLGA nanoparticles

Dexamethasone and GAL-PLGA were dispersed in ethyl acetate in the ratio 1:20. The organic phase was added dropwise in the aqueous phase containing a surfactant, PVA (1-3%) while constantly stirring to form O/W emulsion. The ratio of organic to aqueous phase was kept 1:3. Afterward, the emulsion was probe sonicated (Misonix- XL-2000 series) at 50% amplitude, while immersed in ice-cold water to dissipate heat during sonication. Then stirred overnight to evaporate organic solvents. After solvent removal, nano-suspension was centrifuged thrice at 13500 rpm for 30 min to remove residual solvent and untrapped drug (Figure 2. 2 I-II). The preparation method adopted was suitable and single-stepped to fabricate polymeric nanoparticles loaded with a hydrophobic drug, thus providing a feasible approach. For dye loaded GAL-PLGA nanoparticle, Rhodamine B or fluorescein dye replaced the drug in the organic phase with the same quantity, and the same procedure was adopted. For GAL-PLGA nanoparticle preparation, the QbD based approach was adopted to screen some variables on preliminary grounds and their impact was assessed (Table 2. 2). The interactions between critical attributes and risk assessment was performed using Lean QbD[®] software (QbD works LLC, Fremont, USA) on a 3-level risk assessment scale (low, medium, high) (Table 2. 3). Thereafter, the variables with the most significant impact were further studied and optimized using 3³ Box-Behnken design through STATISTICA[®] 10.0 software. The 3-level Box-Behnken experimental design with different combinations of experimental runs. Nanoparticles obtained after centrifugation were subjected to freeze-drying (lyophilization) for long term stability and storage purpose. Before lyophilization, 5% cryoprotectant either trehalose or sorbitol was incorporated to protect the formulation from the harsh effects of freezing. The nano-formulation was refrigerated at -80°C, followed by main drying and residual drying phase of lyophilization under controlled temperature and pressure.

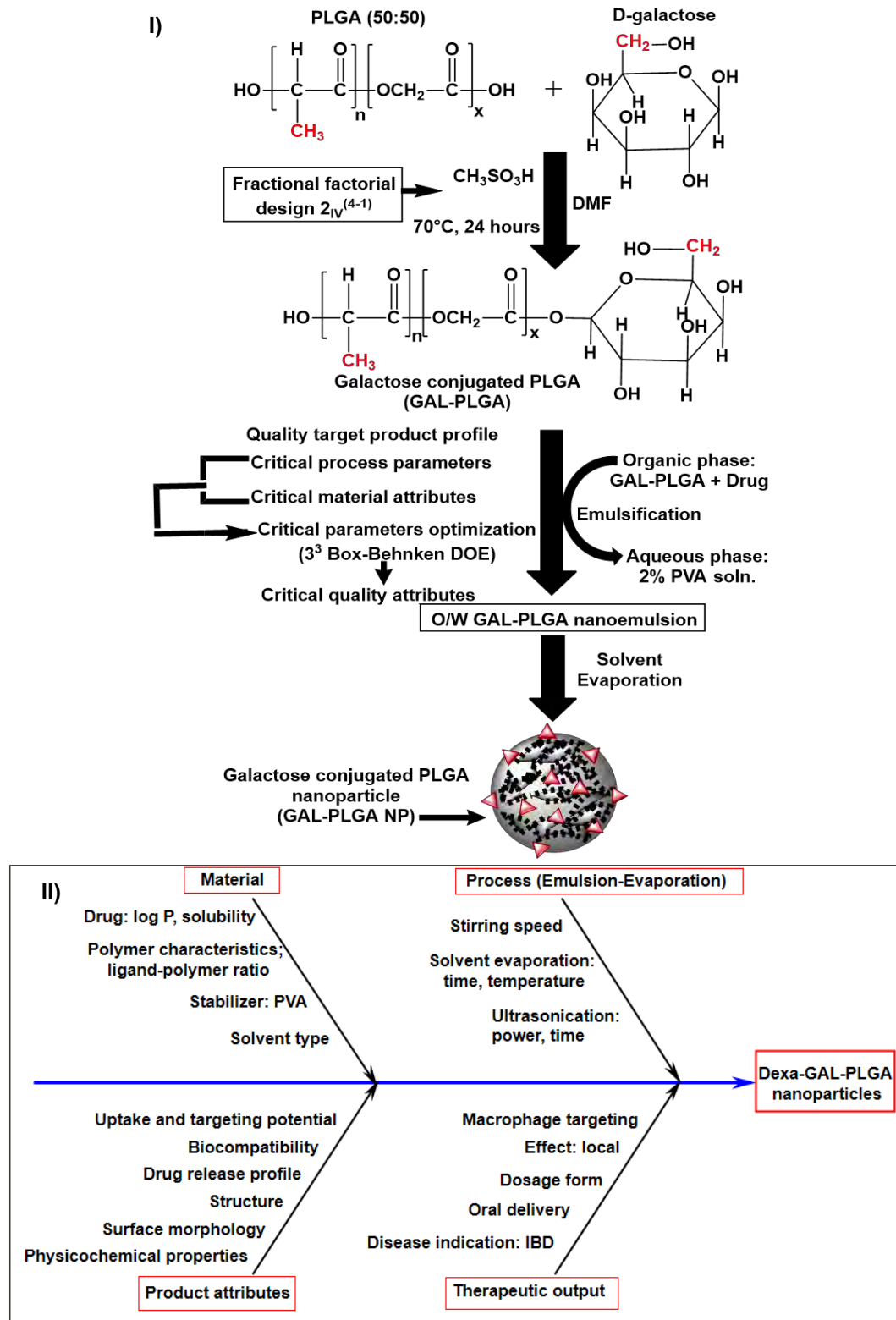


Figure 2. 2: Synthesis of GAL-PLGA polymer and nanoparticles under QbD and DOE approach; (I) Scheme for the synthesis of Galactose conjugated PLGA (GAL-PLGA) polymer under controlled reaction conditions, then QbD based DOE approach to fabricate GAL-PLGA nanoparticles via emulsion-evaporation method incorporating a hydrophobic drug. (II) Ishikawa cause and effect diagram for drug-loaded GAL-PLGA nanoparticle synthesis (Zeeshan *et al.*, 2021)

2.2.4.1. The QbD process for the development of nano-formulation

The QbD approach, at first, starts with the development of “knowledge space”, a systematic collection of concerned scientific data and literature. Knowledge space laid the foundations of ‘quality target product profile (QTPP) that is the main building block in the development of the nanoparticles concerning therapeutic use. Based on knowledge space, QTPP for DEXA-GAL-PLGA nanoparticles was designed (Table 2. 2). Afterward critical material (CMA), and critical process attributes (CPA) were selected that tremendously affect the quality of nano-formulation (Pallagi *et al.*, 2015), listed in Table 2. 2. Both CMAs and CPAs strongly influence the product’s quality as manifested through critical quality attributes (CQA) (Pallagi *et al.*, 2015; Simões *et al.*, 2018). In the case of DEXA-GAL-PLGA nanoparticles, CQAs are particle size, encapsulation efficiency, zeta potential, PDI, appearance, toxicity, and stability that should be within an acceptable range (Table 2. 2). To control these major attributes, an initial risk assessment is performed to know related interdependence and their impact, which is displayed through various charts. The interactions between critical attributes and risk assessment was performed using Lean QbD software® (QbD works LLC, Fremont, USA) on a 3-level risk assessment scale (low, medium, high).

Determination of QTPP for DEXA-GAL-PLGA nanoparticles

International council for harmonization of technical requirements for pharmaceuticals for human use (ICH) Q8 guidelines consider QTPP an essential element of the QbD process and guided about selection criteria of QTPPs (Park *et al.*, 2019). In the present study, ICH guidelines, literature digging, and previous data suggested QTPPs like therapeutic indication, route of administration, dosage form design, dissolution, stability, etc. as mentioned in Table 2. 2.

Determination of CPP, CMA, and CQA for DEXA- GAL-PLGA nanoparticles

Based on knowledge space, critical material, and process attributes are selected that tremendously affect the quality of nano-formulation (Pallagi *et al.*, 2015). The studied CMAs and CPPs for GAL-PLGA nanoparticle synthesis are listed in Table 2. 2. Both CMAs and CPAs strongly influence the product’s quality as manifested through CQA (Pallagi *et al.*, 2015; Simões *et al.*, 2018). In the case of DEXA-GAL-PLGA nanoparticles, CQAs are particle size, encapsulation efficiency, zeta potential, PDI,

appearance, toxicity, and stability that should be within an acceptable range (Table 2.2).

2.2.4.2. Initial risk assessment

The potential influence of CMAs and CPAs on product quality, their impact, and interdependence is determined through a risk assessment tool. After the selection of critical attributes, inter-relation between each QTPP and CQA and between each CPP/CMA and CQA was ascertained using Lean QbD software[®] (QbD works LLC, Fremont, USA) on a 3-level risk assessment scale (low, medium, high). The severity and impact of the attributes were displayed in the charts by the software. Further, attributes/parameters were scrutinized on these bases, screened, and optimized.

Table 2. 2: The selected QTPP elements, CQAs, and CPPs/CMAs with targets and justifications for dexamethasone loaded GAL-PLGA nanoparticles

| | Target | Justification |
|----------------------------------|--|---|
| QTPP elements | | |
| Therapeutic indication | Ant-inflammatory | Easy access to the intestine (colon) through oral route to combat IBD |
| Target patient population | No age specifications | Safer for all age groups |
| Route of administration | Oral | Ease of administration, and it is the safest and natural route to target intestinal mucosa locally |
| Site of activity | Local effect: target macrophages in the inflamed intestine | Accumulation in intestinal tissue, avoid systemic side effects |
| Dosage form design | Freeze-dried nanoparticles, reconstituted nanoparticulate suspension | Solid lyophilized dosage form enhanced formulation's handling and stability; Freeze-dried nano-formulation reconstituted into nano-suspension before use |
| CQAs | | |
| Particle size /surface area (SA) | Increased surface area; nanosized range (~200 nm) | Large specific surface area, increased dissolution rate, enhanced solubility, enhanced eEPR effect, lesser GIT clearance. Nanosized particles have increased uptake by colon epithelial cells |
| Encapsulation efficiency (EE) | Must be greater than 50% | Enough drug should be entrapped within nanoparticles to demonstrate the suitability of a nanocarrier system for better therapeutic efficacy |
| Zeta potential | Negative | Characteristic of polymer, charge indicate stability |
| PDI | Must be less than 0.3 | Demonstrate homogeneous distribution |
| Appearance, homogeneity | Whitish dry lyophilized powder (amorphous) Or reconstituted white translucent liquid suspension | The freeze-dried amorphous powder easily dispersed in distilled water to form stable nanosuspension |
| Dissolution | Sustained; at least up to 24 hours | Effective intestinal mucosa absorption and prolonged therapeutic efficacy |

| | | |
|---|---|--|
| Toxicity/irritation | Non-toxic and non-irritative | Nanoformulation must be biocompatible for living tissues; it must have negligible side effects on the intestinal mucosa, GIT, and vital organs. |
| Stability | Physicochemical and conformational stability at room temperature (25°C), when reconstituted | Nanoformulation must remain stable with minimal precipitation, phase separation, aggregation upon standing. It should be easily re-dispersible after prolong storage either in solid form or liquid. It should not be degraded physically or chemically and retain drug content. |
| CPPs | | |
| Emulsification-solvent evaporation method: Solvent evaporation time/temperature | Overnight evaporation (24 hours) at room temperature (25°C) | Evaporation of solvent is critical to obtain nano-sized particles and to eradicate possible solvent associated toxicity |
| Ultrasonication: Sonication time Sonication power Temperature | Enough time to generate a shear force Enough power to breakdown droplets 20-25°C | Time to apply force to reduce particle size; affects EE Shear stress determine particle size and EE Optimal temperature is required, otherwise leads to instability |
| Stirring speed | For homogeneous dispersion and shear force | Facilitates emulsification process, important for stability and particle size |
| CMAs | | |
| Drug nature | Hydrophilic/lipophilic | To choose solvents to solubilize drug and to develop nanoparticle preparation method, determine EE |
| Ligand: Ligand-polymer bond Ligand-polymer ratio | Covalent linkage 1:20 | Chemical synthesis to effectively adjoin ligand moiety and for effective targeting Established from literature |
| Organic phase: Polymer Type Drug to Polymer Ratio Polymer mol. wt. | Hydrophobic Optimum 7000-17000 | PLGA (50:50) have hydrophobic nature, soluble in organic solvents Established according to the literature; determines EE and drug loading capacity Established in literature and purchasing specification sheet |
| Aqueous phase: Surfactant type Surfactant concentration | PVA, amphiphilic 1-3% | Emulsifier, nanoparticles stabilizer, prevent aggregation and instability According to the literature |
| Organic to aqueous ratio | Optimum (1:3-1:5) | Preliminary experimental optimization based on the values found in the literature; determines nano-formulation stability and EE |

2.2.4.3. Design of experiment (DOE): Box-Behnken design

The surface response optimization designs are a robust way to develop an experimental setup for statistical modeling and estimating the effect of different experimental parameters. After initial risk assessment, the three most influential independent variables were selected including surfactant concentration (A_1), stirring speed (A_2), and sonication time (A_3). Each independent variable has three different levels, -1, 0, and +1

corresponding to lower, middle, and higher values respectively, as described in Table 2. 3. The values of the levels are based on preliminary studies and literature. In this design, the assessed responses or dependent variables are particle size (Z_1), zeta potential (Z_2), and polydispersity index (PDI) (Z_3). Equation 2 describes the polynomial equation for the effect estimation of independent variables on dependent variables:

$$Z = b_0 + b_1A_1 + b_2A_2 + b_3A_3 + b_{12}A_1A_2 + b_{13}A_1A_3 + b_{23}A_2A_3 + b_{11}A_1^2 + b_{22}A_2^2 + b_{33}A_3^2 \dots\dots\dots 2$$

Where Z is the dependent variable, b_0 is the intercept, b_A is the regression coefficient for effect estimate of the independent variable on Z and b_{XY} , b_X^2 corresponds to the interaction of independent variables. Further, ANOVA was applied to determine the statistical significance of independent variables ($\alpha=0.05$) and the adequacy of the regression model. A 3D response surface plots were obtained to ascertain the correlation between two independent variables and the response variable. Moreover, Pareto plot analysis clarified the significance of each independent variable for the selected response variable.

2.2.4.4. Experimental design validation and optimization

The experimental design generated predicted values for response variables which were compared with the experimental values for confirmation. The validation of the experimental design was further conducted by obtaining a desirability profile through the analysis of optimum values of independent variables to produce desirable outcomes (Islam *et al.*, 2012). The most fitted values and the combination of independent variables were experimentally replicated in triplicate to validate the design. The optimized formulation proceeded for further characterization.

Table 2. 3: Studied independent variables at three different levels (-1, 0, +1) in 3³ Box-Behnken DOE to prepare GAL-PLGA nanoparticles of the desirable criteria

| Selected parameters and their levels optimized through 3 ³ Box-Behnken design | | | |
|--|------------------------|------------|-----------|
| Independent variables | Coded levels | | |
| | Low (-1) | Medium (0) | High (+1) |
| A ₁ : Surfactant conc. (%) | 1 | 2 | 3 |
| A ₂ : Stirring speed (rpm) | 1500 | 2000 | 2500 |
| A ₃ : Sonication time (sec) | 30 | 60 | 90 |
| Response variables | Desired criteria | | |
| Y ₁ : Particle size (nm) | Minimum (about 100 nm) | | |
| Y ₂ : Zeta potential (mV) | Minimum | | |
| Y ₃ : PDI | Minimum (> 0) | | |

2.2.5. Physicochemical characterization

Nanoparticles were characterized for particle size, zeta potential, and PDI using Malvern Zetasizer (Malvern Instruments, Worcestershire, UK) and scanning electron microscopy (SEM, Hitachi S4700, Hitachi Scientific Ltd., Tokyo, Japan). Further, drug entrapment and drug loading within polymeric nanoparticles were determined through free drug quantification in the supernatant (Zeeshan *et al.*, 2019b) and through solvent extraction from freeze-dried nanoparticles. Briefly, 10 mg of dried drug-loaded nanoparticles were dispersed in ethyl acetate-acetone mixture, dissolved for 4 hours, and then stirred to evaporate. Thereafter, the obtained residue was dispersed in methanol and left overnight on constant stirring. Then the mixture was centrifuged, and the supernatant was collected to quantify the drug under Agilent 8453 UV spectrophotometer (Agilent Technologies, USA) at 240 nm. All experiments were conducted in triplicate and expressed as mean \pm SD.

2.2.6. Thermogravimetric (TGA) analysis

The thermogravimetric analyzer (TGA) (Mettler-Toledo GmbH, Gießen, Germany) investigated the weight loss of dexamethasone, drug-loaded PLGA nanoparticles, and GAL-PLGA nanoparticles on subsequent temperature elevations. About 5 mg dried sample was placed on a platinum pan and gradually heated from 30°C to 800°C at a heating rate of 10°C/minute under inert nitrogen control.

2.2.7. X-ray powder diffraction (XPRD) analysis

XPRD analysis of pure drug, drug loaded PLGA, GAL-PLGA nanoparticles, and the respective polymers was conducted to find out the crystalline or amorphous nature of the drug inside the nanoparticles using Bruker D8 Advance X-ray powder diffractometer (Bruker®AXS GmbH, Germany). Mounted samples were irradiated with Cu K α source at a wavelength of 1.5406 Å, voltage of 40 kV, and current supply of 40 mA. The XPRD patterns were acquired from 3° to 40° 2 θ through VANTEC-1 detector.

2.2.8. Fourier-transformed Infrared Spectroscopic (FTIR) of excipients and formulation

The molecular vibrations of dried formulation ingredients (dexamethasone, PLGA, GAL-PLGA polymer), their physical mixture, and lyophilized PLGA and GAL-PLGA nanoparticles were investigated to establish drug-polymer compatibility using ATR Cary 630 FTIR (Agilent technologies, USA). A small quantity of powdered sample was placed on the crystal of ATR diamond and FTIR spectra were recorded over the range of 400-4000 cm⁻¹ wavenumber.

2.2.9. In vitro drug release

In vitro release of dexamethasone from PLGA and GAL-PLGA nanoparticles was studied through the dialysis membrane diffusion technique under a controlled environment. Dexa-PLGA or Dexa-GAL-PLGA nanoparticles were loaded in a presoaked dialysis membrane (MW cut-off 12-14 kDa, Millipore Sigma Aldrich (Sigma-Aldrich, Germany) and then sealed from both ends. Immediately, each dialysis bag was immersed in a simulated gastric fluid (0.1N HCl, 2g NaCl per 1L) at a pH of 1.2 in a shaker bath set at 100 rpm at 37°C for 2 hours. Samples were withdrawn after every half an hour and sink conditions were maintained after sampling. Since the normal gastric transit time of the stomach is 2 hours, therefore, the medium was changed to simulated intestinal fluid (pH 7.4) by adding Na₂HPO₄·2H₂O and KH₂PO₄ salts, and pH was adjusted to 7.4 with few drops of 0.1N NaOH (Ali *et al.*, 2014). 0.1% Tween 80 was incorporated as a solubilizing agent, and to achieve sink conditions. Thereafter, the study was continued till 48 hours, and 1 ml aliquots were withdrawn after pre-determined intervals with the replacement of fresh buffer. The samples were analyzed for the drug quantification under UV spectrophotometer at a wavelength of

240 nm and calculations were performed to determine % cumulative release \pm SD (n=3).

Drug release kinetics and mechanism from the nanoparticles were explored by the application of different mathematical models using the DDSolver program (Zhang *et al.*, 2010). The best-fitted model have the highest coefficient of determination (R^2), adjusted coefficient of determination ($\text{adj-}R^2$), model selection criteria (MSC), and lowest Akaike information criterion (AIC) (Zhang *et al.*, 2010).

2.2.10. In vitro hemocompatibility studies

Blood was collected from the healthy volunteers with informed consent, according to standard blood drawing protocol (Organization, 2010). Further, only healthy individuals who met the following criteria were considered for blood withdrawal:

- Healthy, weight above 60 kg, Hemoglobin > 13.5, non-pregnant, normal blood pressure, no blood-borne disease, no communicable disease, normal body temperature.
- Secondly, the amount of blood withdrawn was just 3 ml per 60 kg individual once, which is far less than the standard IRB protocol (i.e., 5 ml/kg in 24 hours), therefore, no special approval from the institutional board was required.

To ascertain the hemocompatibility of Dexa-PLGA and Dexa-GAL-PLGA nanoparticles, fresh human blood from the young healthy volunteers (with consent) was collected in the EDTA tube. Blood samples were purified and diluted with Dulbecco phosphate-buffered saline (PBS) (1:9). Thereafter, various concentrations of nano-formulations (25, 50, and 100 $\mu\text{g/ml}$) were suspended in 1 mL of diluted blood and incubated at 37°C. While 1% Triton-X treated diluted blood sample served as a positive control and PBS as a negative control. After 24 hours, samples were centrifuged at 3000 rpm for 10 min and supernatants were collected to analyze free hemoglobin release using a microplate reader (Perkin Elmer, USA) at a wavelength of 540 nm. % RBC hemolysis was calculated using equation 3:

$$\% \text{ hemolysis} = \frac{\text{sample absorbance} - \text{negative absorbance}}{\text{positive absorbance} - \text{negative absorbance}} \times 100 \dots \dots \dots 3$$

2.2.11. In vitro cell-based studies

2.2.11.1. *Isolation and purification of murine derived peritoneal macrophages and colon cells*

The peritoneal cavity is an enriched source of adhered macrophages, therefore, provides abundant macrophages for the ex vivo experimental studies, mimicking in vivo environment. Thioglycolate elicited macrophages were extracted from the peritoneum of BALB/c mice, according to the protocol (Zhang *et al.*, 2008; Lu and Varley, 2013), washed and grown at 37°C under 5% CO₂ in cRPMI media containing 10% FBS, essential amino acids, antibiotics (penicillin, streptomycin), and 25mM HEPES buffer. Next, colon tissues were excised from healthy mice and treated as per protocol with modifications (Lin *et al.*, 2014). In brief, cells were immersed in HEPES buffer solution with 1% FBS and debris was removed. Colon tissue was fragmented into smaller fragments of about 1 cm and homogenized at 37°C for 3-5 minutes, the resulting single-cell suspensions were centrifuged at 10,000 rpm at 4°C. The obtained pellet was washed thrice with PBS and suspended. The cells were cultured as mentioned above.

2.2.11.2. *Cytotoxicity assay on murine macrophages and colon cells*

In vitro cytotoxicity of pure drug, Dexamethasone-PLGA, and Dexamethasone-GAL-PLGA nanoparticles in the concentration ranging from 25-100 µg/mL was assessed against murine macrophages and murine isolated colon cells using MTT assay. The cells were seeded in a 96-well plate at a density of 5×10^3 cells/well in RPMI-1640 media supplemented with 10% FBS and 1% antibiotics and incubated at 37°C in a humidified 5% CO₂ atmosphere for 24 hours. Then, different concentrations of samples were added to both types of cells in triplicate and incubated for 24 or 48 hours. Thereafter, the culture media was aspirated off and replaced with fresh media with the addition of MTT solution (500 µg/ml) to each well. After 4 hours of incubation, the media was switched with 100 µL DMSO to solubilize the formazan crystals produced from the mitochondrial reduction of MTT. The optical density was recorded at 540 nm using a microplate reader (Perkin Elmer, USA). Untreated cells were served as control. Cell viability was calculated.

2.2.11.3. Cellular uptake studies

Murine-derived peritoneal macrophages were seeded into a 12-well plate at a density of 5×10^3 on a growth medium RPMI-1640 under humidified 5% CO₂ and incubated for 24 hours. Subsequently, free rhodamine-B, rhodamine-B loaded PLGA and GAL-PLGA nanoparticles were added to the medium, incubated for 2 hours, and then washed with pre-warmed PBS and fixed with paraformaldehyde (4%) for 10 min. The cells were mounted on a glass slide to be visualized under fluorescent microscopy. For colon cells, fluorescein-loaded PLGA and GAL-PLGA nanoparticles were used with the same procedure.

2.2.11.4. Elucidation of galactose mediated cell uptake by murine macrophages

Since the conjugation of D-galactose to PLGA make it a more favorable candidate to mediated macrophage MGL-2 (CD301b) driven uptake of GAL-PLGA nanoparticles (Denda-Nagai *et al.*, 2010). Therefore, macrophage cells were pre-treated with D-galactose before the addition of dye loaded GAL-PLGA nanoparticles to competitively inhibit GAL-PLGA nanoparticles uptake.

2.2.12. In vivo preliminary studies to understand nanoparticles behavior in the inflammation

Male BALB/C mice (weight = 25 g) were administered with 3% DSS in drinking water for seven days for the induction of UC. The mice were kept under standard laboratory conditions according to the approved protocols for care and use of lab animals, QAU bioethical codes, based on NIH guidelines. The number of mice was considered based on experimental requirement and principle of 3Rs (replace-refined-reduced) to reduce unnecessary harm to the animals (Festing and Altman, 2002). Daily clinical parameters and indices were observed to ensure the development of the disease.

2.2.13. Harvesting of inflammation led macrophages for flow cytometry analysis

Pro-inflammatory macrophages were recruited to the inflamed tissues, therefore, activated macrophages infiltrated the colon tissues because of DSS-induced inflammation of the colon. The inflamed model completely developed after 7 days; thus, mice were orally administered with fluorescein dye loaded GAL-PLGA nanoparticles on day 7. Thereafter, mice were euthanized after 6 hours, based on the

average transit time of oral formulation to reach the colon (Zeeshan *et al.*, 2019a). Colon tissues were isolated with exudates. The recruited activated macrophages in the colon lamina propria were harvested and purified according to the previous protocol with little modifications (Uronen-Hansson *et al.*, 2014). Cells were washed, centrifuged, resuspended in PBS. Afterward, cells were processed and analyzed to assess cellular uptake of dye loaded nanoparticles under flow cytometry system (FCS) (BD FACSTM, US).

2.2.14. Accumulation of nano-formulation in the visceral organs and colon under inflammation

Free drug suspension and Dexa-GAL-PLGA nanoparticles (drug dose = 10 mg/kg) were orally administered to the DSS induced colitis mice (n=3/group). After 6 hours, mice were euthanized and visceral organs including the stomach, small intestine, colon, spleen, liver, and kidney were excised. Tissue homogenates were prepared, and the drug was extracted overnight from the tissues in PBS and methanol (9:1) mixture. Thereafter, the supernatant was collected through centrifugation and then analyzed spectroscopically ($\lambda = 240$ nm) for the drug quantification. Tissues excised from the mice treated with blank nanoparticles were considered as control.

PART-I (SECTION-B)

Further, the GAL-PLGA (GP) nano-formulation was coated with pH-sensitive polymer for more specific targeting in IBD.

2.2.15. Preparation and characterization of GP/ES100, GP/Pu Nanoparticles (NPs), and G-PLGA/ES/Pu NCs

GP/ES100 NPs were prepared by dissolving Dexa (1 mg) and G-PLGA (10 mg) in ethyl acetate and adding the organic solution into an aqueous phase containing ES100, 2% PVA, methanol and 0.1N NaOH in a dropwise manner, followed by strenuous sonication for about 1 minute and kept stirred for 2-4 hours. Stirring was continued overnight for the evaporation of organic solvents. For GP/Pu NPs, the aqueous phase was replaced with Pu (20 mg) and 2% PVA only.

And GP/ES/Pu NCs were fabricated in the same way except for the aqueous phase, which contains both ES100, and Pu in an optimized ratio with 2% PVA and 0.1N NaOH

solution. The aqueous phase was devoid of methanol because highly soluble pullulan quickly precipitated in methanol, while ES100 was still able to dissolve in 0.1N NaOH solution. The formed O/W nanoemulsion was kept stirred overnight for the organic solvent evaporation. Afterward, GP/ES100, GP/Pu or GP/ES/Pu NCs were centrifuged (13500 rpm, 40 min) for the removal of untrapped drug and residual solvents. Then the obtained pellets were mixed with cryoprotectant (5% trehalose) for the freeze-drying at -80°C. Finally, dried white amorphous powder of GP/ES/Pu NCs were acquired and further used for characterization. Rhodamine-B dye loaded NCs were prepared using the same methodology.

2.2.16. Physicochemical Characterization

Detailed methods for physicochemical characterization (particle size, zeta potential, SEM, TGA, XPRD, FTIR) of nanocargoes can be found in Method sections 2.2.5, 2.2.6, 2.2.7, and 2.2.8. Drug entrapment efficiency (%) was measured through supernatant collected after nanocargoes washing and quantified at 240 nm under RP-HPLC as described above. For the confirmation of actual drug content (%) loaded inside the freeze-dried nanocargoes, about 2.5 mg of particles were dispersed in acetone, stirred for 2-4 hours, and then evaporated to distort nanocargoes. Afterward, the obtained residue was dissolved in acetonitrile: PBS (pH 5.0) solvent mixture to extract the drug overnight and then quantified under HPLC.

2.2.17. Drug Release and Kinetics of GP/ES100, GP/Pu and GP/ES/Pu NCs

Drug release from GP/ES100, GP/Pu, and GP/ES/Pu NCs were estimated through the dialysis membrane diffusion technique. Briefly, NCs equivalent to 1 mg Dexamethasone drug were loaded into the dialysis bag (MW cut off = 12-14 kDa, Sigma Aldrich, Germany) separately and then immediately clamped from both ends. The dialysis bags were placed in 30 ml of simulated gastric fluid (SGF), pH 1.2, in a shaker bath and continued to shake till 2 hours at 37°C. Samples were withdrawn and replaced with fresh buffer at a regular interval. Thereafter, the medium was replaced by phosphate buffer solution, pH 4.5 to mimic acidic conditions of the fed stomach and upper small intestine regions and the release was continued for another 2 hours. Afterward, dissolution media was changed with simulated intestinal fluid (pH 7.4) with or without cecal contents (5% w/v) (Oshi *et al.*, 2018), to match large intestine conditions, and the drug release study was continued till 72 hours with sampling at regular time-period. The time slot for the

pH change was based on average GIT transit time from the stomach to the small intestine and large intestine (Ali *et al.*, 2016). Drug concentration in the samples was quantified at 240 nm and % drug release was calculated (n=3). Drug release kinetics and mechanism were explored through the application of mathematical models using the DDSolver program (Zhang *et al.*, 2010).

2.2.18. Mucin Binding Study

The extent of mucin-nanocargoes interaction was observed through UV spectroscopic analysis at 255 nm, as reported (Yin *et al.*, 2006). Mucin binding efficiency was calculated through formula in Equation 4:

$$\% \text{ Mucin binding} = \frac{\text{Total mucin} - \text{Free mucin}}{\text{Total mucin}} \times 100 \dots\dots\dots 4$$

Next, the interaction was additionally investigated through particle size and zeta potential analysis using Malvern zetasizer. Further, viscoelastic effects of mucin-nanocargoes binding were studied through rheological analysis under cone-plate rheometer (CE AMETEK Brookfield, USA), by varying shear force (Sohail *et al.*, 2016). The calculated parameter was rheological synergism ($\Delta\eta$), described under Equation 5:

$$\Delta\eta = \eta_{mix} - (\eta_{nc} + \eta_{muc}) \dots\dots\dots 5$$

Where η_{mix} is mucin-formulation mix apparent viscosity, η_{nc} is for the apparent viscosity of studied nanocargoes dispersion at a concentration equal to that of the mucin-polymer mix and η_{muc} is the mucin dispersion apparent viscosity equivalent to mucin concentration in the mucin-polymer mix.

2.2.19. In vitro Biocompatibility Studies

The methods of hemolysis Assay, cellular biocompatibility (MTT assay), and in vitro cell uptake assay for the nanocargoes are documented in Methods sections 2.2.10 and 2.2.11.

2.2.20. In vitro Permeability Assay

To determine in vitro permeation and retention of Rhodamine-B dye loaded GP/ES/Pu (Rho-GP/ES/Pu) NCs, 5 cm long goat intestine was taken from the slaughterhouse, washed thoroughly with PBS to remove mucous and luminal content. Thereafter, 1 mL

of Rho-GP/ES/Pu nanosuspension was instilled into the intestine lumen, and both ends of the intestine were secured and closed. The intestinal sac was dipped into the compartment filled with 30 mL PBS (pH 7.4), maintained at a temperature of $37 \pm 1^\circ\text{C}$, and shaken at 50 rpm under a bath shaker. 1 mL samples were withdrawn from the outer compartment at a periodic interval of 2, 4, 6, and 8 hours and replaced with fresh buffer. Samples were quantified under UV-Vis spectrometer at 560 nm to estimate the quantity of dye permeated across the intestine at different time points. Meanwhile, intestine tissues were additionally collected at regular time points. Dye was extracted from the collected tissues and quantified under a UV-Vis spectrophotometer to determine dye retention in the intestinal tissue. The concentration of dye retention is the estimation of the nanocargoes localization in the intestine. Furthermore, the obtained tissues were spliced using a microtome and visualized under a fluorescent microscope to study dye retention. At all time points, free Rhodamine-B control was run to assess the differences in retention and permeability of the free and entrapped dye.

2.3. Animal Studies

2.3.1. Development of DSS induced colitis model for in vivo studies

Male BALB/c mice, 3-4 weeks old, were kept under protocols prescribed for care and use of laboratory animals under QAU, Islamabad bioethical committee, and NIH. UC was developed in the mice through administration of 3% w/v DSS in the drinking water for 7 days. Mice were daily observed for the development of colitis through clinical symptoms like a decline in body weight, rectal bleeding, diarrhea, and signs of anxiety.

2.3.2. NCs Targeting Index and Localization Capacity in the Inflamed Colon

Drug concentration was quantified in the stomach, small intestine, colon, spleen, and the major organs to demonstrate NCs residence in the respective tissues. DSS treated colitis mice (n=5/ group) were administered with Dexa-GP/ES/Pu NCs or with a plain Dexa drug through oral gavage at the same dose of drug separately. After 6 hours of intake, mice were euthanized and GI major segments (stomach, small intestine, and colon) with luminal contents were removed, cleaned, homogenized in phosphate buffer saline (PBS), and stirred overnight in PBS: methanol (9:1) solvent mixture to extract the drug from the tissues. Then the sample mixture was centrifuged (13500 rpm) and the collected supernatant was spectroscopically analyzed to quantify drug concentration

($\lambda = 240$ nm). Samples excised from mice administered with blank nanocargoes were served as a control to eradicate the influence of interfering species during quantification. Other vital organs including the spleen, liver and kidney were treated in the same manner to determine drug amount. NCs targeting index to the colon is estimated as the ratio of the concentration of drug released from nanocargoes in the colon to the drug concentration from free drug solution in the mice colon after oral administration of Dexa-GP/ES/Pu NCs or free Dexa solution respectively (Targeting index = $C_{\text{nanocargoes}}/C_{\text{free drug}}$). Higher the value, the greater the organ targeting efficiency (Gao *et al.*, 2016). Further, NCs selectivity index was determined as a ratio of drug concentration in the targeted organ (colon) to the concentration in the blood plasma after oral administration of Dexa-GP/ES/Pu NCs to the DSS induced colitis mice (Selectivity index of nanocargoes = $C_{\text{colon}}/C_{\text{plasma}}$) (Gao *et al.*, 2016).

After 24 hours of administration of plain Dexa or Dex-GP/ES/Pu NCs, mice were anesthetized and blood was collected through a cardiac puncture in EDTA tube. The collected blood was centrifuged (10,000 rpm) for 10 minutes to separate the plasma, then treated with 1 mL ethyl acetate to extract the drug overnight at optimal temperature. Thereafter, the purified organic phase was collected by centrifugation. Then it was dried, the residue was reconstituted with acetonitrile: PBS (pH 5.0) (32:68) mobile phase solvents to determine drug concentration under HPLC, as described above.

2.3.3. Flow cytometry

Orally treated DSS induced mice with nanocargoes were euthanized after 6 hours of intake, and colon tissues were excised, washed and macrophages were harvested according to the reported protocol (Uronen-Hansson *et al.*, 2014). Harvested cells were centrifuged, suspended in buffer, and processed for uptake analysis under flowcytometer (BD, FACSTM, US).

2.3.4. Therapeutic intervention of DSS induced colitis mice

To investigate the therapeutic effectiveness of Dex-GP/ES/Pu NCs against DSS-induced colitis, mice were randomly distributed following protocols of minimum harm and ARRIVE guidelines into 4 groups (n=5/ group). The number of subjects was selected according to the animal resource equation (Arifin and Zahiruddin, 2017) and considering ethical protocols of minimum harm (3Rs) (Hubrecht and Carter, 2019).

Group I (Normal control): Normal healthy mice, received drinking water

Group II (DSS): DSS-induced colitis mice (disease control), received 3% DSS in drinking water for 7 days

Group III (Dexa): DSS-induced colitis mice after 7 days of disease development received Dexa drug solution (dose= 5 mg/kg) through oral gavage, from day 7-14.

Group IV (Dex-GP/ES/Pu NCs): DSS-induced colitis mice after 7 days of disease development treated with Dex-GP/ES/Pu NCs (at Dexa dose equivalent to 5 mg/kg) through oral gavage, from day 7-14.

2.3.5. Assessment of progression and intervention of colitis thorough morphological parameters and mortality rate

Disease progression was monitored through physical manifestations including bodyweight loss, rectal bleeding, and stool consistency and cumulatively scored as disease activity index (DAI). DAI was calculated according to the reported procedure (Zeeshan *et al.*, 2019b). Further, inflammation indices like colon morphometrics, colon weight to length ratio, spleen weight were estimated to explore the extent of disease. Mice mortality rate in each group was assessed for estimating mice survival after nanocargoes treatment.

2.3.6. Evaluation of colonic vascular integrity

Vascular integrity in IBD is compromised because of altered endothelial function in inflammation (Jerkic *et al.*, 2010). Vascular permeation was assessed through Evans blue assay on the last day of the experiment. In short, mice from all groups including healthy, DSS induced colitis, plain drug and nanocargoes treated mice (n=3) were injected with 100 μ L of Evans blue dye (2% solution in PBS) through the tail vein. 2 hours post-administration, mice were euthanized and perfused with 5 mL normal saline. Colons were isolated, cleaned, and dried at 50°C for 24 hours. The weight of dried colon was recorded. Thereafter, Evans blue was extracted from the colon using dimethylformamide at 50-60°C for 24 hours and quantified at 620 nm through spectroscopic analysis. The results were expressed as a concentration of Evans blue per gram tissue weight (n = 3).

2.3.7. Histopathological assessment

Small colon segments from all groups were fixed in 10% buffered formalin, paraffin-embedded, thin sliced with a microtome and stained with H & E. Afterward, stained samples were observed under microscope and assessed on a scale of 0-12, based on inflammation extent and mucosal injury (Erben *et al.*, 2014).

2.3.8. Immunohistochemistry

Dexa loaded GP/ES100/Pullulan NCs mechanistic action on the expression of NF- κ B, and COX-2 was evaluated through immunohistochemistry, according to the reported protocol (Sana *et al.*, 2021; Khan *et al.*, 2019). Briefly, paraffin-embedded colon tissues were rehydrated through xylene and graded ethanol, followed by quenching with 3% H₂O₂ and incubation with 5% normal goat serum for 20 minutes. Then incubated with mouse anti-COX-2 and anti-NF- κ B antibodies (Santa Cruz Biotechnology, Inc, USA) overnight. The next day, slides were treated with biotinylated goat anti-mouse secondary antibodies and ABC reagents (SCBT, USA); thereafter swept with 0.1M PBS and stained with diaminobenzidine (DAB) (Sigma Aldrich, St. Louis, USA). Quantitative expression of COX-2 and NF- κ B was computed through ImageJ software (NIH, USA).

2.3.9. ATR-FTIR analysis of the colon tissues

Excised dried colon tissues were sliced into thin pieces and mounted on the specimen holder (Baker *et al.*, 2014). Subsequently, tissues were analyzed in the range of 400-4000 cm⁻¹ wavenumber under ATR-FTIR to detect structural and functional changes in the colon before and after disease induction and nanoparticle treatment.

2.3.10. Evaluation of colon microbial content

To determine colon microflora alterations after induction of colitis and to elucidate the effect of nanoparticle treatment on the restoration of flora, fecal samples from all groups were obtained at the end of the experiment. Bacterial colonies from the feces were incubated in the nutrient agar plate at 37°C; colony forming unit (CFU) were counted after 24 hours using the galaxy 230 colony counter instrument. Results were expressed as log CFU/mL \pm SD (n=3).

2.3.11. Real time-polymerase chain reaction (RT-PCR) analysis for the expression of regulatory, inflammatory, and mechanistic proteins

Expression of proteins that regulates tight junction function (E-Cadherin), and mucosal injury (iNOS) was estimated using RT-PCR analysis. Total RNA was extracted from the resected colon of each mice group using TRIzol[®] reagent (Thermo Fisher Scientific, USA), according to the manufacturer's instructions. Total RNA quantitative and qualitative analysis were performed at 260/280 nm using Nanodrop (Skinit RE 4.1, Thermo Scientific, USA) spectrophotometer. Isolated RNA was converted into cDNA through Viva cDNA synthesis kit (Vivantis cDSK01-050, Vivantis technologies, Malaysia). Expression of target genes was quantified through qRT-PCR using Eva Green qPCR Master mix (Solis Biodyne, Estonia) and Magnetic Induction Cycle PCR (Bio Molecular System, Australia) machine. RT-PCR analysis for all samples run in triplicate and primer pair sequences are listed in Table 2. 4. The gene expression was calculated according to $2^{-\Delta\Delta C_t}$ method.

Table 2. 4: Sequence of primers for the gene of interest

| Gene | Forward primer | Reverse primer |
|----------------|---------------------------|--------------------------|
| iNOS | GGCAGCCTGTGAGACCTTTG | GCATTGGAAGTGAAGCGTTTC |
| E-Cadherin | GGCGCCACCTCGAGAGA | TGTCGACCCGGTGCAATCT T |
| GR-Common | AGCAGTGTGCTTGCTCAGGAGAGGG | GAGAGGCTTGCAGTCCTCATTGAG |
| β -actin | CGGTGGACATTGGTTCTGG | CTGAGGAAGGGCAGAAGTTC |

2.3.12. Pro-Inflammatory cytokines detection through ELISA

Exceeding concentrations of pro-inflammatory cytokines in the tissues is the indicator of inflammation. The amount of pro-inflammatory cytokines, TNF- α , and IL-6 were determined in the excised colon tissues from each mice group using commercially available ELISA kits (eBioscience, Inc., CA, USA) according to the manufacturer's directions.

2.3.13. Biochemical antioxidant assays

Antioxidant protection against oxidative stress in the intestine inflammation was evaluated in all experimental groups. The level of antioxidant enzymes including GSH, GST, and catalase were determined in the colon tissues using Ellman's reagent, 1-

Chloro-2,4-dinitrobenzene (CDNB), and H_2O_2 respectively according to reported procedures (Zeeshan *et al.*, 2019b).

Further, inflammation resulted in a heavy load of reactive oxygen species, therefore the concentration of malondialdehyde (MDA) was determined to assess lipid peroxidation (LPO) using the thiobarbituric acid reaction method at 540 nm (Shal *et al.*, 2021). In addition, nitrite (NO) concentration in the colon was estimated using Griess reagent method (Shal *et al.*, 2021).

Next, estimation of myeloperoxidase (MPO) activity indicated the extent of neutrophil infiltration at the inflamed colon (Chami *et al.*, 2018). MPO activity was determined through the CTAB buffer. Briefly, colon tissues were homogenized in 1 mL of PBS (50 mM, pH 6) and 0.5% CTAB, followed by sonication and freeze-thaw cycles. Then centrifuged at 13500 rpm for 5 min at 4°C, collected supernatant was added to 50 mM PBS (pH 6) containing 0.167 mg/mL of o-dianisidine and 0.0005% H_2O_2 , and absorbance was measured at 460 nm using a microplate spectrophotometric reader.

2.3.14. Assessment of hematological parameters

Hematologic analysis was executed to assess variations in the blood parameters after disease induction and to find out the effect of treatment at the end. Complete blood cell count (CBC) and total leukocyte count (TLC) were determined through the blood derived from the cardiac puncture of the mice in each experimental group and collected in the EDTA tube. Moreover, C-Reactive protein (CRP) is a marker of inflammation (Sproston and Ashworth, 2018); therefore, evaluation of CRP in the blood serum indicates the extent of inflammation. The effect of drug-loaded nanocargoes on the blood sugar concentrations was investigated using EasyGluco™ (Infopia, Korea) test strips.

2.3.15. In vivo biocompatibility and toxicity investigations of Dexa-GP/ES100/Pu NCs

BALB/c healthy male mice, weighing 25-30 g, were tested under pathogen-free standard laboratory conditions with *ad libitum* access to food and water. Mice were orally administered with Dexa-GP/ES/Pu NCs (drug dose = 5 mg/kg) for 7 days to explore the possible toxic effects of nanocargoes inside the living system. A control group of mice received plain water only. Mice were daily assessed for acute toxicity

symptoms including bodyweight loss, mortality rate, and behavior patterns like anxious or depressive behavior, lethargy, lacrimation, pain, disturbance in food and water intake, sleep, and defecation. After 7 days, mice were euthanized and assessed for the organ to body weight ratio, histopathological investigations of the vital organs, and biochemical hematological parameters.

Since colon is the major targeting organ, therefore, colon tissues were evaluated for the effect of nanocargoes on cellular death through apoptotic study under flow cytometer (BD, FACS™, USA) using Annexin-V and propidium iodide dyes. The single cell suspension was analyzed for viability, apoptosis, and necrosis with FACScan using CellQuest software (BD, Bioscience, San Jose, CA, USA).

PART-II (SECTION A)

Note: Part-II has two sections, A and B. Section A describes Tofacitinib-citrate (Tofa) loaded PLGA/transferrin nanocarriers (Tofa-P/tfr NCs). And section B describes all experiments for ncoated and ES100 coated Tofa loaded lipidic-PLGA/transferrin nanoshells (Tofa-LP/tfr NSh and Tofa-LP/tfr/ES NSh, respectively).

Section A: Tofa-P/tfr NCs

2.4. HPLC Method for Tofa

HPLC analysis of Tofa was performed through the isocratic method using reversed-phase Agilent HPLC (Agilent technologies 1200 series). The mobile phase consisting of 10mM ammonium acetate (pH 5) and acetonitrile (70:30, v/v), flows at a rate of 1.0 mL/minute. Tofa stock solution was prepared in the mobile phase at a concentration of 1mg/mL, then various dilutions were prepared in the range of 1.5625-100 µg/mL for a standard curve. The volume of injection for the standard or samples was 20 µL and HPLC was assisted with a UV detector that operates at a wavelength of 287 nm. C18 reverse-phase column (250 × 4.6 mm, 5 µm pore size; supelcosil LC-1, Supelco) was used for chromatographic separation of Tofa, which was maintained at a temperature of 35°C. The method proved to be linear with R² value of 0.9994 and obtained a retention time of 9.035 minutes.

Another HPLC method was developed for the quantification of Tofa using reversed phased Agilent HPLC (Agilent 1260 Infinity II series), assisted with C18 phenomene Luna column (150 mm × 4.6 mm, 0.3 um pore size), maintained at 30°C. The mobile

phase was constituted with Millipore water and Acetonitrile (70:30). The method was isocratic, with the similar conditions. Calibration curve was obtained at a concentration of 0.78125-100 $\mu\text{g/mL}$ with a retention time of 5-5.19 min ($R^2 = 0.9998$).

2.5. Preparation of Tofa Loaded PLGA/tfr Nanocarriers (Tofa-P/tfr NCs)

To prepare tfr based polymeric nanocarriers, several procedures were tested to get the maximum amount of adsorbed tfr on the nanocarriers including chemical conjugation and physical adsorption methods. To prepare Tofa-P/tfr NCs with good stability, particle size, and tfr adsorption, the following methods were tried:

- i. The standard method of tfr adsorption on PLGA NCs: This method is the standard method to prepare PLGA/tfr nanocarriers (Frasco *et al.*, 2015). According to this method, blank PLGA nanocarriers were developed by a simple O/W emulsion method. Once PLGA nanosuspension was centrifuged (13500 rpm, 35 minutes) and pellet of purified nanocarriers was obtained, then it was re-dispersed in tfr-HEPES solution (1 mg/mL) and stirred overnight for the adsorption of tfr. The next day, PLGA/tfr nanosuspension was washed and freeze-dried.
- ii. Tfr adsorption during emulsification: The standard method was modified. In this method, PLGA was dissolved in organic solvent and then added dropwise into the aqueous solution comprising 2% PVA solution and tfr-HEPES solution. Then probe sonicated to emulsify the two phases and kept stirred for 4-8 hours. Afterward, solvent was evaporated overnight with stirring. Therefore, tfr adsorbed to the PLGA surface during the formation of nano-emulsion.
- iii. Chemical conjugation of tfr to PLGA NCs: At first PLGA NCs were prepared, and then dispersed in PBS (pH 5.5, 100mM) containing EDC/NHS (400mM/100mM). The reaction was conducted for 1 hour in the dark at 15°C. Afterward, spin it (13000 rpm, 30 min) thrice to obtain a purified pellet. The activated nanocarrier pellet was added to PBS (pH 7.4) containing tfr (1 mg) and stirred for 8 hours for the conjugation of tfr to the nanocarriers. Then centrifuged and freeze-dried to get purified PLGA/tfr NCs.

After selection of method, the following procedure is adopted:

At first, Tofa (2 mg) was dissolved in a chloroform/methanol (0.5:1) mixture, followed by the addition of PLGA (10 mg). The formed organic solution was added into the aqueous solution of 1% PVA (3 mL) and tfr-HEPES solution (1 mg/mL), then homogenized at 13500 rpm for 3 minutes. Stirred overnight to evaporate organic solvents and then the prepared Tofa-PLGA/tfr nanosuspension was washed through centrifugation (13500, 40 minutes) and then freeze-dried using 5% trehalose as a cryoprotectant to form Tofa-PLGA/tfr nanocarriers. The process and formulation parameters were studied and optimized for better quality nanocarriers. The same procedure was opted to prepare Tofa-PLGA nanocarrier without tfr-HEPES solution in the aqueous phase and for Tofa-PLGA/BSA nanocarriers, tfr was replaced with BSA.

The preliminary considerations including method selection and organic solvent screening etc. for the preparation of Tofa-P/tfr NCs were conducted through QbD based approach. The quality target product profile (QTPP) was mentioned in Table 2. 5, indicating major parameters, their role, and outcomes. The interaction of QTPPs and critical material and process parameters (CMAs/CPPs) with critical quality attributes (CQAs)) was evaluated through risk-based assessment using Lean QbD software[®] (QbD works LLC, Fremont, USA) on a scale of 3-levels (low, medium, high). Further, the most influential variables were optimized using Box-Behnken 3³ design using STATISTICA[®] 10.0 software. The studied independent variables with their levels (-1, 0, +1) and the dependent output variables with desired criteria are mentioned in Table 2. 6. 3³ Box-Behnken design provided various experimental runs of the most affecting independent variables including tfr concentration (A), drug concentration (B) and surfactant concentration (C). The studied outputs were particle size (X), drug entrapment (Y), and tfr adsorption (Z). Independent variables effect estimate on output is described under polynomial Equation 6:

$$\mathbf{X^* = b_0 + b_1A + b_2B + b_3C + b_{12}AB + b_{13}AC + b_{23}BC + b_{11}A^2 + b_{22}B^2 + b_{33}C^2 \dots 6}$$

X* is any studied dependent variable, b₀ is the intercept, b₁ is the effect estimate of the independent variable on X*. While b_{ab} and b₁₁² are linear and quadratic interactions of independent variables. Each variable was analyzed under ANOVA for statistical significance (α=0.05). Pareto charts and 3D response plots were obtained to understand the effect of each variable on a particular outcome.

To validate the experimental design, the difference between predicted and experimental values was observed using statistical graphs. And a desirability profile was obtained to determine the optimum combination of variables that produced the desired outcome responses (Islam *et al.*, 2012). The best combination of independent variables was considered and experimentally replicated thrice to validate the design.

Table 2. 5: QTPP for Tofa-P/tfr NCs

| | Target | Justification |
|-------------------------------|---|--|
| QTPP elements | | |
| Therapeutic indication | Inflammatory bowel disease (ulcerative colitis) | Targeted delivery of Tofacitinib citrate (Tofa) to combat intestinal inflammation via JAK/STAT inhibition |
| Target patient population | Not specified | Children, adults, old aged |
| Administration | Oral route | Natural and safest route to GIT, Ease of administration with good patient compliance |
| Site of activity | Colon targeted drug delivery; interact with macrophage-surface receptor in the inflamed intestine | Accumulation in intestinal tissue, local therapeutic action, avoid systemic side effects |
| Dosage form design | Freeze dried nanoparticles, reconstituted nanoparticulate suspension | Solid lyophilized dosage form enhanced formulation's handling and stability; Freeze dried nano-formulation reconstituted into nano-suspension prior to use |
| Therapeutic outcome | Ameliorate bowel inflammation by targeted, localized, sustained release of drug | Enhanced uptake by immune cells and macrophages, high residence time and improved immunosuppressant and anti-inflammatory activity |
| CQAs | | |
| Particle size | Increased surface area; nanosized range (100-300 nm) | Large specific surface area, enhanced solubility, enhanced eEPR effect, lesser GIT clearance. Nanosized particles have increased uptake by colon epithelial cells and the immune cells |
| Encapsulation efficiency (EE) | Must be greater than 50% | Enough drug should be entrapped within nanoparticles to demonstrate suitability of nanocarrier system for better therapeutic efficacy |
| Zeta potential | Negative | Characteristic of polymer, charge indicate stability |
| PDI | Must be less than 0.3 | Demonstrate homogeneous distribution |
| Ligand (tfr) adsorption | High | For efficient uptake by TFR-1/CD71 receptor on macrophages and colon epithelial cells |
| Dissolution | pH-dependent, sustained; at least up to 24 hours | Minimum at acidic pH (Gastro-protection), sustained drug release at colon pH that leads to effective intestinal mucosa absorption and prolonged therapeutic efficacy |
| Toxicity/irritation | Non-toxic and non-irritative | Nanoformulation must be biocompatible for living tissues; it must have negligible side effects on intestinal mucosa, GIT, and vital organs. |
| Stability | Physicochemical and conformational stability at room temperature (25°C), when reconstituted | Nanoformulation must remain stable with minimal precipitation, phase separation, aggregation upon standing. It should be easily re-dispersible after prolong storage either in solid form or liquid. It should not be degraded physically or chemically and retain drug content. |
| CPPs | | |

| | | |
|---|---|--|
| Method selection: Mode of tfr adsorption | Modified emulsion evaporation Physical mode of adsorption | The method was modified to ensure maximum tfr adsorption during emulsification |
| Homogenization: Time Speed Temperature | Enough time to generate shear force Enough power to breakdown droplets 0-4°C using ice bath | Time to apply force to reduce particle size; affects EE Shear stress determine particle size and EE Homogenization temperature should be lower to minimize tfr degradation |
| Stirring speed | For homogeneous dispersion and shear force | Facilitates emulsification process, important for stability and particle size |
| CMAs | | |
| Drug properties | Moderately hydrophilic, Soluble in mixture of organic solvents and DMSO | For O/W emulsion: mixture of solvents must be considered to dissolve with PLGA in the internal organic phase |
| Ligand: Ligand-polymer linkage Ligand-polymer ratio | Physical adsorption 0.25-1 to 10 (to be optimized) | Physical method enabled maximum tfr amount on the PLGA nanocarriers Chemical conjugation utilized toxic reagents and have low tfr conjugation Established from literature |
| Organic phase: Core polymer Type Drug to core polymer Ratio Aqueous phase: Type of Surfactant Tfr conc. | Hydrophobic Optimum PVA: hydrophilic (1-3%) Should be optimum | PLGA have hydrophobic nature, soluble in organic solvents Optimized with DOE; determines EE and drug loading capacity The concentration of PVA should be optimum for desired effects, stability, and prevention of aggregation; tfr should be enough for targeting purpose |
| Organic to aqueous ratio | Optimum (1:3-1:5) | Pre-liminary experimental optimization based on the values found in the literature; determines nano- formulation stability and EE |

Table 2. 6: Studied independent variables at three different levels (-1, 0, +1) in 3³ Box-Behnken DOE to prepare Tofa-P/tfr NCs of desired characteristics

| Studied variables at 3 levels, optimized through 3³ Box-Behnken design | | | |
|--|-------------------------|-------------------|------------------|
| Independent variables | Coded levels | | |
| | Low (-1) | Medium (0) | High (+1) |
| A: Tfr conc. (mg) | 0.50 | 0.75 | 1.00 |
| B: Drug conc. (mg) | 0.50 | 1.00 | 2.00 |
| C: Surfactant conc. (%) | 1.00 | 2.00 | 3.00 |
| Response variables | Desired criteria | | |
| X: Particle size (nm) | Minimum | | |
| Y: Drug entrapment (%) | Maximum | | |
| Z: Tfr adsorption (mg) | Maximum | | |

2.6. Physicochemical Characterization

The nano-formulation was characterized for particle size, zeta potential, PDI, and conductivity using Malvern zeta sizer ZS90 (Malvern Instruments, Worcestershire, UK). Particle size distribution and morphology were further assessed through a scanning electron microscope (SEM, Hitachi S4700, Hitachi Scientific Ltd., Tokyo, Japan). Encapsulation efficiency (EE) was determined from the free amount of drug in the supernatant collected during washing of nanocarriers using HPLC method at 287 nm. Further, drug content loaded into the nanocarrier was estimated by dispersing freeze-dried nanocarriers in acetone-methanol (1:1) solution for the dissolution of excipients and polymers for 4 hours, then evaporated to a residue. Afterward acetonitrile: Millipore water mixture (3:7) was added to extract the drug overnight into the solvent system, then centrifuged to remove the residue, and collected supernatant was analyzed under HPLC for drug quantification. The formulas used to determine EE and drug content are mentioned in Equation 7 and 8:

$$\% \text{ EE} = \frac{\text{Total conc.of drug}-\text{Free drug conc.}}{\text{Total conc.of drug}} \times 100 \dots\dots 7$$

$$\text{Drug content } (\mu\text{g}/\text{mg}) = \frac{\text{Drug conc.extracted from nanocarriers}}{\text{Total amount of nanocarrier}} \dots\dots\dots 8$$

2.6.1. Protein quantification

Tfr content was determined through Bradford assay and Nanodrop instrument named as Titertek-Berthold Colibri Microvolume Spectrometer (Berthold Detection Systems GmbH, Germany). Nanodrop measured the adsorption of tfr onto the nanocarriers through quantification of free tfr in the supernatant of the blank nanocarriers at 280/260 nm. Then the amount of adsorbed tfr was calculated using Equation 9.

$$\text{Conc. of tfr adsorbed} = \frac{\text{total conc.of tfr}-\text{free tfr content}}{\text{total conc.of tfr}} \dots\dots\dots 9$$

Further, tfr or BSA protein content was assessed through Bradford assay (Bradford, 1976). To prepare a standard curve, BSA was dissolved in distilled water at various concentrations (7.8125-1000 $\mu\text{g}/\text{mL}$), 100 μL from each BSA dilution was mixed with Bradford reagent (5mL, 5X) and incubated for 5-10 minutes and analyzed at 595 nm. For samples, unbound tfr in the supernatants of the centrifuged nanocarriers were collected (100 μL) and mixed with Bradford reagent (5 mL) separately, followed by

incubation for 5-10 minutes. Then the standards and samples were analyzed under a spectrophotometer at 595 nm.

2.6.2. TGA, ATR-FTIR and XPRD

Effect of temperature elevations (10°C/ minute) on the degradative behavior of the drug and the drug-loaded nanocarriers (2 mg) was evaluated through thermogravimetric analysis (TGA) at 30-450°C using TG analyzer (Mettler-Toledo GmbH, Gießen, Germany).

ATR-FTIR analysis was conducted to determine computability between drug and excipients in the nanoshells using ATR FTIR Cary 630 (Agilent Technologies, USA). XPRD was performed to detect the crystallinity of the drug in the pure form and inside the nanoshells using XPRD instrument (Bruker® AXS GmbH, Germany). Samples were prepared by mounting powders on aluminum stages with leveling of the upper surface to a smooth layer.

2.6.3. DSC

Differential scanning calorimetry (DSC, Mettler-Toledo DSC822e, Gießen, Germany) was performed to determine the physical state of Tofa inside the nanocarriers and the effect of subsequent heating on the degradative pattern of nanocarriers. Briefly, samples were weighed, crimped into an aluminum pan, placed on the holder, and ran at a scanning temperature of -10°C to 220°C and at a heating rate of 10°C/minute under nitrogen purge. An empty pan was served as a reference pan. Data analysis has been done using STARe software (Mettler Toledo Mettler Inc.).

2.7. Drug Release and Kinetics

In vitro drug release studies of Tofa-PLGA NCs and Tofa-P/tfr NCs were carried out using the dialysis bag method at 37±1°C. The release was conducted in simulated gastric fluid (SGF: 0.1N HCl + 2g of NaCl/L) at pH 1.2 for the first two hours and then the bag was shifted to simulated intestinal fluid (SIF, pH 7.4) (Zeeshan *et al.*, 2019b), and release was conducted till 72 hours. The pH values were screened and selected according to natural variations of pH in the GIT (Ali *et al.*, 2014). Samples are withdrawn at pre-determined intervals and replaced with fresh medium aliquots to maintain the sink conditions. Then the samples were analyzed under UV/HPLC at 287 nm and cumulative drug release was calculated (mean ± SD, n=3). Kinetics and

mechanistic of drug release from the nanocarriers were evaluated using the DDSolver program (Zhang *et al.*, 2010).

2.8. Mucin Binding Study

Mucin-nanocarrier interaction was studied to determine mucoadhesion properties. Briefly, 5% artificial mucin (Sigma Aldrich, US) solution in PBS (pH 7.4) was combined with 1% nanosuspension of Tofa-P/tfr NCs, followed by incubation for 4 hours at $37 \pm 0.5^\circ\text{C}$. Then the mixture was assessed for % mucin binding efficiency using UV-Vis spectrophotometer and evaluated for changes in viscosity using DV3T Brookfield rheometer (Brookfield Engineering Laboratories, USA) and particle size distribution using Malvern zeta sizer ZS90 (Malvern Instruments, Worcestershire, UK)

2.9. In Vitro Biocompatibility and Toxicity Studies

2.9.1. Hemolysis assay

Hemo-toxicity was investigated as per the method described in Methods section 2.2.10.

2.9.2. Cellular biocompatibility on murine derived colon cells and macrophages

Mice were given IP injection of 3% thioglycolate medium to elicit macrophages in the peritoneal cavity. The harvested macrophages and murine colon cells were analyzed under MTT assay (See Methods section 2.2.11.1 and 2.2.11.2).

2.9.3. Cellular uptake study

2.9.3.1. Colon and macrophage uptake

The murine-derived colon and macrophages were seeded into 12-well plates in a cRPMI- 1640 media under a controlled humidified CO₂ (5%) environment at 37°C for 24 hours. Afterward, Dye-P/tfr NCs were added into the medium and incubated for 2 hours, then washed and fixed with paraformaldehyde and visualized under a fluorescent microscope (Olympus CX41, Olympus Corporation, Japan) and quantified through ImageJ (NIH, USA) software. Plain dye was used as a control.

2.9.3.2. Macrophage uptake and tfr inhibition assay

THP-1 monocytes were treated with 10 ng/mL phorbol myristate acetate (PMA) in the RPMI media for 24 hours, followed by PMA free RPMI media for the next 24 hours.

Thereafter, monocytes had been grown into macrophages. The developed macrophages were assessed for F4/80 and CD71 (TFR-1) surface markers. About 90% were found to be F4/80 positive and about 22% F4/80+CD71 positive. The CD71 expressing macrophages were considered for macrophage uptake assay. Briefly, coumarin-6 (Dye) loaded nanocarriers were prepared using the same method. Dye-PLGA NCs and Dye-P/tfr NCs were added to the grown macrophages in the RPMI media under controlled conditions (37°C, 5% CO₂) for 2 hours. Then washed, fixed, and visualized for cellular uptake under the fluorescent microscope. In another set of parallel experiments, purified anti-mouse CD71 antibody (R17217, BioLegend, USA) was added to the macrophage media before adding nano-formulation. After 30 minutes, nano-formulations were added to the respective wells, and uptake was observed after 2 hours of incubation under a fluorescent microscope (Leica microsystem GmbH, Germany).

2.10. Stability Studies

Physicochemical parameters of nanocarriers were assessed after 6 months at 4°C and 25°C, according to ICH guidelines.

2.11. Animal Studies

Male BALB/c mice (weight=25g) were acclimatized in pathogen-free, standard laboratory conditions (37±1°C). The study was conducted according to the approved protocols for care and use of laboratory animals, QAU bioethical code of conduct, and NIH guidelines.

2.11.1. Induction of ulcerative colitis (UC)

The mice were induced with UC by oral administration of 3% DSS (MW 40000) in the drinking water for 7 days. After induction, mice were segregated randomly for two domains of animal studies i.e., nanocarrier targeting studies and therapeutic studies.

2.11.2. Nanocarrier targeting ability and biodistribution

The targeting potential of Tofa-P/tfr NCs to the colon tissues was assessed by oral administration of nanocarrier (drug dose=0.43 mg/mice) to the DSS-induced colitis (n=3). Mice were euthanized post 6 hours of intake and the colon was excised. Additionally, the GI organs like stomach, small intestine, spleen, and organs of elimination like liver and kidney had been taken out to determine drug concentration in

the respective organs. Tissue homogenates were prepared, and drug was extracted using acetonitrile: PBS (1:1) solution from the tissues by overnight shaking (37°C). Clean supernatants were collected the next day and the drug was quantified through the RP-HPLC method (287 nm). The estimation of the released drug at colon and other organs provides an indirect insight of nanocarrier targeting and localization to the colon (Zeeshan *et al.*, 2021). A blank nanocarrier treated mice was used as a control to minimize the influence of nanocarrier excipients and the tissue remnants.

Further, fluorescein dye loaded P/tfr NCs were prepared, and the study was repeated. After 6 hours of administration, colons were excised with exudates. The activated macrophages in the colon lamina propria were harvested according to the protocol (Uronen-Hansson *et al.*, 2014). Cells were processed and resuspended in the buffer to analyze under flow cytometer (BD FACS™, US) for the uptake of dye loaded nanocarriers by the harvested cells.

2.11.3. Evaluation of therapeutic efficacy in the DSS induced colitis mice

After the establishment of DSS-induced colitis, the ameliorative effects of the drug either as a free form or inside the nanocarrier were evaluated after 7-day treatment. Tofa or Tofa-P/tfr NCs were administered to the mice at the drug equivalent dose of 17.5 mg/kg or 0.4375 µg for 25g mice. The number of mice per group was selected according to the resource equation, ARRIVE guidelines, and 3Rs of minimum harm (Arifin and Zahiruddin, 2017; Hubrecht and Carter, 2019).

Group I (Normal control): Healthy mice, administered with drinking water (n=5)

Group II (DSS-colitis): DSS- induced colitis mice (n=5). The DSS was orally administered in the drinking water from day 0-7 and left untreated from day 7-14

Group III: Tofa drug was administered to DSS-induced colitis mice from day 7-14 (n=5), through oral gavage

Group IV: Tofa-P/tfr NCs administered to DSS-induced colitis mice from day 7-14 (n=5), through oral gavage

2.11.4. Assessment of progression and intervention of colitis through morphological parameters and mortality rate

The colitis progression and severity were assessed on daily basis through body weight changes and DAI from day 0-14. DAI was the cumulative of body weight loss, stool consistency, and rectal bleeding, and protrusion (Zeeshan *et al.*, 2019b). Mice mortality was recorded in each group to know the survival rate at the end. At the termination of the experiment, mice were sacrificed and the organs of interest including colon, stomach, small intestine, spleen, liver, kidney, heart, and lungs were resected from each group. The intestine length, weight, and other morphometric parameters were calculated to know inflammation extent.

2.11.5. Histological investigations

1-cm colon tissue was treated with 10% formalin-PBS, then embedded in paraffin and cryosection with a microtome. The sample embedded slide was stained with hematoxylin and eosin (H&E). Then the H&E stained slides from each group were observed under a light microscope and scored according to the pre-determined criteria of colon inflammation (Erben *et al.*, 2014).

2.11.6. Assessment of vascular integrity

The endothelial membrane structure is compromised function in colitis (Jerkic *et al.*, 2010). The vasculature became leaky with endothelial gaps at the inflammation region; therefore, we have performed Evans blue assay to determine endothelial function. The Evans blue (2%, 100 μ L) solution was injected IV through the mice tail vein on the 14th day of study. After 2 hours, mice were perfused with 5% normal saline and euthanized, colons were resected, cleaned, and dried. Afterward the amount of Evans blue permeated into the colon tissue from the malfunctioned vasculature was extracted in DMF at 50-60°C for 24 hours and quantified spectroscopically at 620 nm.

2.11.7. RT-PCR analysis of expression of inflammatory and regulatory proteins

The expression of proteins like E-cadherin (tight junction protein), iNOS (inflammation mediator), STAT-1 (inflammation regulator, Tofa target), and TFR-1/CD71 (the increased expression on macrophages and colon epithelial cells surface) was determined through RT-PCR. Total RNA was extracted from the harvested colon

tissues of each group using TRIzol[®] reagent (Thermo Fisher Scientific, USA), according to manufacturer protocol. The RNA concentration was determined using Nanodrop (Skagit RE 4.1, Thermo Scientific, USA) instrument. cDNA was constructed from extracted RNA using a cDNA synthesis kit (Vivantis technologies, Malaysia). Then the expression of target mRNA was estimated by RT-PCR using Eva Green qPCR Master mix (Solis Biodyne, Estonia). The target gene primer pair sequences are mentioned in Table 2. 7.

Table 2. 7: Forward and reverse primer sequence of the targeted genes

| Gene | Forward primer | Reverse primer |
|-------------------|-----------------------|------------------------|
| STAT-1 | CTGAATATTTCCCTCCTGGG | TCCCGTACAGATGTCCATGAT |
| TFR-1 | GGTAAACTGGTCCATGCTAAT | CCCTGCTCTAACAATCACTAAA |
| iNOS | GGCAGCCTGTGAGACCTTTG | GCATTGGAAGTGAAGCGTTTC |
| E-Cadherin | GGCGCCACCTCGAGAGA | TGTCGACCGGTGCAATCT T |
| β-actin | CGGTGGACATTGGTTCTGG | CTGAGGAAGGGCAGAAGTTC |

2.11.8. Pro-inflammatory cytokines analysis (ELISA)

Pro-inflammatory cytokines including IL-6 and TNF- α in the colons from the mice of each group were quantified using ELISA kits (eBioscience, Inc., CA, USA), as per manufacturer instructions.

2.11.9. Assessment of antioxidant protection level

Biochemical antioxidant assays were performed to detect the level of tissue protection by the quantification of antioxidant (GSH, GST, catalase) and oxidants (NO, MDA/LPO, MPO) in the colon, excised from the mice of different groups. In short, colon tissue homogenates were prepared in PBS, centrifuged (13500 rpm, 10 minutes) and the supernatant was collected. Then the samples were used to detect GSH concentration using Ellman's reagent (Moron *et al.*, 1979). The obtained amount was expressed as nmole/g tissue. GST worked by enzymatically conjugating CDNB to the GSH. The GST enzyme activity to react the sample and CDNB was detected spectroscopically at 340 nm (Habig *et al.*, 1974). Further, catalase enzymatic activity was determined by its ability to decompose H₂O₂ and measured spectroscopically at 240 nm (Senthilkumar *et al.*, 2021). Next, the oxidant NO was estimated by the Griess reagent method (Tsikas, 2007). And lipid peroxidation was assessed by MDA levels through thiobarbituric acid and detected spectroscopically at 540 nm (Shal *et al.*, 2021). The neutrophil marker activity, myeloperoxidase (MPO), increased in colitis.

Therefore, MPO activity was evaluated using CTAB buffer and o-dianisidine reagent at 460 nm (Pulli *et al.*, 2013).

2.11.10. Biochemical hematological parameters

Blood-borne parameters suggested a disease condition and we can assess the treatment efficacy through it. The blood was withdrawn from the cardiac puncture of the mice from each group and assessed for CBC. Further, the blood serum was collected and analyzed for the inflammatory marker, C-reactive protein (CRP). We investigated the effect of nano-formulation treatment in DSS-colitis on the kidney, therefore sera were evaluated for RFTs.

2.11.11. Evaluation of colon microbiome

Colitis leads to several changes in the colon microenvironment and disturbs the natural microbiome of the colon. Some bacteria exceed in amount while some beneficial bacteria decline in growth (Zeeshan *et al.*, 2019a). Therefore, we evaluated the effect of DSS-colitis and the course of treatment on the microbiome of the colon by collecting and culturing the feces and colon exudates at the end of the animal experiment. The samples were cultured in a nutrient agar plate at 37°C for 48 hours to assess bacterial growth. The CFU were counted and represented as \log_{10} CFU/ mL (n=3).

PART-II (SECTION B)

Tofa-LP/tfr NSh and Tofa-LP/tfr/ES NSh

2.12. Preparation of Tofa-LP/tfr NSh and Tofa-LP/tfr/ES NSh

Tofa-LP/tfr NSh: Tofa-LP/tfr NSh was prepared using the W/O/W double emulsion method. Briefly, Tofa (2 mg/mL) was dissolved in PBS (Ph 7.4). An organic solution of PLGA (10 mg) and lipid phospholipon-90G (2.5 mg) in ethyl acetate (1 mL) was prepared. The aqueous solution was added to the organic solution, with continuous stirring. The formed W/O emulsion was probe sonicated for 30 seconds and immediately added to the external aqueous solution made up of 2% PVA solution (2mL) and tfr-HEPES solution (1 mg/mL) in a dropwise fashion. Then, again sonicated for 1 minute, 30 seconds, and stirred for 6 hours to prepare W/O/W nano-emulsion. Then remove the coverlid of the vial and kept stirred overnight for the removal of

organic solvents. The formed Tofa-LP/tfr nanosuspension was centrifuged (13500 rpm, 40 minutes) thrice for the removal of unentrapped drug and residual solvents. Thereafter, 5% trehalose solution was added as a cryoprotectant, and the nano-formulation was freeze-dried at -80°C using a lyophilizer.

Tofa- LP/tfr/ES NSh: The procedure was the same for Tofa-LP/tfr/ES NSh except an additional coating step was incorporated. For ES100 coating, ES100 (20 mg) in 1 mL methanol and a few drops of 0.1N NaOH. The formed Tofa-LP/tfr nano-emulsion was added to ES100 solution and kept stirred for 4 hours, then remove the lid for overnight evaporation of the solvent. Then the nano-formulation was centrifuged thrice and freeze-dried to get lyophilized powder of Tofa-LP/tfr/ES NSh.

2.13. Physicochemical Characterization

The nano-formulations were assessed for particle size, PDI and zeta potential, tfr adsorption, TGA, DSC, and ATR-FTIR using the methods described in Methods section 2.6.

2.14. Drug Release and Kinetics

In vitro release and kinetics of Tofa from Tofa-LP/tfr NSh and Tofa-LP/tfr/ES NSh were conducted through dialysis membrane technique, as per method in section 2.7.

2.15. Mucin Binding Study

See section 2.8 for the method of mucin-interaction study.

2.16. In Vitro Cell-Based Assays

2.16.1. Hemo-toxicity assay

The compatibility of nanoshells with the blood was investigated through a reported procedure (Zeeshan *et al.*, 2021). Consent and approvals from the young healthy individuals were taken before the experiment.

2.16.2. Cellular biocompatibility assay

2.16.2.1. *MTT viability assay (colon, macrophages)*

MTT assay was performed to study the biocompatibility of Tofa-LP/tfr NSh and Tofa-LP/tfr/ES NSh (25-100 µg/mL) towards murine-derived macrophages, and colon cells (Zeeshan *et al.*, 2021).

2.16.2.2. *Colon apoptosis study (7-AAD, PI)*

Caco-2 cells were seeded into the 12-well plate in the RPMI media at 37±0.5°C under humidified 5% CO₂. The caco-2 cells were treated either with 100 µL of Tofa-LP/tfr NSh or Tofa-LP/tfr/ES NSh for 6 hours and 24 hours. At the fixed time points, the cells were taken in the FACS tube, diluted with Millipore water (1:10), and washed with centrifugation (5000 rpm, 5 minutes). Decant the supernatant and collect the cell pellet and add 100 µL of FACS buffer, then stained either with 5µL of propidium iodide (PI) (BioLegend, US) or 7-Aminoactinomycin D (7AAD) (BioLegend, US) and incubate for 10 minutes in the dark. Afterward, the prepared samples were run under flowcytometer (BD Accuri Flow Cytometer, USA) to investigate nano-formulations' impact on caco-2 viability and death. Unstained untreated cells served as negative control. And only PI or 7AAD treated cells served as a positive control, it was not incubated with any nano-formulation.

2.16.3. Colon uptake study

Caco-2 colon cells were used to investigate the uptake potential of Dye-LP/tfr NSh and Dye-LP/tfr/ES. Briefly, Caco-2 cells at a density of 5 x 10⁵/ well were grown in RPMI-media, supplemented with 10% FBS and 1% antibiotics (penicillin-streptomycin) at 37°C under humidified 5% CO₂ for 24 hours. Afterward, the Caco-2 cells were treated with Dye-LP/tfr NSh and Dye-LP/tfr/ES, separately for 2 and 4 hours. Thereafter cells were washed and observed under Leica fluorescent microscope (Germany). The images were processed using Leica Application Suite (LAS) X software.

2.16.4. Macrophage assays

2.16.4.1. *THP-1 monocyte differentiation into macrophages*

THP-1 monocyte cells were grown in RPMI 1640 media (10% FBS, 1% Pen/Strep) at 37°C with 5% CO₂. The THP-1 cells were converted into macrophages by the reported

protocol (Genin *et al.*, 2015). In short, THP-1 cells were sensitized with 10 ng/mL PMA (Sigma Aldrich, US) for 24 hours and then incubated with RPMI media without PMA for the next 24 hours to differentiate into macrophages. Harvested macrophages were washed with RPMI 1640 media containing 10% FBS and then counted using trypan blue. The formed macrophages were observed under the microscope to confirm morphological changes and macrophage surface markers like F4/80 and CD71 were confirmed by FACS.

2.16.4.2. Macrophage uptake and tfr inhibition assay

Then the CD71 receptor expressing macrophages were treated with Dye-LP/tfr NSh and Dye-LP/tfr/ES NSh to the respective wells in the RPMI media (with 10% FBS and 1% Pen/Strep) for 2 hours at 37°C under humidified 5% CO₂. Then cells were washed, fixed, and observed for the cellular uptake under a fluorescent microscope. To visualize tfr mediated uptake, the receptor was blocked by the addition of purified anti-mouse CD71 antibody (R17217, BioLegend, US) to the media, 30 minutes prior to nanoshells addition. Then the experiment was carried out in the same way.

2.16.4.3. Macrophage JAK-1/STAT-1 inhibition assay

The THP-1 derived macrophages were further stimulated by the addition of LPS (100 ng/mL) and IF- γ (20 ng/mL) in RPMI 1640 media (10% FBS + 1% Penicillin/Streptomycin) for 24 hours. Then the activated M1 macrophages were washed, and media was replaced. Both LPS and IF- γ activated the JAK/STAT signaling in the M1 macrophages (Dell'Albani *et al.*, 2001; Venkatesan *et al.*, 2018). Since Tofa is well known JAK/STAT inhibitor, therefore, we have evaluated JAK-1/STAT-1 inhibition activity by incubating Tofa loaded nanoshells (Tofa-LP/tfr NSh and Tofa-LP/tfr/ES NSh) with M1 macrophages for 4 hours. Tofa drug was also incubated separately. And PBS-treated M1 cells served as a positive control. After 4 hours, total RNA was extracted from the cells using RNA micro kit (Macherey-Nagel GmbH, Germany), and cDNA was synthesized by SCRIPT cDNA Synthesis kit (Jena Bioscience GmbH, Germany). qRT-PCR expression of JAK-1 and STAT-1 was measured using SYBR Green dye with respective primers on C1000 RT-PCR system (BioRad, Hercules, CA). 18S rRNA was used as a reference gene.

2.17. Stability Studies

Tofa-LP/tfr/ES NSh were stored at -4°C and at room temperature (25°C) to observe changes in physicochemical properties including particle size, zeta potential, PDI, and % drug entrapment.

2.18. Animal Studies

Mice were induced with DSS to develop UC. Thereafter, mice were separated for targeting and biodistribution studies and the rest were randomly divided into different groups for the therapeutic investigations.

2.19. Preliminary In Vivo Studies

2.19.1. Nanoshells localization and colon targeting ability

The nanoshells colon targeting and localization potential were determined by oral administration of nanoshells (drug dose=0.43 mg/mice) to the DSS-induced mice (n=3). After 6 hours, mice were euthanized and all vital organs including the colon were excised out. The released drug was extracted from the tissues and quantified to determine drug retention using HPLC at 287 nm.

2.19.2. Flow cytometry uptake study

Nanoshell colon-macrophage targeting ability was assessed through flowcytometry by administering dye-loaded LP/tfr NSh and dye loaded LP/tfr/ES NSh to the DSS induced mice, according to the protocol (Zeeshan *et al.*, 2021).

2.19.3. In vivo biodistribution and visualization study

Coumarin-6 (Co-6) dye was loaded into the nanoshells using the same preparation method for the in vivo visualization experiment. To study the biodistribution of dye loaded nanoshells in the healthy and colitis mice, mice (weight=20-25 g) were distributed into 4 groups. Group 1 and 2 have healthy mice, while Group 3 and 4 are DSS (3%) challenged colitis mice. Group 1 and 3 received Co-6 loaded LP/tfr NSh and group 2 and 4 got Co-6 loaded LP/tfr/ES NSh through oral administration. After 18 hours of nano-formulation intake, mice were euthanized and the whole GIT was resected, then kept under Maestro In Vivo Imaging System (CRI-InTAS, Woburn USA) to visualize the biodistribution of dye loaded nanoshells.

To determine the localized retention of Co-6 loaded LP/tfr/ES NSh in the colon of healthy and DSS-colitis mice, colon tissues (from group 2 and 4) were sliced using cryostat microtome and fixed with 0.5% paraformaldehyde (histofix), rinsed with PBS twice and stained with DAPI. A small drop of Mowiol[®] (PVA) was added to adjust the coverslips on the slide. Then the slides were observed under a confocal microscope (Leica SP5 II and Leica Stellaris 8, Leica microsystem, Germany) to study the accumulation of nanoshells within colon tissue.

2.20. In Vivo Therapeutic Efficacy in DSS-Induced Colitis Mice

2.20.1. Evaluation of therapeutic efficacy in the DSS-induced colitis mice

To evaluate in vivo therapeutic efficacy of nanoshells, mice were randomly divided into 5 groups (n=5/group) following the ethical protocol of minimum harm and ARRIVE guidelines and resource equation (Arifin and Zahiruddin, 2017; Hubrecht and Carter, 2019). The groups are:

Normal control: The normal healthy mice (n=5), received only drinking water from Day 0-14

DSS-colitis: UC was induced in the mice by DSS administration in the drinking water from day 0-7, and left untreated from Day 7-14 (n=5)

Treatment I: Tofa: (drug dose=17.5 mg/kg) was administered to DSS-induced colitis mice from Day 7-14 through oral gavage(n=5)

Treatment II: Tofa-LP/tfr NSh (equivalent drug dose=17.5 mg/kg) were administered to DSS-induced colitis mice from day 7-14 through oral gavage (n=5)

Treatment III: Tofa-LP/tfr/ES NSh (equivalent drug dose=17.5 mg/kg) were administered to DSS-induced colitis mice from day 7-14 (n=5) through oral gavage.

2.20.2. Morphological assessment for colitis severity and treatment efficacy, histopathology, and vascular membrane integrity

Detailed methods are mentioned in sections 2.11.4, 2.11.5, and 2.11.6.

2.20.3. RT-PCR analysis for the expression of the epithelial membrane (E-cadherin), inflammatory (iNOS), mechanistic (STAT-1), and receptor-oriented proteins (TFR-1)

RT-PCR analysis was conducted to determine the expression of STAT-1, TFR-1, iNOS, and E-cadherin proteins. β -actin was used as a control. Total RNA from the isolated colons was harvested using TRIzol reagent (Thermo Fisher Scientific, USA) and transformed into cDNA using a cDNA synthesis kit (Vivantis cDSK01-050, Vivantis technologies, Malaysia). Target mRNA expression was assessed using Eva Green Master Mix (Solis Biodyne, Estonia) and cycler PCR machine (BioMolecular System, Australia). The calculations were performed according to $2^{-\Delta\Delta Ct}$ method.

2.20.4. Assessment of pro-inflammatory cytokines

The quantity of pro-inflammatory cytokines (IL-6, TNF- α) in the excised colons of mice (from 5 groups) was assessed through commercially available ELISA kits for IL-6 and TNF- α (eBioscience, Inc., USA), under the manufacturer's directions.

2.20.5. Antioxidant protection by the nano-formulations

2.20.5.1. *Immunohistochemistry for the expression of antioxidant proteins*

The protective effects of drug loaded nanoshells on restoring the antioxidants levels of the colon were investigated by measuring the expression of antioxidant proteins including Nrf2, and HO-1 through immunohistochemistry (Sana *et al.*, 2021; Khan *et al.*, 2019). In short, xylene was used to rehydrate paraffin-colon tissues, followed by the treatment of graded ethanol. Then treated with Proteinase-K and normal goat serum and incubated for 20 minutes. Thereafter, the antibodies, either mouse anti-Nrf2 or HO-1 (Santa Cruz Biotechnology, Inc, USA) was applied to the slides with an overnight incubation at 4°C. Then treated with secondary biotinylated goat anti-mouse antibodies and ABC reagents. After washing with 0.1M PBS, stained with 3,3'-diaminobenzidine (DAB) (Sigma Aldrich, USA). The prepared slides were visualized under a light microscope and expression was computed using ImageJ software (NIH, USA).

2.20.5.2. *Biochemical antioxidant assays*

The increased oxidative stress in the colitis lowered the protective antioxidants and increased the oxidative species. We evaluated the levels of antioxidants like GSH, GST,

and catalase enzymatic activity from the colon samples of the disease and treatment groups using Ellman's reagent method, CDNB conjugation method (340 nm), and H₂O₂ decomposition by catalase, respectively (Zeeshan *et al.*, 2019b).

Further, the oxygen species including malondialdehyde (MDA) was estimated to know lipid peroxidation using the thiobarbituric acid method (540 nm). And nitrite (NO) was measured using the Griess reagent method (Shal *et al.*, 2021). Sodium nitrite was used as a standard to develop a standard calibration curve. Further myeloperoxidase (MPO) activity was determined through the CTAB method (460 nm) (Pulli *et al.*, 2013).

2.20.6. Biochemical hematological parameters

Hematologic parameters get altered in bowel inflammation. Therefore, we assessed complete blood count (CBC) at the end of the experiment. And C-reactive proteins (CRP) levels to determine the extent of inflammation (Masoodi *et al.*, 2011). Further, RFTs were conducted from the collected blood sera (each group mice) to determine any detrimental effects on kidney function.

2.20.7. Colon microbiome growth evaluation

To ascertain the DSS-colitis effects and the treatment led recovery of the colon microenvironment, we collected feces and exudates from the colon of the mice from each group. The samples were mixed with PBS, thoroughly shaken, and centrifuged. Then supernatants were used to culture on nutrient agar at 37°C for 48 hours. The bacterial growth was estimated as log₁₀CFU/ mL (n=3).

2.20.8. In vivo biocompatibility of nanoshells in the healthy mice

Healthy BALB/c male mice were housed in a standard laboratory environment. To evaluate the toxic potential of the Tofa-LP/tfr/ES NSh, the nano-formulation was orally administered to the mice (n=3) for 7 days. The dose was kept the same as that of the therapeutic study experiment. Mice were daily examined for body weight, mortality, distress symptoms, food-water intake patten, allergies, lethargy, lacrimation, and any signs of changed behavior. The mice were euthanized after 7 days, and organs of interest were resected for investigations. Colon fecal content was collected to evaluate the influence of nanoshells on the natural microbiome. The colon was assessed for necrosis and apoptosis using Annexin-V/ Propidium iodide (PI) dyes under flowcytometry ((BD, FACSTTM, USA). In short, the colon tissue homogenate was

prepared in PBS and cell counting was done through preparation of 1x trypan blue solution, followed by mixing of trypan blue with cell suspension (1:1) and loading into a hemocytometer. Then hemocytometer was visualized under a light microscope and viable cells were counted. For Annexin-V/PI staining, take 1×10^6 cells and add 500 μL of 1% FBS and 200 μL of Annexin-V binding buffer and incubate for 5 minutes at room temperature. Centrifuged at 400 rcf for 5 minutes and collect the pellet. Add 100 μL of Annexin-V binding buffer and resuspend the cell pellet in it, then add 5 μL of Annexin-V and 5 μL of PI dyes, incubate for a few minutes and run under flowcytometer.

PART-III

Note: This section describes tacrolimus (TAC) loaded PLGA/L-Lysine nanocarriers (TAC-P/Lys NCs) and ES100 and EL100 coated TAC loaded PLGA/L-Lysine nanocarriers (TAC-P/Lys/ES-L100 NCs).

2.21. HPLC Analysis of TAC

RP-HPLC method was developed for quantification of TAC (FK506) using Agilent 1260 Infinity II HPLC instrument (Agilent Technologies, Santa Clara, CA, USA), and C18 Phenomenex Luna (150 mm x 4.6 mm, 100 Å, 0.3 μm pore size) column at 60°C. The isocratic method worked at a wavelength of 210 nm and the injection flow rate was adjusted to 1 mL/min. The mobile phase was composed of 0.1% trifluoroacetic acid-Millipore water and acetonitrile (1:1). To construct a standard curve, a stock solution of 1 mg/mL was prepared in acetonitrile, and dilutions were prepared accordingly. TAC in the concentration of 3.09 μg to 500 μg was estimated under HPLC to plot a standard calibration curve. The obtained retention time was about 26 minutes and the correlation coefficient has a linearity of 0.995.

2.22. Preparation and Optimization of TAC-P/Lys NCs and TAC-PLGA/Lys/ES-L100 NCs

TAC-P/Lys NCs were prepared using O/W emulsion-evaporation method. In short, TAC (1 mg) and PLGA (10 mg) were dissolved in ethyl acetate (1 mL) to constitute the organic phase. Then the organic solution was added dropwise into the aqueous phase, containing 2% PVA and L-Lysine (5 mg). The resultant mixture was sonicated using a probe sonicator for 1 minute, 30 seconds (97% Amplitude), and then stirred for 2 hours. The lid of the vial was removed to remove organic solvents, under continuous

stirring at 780-850 rpm. The formed nanosuspension was purified through centrifugation at 14000 rpm for 40 minutes thrice. The obtained pellet was resuspended in 1 ml of distilled water with 5% trehalose (cryoprotectant). Afterward, the nanocarriers were freeze-dried at -80°C using a lyophilizer (Vir tis Genesis 25EL, US).

TAC-P/Lys/ES-L100 NCs were prepared using the same method with the addition of another last step. The organic phase had the same composition. It was added to the aqueous phase of L-lysine (5 mg) + 1% PVA (1 mL), probe sonicated for 1 minute, 30 seconds (97% amplitude), and stirred for 2 hours to form O/W TAC-P/Lys nanoemulsion. The pH-sensitive polymer solution was made up of ES100 (10 mg) and EL100 (10 mg) in methanol (2 mL), a few drops of 0.1N NaOH, and 2% PVA solution (2mL). The O/W TAC-P/Lys nanoemulsion was added into the pH-sensitive polymer solution, probe sonicated (97% amplitude) for 2 minutes, and kept on stirring (800-1000 rpm) for 2 hours. Afterward, the organic solvent was evaporated through overnight stirring, followed by centrifugation and freeze-drying to obtain powdered TAC-P/Lys/ES-L100 NCs.

2.23. Physicochemical properties

The main physicochemical characteristics including particle size, zeta potential, and PDI were determined using dynamic light scattering technique under Malvern Nano-ZS90 zetasizer (Malvern Instruments Ltd, Worcestershire, UK). The morphology was examined using SEM and scanning transmission electron microscope (STEM, Thermo Fisher Scientific Spectra 200 C-FEG, Massachusetts, US). The TAC loaded nanocarriers were centrifuged at 14000 rpm for 40 minutes and the supernatant was collected and assessed for the quantification of free unbound TAC using the RP-HPLC method at 210 nm. The entrapment efficiency and loaded drug content were determined from the unbound drug. Differential scanning calorimetry (DSC) of TAC and TAC loaded nanocarriers was performed through the same method in **section 2.6.3**.

2.24. Drug Release Studies and Kinetics

The TAC (FK506) release profiles from TAC-PLGA NCs, TAC-P/Lys NCs, and TAC-P/Lys/ES-L100 NCs were obtained at the simulated gastric fluid (SGF) of pH 1.2 for initial 2 hours, and at the simulated intestinal fluid (SIF) of pH 7.4 from 2-72 hours with continuous rotation at 37°C. The pH values were selected according to the variation of pH within GIT from the stomach to colon (Zeeshan *et al.*, 2019a). The

samples were withdrawn at pre-determined time intervals and replaced with fresh media. The drug concentration was quantified at 210 nm.

2.25. In Vitro Cell-Based Studies

2.25.1. Caco-2 viability assay with 7-AAD and PI staining

Caco-2 cells were cultured in RPMI 1640 media, supplemented with 10% FBS, 1% Penicillin-Streptomycin antibiotics, 1% sodium pyruvate in a humidified 5% CO₂ atmosphere at 37°C. The viability dyes 7-AAD and PI were used to assess the effect of nanocarriers on the viability of Caco-2 cells. Briefly, the Caco-2 cells were seeded in a 24-well plate at a density of 1×10^5 cells/well and incubated for 24 hours. TAC-P/Lys NCs and TAC-P/Lys/ES-L100 NCs (100 µg/mL) were added to the wells and incubate for either 6 hours or 24 hours. Then, the cells were collected in FACS buffer and washed with centrifugation (5000 rpm, 5 minutes). Then the cells were treated with either 5 µL of 7-AAD (BioLegend, USA) or PI (BioLegend, US) dye and 100 µL of FACS buffer was added to it. After 5-10 minutes of incubation, the samples were analyzed under flowcytometry (BD Accuri Flow Cytometer, USA). Data were analyzed through FlowJo™ LLC Software v10.6.2 (BD Life Sciences, USA). Unstained untreated cells had been taken as negative, while only dye (7-AAD or PI) stained cells with no nanocarrier treatment served as a positive control.

2.25.2. Caco-2 uptake studies

Caco-2 cells were grown under the same conditions and incubated with Coumarin-6 dye loaded PLGA/Lys NCs and PLGA/Lys/ES-L100 NCs for 4 hours. Untreated cells served as a control and only dye treated cells served as a positive control. After 4 hours, cells were washed to remove excessive nanocarrier, fixed and visualized under Leica fluorescent microscope (Germany), assisted with Lecia Application Suite (LAS) X software.

2.25.3. Macrophage uptake studies

Macrophages were derived from THP-1 monocytes using PMA, according to the mentioned protocol (Genin *et al.*, 2015). The formed macrophages were seeded in a 24-well plate in RPMI 1640 media (10% FBS, 1% antibiotics) under 5% CO₂ at 37°C for 24 hours. Afterward, Coumarin-6 dye loaded nanocarriers were added and incubated

for 4 hours. Then washed, fixed, and visualized under a fluorescent microscope for the uptake of nanocarriers

2.26. Animal Studies

C57BL/6J mice (weighing 20-22 g) were housed and acclimatized to a pathogen-free hygienic environment under standard environmental conditions and proceeded for the development of colitis and therapeutic investigations.

2.26.1. Instillation of oxazolone (OXA) to induce UC

2.26.1.1. *Pre-sensitization with OXA*

At first, the solvent mixture of acetone and olive oil (4:1) was prepared by vigorous mixing. Then 3% OXA solution was prepared in the solvent mixture with vortex mixing and under proper precautions and careful handling. The mice were pre-sensitized with this 3% OXA solution by spreading it to the mice abdominal skin.

2.26.1.2. *Intra-rectal instillation of 0.6% OXA solution*

0.6% OXA solution was prepared in 50% ethanol. On the 4th day of pre-sensitization, mice were anesthetized with ketamine/xylene solution, and 100 μ L of 0.6% OXA solution was administered intrarectally.

2.27. Therapeutic Evaluation of Nanocarriers

After intra-rectal administration of OXA, mice were randomly distributed into 4 groups. And the treatment with a plain drug (TAC), TAC-P/Lys NCs, and TAC-P/Lys/ES-L100 was started on the same day and continued for 4 days. One group was left untreated as a disease control (OXA-colitis). And the group of mice consisted of normal healthy mice considered normal control. TAC either as a free drug or within nanocarriers was given at a dose of 1 mg/kg (n=4/ group).

1. Normal: Untreated healthy mice
2. OXA-Colitis
3. TAC only treated OXA-colitis mice
4. TAC- PLGA/Lys NCs treated OXA-colitis mice
5. TAC- PLGA/Lys/ES-L100 NCs treated OXA-colitis mice

2.27.1. Assessment of therapeutic efficacy through morphological indices

Colitis severity and progression were monitored using high-resolution mini endoscopy to visualize the interior of the colon under the Coloview system (Storz) and graded according to the Murine Endoscopy Index of Colitis Severity (MEICS) score (Becker *et al.*, 2005). The MEICS score is based on several symptoms and manifestations of IBD, with a maximum score of 15 (Table 2. 8). Briefly, mice were anesthetized using Isoflurane under oxygen supply. The miniature endoscope rod (1.9 mm outer diameter) assisted with xenon light, triple chipped camera, and air pump was inserted through the rectum and moved upward towards the intestine, carefully without damaging the mice interior. Further, mice body weight was daily assessed for any changes. At the termination of the experiment, the colon was excised, and morphometric parameters were assessed.

Table 2. 8: Inflammation indices determining the MEICS

| Inflammation Index | Endoscopy score (MEICS) levels | | | |
|--------------------|--------------------------------|--------|----------|------|
| | Nil | Little | Moderate | High |
| Translucent | 0 | 1 | 2 | 3 |
| Granularity | 0 | 1 | 2 | 3 |
| Fibrin | 0 | 1 | 2 | 3 |
| Vascularity | 0 | 1 | 2 | 3 |
| Stool | 0 | 1 | 2 | 3 |

2.27.2. Histopathological analysis

Excised colon tissues were preserved in the cryo-molds using Tissue-Tek OCT and frozen down under liquid nitrogen. Then 5µm sections of the colon were sliced using Leica CM3050 S cryostat (Leica, Germany) onto the slides. The slides were stained with H & E for histological evaluation of the tissue. The histopathological features were observed under NanoZoomer (Hamamatsu NanoZoomer 2.0HT) and graded on a scale of 0-12 (Erben *et al.*, 2014).

2.27.3. IVIS imaging to assess myeloperoxidase (MPO) activity

In vivo imaging of inflammation intensity and MPO activity was assessed using In Vivo Imaging System (IVIS). Briefly, mice were injected with 100 µL of 5-amino-2,3-dihydro-1,4-phthalazine-dione (luminol) dye through the IP route. Immediately, mice were anesthetized using isoflurane, while oxygen supply was maintained. Then placed

inside the chamber of IVIS and the bioluminescence signals were obtained and captured by charged couple device (CCD) camera. Luminol is a redox compound that radiates blue fluorescence ($\lambda_{\text{max}}=425$ nm) on exposure to oxidizing agents. Therefore, the strength of the bioluminescence signal is the indicator of inflammation severity and MPO activity.

2.27.4. Immunohistochemistry for the pITK expression in the CD3⁺ T cells of the colon tissue

Cryo-sections of colon tissue were embedded on glass slides and fixed with 2% Histofix (paraformaldehyde). Wash slides with PBS for 5 minutes thrice and then add 50 μL of 0.2% Triton-X100 per section for 5 minutes. Again, wash with PBS for 5 minutes. Block the sections with 50 μL Dako and incubate for 30 minutes at room temperature. Wash with PBS for 5 minutes. Then add 5% BSA and 20% FBS and incubate for 30 minutes. Again, wash with PBS one time. Prepare ROTI[®]ImmunoBlock mixture (1x) with primary antibody anti-Human/Mouse phospho-BTK/ITK (pITK) (Invitrogen [™], eBioscience [™]) in the ratio 1:25 and add 50 μL of the mixture per section and incubate overnight at 4°C. For isotype control, use anti-mouse IgG2b kappa isotype control (Invitrogen [™], eBioscience [™]) instead of pITK on the control section. The next day, wash three times with PBS for 5 minutes. Prepare the mixture of ROTI[®]ImmunoBlock and antibody anti-Human/Mouse CD3 (Invitrogen [™], eBioscience [™]) in the ratio of 1:50 and add 50 μL of this mixture to the section and incubate overnight at 4°C. Then wash three times with PBS.

Afterward, prepare a mixture of ROTI[®]ImmunoBlock and secondary antibody, Goat anti-hamster Dylight [™] -488 (BioLegend[®], San Diego, CA, USA), add to the slide tissue sections, and incubate for 1-2 hours. Then wash with PBS three times. Add DAPI (1:5000) to all sections and leave it for 7 minutes. Instill a drop of Mowiol[®] to the slide and place a coverslip on it. Store the prepared slides at 4°C. Visualize under a high-resolution confocal microscope (Leica SP5 II and Leica Stellaris 8, Leica microsystem, Germany) to assess the expression of pITK in the CD3⁺ T-cells of the colon.

2.27.5. RT-PCR analysis of inflammation markers and ELISA for pro-inflammatory mediators' analysis

The colon tissues from the mice of all experimental groups were sliced and total RNA was extracted using RNA micro kit (Macherey-Nagel GmbH, Germany), according to the manufacturer's instructions. The RNA content was quantified using Nanodrop at 260/280 nm. The cDNA was synthesized from RNA using a SCRIPT cDNA synthesis kit (Jena Bioscience GmbH, Germany). Then the qRT-PCR expression of pITK, NFATc-1, NF- κ B, Ocln-1, TGF- β , and VEGF-A were measured against respective primers on thermal cycler C1000 RT-PCR system (BioRad, Hercules, CA) using SYBR Green dye. 18S rRNA served as a reference gene. The pro-inflammatory cytokine was determined using ELISA kits (BioLegend, USA), as per instructions.

2.27.6. Flowcytometry

2.27.6.1. *Isolation of T-cells and macrophages from spleen cells*

The spleen was excised from the mice of all groups at the end of the experiment. Spleens were smashed using glass slides, add into the PBS, and filtered using cell strainers. Then incubate at 37°C and add 5-10 mL of PBS and centrifuge down the cell pellet at 5000 rpm for 5 minutes. Add 3 mL of lysis buffer to exclude RBC cells. Incubate it at room temperature (RT) for 15 minutes and wash with PBS, centrifuged (5000 rpm, 5 minutes), and collect the cell pellet. Resuspend pellet in PBS, count the cells using trypan blue, and culture in RPMI 1640 media (supplement with FBS and antibiotics) for further activity.

2.27.6.2. *Assessment of pITK expression in the T-cells*

Take 1-2 million isolated spleen cells from the culture and pipette into the FACS tubes. Wash with 200 μ L FACS buffer with centrifugation. Take the pellet and add 200 μ L of 30% H₂O₂-PBA solution and incubate for 20 minutes at 4°C. The wash with FACS buffer, centrifuge, and incubated with 2 μ L of anti-CD4 antibody for 20 minutes at 4°C. Then wash with FACS buffer and fix with FOXP3/PERM buffer kit (Invitrogen™, eBioscience™) and incubate overnight at 4°C. After washing, incubate with 2x Perm buffer for 10 minutes at RT. Centrifuged and add 200 μ L of 30% H₂O₂-PBA solution with incubation for 2 minutes at RT. Was with FACS buffer and add 2x Perm-buffer to it, followed by the addition of 3-5 μ L of anti-pITK PE antibody (BioLegend, USA) and

incubate for 30 minutes at RT. Wash and add 200 μ L of FACS buffer to analyze under flowcytometer.

2.27.6.3. *Assessment of pro-inflammatory M1-macrophages in the spleen cells*

Take 1-2 million spleen cells into the FACS tube. Wash and add FACS buffer to each tube, then sequentially stain with anti-F4/80, CD11b, and CD38 antibodies (BioLegend, USA) with all in between necessary washings and steps. In the end, add FACS buffer and run under flowcytometer (BD Accuri Flow Cytometer, USA). Sort out the cells and estimate CD38⁺ M1 cells among F4/80⁺CD11b⁺ macrophage populations.

2.28. Statistical Analysis

The data were expressed as mean \pm standard deviation (SD) (n=3) unless otherwise stated. Statistical analysis was conducted using t-test and one-way ANOVA with Bonferroni post hoc analysis. The level of significance was 0.05 ($p < 0.05^*$), 0.01 ($p < 0.01^{**}$) and 0.001 ($p < 0.001^{***}$).

CHAPTER 3

RESULTS

3. RESULTS

PART-I (SECTION A)

3.1. HPLC Calibration Curve of Dexa

Dexa standard curve was successfully achieved at a concentration of 6.25-100 $\mu\text{g/mL}$, with linearity ($R^2=0.9984$) (Figure 3. 1).

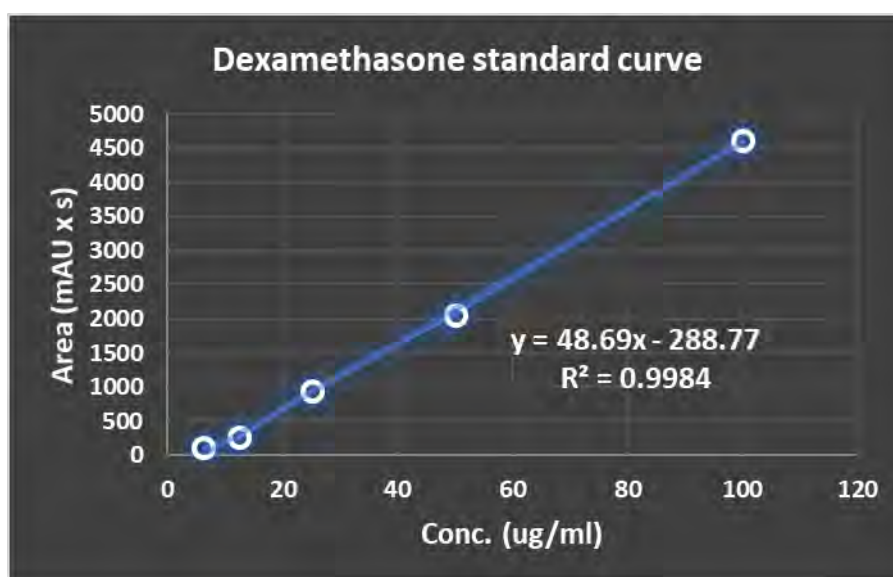


Figure 3. 1: HPLC standard curve of Dexamethasone (Dexa)

3.2. Molecular Docking

MGL-2 homology model (5JPV) has two coordinates, A and B, illustrated in . The protein model was accessed through the Ramachandran plot and Z-scores using PROCHECK and ProSA online servers, respectively. Ramachandran plot have shown that amino acid residues are distributed about 90.6% in the most favored regions for the MGL-2 receptor (Figure 3. 2 a). Further, Z-score determines the model quality and the negative residual energy of -7.34 confirmed model uniformity (Figure 3. 2 b).

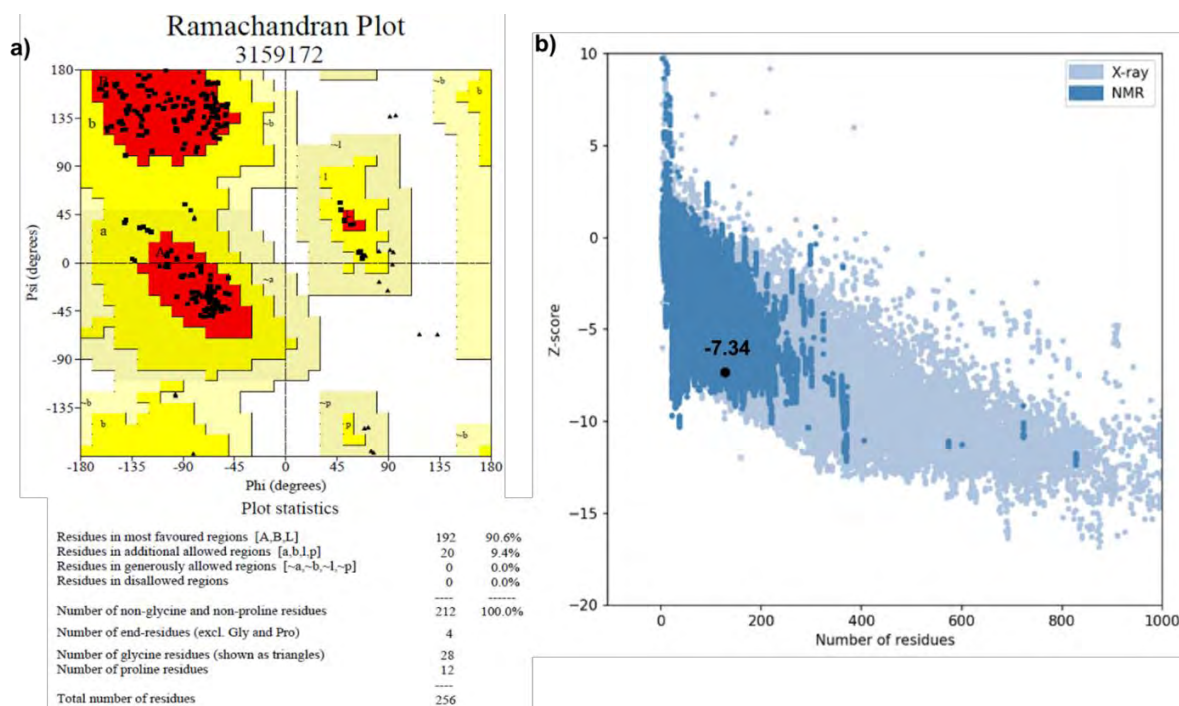


Figure 3. 2: Evaluation of quality of MGL-2 homologous model through Ramachandran plot (a) and, Z-score plot (b) (Zeeshan *et al.*, 2021)

Docking studies of the prepared ligands with galactose (carbohydrates) binding domains of MGL-2 receptor (Q8IUN9, PDB: 5JPV) were carried out using the AutoDock Vina tool in the PyRx program. The protein receptor has two chains, A and B; both chains were individually docked with the ligands. To determine the strength of binding interaction between ligands (D-galactose or GAL-PLGA polymer) and the protein receptor, binding energies were obtained. The best ligand binding pose is considered with the least binding energy. The amino acid residues of the receptor that interact with GAL-PLGA ligand either through hydrogen bonding or electrostatic interactions are Arg298, Asp294, Asn292, Glu280, Asp269, Gln267, and Lys264 (). For D-galactose, the main binding residues are Asp294, Asn292, Glu280; while chains A and B differ in terms of Tyr300, Tyr236, and Gln267 bonding with D-galactose (). Besides, obtained binding energy scores make it obvious that GAL-PLGA ligand have better recognition by both coordinates (A, B) of the MGL-2 receptor as compared to plain D-galactose.

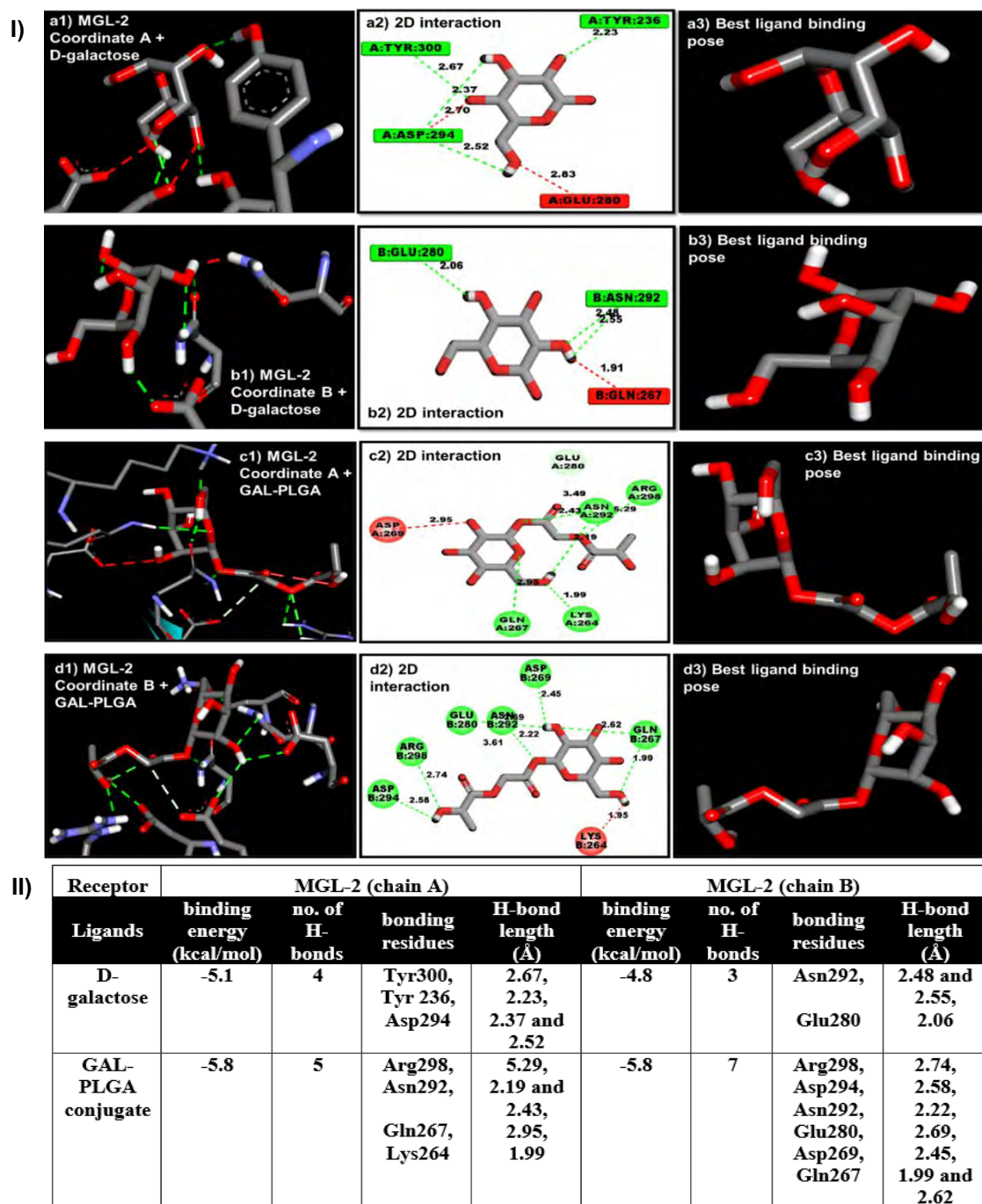


Figure 3. 3: Molecular docking: simulated ligand interaction with MGL-2 homologous receptor (model/coordinates A and B) with binding energies, H-bonds, and binding amino acid residues; (I) H-bonding between D-galactose and MGL-2, coordinates A and B (a1,b1), their 2D interaction depicting binding amino acids (a2, b2), and D-galactose best receptor binding pose (a3, b3). H-bonding between GAL-PLGA and MGL-2, coordinates A and B (c1,d1), their 2D interaction depicting binding amino acids (c2, d2), and GAL-PLGA best receptor binding pose (c3, d3). Green dashed line indicated H-bond, Red line indicated other unfavorable bonds, (II) Ligand-receptor interaction with respective binding energies and other details (Zeeshan *et al.*, 2021)

3.3. GAL-PLGA Polymer Synthesis

The reaction between D-galactose and PLGA was a conventional esterification reaction (Peça *et al.*, 2012; Park *et al.*, 2017; Margarida Cardoso *et al.*, 2016), that was opted to successfully produce GAL-PLGA polymer, as shown in Figure 2. 2. The acid-catalyzed esterification reaction was feasible, easy to proceed using distillation apparatus, and cost-effective as compared to the other methods of synthesis like microwave irradiation, etc. (Peça *et al.*, 2012; Park *et al.*, 2017; Margarida Cardoso *et al.*, 2016).

It was carried out in mildly acidic conditions, using DMF as a solvent and methanesulfonic acid as a catalyst in a quantity of 0.004 mL (0.056 mmol), which is minute and constitutes pH of around 4. And the reaction was completed in 24 hours. It was noticed that several days (>15) are required to change the internal pH of PLGA based particulate systems that tend to degrade its polymeric structure and the encapsulant (Fu *et al.*, 2000). A study reported a little deviation in the thermograph (TGA) of PLGA at pH 2.4 over 5 days and smooth morphology of PLGA microspheres at pH 2.4 with homogenous degradation (Zolnik and Burgess, 2007). As per our examination, PLGA degraded only under strongly acidic conditions (pH 1-1.5) but does not degrade faster in mild-moderate acidic conditions. It tends to degrade over time. Thus, these mild acidic conditions facilitated deprotonation of PLGA to aid ester formation but does not disintegrate its polymeric structure.

PLGA carboxylic group at the terminal end was covalently linked with the anomeric hydroxyl groups of D-galactose under mild acidic or basic conditions. Although, the reaction was susceptible between any hydroxyl group of D-galactose and PLGA, however, we assume linkage to anomeric hydroxyl because it is the most reactive one with the highest coupling constant and therefore more prone to undergo ester linkage with PLGA carboxylic group (Miljković, 2010; Lim and Fairbanks, 2017; Peça *et al.*, 2012). Therefore, no prior activation of D-galactose was required. Mostly, OH groups on other carbon atoms were protected when reaction involves any OH group of galactose, other than anomeric -OH, here, it was not the case (Miljković, 2010; Lim and Fairbanks, 2017). In the case of unprotected OH, the reaction with anomeric OH is most feasible (Lim and Fairbanks, 2017)

Further, DMF was used as a reaction media because both reactants are solubilized in it, have a higher boiling point (153°C) and facilitated nucleophilic substitution (Peça *et*

al., 2012). The reaction conditions that affect resultant GAL-PLGA polymeric powder quality and yield were further studied and optimized. To study the effect of interfering reaction variables, the $2_{IV}^{(4-1)}$ fractional factorial design was adopted which provides different experimental runs with varying conditions, as presented in Table 3. 1.

Effect of independent variables on GAL-PLGA polymer yield (Y_1) and powder consistency (Y_2):

In a two-level fractional factorial design, four independent variables including temperature (X_1), heating conditions (X_2), drying conditions (X_3), and atmospheric conditions (X_4) were studied with different experimental combinations to determine their effect on dependent variables (response) i.e., % age yield (Y_1) and powder consistency (Y_2) of the synthesized polymer (Table 3. 1). The generated effect estimates, and corresponding polynomial equation show the main and interacting effect of the independent variables on the response variables with the help of STATISTICA® software. The mathematical model to compute the effect of independent variables on %age yield through $2_{IV}^{(4-1)}$ fractional factorial design is represented by Equation 10:

$$Y_1 = 75 + 14.5X_1 + 5.5X_2 + 5X_3 + 7X_4 + 0X_1X_2 - 2.5X_1X_3 + 3.5X_1X_4 \dots\dots 10$$

The positive sign in the polynomial equation indicates a synergistic effect whereas the negative sign suggests an inverse effect. Moreover, the higher associated coefficient of each variable (pre-factor of X_A) has more control over the response variable. In the above equation, the highest coefficient is accredited to temperature (X_1), which indicates that the temperature affects polymeric yield more than other variables. Further, an analysis of variance (ANOVA) was carried out to authenticate the statistical significance of each variable. ANOVA analysis indicates that the regression sum of squares, p-values, and F-values are statistically significant for the effect of temperature on % yield (Table 3.2), at a significance level of 0.05 ($\alpha=0.05$). Other independent variables affect % yield to some extent. Furthermore, Pareto chart analysis (Figure 3.4 I) graphically illustrated the influence of each variable on the response variable, % yield (Y_1), highlighting the influence of temperature to obtain a better yield of GAL-PLGA polymer. Similarly, the polynomial equation for the response variable powder consistency (Y_2) using $2_{IV}^{(4-1)}$ fractional factorial design is:

$$Y_2 = 43.75 + 0X_1 + 0X_2 + 37.5X_3 + 62.5X_4 + 12.5X_1X_2 + 0X_1X_3 + 0X_1X_4 \dots\dots\dots 11$$

The equation indicates that the independent variable atmospheric conditions (X_4) have the maximum influence to obtain a better quality dried polymeric powder. It represents that a nitrogen-controlled environment is the utmost for good quality dried powder. In addition, drying conditions (X_3) affect powder consistency pronouncedly; it demonstrates polymer obtained at the end of the reaction when dried in the desiccator overnight produced better results as compared to the freeze-drying (lyophilization) procedure. Whilst temperature and heating conditions minorly influence final polymeric powder quality. ANOVA confirmed the statistical significance of atmospheric and drying conditions on powder consistency (Table 3. 3). Moreover, Pareto charts graphically showed the effect of atmospheric and drying conditions are statistically superior to other independent variables to produce freely flowing dried powder (Figure 3.4 II)

Table 3. 1: Two-level $2_{IV}^{(4-1)}$ fractional factorial design to study the effect of reaction variables on % yield and powder consistency of the synthesized GAL-PLGA polymer

| Runs | X ₁ : Temperature (°C) | X ₂ : Heating conditions | X ₃ : Drying conditions | X ₄ : Atmospheric conditions | Y ₁ : Yield (%) | Y ₂ : Powder consistency |
|------|---|---|--|---|----------------------------------|---|
| 1 | 60 | Sand bath | Lyophilizer | Air | 60 | 0 |
| 2 | 70 | Sand bath | Lyophilizer | Nitrogen | 84 | 50 |
| 3 | 60 | Oil bath | Lyophilizer | Nitrogen | 69 | 50 |
| 4 | 70 | Oil bath | Lyophilizer | Air | 79 | 0 |
| 5 | 60 | Sand bath | Desiccator | Nitrogen | 71 | 100 |
| 6 | 70 | Sand bath | Desiccator | Air | 76 | 25 |
| 7 | 60 | Oil bath | Desiccator | Air | 73 | 25 |
| 8 | 70 | Oil bath | Desiccator | Nitrogen | 92 | 100 |

Table 3. 2: ANOVA analysis to study the influence of independent variables on % Yield (Y_1) of GAL-PLGA polymer under $2_{IV}^{(4-1)}$ fractional factorial design

| Independent variable | SS | df | MS | F | p | Result |
|----------------------------|----------|----|----------|----------|----------|-------------|
| (1) Temperature (°C) | 420.5000 | 1 | 420.5000 | 34.09459 | 0.010009 | Significant |
| (2) Heating conditions | 60.5000 | 1 | 60.5000 | 4.90541 | 0.113590 | |
| (3) Drying conditions | 50.0000 | 1 | 50.0000 | 4.05405 | 0.137521 | |
| (4) Atmospheric conditions | 98.0000 | 1 | 98.0000 | 7.94595 | 0.066802 | |
| Error | 37.0000 | 3 | 12.3333 | | | |
| Total SS | 666.0000 | 7 | | | | |

Table 3. 3: ANOVA analysis to study influence of independent variables on powder consistency (Y_2) of GAL-PLGA polymer under $2_{IV}^{(4-1)}$ fractional factorial design

| Independent variable | SS | df | MS | F | P | Result |
|----------------------------|----------------|----------|-----------------|-----------------|-----------------|--------------------|
| (1) Temperature (°C) | 0.00 | 1 | 0.000 | 0.00000 | 1.000000 | |
| (2) Heating conditions | 0.00 | 1 | 0.000 | 0.00000 | 1.000000 | |
| (3) Drying conditions | 2812.50 | 1 | 2812.500 | 27.00000 | 0.013847 | Significant |
| (4) Atmospheric conditions | 7812.50 | 1 | 7812.500 | 75.00000 | 0.003239 | Significant |
| Error | 312.50 | 3 | 104.167 | | | |
| Total SS | 10937.50 | 7 | | | | |

3.3.1. Confirmation of synthesized polymer through ATR-FTIR, NMR, and TGA

Obtained ATR-FTIR spectra of D-galactose conjugated PLGA polymer confirmed the conjugation reaction and formation of ester linkage (Figure 3.4). In FTIR, the peak at 3389 cm^{-1} corresponds to the O-H functional group which demonstrated galactose attachment. Next, the prominent peak at 1748 cm^{-1} represented the ester group, another minute peak at 1672 cm^{-1} presented the C=O group in the structure. Further, esteric C-O bend is present at 1165 cm^{-1} and 1130 cm^{-1} . The CH₃ stretches were allocated at 2922 and 2953 cm^{-1} and CH₂ at 2852 cm^{-1} vibrations.

Further, NMR spectroscopy of the synthesized polymer under Agilent VNMR 400 NMR (¹H NMR at 400 MHz and ¹³C NMR at 101 MHz) spectrometer provided H and C details associated with each functional group. ¹H-NMR (CDCl₃) spectra of the synthesized polymer have representative areas of galactose moiety and PLGA (PLA, PGA), as shown in Figure 3.4. The main chemical shifts of PLA appeared at 5.2-5.3 ppm (CH) and 1.55-1.59 ppm (CH₃); and the PGA peak of CH₂ present at 4.8 ppm. While chemical shifts at 4.31 and 6.2-6.3 ppm are the representatives of C-H and other CH protons linked to the hydroxyl group of D-galactose moiety, respectively (Figure 3.4) (Dong *et al.*, 2017). The specific chemical shifts (4.31) and methyl, methylene protons mole ratio indicated galactose conjugation to PLGA. Both FTIR and NMR analysis assured galactose conjugation with PLGA polymer.

Furthermore, TGA investigations confirmed polymer synthesis as indicated by large deviations between PLGA and GAL-PLGA thermal degradation patterns (Figure 3.4). PLGA polymer was completely burnt (about 99%) at 300-400°C, which is the characteristic of PLGA (Wang *et al.*, 2016). Whereas TGA spectrum of GAL-PLGA polymer started declining after 150°C, then GAL-PLGA decomposed in shifts from 240°C to 460°C gradually, resting about more than 50% residue till 550°C (Figure 3.4). Gradual melting and decomposition is the characteristic of sugars (Hurtta *et al.*, 2004), that imparted a slow decomposition pattern to the synthesized polymer rather than a

sharp decline (Goel *et al.*, 2021). Galactose-based polymers have multiple phases of degradation, with initial loss of OH groups, followed by decomposition of sugar residue and polymeric backbone (Goel *et al.*, 2021; Saltan and Akat, 2013). It is expected that during water loss in the initial phase, the sugar-based structure caramelizes, thus leaving 60% water and 40% of carbon black (Hurtta *et al.*, 2004). It indicated that ~50% weight of GAL-PLGA polymer left at 550°C might be the carbon black content (Figure 3.4). Further, sugar-based products might continue to burn over a range of temperatures, for instance, complete degradation occurs at 1050°C during sintering (Le Ray *et al.*, 2010). Thus, we can say that GAL-PLGA polymer decomposed almost 50% till 550°C, however, chances existed that it underwent another phase of decline at higher temperatures. Overall, GAL-PLGA polymer have an earlier onset of degradation than underived PLGA polymer (Figure 3.4), however, the GAL-PLGA polymer gradual degradation pattern at higher temperature assisted the polymer to completely deteriorate over a broader time and temperature range.

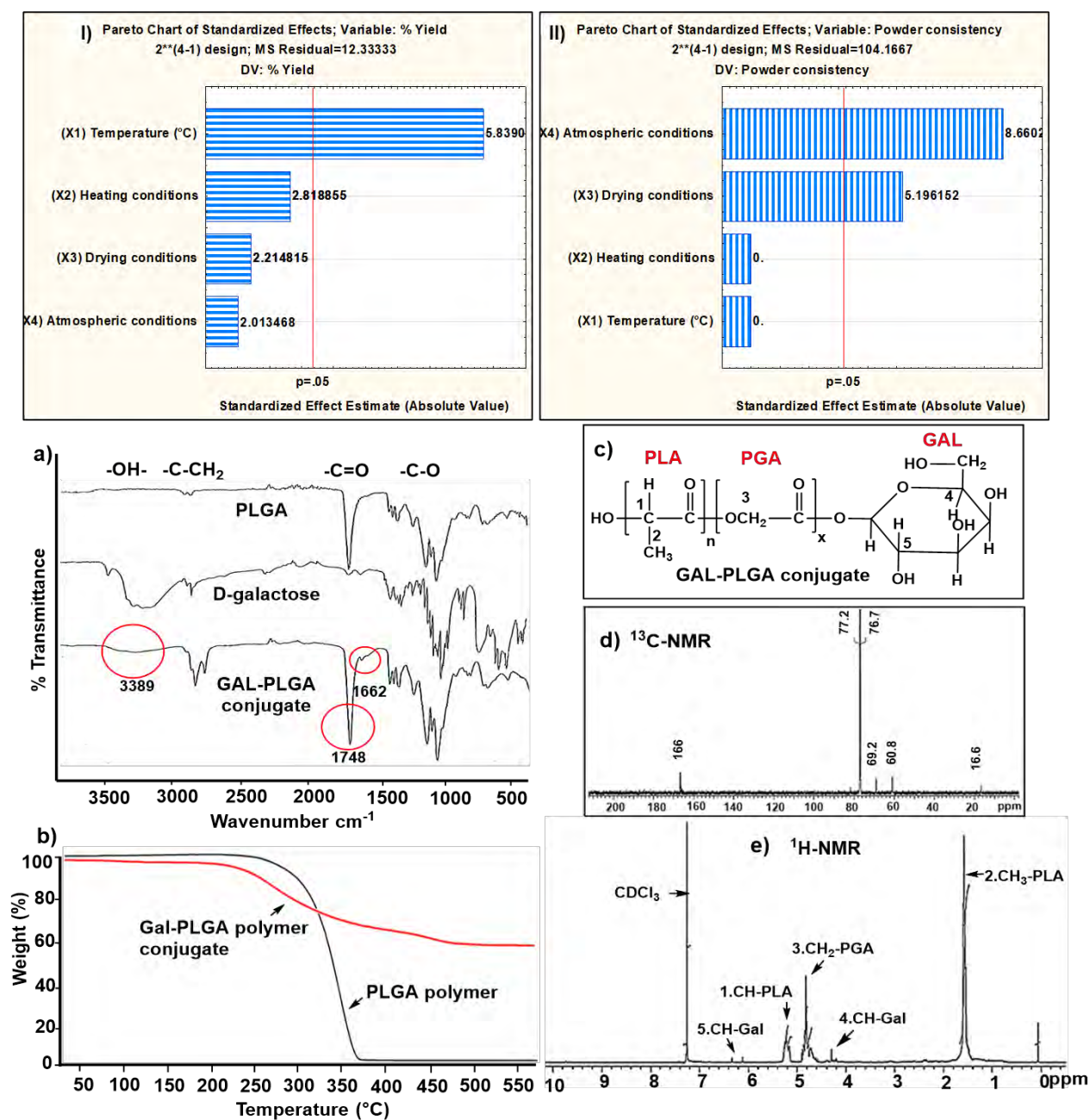


Figure 3. 4: Effect of reaction variables on quality of GAL-PLGA powder and physicochemical characterization of GAL-PLGA polymer; (I-II) Pareto chart analysis for the effect of independent variables on % Yield (Y_1) and powder consistency (Y_2) of GAL-PLGA polymer, (a-e) Characterization: Investigation of GAL-PLGA polymer synthesis through FTIR and TGA techniques (a, b) chemical structure of GAL-PLGA for the display of main functional groups (c) ¹³C-NMR and ¹H-NMR (d, e) of GAL-PLGA polymer for the confirmation of main groups (Zeeshan *et al.*, 2021)

3.3. Preparation of Drug-Loaded GAL-PLGA Nanoparticles & Optimization

3.3.1. QbD process for Dexamethasone-GAL-PLGA nanoparticles

QbD process started with defining quality target product profile (QTPP) for dexamethasone incorporated GAL-PLGA nanoparticles for macrophage targeting under inflammation with appropriate particle size control and physiochemical profile (Table 2. 2). For the fabrication of nanoparticles, initially, the critical material (CMA) and critical process attributes (CPA) were considered based on literature and preliminary experiments (Table 2. 2), and their relative impact on critical quality attributes, CQA, were determined through risk assessment using lean QbD software. Estimated inter-relations between each QTPP and CQA and between each CPP/CMA and CQA were mentioned in Figure 3. 5 (I-II) and rated on 3-levels (low, medium, and high). Severity scores clarified the significance of each variable. CPPs/CMAs with the highest impact on quality are in the order: surfactant concentration > sonication time > stirring speed (Figure 3. 5). From risk assessment scrutinization, the most influential CPPs and CMAs were further optimized during the Box-Behnken DOE. Among CQAs, particle size, encapsulation efficiency, PDI, dissolution, and zeta potential have the maximum effect on the product's quality (Figure 3. 5). Herein, we consider particle size, PDI, and zeta potential to develop a blank formulation. Classic Ishikawa cause and effect diagram categorizes influencing variables/factors into 4 major groups affecting the final product quality (Figure 2. 2 II).

3.3.2. DOE: Box-Behnken design

A 3^3 Box-Behnken design (Magalhães *et al.*, 2020) was considered because it provides fewer experimental runs, avoids extreme combinations, easy to interpret, and saves cost and time (Islam *et al.*, 2012). After initial preliminary studies and risk assessment process, surfactant concentration (A_1), stirring speed (A_2), and sonication time (A_3) were selected to be the most influential independent variables affecting product outcomes. The 3^3 Box-Behnken design, a response surface model, was chosen to design experimental conditions based on these variables and their corresponding effects. It generated 15 different combinations of independent variables and their effect on response variables particle size (Z_1), zeta potential (Z_2), and PDI (Z_3), presented in Table 3. 4. The model regression coefficient of determination (R^2) estimates its goodness of fit. R^2 for the particle size (Z_1), zeta potential (Z_2), and PDI (Z_3) were found

to be 0.97, 0.91, and 0.79 respectively, and statistical significance for all independent variables is confirmed through $p\text{-value} \ll 0.05$, indicating reasonable agreement of the results with the predicted values.

Table 3. 4: 3-level, 3-factor Box-Behnken DOE to explore the effect of independent variables (A_1 - A_3) on experimental and predicted values of response variables (particle size (Z_1), zeta potential (Z_2) and PDI (Z_3)) to control GAL-PLGA nanoparticles quality

| Runs | A ₁ - Surfactant conc. (%) | A ₂ - Stirring speed (rpm) | A ₃ - Sonication time (sec) | Z ₁ -Particle size (nm) | | Z ₂ -Zeta potential (mV) | | Z ₃ -PDI | |
|------|---|---|--|------------------------------------|-----------|-------------------------------------|-----------|---------------------|-----------|
| | | | | Experimental | Predicted | Experimental | Predicted | Experimental | Predicted |
| 1 | 1.000000 | 1500.000 | 60.00000 | 269.1 | 262.8649 | -4.63000 | -3.81793 | 0.032000 | -0.010516 |
| 2 | 3.000000 | 1500.000 | 60.00000 | 598 | 560.5099 | -7.42000 | -7.35793 | 0.181000 | 0.170734 |
| 3 | 1.000000 | 2500.000 | 60.00000 | 137 | 165.9549 | -7.50000 | -7.69793 | 0.009000 | 0.013484 |
| 4 | 3.000000 | 2500.000 | 60.00000 | 546.7 | 544.3999 | -2.80000 | -3.74793 | 0.048000 | 0.084734 |
| 5 | 1.000000 | 2000.000 | 30.00000 | 280.5 | 229.0150 | -6.05000 | -6.31500 | 0.068000 | 0.053000 |
| 6 | 3.000000 | 2000.000 | 30.00000 | 656.7 | 636.4700 | -6.64000 | -6.15500 | 0.272000 | 0.224750 |
| 7 | 1.000000 | 2000.000 | 90.00000 | 145.3 | 174.0652 | -7.00000 | -7.34913 | 0.005000 | 0.058033 |
| 8 | 3.000000 | 2000.000 | 90.00000 | 382.68 | 442.7002 | -7.50000 | -7.09913 | 0.118000 | 0.138783 |
| 9 | 2.000000 | 1500.000 | 30.00000 | 179.5 | 232.9525 | -7.01000 | -7.62500 | 0.032000 | 0.086625 |
| 10 | 2.000000 | 2500.000 | 30.00000 | 150.43 | 168.6925 | -8.30000 | -7.90500 | 0.005000 | 0.012625 |
| 11 | 2.000000 | 1500.000 | 90.00000 | 110.57 | 100.8427 | -8.50000 | -8.75913 | 0.005000 | 0.003158 |
| 12 | 2.000000 | 2500.000 | 90.00000 | 97 | 52.0827 | -9.50000 | -8.74913 | 0.064000 | 0.015158 |
| 13 | 2.000000 | 2000.000 | 90.00000 | 99.5 | 65.3591 | -8.60000 | -9.14348 | 0.064000 | 0.040870 |
| 14 | 2.000000 | 2000.000 | 60.00000 | 124.02 | 129.3052 | -8.20000 | -7.96413 | 0.005000 | 0.038783 |
| 15 | 2.000000 | 2000.000 | 60.00000 | 117.52 | 129.3052 | -8.00000 | -7.96413 | 0.061000 | 0.038783 |

Effect of independent variables on particle size (Z_1): Different experimental combinations of independent variables generated particle size in the range of 97-656 nm (Table 3. 4). The second-order polynomial equation 12 for establishing an empiric relationship between particle size (Z_1) and independent variables is:

$$Z_1 = 297.621 + 338A_1 - 56.51A_2 - 124.36A_3 + 40.4A_1A_2 - 69.410A_1A_3 + 7.75A_2A_3 - 243.129A_1^2 - 11.1A_2^2 + 1.76A_3^2 \dots\dots\dots 12$$

The equation shows a multi-variable effect on particle size, the positive sign is for synergy and the negative indicates the opposing effect. Surfactant concentration (A_1) have the maximum impact on particle size with a positive sign indicating an increase in concentration produces larger particles. It was obvious from the 3D response surface plot (Figure 3. 5 A) that initially increase in surfactant concentration from 1% to 2% decreased the particle size, however, greater than 2% concentration drastically

increased the size. Initially, particle size reduction is attributed to enhanced interfacial stabilization on increasing surfactant concentration which prevents particles agglomeration; while surfactant concentration beyond a certain limit saturates the medium and increases the viscosity with lowering of cumulative shear stress to split the droplets or it can be referred to the point of micelles formation. Further, the second effect is confirmed by quadratic relation, A_1^2 , that depicted a negative correlation i.e., particle destabilization if the surfactant concentration is highly exceeded. Next, prolongation of probe sonication time (A_3) produced greater energy density in the medium, thus elevating the intensity of shear stress which ultimately diminished particle size (Figure 3. 5 A), the effect agreed with the literature (Sharma *et al.*, 2016; Bhatt *et al.*, 2017). Likewise, stirring speed (A_2) is negatively linked with the particle size, thus increasing speed generates greater shear force to break down the droplets which reduced the particle size (Figure 3. 5 A). ANOVA confirms the significant effect of surfactant concentration and sonication time on the particle size, as $p < 0.05$ (Table 3. 5), while stirring speed although reduced the size but not significantly. Pareto chart analysis emphasizes the same results (Figure 3. 5 a).

Effect of independent variables on zeta potential (Z_2): Different combinations of independent variables generated negative zeta potential (Table 3. 4, Figure 3. 5 B). The multivariate regression equation 13 for zeta potential and its relationship with independent variables is:

$$Z_2 = -6.882 + 0.205A_1 - 0.135A_2 - 0.989A_3 + 3.745A_1A_2 + 0.045A_1A_3 + 0.145A_2A_3 - 1.919A_1^2 - 0.389A_2^2 + 0.684A_3^2 \dots \dots \dots 13$$

The model applied provides results within a 95% confidence interval. From the equation and 3D plot (Figure 3. 5 B), it is comprehended that surfactant concentration positively correlated with zeta potential, increasing concentration shifted the anionic nature of the polymer towards the neutral side. The effect was found to be consistent with studies on PLGA nanoparticles (Takeuchi *et al.*, 2017). Though the linear impact is not wide enough to be significant, its quadratic impact stood significant ($p < 0.05$), as presented through the Pareto chart (Figure 3. 5 b) and ANOVA analysis (Table 3. 6). Stirring speed have non-significant positive, while sonication time have an antagonist effect on zeta potential.

I)

| QTPP | Therapeutic indication | Route of administration | Site of activity | Target population | Dissolution profile | Physicochemical properties | Dosage form design | Severity score |
|----------------------------|------------------------|-------------------------|------------------|-------------------|---------------------|----------------------------|--------------------|----------------|
| CQA | | | | | | | | |
| Encapsulation efficiency % | Medium | Medium | Low | Medium | Medium | High | High | 41 |
| Zeta potential | Low | Low | Medium | Low | Medium | High | High | 37 |
| PDI | Low | Medium | Medium | Low | Medium | High | High | 40 |
| Appearance | Low | Medium | Low | Low | Medium | Medium | High | 34 |
| Dissolution | Low | Medium | Medium | Low | High | High | Medium | 40 |
| Particle size | High | High | High | Low | High | High | High | 55 |
| Toxicity/Irritation | Medium | Medium | High | Low | Low | Medium | Low | 34 |
| Stability | Low | Medium | Medium | Low | Low | High | Medium | 34 |

II)

| CPP/CMA | Solvent evaporation time | Sonication time | Sonication power | Drug nature | Drug to polymer ratio | Surfactant conc. | Organic-Aqueous ratio | Stirring speed |
|----------------------------|--------------------------|-----------------|------------------|-------------|-----------------------|------------------|-----------------------|----------------|
| CQA | | | | | | | | |
| Encapsulation efficiency % | High | High | Medium | High | Medium | High | Medium | High |
| Zeta potential | Medium | High | Low | Low | Medium | High | Medium | Medium |
| PDI | Medium | Medium | Low | Low | Medium | High | Medium | High |
| Appearance | Low | Medium | Low | Low | Low | High | Low | Low |
| Dissolution | Low | Low | Low | High | Medium | Medium | Medium | Low |
| Particle size | High | High | High | Medium | Medium | High | Medium | High |
| Toxicity/Irritation | Medium | Low | Low | Medium | Medium | Medium | Low | Low |
| Stability | Medium | Medium | Medium | Low | Medium | High | Low | Medium |
| Severity score | 652 | 689 | 500 | 566 | 596 | 871 | 528 | 658 |

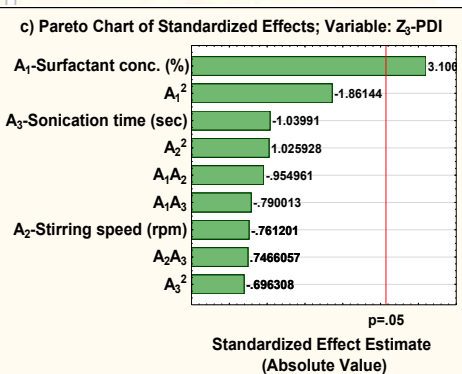
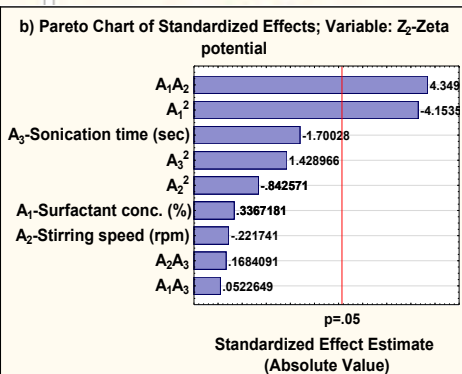
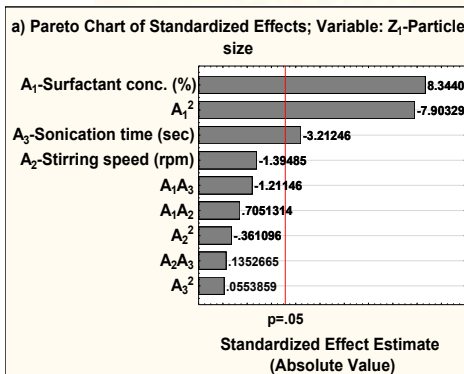
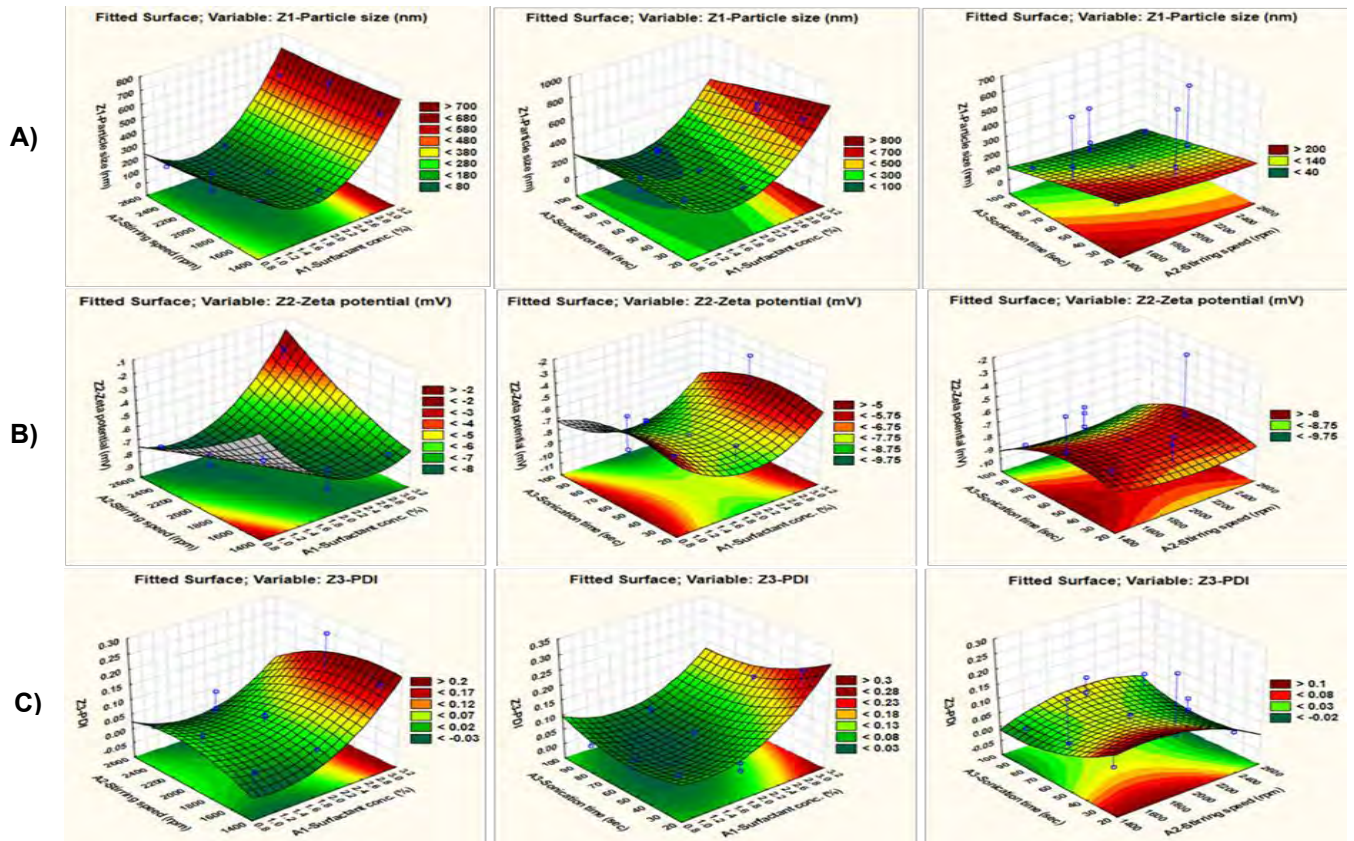


Figure 3. 5: QbD risk assessment and 3^3 Box-Behnken DOE to investigate effect of independent variables on nanoparticles outcomes; (I) Evaluation of inter-relation between each QTPP-CQA and (II) CPP/CMA-CQA with their severity scores; 3-dimensional surface (3D) plots to depict the effect of independent variables on (A) particle size, (B) zeta potential, and (C) PDI of GAL-PLGA nanoparticles under 3^3 Box-Behnken design; Pareto chart analysis of standardized effects on a) particle size, b) zeta potential and c) PDI of GAL-PLGA nanoparticles (Zeeshan *et al.*, 2021)

Effect of independent variables on PDI (Z_3): Box-Behnken model provides regression equation 14 describing influence of independent variables on PDI:

$$Z_3 = 0.0709 + 0.126A_1 - 0.031A_2 - 0.0404A_3 - 0.055A_1A_2 - 0.045A_1A_3 + 0.043A_2A_3 - 0.0575A_1^2 + 0.0317A_2^2 - 0.0223A_3^2 \dots\dots 14$$

Nearly all experimental runs provided PDI in a narrow suitable range ($\ll 0.3$) (Table 3.4). The most promising influencing parameter was surfactant concentration which directly increases PDI (Figure 3. 5 C). The significance is established through ANOVA (

Table 3. 7) and Pareto plot (Figure 3. 5 c). The increased surfactant concentration might escalate the medium viscosity which reduced shear stress and generate particles of various size distributions (Patel *et al.*, 2016b). Other variables have minimal effect on PDI. 3D response surface plots are drawn to illustrate the effects (Figure 3. 5 C).

Table 3. 5: ANOVA analysis to study effect of independent variables (A_1 - A_3) on particle size (Z_1) of GAL-PLGA nanoparticles under 3^3 Box-Behnken DOE

| Independent variable | SS | df | MS | F | P | Result |
|--------------------------------|-----------------|----------|-----------------|-----------------|-----------------|--------------------|
| A_1 -Surfactant conc. (%) | 228548.8 | 1 | 228548.8 | 69.52296 | 0.000406 | Significant |
| A_1^2 -Surfactant conc. (%) | 205218.2 | 1 | 205218.2 | 62.42595 | 0.000523 | Significant |
| A_2 -Stirring speed (rpm) | 6286.6 | 1 | 6286.6 | 1.91233 | 0.225276 | |
| A_2^2 -Stirring speed (rpm) | 471.5 | 1 | 471.5 | 0.14343 | 0.720440 | |
| A_3 -Sonication time (sec) | 33872.3 | 1 | 33872.3 | 10.30373 | 0.023730 | Significant |
| A_3^2 -Sonication time (sec) | 8.8 | 1 | 8.8 | 0.00268 | 0.960694 | |
| A_1A_2 | 1632.2 | 1 | 1632.2 | 0.49649 | 0.512503 | |
| A_1A_3 | 4817.7 | 1 | 4817.7 | 1.46553 | 0.280151 | |
| A_2A_3 | 74.6 | 1 | 74.6 | 0.02271 | 0.886110 | |
| Error | 16436.9 | 5 | 3287.4 | | | |
| Total SS | 529675.3 | 14 | | | | |

Table 3. 6: ANOVA analysis to study effect of independent variables (A_1 - A_3) on zeta potential (Z_2) of GAL-PLGA nanoparticles under 3^3 Box-Behnken DOE

| Independent variable | SS | df | MS | F | p | Result |
|--------------------------------|-----------------|----------|-----------------|-----------------|-----------------|--------------------|
| A_1 -Surfactant conc. (%) | 0.08405 | 1 | 0.08405 | 0.11338 | 0.750002 | |
| A_1^2 -Surfactant conc. (%) | 12.78938 | 1 | 12.78938 | 17.25220 | 0.008879 | Significant |
| A_2 -Stirring speed (rpm) | 0.03645 | 1 | 0.03645 | 0.04917 | 0.833287 | |
| A_2^2 -Stirring speed (rpm) | 0.52628 | 1 | 0.52628 | 0.70993 | 0.437904 | |
| A_3 -Sonication time (sec) | 2.14312 | 1 | 2.14312 | 2.89095 | 0.149823 | |
| A_3^2 -Sonication time (sec) | 1.51373 | 1 | 1.51373 | 2.04194 | 0.212392 | |
| A_1A_2 | 14.02503 | 1 | 14.02503 | 18.91903 | 0.007362 | Significant |
| A_1A_3 | 0.00203 | 1 | 0.00203 | 0.00273 | 0.960341 | |
| A_2A_3 | 0.02103 | 1 | 0.02103 | 0.02836 | 0.872862 | |
| Error | 3.70659 | 5 | 0.74132 | | | |
| Total SS | 39.68733 | 14 | | | | |

Table 3. 7: ANOVA analysis to study effect of independent variables (A_1 - A_3) on PDI (Z_3) of GAL-PLGA nanoparticles under 3^3 Box-Behnken DOE

| Independent variable | SS | df | MS | F | p | Result |
|--------------------------------|-----------------|----------|-----------------|-----------------|-----------------|--------------------|
| A_1 -Surfactant conc. (%) | 0.031878 | 1 | 0.031878 | 9.610334 | 0.026852 | Significant |
| A_1^2 -Surfactant conc. (%) | 0.011493 | 1 | 0.011493 | 3.464957 | 0.121745 | |
| A_2 -Stirring speed (rpm) | 0.001922 | 1 | 0.001922 | 0.579427 | 0.480876 | |
| A_2^2 -Stirring speed (rpm) | 0.003491 | 1 | 0.003491 | 1.052528 | 0.351973 | |
| A_3 -Sonication time (sec) | 0.003587 | 1 | 0.003587 | 1.081421 | 0.346029 | |
| A_3^2 -Sonication time (sec) | 0.001608 | 1 | 0.001608 | 0.484844 | 0.517270 | |
| A_1A_2 | 0.003025 | 1 | 0.003025 | 0.911950 | 0.383454 | |
| A_1A_3 | 0.002070 | 1 | 0.002070 | 0.624121 | 0.465319 | |
| A_2A_3 | 0.001849 | 1 | 0.001849 | 0.557420 | 0.488898 | |
| Error | 0.016585 | 5 | 0.003317 | | | |
| Total SS | 0.079142 | 14 | | | | |

3.3.3. Experimental design validation and optimization

Box-Behnken model predicted values for the response variables including particle size (Z_1), zeta potential (Z_2), and PDI (Z_3) are found to be in good agreement with the experimental values apart from little variations (Table 3. 4). The profiles for predicted response values and desirability was obtained using STATISTICA[®] 10.0 software, as presented in Figure 3. 6. The suitable combination of independent variables (2% surfactant concentration, 2500 rpm stirring speed, and 90 seconds sonication time) that produced desirable outcomes have proceeded for characterization.

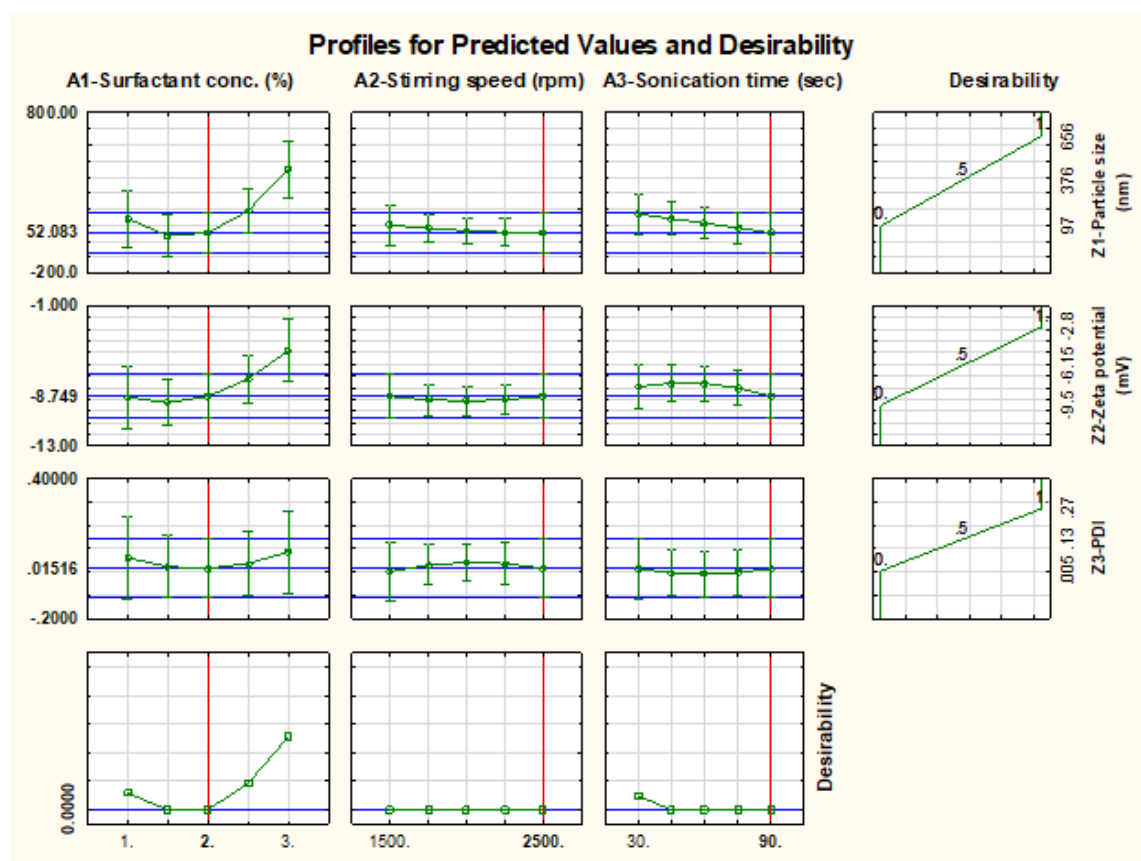


Figure 3. 6: Prediction and desirability profiling of the optimum values of independent variables to produced GAL-PLGA nanoparticles with desired characteristics (Zeeshan *et al.*, 2021)

3.3.4. Physicochemical characterization

The optimized formulation from the Box-Behnken design was replicated thrice and characterized for physicochemical properties; and loaded with dexamethasone drug. The average hydrodynamic particle size for blank and drug-loaded GAL-PLGA nanoparticles was $97.74 \text{ nm} \pm 0.72 \text{ nm}$ and $118.77 \text{ nm} \pm 0.74 \text{ nm}$, respectively (Figure 3. 7 a-c). Additionally, SEM morphological examination indicated nanoparticles with round spherical shape and smooth topology (Figure 3. 7 b). Particle size below 200 nm is favorable for enhanced epithelial permeability and retention effect at the inflamed region and the efficient immune cells uptake (Zeeshan *et al.*, 2019a). Moreover, zeta potential was found to be $-9.58 \pm 0.19 \text{ mV}$ (Figure 3.7 c). Negative zeta potential value is the characteristic for PLGA and similar values were reported for GAL-PLGA nanoparticles (Gupta *et al.*, 2013). The negative charge may persist because of remaining PLGA carboxylic functional groups. The anionic nature represented PLGA and galactose moiety and stabilizes the structure with charge-charge repulsion among

particles. Furthermore, PDI lesser $\ll 0.1$ indicated homogenous particle size distribution (Figure 3. 7 a-c) and this mono-disperse system is more reluctant to be removed by the reticuloendothelial system (Sipos *et al.*, 2020). Various drug-polymer ratios were investigated in the preliminary studies with minor differences in EE, therefore, 1:10 was chosen with EE of about $87.33 \pm 3.47 \%$ and drug loading of about $79.39 \pm 3.15 \mu\text{g}$ per mg GAL-PLGA nanoparticles (Figure 3. 7 c). Stability analysis of Dexamethasone (Dexa)-GAL-PLGA nanoparticles according to ICH guidelines for 6 months revealed particle size and zeta potential lied within a suitable range, and the drug content was little bit decreased but within the limit, as listed in Table 3. 8.

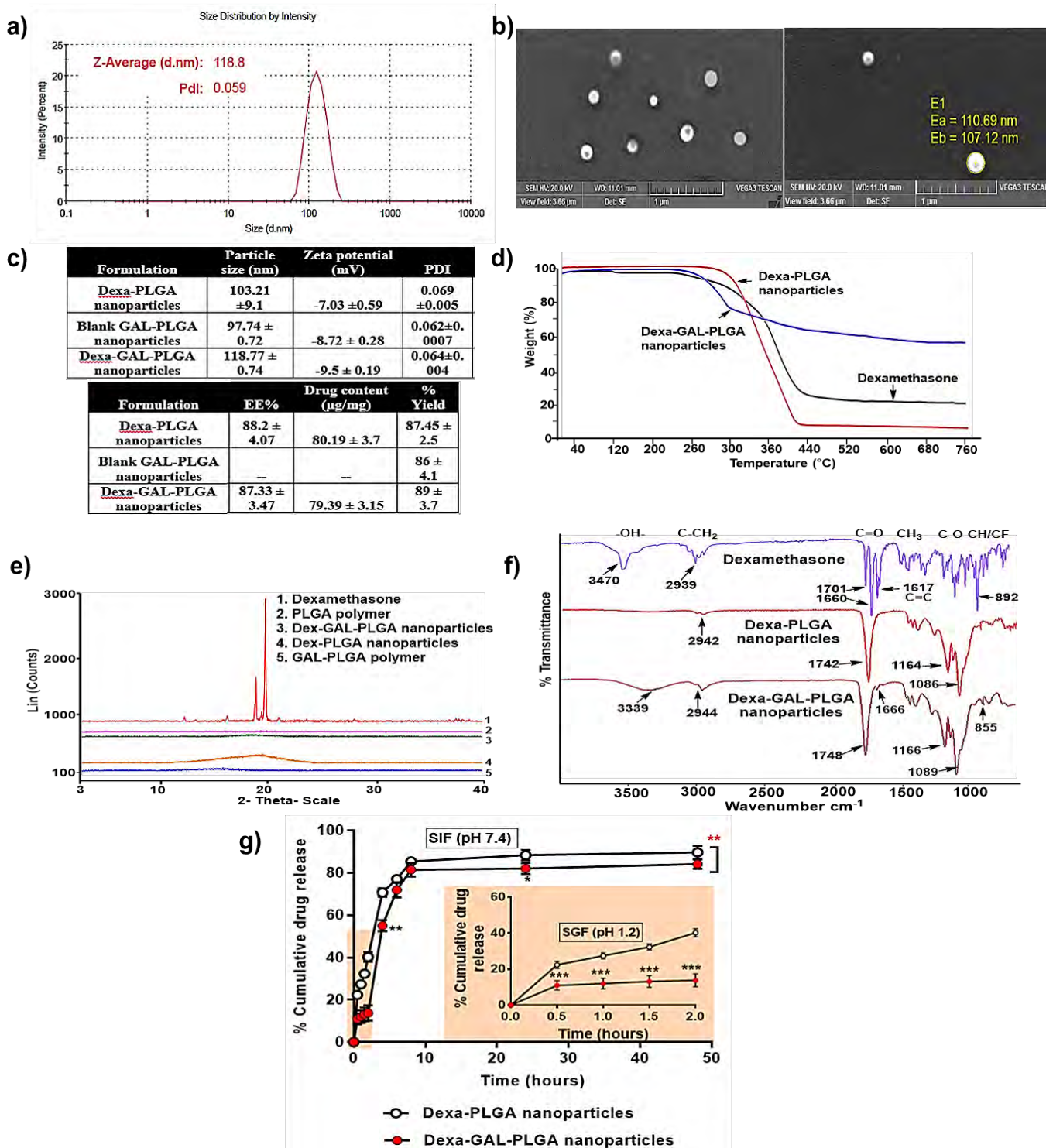


Figure 3. 7: Physicochemical and *In vitro* characteristics of Dexa-GAL-PLGA nanoparticles (a) particle size (nm) and PDI (b) surface morphology through SEM analysis (c) physicochemical properties and drug content (d) thermal analysis under TGA (e) XPRD spectra of drug, polymers and drug loaded nanoparticles; (f) FTIR spectra of drug and drug loaded nanoparticles; (g) *In vitro* dexamethasone release from plain PLGA and GAL-PLGA nanoparticles at pH 1.2 (SGF) and pH 7.4 (SIF), statistical comparison (t-test) between release profiles $p < 0.05^*$, $p < 0.01^{**}$, $p < 0.001^{***}$, (n=3) (Zeeshan *et al.*, 2021)

Table 3. 8: Effect of storage conditions on physicochemical characteristics of Dexamethasone loaded GAL-PLGA nanoparticles

| Dexa-GAL-PLGA nanoparticles | Initial | | After 1 month | | After 6 months | |
|-----------------------------|------------|------------|---------------|------------|----------------|------------|
| | 4°C | 25°C | 4°C | 25°C | 4°C | 25°C |
| Particle size (nm) | 118.8±0.74 | 118.8±0.74 | 118.8±0.74 | 123.5±1.2 | 121.9±1.5 | 137.1±1.87 |
| Zeta potential (mV) | -9.5±0.19 | -9.5±0.19 | -9.5 ± 0.5 | -9.1±0.25 | -9.4±1.1 | -9.05±0.75 |
| Drug content (µg/mg) | 79.39±3.15 | 79.39±3.15 | 77.45±1.35 | 76.15±0.55 | 77.0±2.25 | 75.45±1.25 |

3.3.5. TGA

The thermal behavior of pure dexamethasone, Dexa-PLGA nanoparticles, and Dexa-GAL-PLGA nanoparticles was evaluated through TGA analysis. Dexamethasone thermal evaluation indicated about 80% of the mass loss gradually between 250-440°C (Figure 3. 7 e), because of drug decomposition into various products including β -hydroxy dexamethasone and dexamethasone-21-oic acid (Jain and Datta, 2015). After then, the weight became constant (about 20%) due to the formation of carbon black. Dexa-PLGA nanoparticles showed complete single-step thermal degradation started at a temperature of 300°C with 94.11 % weight loss, followed by a constant weight (~6 %) due to carbon black. For Dexa-GAL-PLGA nanoparticles, total mass loss was 35.41% as signaled by an initial peak around 260-300°C followed by a broad down peak gradually declined from 300°C to 680°C. Thereafter, the peak became constant. Although degradation was continuous and started earlier, however, approximately 64 % of the mass either remained stable against degradation or constituted residual matter (Figure 3. 7 e). It has been established that the addition of D-galactose moiety to the polymers brought decomposition more gradual with more char content at the end (Saltan and Akat, 2013). The pattern matches to thermal decomposition pattern of GAL-PLGA polymer and depicted that polymer properties stayed unchanged while fabricating their nanocarriers.

3.3.6. X-ray powder diffraction (XPRD) analysis

XPRD patterns of dexamethasone, polymers, and nanoparticles were obtained to investigate the physical form of the entrapped drug inside the polymeric nanocarrier. Dexamethasone in the pure state had peaks at 12.5, 16.5, and between 18-20 2 θ (Figure 3. 7 f), reflecting crystalline nature. On contrary, polymers including PLGA and GAL-

PLGA are amorphous in nature and their spectra have no sharp peak. While dexamethasone inside the PLGA and GAL-PLGA nanoparticles resided in the amorphous form, as reflected from smooth, low-intensity spectra of the nanoparticles, as shown in Figure 3. 7 f. Additionally, the absence of dexamethasone sharp peak in the PLGA and GAL-PLGA nanoparticles spectra confirmed complete encapsulation of the drug and negate the presence of surface-bound drug traces. During preparation, dexamethasone was dispersed in a molecular state and entrapped within PLGA polymeric structure in an amorphous form.

3.3.7. FTIR of excipients and formulation

FTIR spectra of dexamethasone drug, drug-loaded PLGA, and GAL-PLGA nanoparticles were obtained to identify possible drug-polymer molecular interaction and drug entrapment inside nanoparticles. The FTIR spectrum of dexamethasone (Figure 3. 7 g) exhibited main peaks at 3470 cm^{-1} , 2939 cm^{-1} , 1701 cm^{-1} , 1660 cm^{-1} , 1617 cm^{-1} , 1392 cm^{-1} , 1080 and 892 cm^{-1} corresponding to -OH, -CH₂, aldehyde C=O, ketone C=O, C=C, CH₃, C-O and C-F functional groups respectively. The Dexa-PLGA nanoparticles spectra, Figure 3. 7 g, have representative bands of -CH₂, C=O, C-OH in-plane, -CH₃, esteric C-O, alcoholic C-O at 2942 cm^{-1} , 1742 cm^{-1} , 1422 cm^{-1} , 1382 cm^{-1} , 1164 cm^{-1} , 1086 cm^{-1} respectively, the spectra mimics previous findings (Nejad *et al.*, 2019). FTIR spectrum of Dexa-GAL-PLGA nanoparticles (Figure 3. 7 g) have a broadened peak of -OH at 3339 cm^{-1} and a pointed peak of CH₃ at 2944 cm^{-1} . Furthermore, ester C=O stretch at 1748 cm^{-1} and 1666 cm^{-1} , ester C-O peak at 1166 cm^{-1} and alcoholic C-O pointed at 1089 cm^{-1} . A smaller peak at 855 cm^{-1} indicated either C-F or C-H group of drug or GAL-PLGA, respectively. The spectra of drug-loaded PLGA and GAL-PLGA nanoparticles negate new bond formation or changes in the bond position which nullify drug-polymer interaction. Further, nanoparticles spectra retained the position of the peaks as found in the respective polymer, Figure 3.4 a, which confirmed the physical entanglement of the drug in the polymeric nanocarrier. Drug bands were not obvious in both types of nanoparticles which ensured complete drug encapsulation with minimal chances of the surface-bound drug. However, a bit sharper bond intensity represented drug presence inside the nanoparticles (Figure 3. 7 g).

3.4. *In Vitro* Drug Release Study

Drug release study was performed in simulated fluids, SGF (pH 1.2) and SIF (pH 7.4), Figure 3. 7 h, based on the physiological pH of the stomach and large intestine (Ali *et al.*, 2014). In the first 2 hours, DEXA-PLGA nanoparticles showed an abrupt release of a drug, accounting for almost 40% of drug release. Whereas DEXA-GAL-PLGA nanoparticles have statistically relevant control over immediate drug release in the initial 2 hours in SGF. After pH change to 7.4 (SIF), the drug release pattern of both PLGA and GAL-PLGA nanoparticles was almost parallel and sustained. About 89.6% drug was released in SIF till 48 hours from PLGA nanoparticles. While 84% drug was released from GAL-PLGA nanoparticles in 48 hours (Figure 3. 7 h).

Basically, the polymeric nanocarriers like PLGA and derived-PLGA nanoparticles exhibited a biphasic drug release pattern, an initial burst release of the drug which is followed by a sustained release pattern (Ali *et al.*, 2016; Godse *et al.*, 2021). Attachment of galactose to the PLGA backbone has the same biphasic pattern of drug release (Godse *et al.*, 2021). That is why a slowdown occurred in the drug release pattern of the GAL-PLGA nanoparticles, which demonstrated the typical sustained release pattern after an initial phase.

However, GAL-PLGA predominantly controlled the burst release effect of bare PLGA particles and is, therefore, suitable to be considered for colon drug delivery. The student's t-test was applied to differentiate between time points of release profiles of PLGA and GAL-PLGA nanoparticles. At pH 1.2, each time point significantly differs from the other ($p < 0.001$); whereas only two-time points showed a difference at pH 7.4, the rest of the points did not differ (Figure 3. 7 h).

If we compare the drug release from plain PLGA and GAL-PLGA nanoparticles in the first 2 hours at acidic pH (1.2), the burst release content was very much controlled in the case of GAL-PLGA nanoparticles because of possible steric hindrance conferred by the galactose moiety on attachment to PLGA backbone. The addition of galactose conferred structural stability to the GAL-PLGA nanostructure from initial abrupt disintegration at acidic conditions (pH 1.2), thus offering a steric barrier to the initial burst of the drug (Jain *et al.*, 2015). Further, when pH was changed to 7.4 after 2 hours, the first time point (at 4th hour) also significantly differ between the two profiles. Therefore, we can postulate that galactose moiety induced structural integrity which

hinders abrupt diffusion of drug in the initial hours, thereafter, the profile pattern became parallel to PLGA nanoparticles. It does not depict pH-mediated drug release, however, controlled earlier burst release avoids drug dumping in upper GIT regions and facilitates colon targeting.

One-way ANOVA analysis compared whole release profiles and declared both to differ insignificantly with p-value >0.05 . Thus, difference occurred in the initial time points (0.5-4 hours) drug release, thereafter the pattern of the two profiles became similar

3.4.1. Drug release kinetic modeling

With more advancement, it is necessary to evaluate release kinetics through mathematical models and evaluate the behavior and mechanism of drug release from nanoparticles using the DDSolver program. Based on R, R^2 , RMSE, MSC, and AIC parameters, both Korsmeyer-Peppas and Peppas-Sahlin models were best fitted for the drug release profile of GAL-PLGA nanoparticles at pH 1.2 (Table 3. 9). The reason behind this is when Peppas-Sahlin's coefficients $k_1 > k_2$, then the system favored the release of drug molecule more towards diffusion mechanism rather than polymer chain relaxation and its m-value becomes equal to the n-value of Korsmeyer-Peppas (Freire *et al.*, 2017). Therefore, both models explained the drug release in the same manner without the involvement of polymer chain relaxation or elongation. In this case, the value is near to n-value ($m=0.128$, $n=0.17$) and Fickian was the major drug release mechanism because n/m are lesser than 0.5. The same trend was observed for drug release data from the PLGA nanoparticles with $k_1 > k_2$, $n=0.43$, and $m=0.33$. Peppas-Sahlin and Korsmeyer-Peppas models describe the release of a drug from the polymeric systems as a function of either diffusion or polymer relaxation or both (Bruschi, 2015). At pH 7.4, Peppas-Sahlin remains the best-fitted model for both PLGA and GAL-PLGA nanoparticles with the highest R, R^2 and MSC, lowest RMSE, and AIC and $k_1 > k_2$, m-value was approaching n-value and Fickian diffusion as a drug release mechanism (Table 3. 9).

Table 3. 9: Mathematical models describing drug release kinetics from GAL-PLGA and PLGA nanoparticles at pH 1.2 (SGF) and pH 7.4 (SIF)

| a) Dexamethasone loaded GAL-PLGA nanoparticles (pH 1.2) | | | | | | |
|--|-------------------|--------------------|----------------|-------------------------------|----------------------|------------------------------------|
| Parameter | Zero order | First order | Higuchi | Korsmeyer-Peppas | Hixon-Crowell | Peppas-Sahlin |
| R | 0.9177 | 0.9286 | 0.9883 | 0.9947 | 0.9250 | 0.9950 |
| R ² | 0.7394 | 0.7823 | 0.9734 | 0.9894 | 0.7686 | 0.9901 |
| RMSE | 3.8079 | 3.4800 | 1.2162 | 0.8850 | 3.5877 | 1.0503 |
| AIC | 22.3022 | 21.4017 | 10.8892 | 8.2716 | 21.7066 | 9.9568 |
| MSC | -0.2161 | -0.0360 | 2.0665 | 2.5900 | -0.0970 | 2.2530 |
| Other | k0=11.13 | k1=0.124 | kH=14.005 | kkp=14.6379, n=0.36 | Khc=0.04 | k1=9.74, k2=4.86, m=0.271 |
| b) Dexamethasone loaded PLGA nanoparticles (pH 1.2) | | | | | | |
| Parameter | Zero order | First order | Higuchi | Korsmeyer-Peppas | Hixon-Crowell | Peppas-Sahlin |
| R | 0.9419 | 0.9607 | 0.9942 | 0.9953 | 0.9550 | 0.9957 |
| R ² | 0.8138 | 0.8857 | 0.9885 | 0.9906 | 0.8647 | 0.9915 |
| RMSE | 6.5500 | 5.1330 | 1.8800 | 1.6990 | 5.5840 | 1.9800 |
| AIC | 27.7260 | 25.2800 | 15.8100 | 14.7900 | 26.1300 | 16.3110 |
| MSC | 0.2340 | 0.7220 | 2.6200 | 2.8200 | 0.5500 | 2.5000 |
| Other | k0=22.33 | k1=0.284 | kH=27.3 | Kkp=28.49, n=0.43 | kHC=0.087 | k1=19.1, k2=9.28, m=0.33 |
| c) Dexamethasone loaded GAL-PLGA nanoparticles (pH 7.4) | | | | | | |
| Parameter | Zero order | First order | Higuchi | Korsmeyer-Peppas | Hixon-Crowell | Peppas-Sahlin |
| R | 0.5756 | 0.9773 | 0.7886 | 0.9768 | 0.8361 | 0.9865 |
| R ² | -1.0522 | 0.8951 | 0.6219 | 0.9541 | 0.4785 | 0.9732 |
| RMSE | 46.4470 | 10.4993 | 22.2900 | 7.7700 | 23.4100 | 6.8600 |
| AIC | 57.7165 | 39.8723 | 49.5676 | 36.9218 | 49.4966 | 35.6968 |
| MSC | -2.4020 | 0.5720 | -1.0439 | 1.0638 | -1.0320 | 1.2679 |
| Other | k0=2.439 | k1=0.203 | kH=10.584 | kkp=56.13, n=0.115 | khc=0.03 | k1=46.99, k2=-6.33, m=0.392 |
| d) Dexamethasone loaded PLGA nanoparticles (pH 7.4) | | | | | | |
| Parameter | Zero order | First order | Higuchi | Korsmeyer-Peppas | Hixon-Crowell | Peppas-Sahlin |
| R | 0.5414 | 0.9894 | 0.7635 | 0.9947 | 0.8046 | 0.9978 |
| R ² | -1.2858 | 0.9524 | 0.5830 | 0.9895 | 0.3680 | 0.9957 |
| RMSE | 51.9100 | 7.4900 | 24.7900 | 3.9300 | 27.2900 | 2.9100 |
| AIC | 59.0503 | 35.8231 | 50.8419 | 28.7405 | 51.3367 | 25.4115 |
| MSC | -2.7502 | 1.1210 | -1.3822 | 2.3014 | -1.4646 | 2.8562 |
| Other | k0=2.62 | k1=0.268 | kH=10.86 | kkp=67.05, n=0.082 | khc=0.032 | k1=66.28, k2=-12, m=0.296 |

3.5. In Vitro Biocompatibility Studies

3.5.1. Hemolysis assay

RBCs *In vitro* compatibility experiment assured that both Dexamethasone (Dexa)-PLGA and Dexa-GAL-PLGA nanoparticles have negligible toxicity potential. Different concentrations of dexamethasone loaded PLGA nanoparticles have 1.3-1.538% and GAL-PLGA nanoparticles have 0.53-0.68% hemolytic activity compared to the positive control (Triton-X) after 24 hours (Figure 3. 8 a). Both types of polymeric nanocarriers were found to be RBCs friendly and thus safe and compatible to be delivered through any route and exposure to blood content.

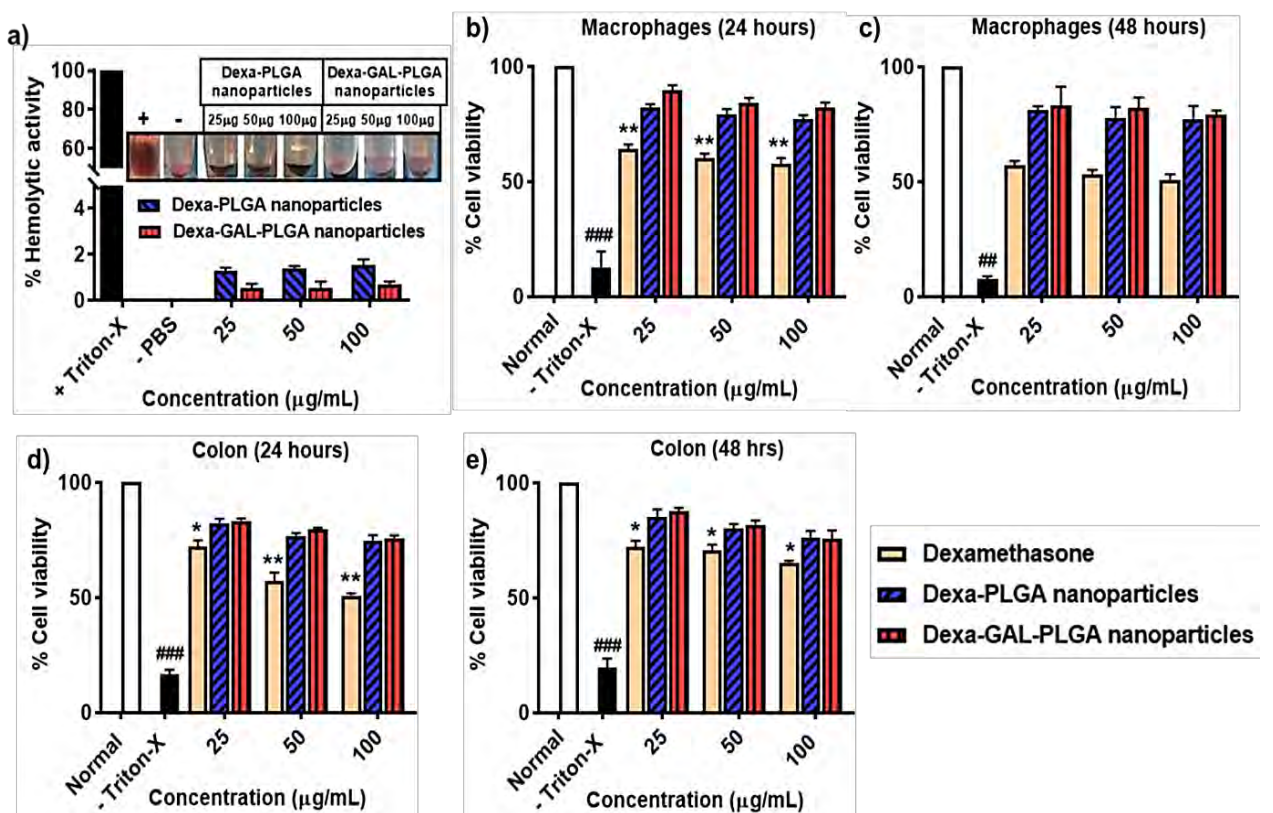


Figure 3. 8: In vitro hemolysis and cellular biocompatibility assessment of GAL-PLGA nanoparticles; In vitro hemocompatibility of drug-loaded PLGA and GAL-PLGA nanoparticles (a), In vitro cytotoxic evaluation of drug-loaded PLGA and GAL-PLGA nanoparticles on macrophages after 24 hours (b) and 48 hours (c), and colon cells biocompatibility of drug-loaded PLGA and GAL-PLGA nanoparticles after 24 hours (d) and 48 hours (e); Statistical comparison of groups with Normal control $p < 0.05^*$, $p < 0.01^{**}$, $p < 0.001^{***}$, Normal vs Triton-X: $p < 0.05^{\#}$, $p < 0.01^{\#\#}$, $p < 0.001^{\#\#\#}$ (Zeeshan *et al.*, 2021)

3.5.2. *In vitro* cell-based cytotoxicity assay on derived macrophages and colon cells

Extracted macrophages and colon cells were morphologically analyzed, and trypan blue exclusion assay and FACS apoptotic assay of colon cells validated their viability. Drug loaded PLGA and GAL-PLGA nanoparticles were incubated at various concentrations with murine-derived macrophages and colon cells and evaluated for cytotoxic potential using MTT assay. Various concentrations of PLGA nanoparticles remained biocompatible with 77-82% and 77-81% macrophage viability and 74-82% and 76-85% colon cell viability after 24 and 48 hours, respectively. Likewise, Dexa-GAL-PLGA, in different strengths, proved to be more bio-safer with 82-89% and 79-83% macrophage viability and 75-83% and 75-87% colon cells viability after 24 and 48 hours, respectively (Figure 3. 8 b-e). All groups were compared with normal (untreated) cells control and differ insignificantly. Whereas dexamethasone free drug lowered viable cell count to a statistically significant level. A negative control (triton X) was run to control experimental validity and found to reduced cell viability widely (Figure 3. 8 b-e). Hence, Dexa-GAL-PLGA nanoparticles proved to be non-toxic on living cells and safer to be delivered to the large intestine. Moreover, conjugation of D-galactose moiety enhanced the inert nature of the drug-loaded polymeric nanocarrier and neither the solvents nor the synthesis reaction declined biocompatibility.

3.5.3. Cellular uptake studies

Cell-mediated endocytosis by murine macrophages and colon cells was observed through loading of nanoparticles with a fluorescent dye (rhodamine-B for macrophage study, fluorescein for colon cells), then incorporated nanoparticles to the cell cultures and visualized radiating fluorescence of the fed cells. Plain dye was used as an experimental control and have minimal uptake by the cells. It was obvious that GAL-PLGA nanoparticles have greater cellular uptake compared to PLGA nanoparticles by macrophages and colon cells (Figure 3. 9 a, b). Furthermore, the fluorescence intensity of GAL-PLGA nanoparticles was found significantly superior to the counterpart in the macrophages ($p < 0.001$) and colon cells ($p < 0.001$) (Figure 3. 9 c, d), measured through ImageJ software (NIH, USA). Thus, D-galactose anchored PLGA nanoparticles are preferable for macrophage targeting under inflammation of the intestine.

3.5.4. Elucidation of galactose mediated cell uptake by murine macrophages

To further investigate the role of D-galactose in the GAL-PLGA nanoparticles in targeting macrophages via the MGL-2 receptor, we added free D-galactose to the cell culture and visualized after 4 hours. Cellular uptake efficiency of GAL-PLGA nanoparticle markedly diminished in the presence of D-galactose ($p < 0.001$) (Figure 3. 9 a), suggesting MGL-2 governed major contribution in the endocytosis of GAL-PLGA nanoparticles into the macrophages. Investigations hypothesized the higher intensity was a combined effect of size-mediated uptake and galactose-binding MGL-2 receptor-mediated uptake of GAL-PLGA nanoparticles by the macrophages (Figure 3. 9 a). In the colon cells, though PLGA nanoparticles endocytosed because of nano-size range, still GAL-PLGA nanoparticles engulfed with more preference than PLGA nanoparticles (Figure 3. 9 b) either because of clathrin-mediated endocytosis rather than lipid raft/ caveolae facilitated uptake (Dalal and Jana, 2018) or SGLT1/GLUT mediated transport across colon epithelium (Merigo *et al.*, 2018). Thus, GAL-PLGA nanoparticles have a more chance to reside at the inflamed colon tissues which prolonged drug release and therapeutic efficacy. GAL-PLGA nanoparticles have an additional advantage of ligand directed uptake through the MGL-2 receptor which subsides plasma membrane barrier potential in the uptake of PLGA nanoparticles (Lu *et al.*, 2019).

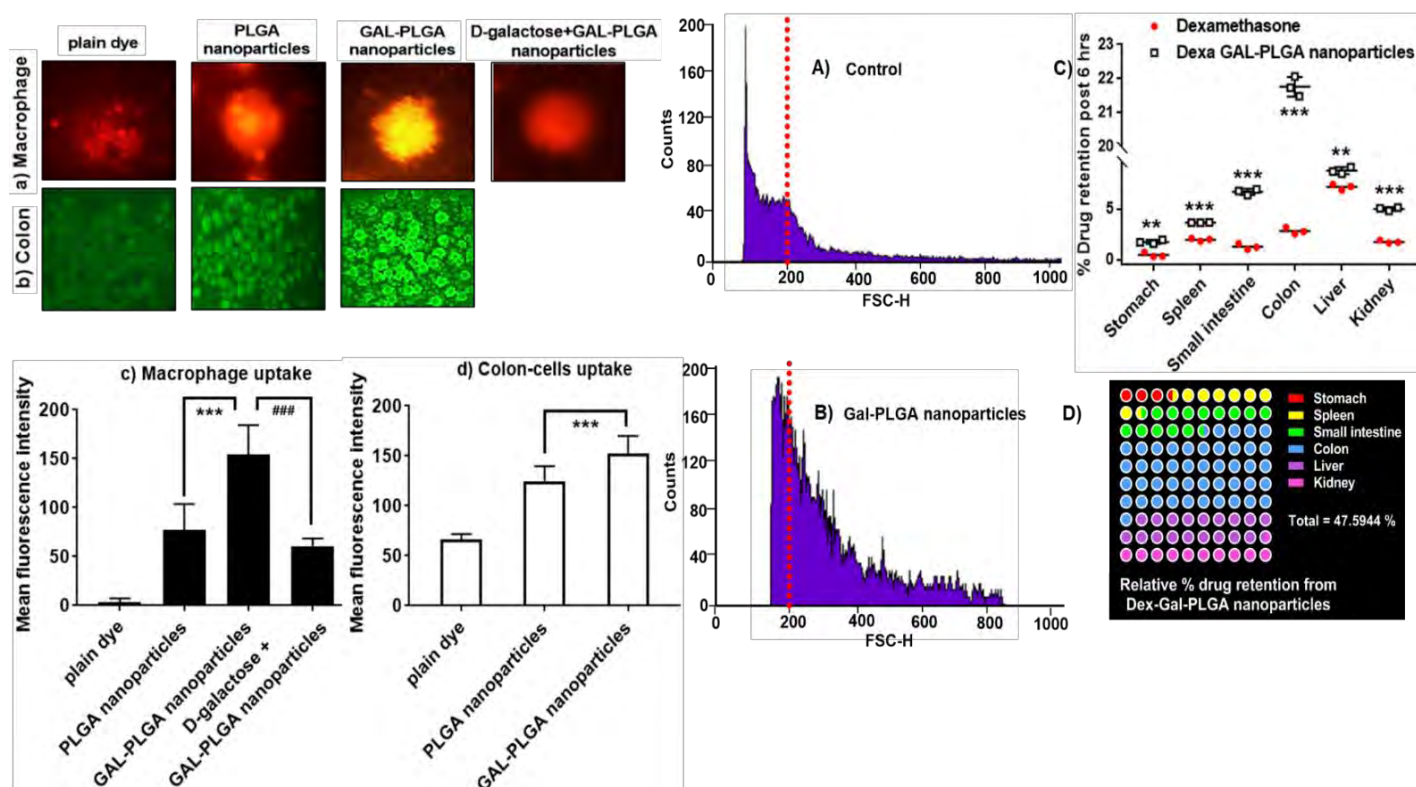


Figure 3. 9: Cell uptake assays and in vivo biodistribution studies of GAL-PLGA nanoparticles; Cellular uptake of dye loaded PLGA and GAL-PLGA nanoparticles by macrophages (a) and colon cells (b) visualized through fluorescent microscopy (100X); mean fluorescence exhibited by macrophages (c) and colon cells (d), Statistical comparison between PLGA and GAL-PLGA nanoparticles groups $p < 0.001$ *** (c), and between GAL-PLGA and D-galactose treated GAL-PLGA nanoparticles $p < 0.001$ ### (d) ($n=3$); Flow cytometry analysis of cellular uptake of fluorescein loaded GAL-PLGA nanoparticles by colon derived macrophages recruited under inflammation (A-control cells, B-GAL-PLGA nanoparticles treated); % drug released and retained in the major organs from GAL-PLGA nanoparticles after 6 hours of oral administration in the DSS-induced colon inflamed mice (C, D), Statistical comparison between GAL-PLGA nanoparticles and Dexamethasone groups $p < 0.05$ *, $p < 0.01$ **, $p < 0.001$ ***, $n=3$. (Zeeshan *et al.*, 2021)

3.6. *In Vivo* Preliminary Studies to Understand Nanoparticles Behavior in the Inflammation

3.6.1. Flow cytometric analysis

Fluorescein dye loaded GAL-PLGA nanoparticles were administered to the DSS mice and then harvested colon-macrophage mediated uptake was studied under flow cytometry. Untreated cells were used as control. The FCS analysis was performed to assess morphological and molecular deviations in the cells upon nanoparticles

treatment (Patel *et al.*, 2016a; Alwani *et al.*, 2016). A pronounced internalization of GAL-PLGA nanoparticles was observed with a right-shift in the forward scattered plot (FSC-H) because of the size increase and structural complexity of the cells (Figure 3. 9 A, B), demonstrating the potential of nano-formulation to efficiently target macrophages under intestine inflammation.

3.6.2. Accumulation of nano-formulation in the visceral organs and colon under inflammation

To evaluate nanoparticles targeting potential, localization, and distribution, the released drug was quantified in the major GI sections, stomach, small intestine and colon, and visceral organs namely liver, spleen, and kidney. % Drug concentration was found to be highest in the colon of DSS induced colitis mice (n=3) followed by liver and small intestine (Figure 3. 9 C, D). The greater proportion in the colon indicated higher GAL-PLGA nanoparticle residence at the inflamed colon, because of a large number of macrophages with galactose bound MGL-2 receptor. After the inflamed colon, drug retention in the liver might be because of asialoglycoprotein receptors with galactose affinity. An experiment of blank GAL-PLGA nanoparticles was run in parallel for control. The role of MGL-2 is established more in the case of inflammation, otherwise, in normal conditions, galactose anchored carriers have low accumulation in the large intestine because of lack of activated macrophages at the site and involvement of sugar transport receptors (Siu *et al.*, 2018). On contrary, plain dexamethasone drug failed to reside in the inflamed colon tissues and was found mostly in the liver because early absorption of plain drug enabled its reach to the organ of metabolism (liver) in a shorter period eliminates rapidly (Figure 3. 9 C). It demonstrated macrophage receptor MGL-2 targeting through galactose anchored PLGA nanoparticles prolonged drug residence at the inflamed colon, thus, prolonging drug release and therapeutic action, and could have promising potential to cure IBD and associated intestinal diseases.

PART-I (SECTION B)

Note: This section is further modification of GAL-PLGA Nanoparticles with specific stimuli sensitive coatings to make the particles more efficient in targeting inflamed colon. The prepared nanocargoes in this section are designated as Dexa loaded GAL-PLGA nanoparticles (Dexa-GP NPs), ES100 coated Dexa-GP nanocargoes (Dexa-GP/ES NCs), Pullulan coated Dexa-GP nanocargoes (Dexa-GP/Pu NCs) and ES100/Pullulan coated Dexa-GP nanocargoes (Dexa-GP/ES/Pu NCs). The focus is on the last one for the activities

3.7. Synthesis of Nanocargoes and Characterization

Dexa loaded GP (Dexa-GP) NPs were prepared through a modified O/W emulsion method with desired attributes. Next, Dexa-GP NPs coating with ES100 and pullulan produced Dexa-GP/ES/Pu NCs having both pH sensitive and microbial sensitive characteristics. For coating, ES100 to pullulan in 1:1 and 2:1 ratio were considered and further evaluated for drug release function at pH 1.2 to avoid pre-colonic dose dumping.

The best prepared Dexa-GP/ES/Pu NCs (2:1) have particle size around $254.23 \text{ nm} \pm 1.95 \text{ nm}$, zeta potential of $-27.6 \text{ mV} \pm 0.115 \text{ mV}$, and PDI of 0.147 ± 0.018 (Table 3.10), which satisfy the demands to target inflamed mucosa and epithelial cells of the large intestine with enhanced sensitivity to pH and microbial content. The monodispersed nano-system possessed the properties to avoid gastric pH degradation (pH 1.2) and stability against gastric enzymes. The negative zeta potential is attributed to the presence of free acrylic acid and carboxylic groups of the ES100. Therefore, the highest negative charge appeared on Dexa-GP/ES NPs. While pullulan has comparatively lower negative charge, that contributed to a decline in the zeta potential of Dexa-GP/ES/Pu NCs compared to the Dexa-GP/ES NPs (Table 3.10). Furthermore, ES to Pu in the ratio of 2:1 has more negative zeta potential compared to 1:1 because of increased ES100 content (Table 3.10).

Table 3. 10: Physicochemical characteristics of Dexa loaded nanocargoes

| Formulation | Particle size (nm) | Zeta potential (mV) | PDI | EE% | DL (ug/mg NPs) | % Yield | Conductivity (mS/cm) |
|-------------------------|--------------------|---------------------|----------------|--------------|----------------|--------------|----------------------|
| Dexa-GP NPs | 118.77 ± 0.74 | -9.5 ± 0.19 | 0.064 ± 0.004 | 89.97 ± 0.4 | 81.79 ± 0.35 | 89.2 ± 3.7 | 0.0374 ± 0.000115 |
| Dexa-GP/ES NPs | 189.57 ± 0.865 | -34.9 ± 0.611 | 0.228 ± 0.0132 | 92.64 ± 3.5 | 43.77 ± 1.705 | 89.33 ± 1.38 | 0.0596 ± 0.000611 |
| Dexa-GP/Pu NPs | 213.067± 0.5 | -10.83 ± 0.154 | 0.059 ± 0.015 | 91.97 ± 3.36 | 43.32 ± 1.6 | 90 ± 3.21 | 0.0709 ± 0.00025 |
| Dexa-GP/ES/Pu NCs (1:1) | 200.667± 4.8 | -22.52 ± 0.155 | 0.252 ± 0.0023 | 92.76 ± 2.7 | 44.17 ± 1.3 | 91.41 ± 3.75 | 0.056 ± 0.00015 |
| Dexa-GP/ES/Pu NCs (2:1) | 254.23± 1.95 | -27.6 ± 0.115 | 0.147 ± 0.018 | 94.56 ± 1.6 | 45.78 ± 1.7 | 91.83 ± 3.4 | 0.058 ± 0.000154 |

Moreover, SEM analysis revealed spherical smooth morphology of the Dexa-GP/ES/Pu NCs with the particle size ranging around 100-200 nm, consistent with zeta sizer findings (Figure 3. 10). ATR-FTIR evaluation of drug, polymers and the nanocargoes negate the presence of polymer-polymer or drug-polymer interaction. Furthermore, FITR spectra obtained for Dexa-GP/ES/Pu NCs confirmed complete entrapment of drug inside polymeric structure and absence of any surface-bound or untrapped drug on the surface (Figure 3. 10). XPRD findings suggested Dexa conversion into amorphous form when entrapped in the polymeric nanocargoes with low-intensity peaks (Figure 3. 10). While plain Dexa exists in the crystalline form as indicated through sharp peaks in the spectrum. Polymers including PLGA, GP, ES100, and pullulan are amorphous in nature, as shown in the XPRD spectra (Figure 3. 10). Thermal withstanding of nanocargoes was assured through TGA investigations. It demonstrated that Dexa inside the polymeric nanocargoes attained enhanced thermal stability as compared to its free form (Figure 3. 10).

Dexa-GP/ES/Pu NCs were evaluated for physicochemical characteristics after 1 and 6 months of storage at 4°C and 25°C. Nanocargoes retained the particle size, zeta potential, PDI, and EE% within the acceptable limits (Table 3. 11). Further, Dexa-GP/ES/Pu NCs were dispersed in SIF (pH 7.4) with or without cecal contents. After 72 hours of incubation, the particles were within the size limits, PDI was still lower, the

zeta potential was representative of GP NPs because of dissolution of ES100 and Pu coat at pH 7.4 which is the threshold to dissolve the enteric coat (Table 3. 12).

Table 3. 11: Effect of storage conditions on physicochemical characteristics of Dexa-GP/ES/Pu NCs (ICH guidelines)

| Dexa-GP/ES/Pu NCs | Initial | | After 1 month | | After 6 months | |
|----------------------------|---------------|---------------|---------------|---------------|----------------|-------------|
| | 4°C | 25°C | 4°C | 25°C | 4°C | 25°C |
| Particle size (nm) | 254.23±1.95 | 254.23±1.96 | 257 ± 1.86 | 265.55 ± 2.05 | 264.23±1.99 | 288.6±2.12 |
| Zeta potential (mV) | -27.6 ± 0.115 | -27.6 ± 0.116 | -27.2 ± 0.05 | -25 ± 0.135 | -23.6 ± 2.3 | -19± 3.1 |
| PDI | 0.147 ±0.0178 | 0.147 ±0.0179 | 0.147 ±0.0180 | 0.147 ±0.0181 | 0.282±0.09 | 0.332±0.15 |
| EE% | 94.56 ± 1.6 | 94.56 ± 1.7 | 92.22 ± 2.1 | 91.05 ± 1.85 | 91.5 ± 1.10 | 89.98 ± 2.6 |

Table 3. 12: Evaluation of Dexa-GP/ES/Pu NCs in physiological buffers (pH 7.4)

| Stability in buffers after 72 hours | | |
|-------------------------------------|------------------|-------------------------------|
| Dexa-GP/ES/Pu NCs | SIF (pH 7.4) | SIF + cecal contents (pH 7.4) |
| Particle size (nm) | 235 ± 4.45 | 235.65 ± 9.97 |
| Zeta potential (mV) | -7.93 ± 0.36 | -7.71 ± 0.55 |
| PDI | 0.088 ± 0.034 | 0.06 ± 0.019 |
| conductivity (mS/cm) | 0.0614 ± 0.00023 | 0.0403 ± 0.00035 |

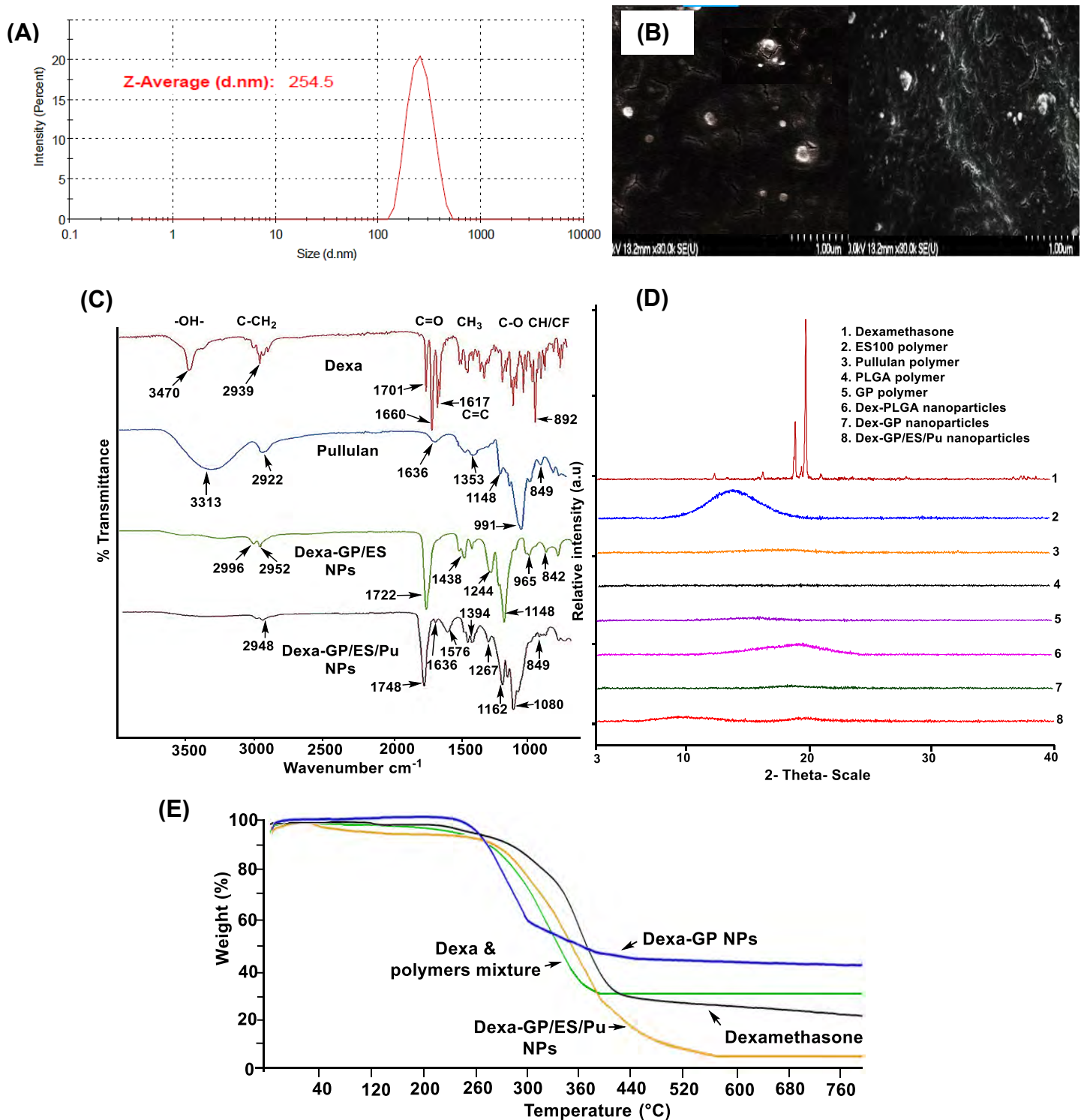


Figure 3. 10: Physicochemical characterization of DEXA-GP/ES/Pu NCs (A-E); (A) Particle size analysis, (B) SEM analysis, (C) ATR-FTIR, (D) XPRD, and (E) TGA analysis drug, excipients and nanocargoes

3.8. Drug Release and Kinetics

DEXA release from GP/ES/Pu NCs was determined through the dialysis diffusion method in SGF (pH 1.2), phosphate buffer solution (pH 4.5), and SIF (pH 7.4). The range of pH was selected because of variations across GIT; the acidic range over pH

1.2-4.5 covers the upper GIT portion including the stomach and upper region of the small intestine, while pH 7.4 is specific to the colon (Zeeshan *et al.*, 2019a). In comparison, Dexamethasone release from GP/ES and GP/Pu NPs were studied to elucidate the effect of dual ES/Pu coat on drug release at the colon. Moreover, drug release in the presence of cecal contents (5% w/v) was observed to simulate the colonic microenvironment. At pH 1.2, GP/Pu NPs have released 25.3-29.6%, GP/ES NPs exhibited 9.8-11.8%, while GP/ES/Pu NCs have released 4.3-7.2% of the drug (Figure 3.11 A). Dual GP/ES/Pu NCs have significantly reduced the burst release of the drug at pH 1.2, in comparison to GP/Pu NPs, while a non-significant difference was observed in the drug release at pH 1.2 between Dual GP/ES/Pu NCs and GP/ES NPs. At pH 4.5, GP/ES/Pu NCs markedly reduced the drug release, in comparison to both GP/Pu and GP/ES NPs (Figure 3.11 A).

At pH 7.4, drug release from GP/Pu, GP/ES and GP/ES/Pu NCs were parallel and in a sustained manner, with approx. 82.5%, 84.3% and 83.5% drug release at 72 hours, respectively (Figure 3.11 A).

In SIF (pH 7.4) with cecal contents, GP/Pu NPs have drug release approximating 90%, GP/ES NPs released about 81% and GP/ES/Pu NCs have 86% of drug release till 72 hours (Figure 3.11 B). The addition of cecal content in SIF (pH 7.4) have majorly affected drug release from nanoparticles with pullulan coat because cecal contents are the source of microbial enzymes that consume pullulan, thus majorly affecting drug release from GP/Pu NPs and moderately affected drug release from GP/ES/Pu NCs, while the negligible effect on GP/ES NPs drug release (Figure 3.11 B).

For GP/ES/Pu NCs, the drug release kinetics fitted to Peppas-Sahlin model at acidic pH 1.2 and pH 7.4, both in the presence and absence of cecal contents (Table 3. 13). The value of Korsmeyer's 'n' and Peppas-Sahlin 'm' are greater than 0.5 at acidic pH that corresponds to non-Fickian drug release mechanism, while the values are lesser than 0.5 at pH 7.4 (\pm cecal material) that describes Fickian diffusion of drug to move outside the polymeric nanocargoes (Table 3. 13). Both Korsmeyer and Peppas-Sahlin described drug release from the polymers and polymeric nanoparticles either because of polymer chain elongation or diffusion or both mechanisms (Zeeshan *et al.*, 2021). The major mechanism at pH 7.4 is Fickian diffusion that negates polymer relaxation because the

outer enteric coat dissolved at the threshold pH that uncovered the galactosylated-PLGA (GP) nanocore, from where the drug was released through a diffusion process.

At acidic pH (pH 1.2-4.5), GP/ES NPs followed the Peppas-Sahlin model and at pH 7.4, the particles had relevance to Korsmeyer-Peppas (Table 3. 14). The mechanism of drug release as described from the 'n' value was non-Fickian and Fickian at acidic and pH 7.4, respectively. In the presence of cecal contents, GP/ES NPs had followed both Peppas-Sahlin and Korsmeyer-Peppas models with a similar mode of drug release at acidic and 7.4 pH (Table 3. 14).

GP/Pu NPs followed the same kinetics at acidic pH with a non-Fickian mechanism of drug release. While at pH 7.4 without cecal contents, GP/Pu NPs have acceptance to both Korsmeyer-Peppas and Peppas-Sahlin models. In the presence of cecal content, the drug pattern more coincided with the Peppas-Sahlin model with drug release under Fickian diffusion (Table 3.15).

Table 3. 13: Drug release from Dexa-GP/ES/Pu NCs at acidic pH and pH 7.4, without or with cecal content

| Dexa-GP/ES/Pu NCs (pH 1.2-4.5; 0-4 hours) | | | | | | | Dexa-GP/ES/Pu NCs (pH 7.4; 4-72 hours) | | | | | |
|---|--------------|-------------|--------------|------------------------------|---------------|--|---|--------------|---------------|--------------------------------|---------------|---|
| Parameter | Zero order | First order | Higuchi | Korsmeyer-peppas | Hixon-Crowell | Peppas-Sahlin | Zero order | First order | Higuchi | Korsmeyer-peppas | Hixon-Crowell | Peppas-Sahlin |
| R_obs-pre | 0.9702 | 0.9672 | 0.9052 | 0.9740 | 0.9682 | 0.9788 | 0.6192 | 0.9656 | 0.8178 | 0.9970 | 0.8560 | 0.9996 |
| Rsqr | 0.9410 | 0.9354 | 0.7872 | 0.9447 | 0.9374 | 0.9546 | -1.1196 | 0.8122 | 0.3385 | 0.9940 | 0.4699 | 0.9992 |
| RMSE | 1.2422 | 1.2989 | 2.3582 | 1.3885 | 1.2795 | 1.5398 | 42.4093 | 12.6244 | 23.6924 | 2.4660 | 21.2091 | 1.0153 |
| AIC | 11.1005 | 11.5465 | 17.5103 | 12.7752 | 11.3959 | 13.7821 | 67.0055 | 50.0411 | 58.8544 | 27.9025 | 57.3043 | 15.9166 |
| MSC | 2.1786 | 2.0894 | 0.8966 | 1.8436 | 2.1195 | 1.6422 | -2.5736 | -0.1501 | -1.4092 | 3.0125 | -1.1877 | 4.7248 |
| Other | k0= 3.176 | k1=0.034 | kH=5.14 2 | kKp=2.761, n=1.119 | Khc=0. 011 | k1= 2.108, k2=0.673, m=0.82 | k0= 1.637 | k1= 0.121 | kH=13. 212 | kKp=51.605 , n=0.119 | Khc= 0.02 | k1=46.726, k2= -6.538, m=0.312 |
| Dexa-GP/ES/Pu NCs (pH 1.2-4.5; 0-4 hours) | | | | | | | Dexa-GP/ES/Pu NCs (pH 7.4; 4-72 hours; with cecal contents) | | | | | |
| Parameter | Zero order | First order | Higuchi | Korsmeyer-peppas | Hixon-Crowell | Peppas-Sahlin | Zero order | First order | Higuchi | Korsmeyer-peppas | Hixon-Crowell | Peppas-Sahlin |
| R_obs-pre | 0.9639 | 0.9622 | 0.9390 | 0.9627 | 0.9628 | 0.9677 | 0.6016 | 0.9755 | 0.8044 | 0.9956 | 0.8467 | 0.9988 |
| Rsqr | 0.9013 | 0.9053 | 0.8733 | 0.9245 | 0.9042 | 0.9341 | -1.1892 | 0.8658 | 0.2972 | 0.9913 | 0.4623 | 0.9976 |
| RMSE | 2.0492 | 2.0074 | 2.3220 | 2.0697 | 2.0190 | 2.3684 | 44.6120 | 11.0474 | 25.2766 | 3.0854 | 22.1090 | 1.8219 |
| AIC | 16.1062 | 15.8998 | 17.3558 | 16.7673 | 15.9577 | 18.0879 | 67.7144 | 48.1731 | 59.7606 | 31.0394 | 57.8861 | 24.1024 |
| MSC | 1.5300 | 1.5713 | 1.2801 | 1.3978 | 1.5597 | 1.1337 | -2.6373 | 0.1543 | -1.5010 | 2.6020 | -1.2332 | 3.5930 |
| Other | k0= 4.477 | k1=0.049 | kH=7.49 4 | kKp=5.805, n=0.772 | Khc=0. 016 | k1= 4.158, k2= 1.572, m=0.579 | k0= 1.69 | k1= 0.137 | kH=13. 686 | kKp=55.11, n=0.11 | Khc= 0.02 | k1=49.427, k2= -7.103, m=0.313 |

Table 3. 14: Drug release from Dexa-GP/ES NPs at acidic pH and pH 7.4, without or with cecal content

| Dexa-GP/ES NPs (pH 1.2-4.5; 0-4 hours) | | | | | | | Dexa-GP/ES NPs (pH 7.4; 4-72 hours; without cecal contents) | | | | | |
|--|------------|-------------|------------|-----------------------------|---------------|---------------------------------------|---|-------------|------------|------------------------------|---------------|---|
| Parameter | Zero order | First order | Higuchi | Korsmeyer-peppas | Hixon-Crowell | Peppas-Sahlin | Zero order | First order | Higuchi | Korsmeyer-peppas | Hixon-Crowell | Peppas-Sahlin |
| R_obs-pre | 0.9555 | 0.9473 | 0.9010 | 0.9558 | 0.9501 | 0.9622 | 0.5550 | 0.9508 | 0.7611 | 0.9994 | 0.7871 | 0.9841 |
| Rsqr | 0.9078 | 0.8959 | 0.7921 | 0.9078 | 0.9003 | 0.9205 | -1.4317 | 0.7668 | 0.1450 | 0.9987 | 0.2690 | 0.9653 |
| RMSE | 3.5349 | 3.7564 | 5.3078 | 4.0814 | 3.6756 | 4.6416 | 45.9451 | 14.2286 | 27.2433 | 1.1564 | 25.1911 | 7.7584 |
| AIC | 21.558 | 22.166 | 25.6233 | 23.5574 | 21.9487 | 24.8162 | 68.1266 | 51.715 | 60.8096 | 17.3006 | 59.7132 | 44.3732 |
| MSC | 1.6961 | 1.5746 | 0.8831 | 1.2963 | 1.6181 | 1.0446 | -2.9500 | -0.6057 | k1= 0.15 | 4.3108 | -1.7481 | 0.4433 |
| Other | k0= 7.42 | k1= 0.085 | kH= 12.151 | kkp=7.354, n= 1.008 | Khc=0.027 | k1= 5.452, k2= 1.852, m= 0.747 | k0= 1.658 | k1= 0.15 | kH= 13.512 | kKp= 61.869, n= 0.072 | Khc= 0.02 | k1= 40.469, k2= -4.758, m= 0.382 |
| Dexa-GP/ES NPs (pH 1.2-4.5; 0-4 hours) | | | | | | | Dexa-GP/ES NPs (pH 7.4; 4-72 hours; with cecal contents) | | | | | |
| Parameter | Zero order | First order | Higuchi | Korsmeyer-peppas | Hixon-Crowell | Peppas-Sahlin | Zero order | First order | Higuchi | Korsmeyer-peppas | Hixon-Crowell | Peppas-Sahlin |
| R_obs-pre | 0.9434 | 0.9420 | 0.9400 | 0.9486 | 0.9425 | 0.9534 | 0.5595 | 0.9513 | 0.7697 | 0.9988 | 0.8064 | 0.9998 |
| Rsqr | 0.8269 | 0.8433 | 0.8823 | 0.8981 | 0.8385 | 0.9072 | -1.3962 | 0.7375 | 0.1760 | 0.9977 | 0.3026 | 0.9996 |
| RMSE | 4.1829 | 3.9789 | 3.4492 | 3.7062 | 4.0399 | 4.3316 | 44.2318 | 14.6404 | 25.9375 | 1.5043 | 23.8622 | 0.6947 |
| AIC | 23.2416 | 22.7415 | 21.3130 | 22.5930 | 22.8936 | 24.1252 | 67.5945 | 52.1153 | 60.1220 | 20.9825 | 58.9545 | 10.6037 |
| MSC | 0.8856 | 0.9856 | 1.2713 | 1.0153 | 0.9552 | 0.7089 | -2.8880 | -0.6766 | -1.8204 | 3.7709 | -1.6537 | 5.2536 |
| Other | k0= 7.161 | k1=0.083 | kH=12.18 | kkp=10.746, n= 0.637 | Khc=0.026 | k1=7.587, k2=3.003, m=0.483 | k0=1.604 | k1=0.132 | kH=13.076 | kkp=58.029, n= 0.082 | Khc=0.02 | k1= 60.79, k2= -11.44, m=0.232 |

Table 3. 15: Drug release from Dexa-GP/Pu NPs at acidic pH and pH 7.4, without or with cecal content

| Dexa-GP/Pu NPs (pH 1.2-4.5; 0-4 hours) | | | | | | | Dexa-GP/Pu NPs (pH 7.4; 4-72 hours) | | | | | |
|--|---------------|--------------|---------------|----------------------------------|---------------|--|--|--------------|---------------|---------------------------------|---------------|---|
| Parameter | Zero order | First order | Higuchi | Korsmeyer-r-peppas | Hixon-Crowell | Peppas-Sahlin | Zero order | First order | Higuchi | Korsmeyer-r-peppas | Hixon-Crowell | Peppas-Sahlin |
| R_obs-pre | 0.9716 | 0.9781 | 0.9831 | 0.9888 | 0.9766 | 0.9909 | 0.5545 | 0.9370 | 0.7589 | 0.9986 | 0.7802 | 0.9985 |
| Rsqr | 0.8766 | 0.9278 | 0.9639 | 0.9774 | 0.9142 | 0.9815 | -1.4341 | 0.7043 | 0.1391 | 0.9972 | 0.2339 | 0.9970 |
| RMSE | 5.9033 | 4.5152 | 3.1918 | 2.9155 | 4.9235 | 3.2303 | 44.9464 | 15.6646 | 26.7296 | 1.6557 | 25.2154 | 2.2342 |
| AIC | 26.6866 | 24.0059 | 20.5373 | 20.1935 | 24.8716 | 21.1914 | 67.8189 | 53.0619 | 60.5431 | 22.3253 | 59.7267 | 26.9448 |
| MSC | 1.1870 | 1.7231 | 2.4168 | 2.4856 | 1.5500 | 2.2860 | -2.9529 | -0.8448 | -1.9135 | 3.5462 | -1.7969 | 2.8863 |
| Other | k0= 12.336 | k1=0.16 3 | kH=21.0 87 | kKp=19.01 2, n= 0.614 | Khc=0.05 | k1=13.44, k2= 5.43, m=0.46 | k0= 1.621 | k1= 0.142 | kH=13.2 08 | kKp=60.88 9, n= 0.07 | Khc= 0.02 | k1=72.959 , k2= -12.865, m=0.102 |
| Dexa-GP/Pu NPs (pH 1.2-4.5; 0-4 hours) | | | | | | | Dexa-GP/Pu NPs (pH 7.4; 4-72 hours; with cecal contents) | | | | | |
| Parameter | Zero order | First order | Higuchi | Korsmeyer-r-peppas | Hixon-Crowell | Peppas-Sahlin | Zero order | First order | Higuchi | Korsmeyer-r-peppas | Hixon-Crowell | Peppas-Sahlin |
| R_obs-pre | 0.9466 | 0.9645 | 0.9929 | 0.9929 | 0.9592 | 0.9940 | 0.4940 | 0.9880 | 0.7162 | 0.9986 | 0.7590 | 0.9995 |
| Rsqr | 0.7594 | 0.8642 | 0.9857 | 0.9858 | 0.8340 | 0.9880 | -1.6464 | 0.9378 | 0.0138 | 0.9972 | 0.2100 | 0.9990 |
| RMSE | 8.5263 | 6.4061 | 2.0811 | 2.3938 | 7.0817 | 2.6879 | 53.2622 | 8.1654 | 32.5147 | 1.9143 | 29.1015 | 1.2873 |
| AIC | 30.3631 | 27.5040 | 16.2602 | 18.2219 | 28.5066 | 19.3533 | 70.1955 | 43.9411 | 63.2860 | 24.3574 | 61.7334 | 19.2400 |
| MSC | 0.3783 | 0.9501 | 3.1989 | 2.8065 | 0.7496 | 2.5802 | -3.1119 | 0.6387 | -2.1249 | 3.4364 | -1.9031 | 4.1674 |
| Other | k0= 13.364 | k1= 0.185 | kH= 23.291 | kkp= 23.477, n= 0.5 | Khc=0.05 5 | k1=16.47 5, k2=6.9, m=0.369 | k0= 1.815 | k1= 0.223 | kH= 14.961 | kKp=74.53 9, n= 0.048 | Khc= 0.022 | k1=82.821, k2= -18.984, m=0.201 |

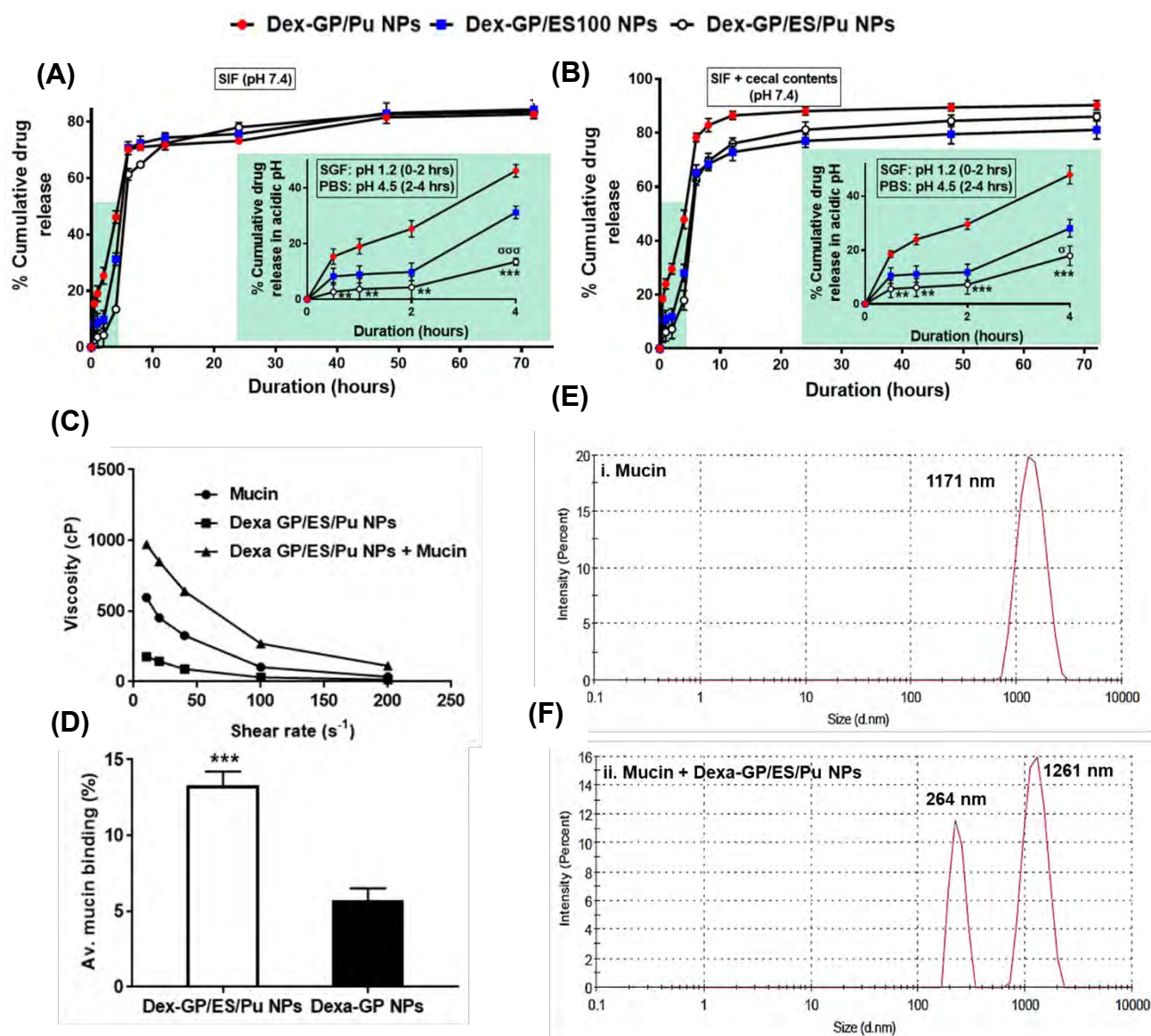


Figure 3. 11: Drug release study of GP/ES/Pu NCs and mucin-nanocargoes binding investigations; Dexamethasone (Dexa) release from GP/Pu NPs, GP/ES NPs and GP/ES/Pu NCs at acidic pH (pH 1.2-4.5) and pH 7.4, without or with cecal contents (A, B); Rheological investigations of mucin and nanocargoes interaction (C); Spectrophotometric analysis of % mucin binding to nanocargoes (D); Size analysis of Mucin (E); Size analysis after mucin-nanocargoes interaction (F)

3.9. Mucin Binding Study

The rheological investigations of mucin-nanocargoes mixture suggested an increase in viscosity compared to the viscosities of Dex-GP/ES/Pu NCs or mucin alone. The consistent viscosity increase was observed at different shear rates (10-200 s⁻¹) at a fixed mucin-nanocargoes concentration (1:1) (Figure 3.11 C). The rheological synergism is the mucoadhesion evaluation parameter for the polymeric systems (Ding *et al.*, 2018).

The synergism findings showed viscosity for mucin-formulation mixture (η_{mix}) was higher than the $\eta_{\text{NCs}} + \eta_{\text{muc}}$ values, thus, indicating positive rheological synergism.

Rheological studies indicated an interaction between mucin and Dexa-GP/ES/Pu NCs. To further elucidate, the extent of mucin binding was explored. It was found that the binding efficiency of mucin to Dexa-GP/ES/Pu NCs was about 13.3%, compared to 5.7% binding with Dexa-GP NPs, indicating 2 folds higher interaction in presence of ES100 and pullulan coat on GP NPs (Figure 3.11 D). Though the enteric coat increased the mucin interaction, still the % binding was not high enough. Further, particle size distribution analysis of the mucin-nanocargoes mixture revealed the presence of bimodal peaks, because of nanocargoes (264 nm) and mucin (1261 nm). Size of nanocargoes have insignificant difference ($\sim 10\text{-}20$ nm) after incubation with mucin, pointing to little mucin adsorption on the surface due to the anionic nature of the GP/ES/Pu NCs (Figure 3.11 E, F).

Together, findings suggested that polymethacrylate and pullulan-based coating improved mucoadhesion to some extent because of swelling properties of the polymers (Chaves *et al.*, 2018), however, the anionic nature of the system work against extensive mucin binding (Rossi *et al.*, 2019; Hua *et al.*, 2015).

3.10. In vitro Biocompatibility Studies

3.10.1. Hemolysis assay

RBCs hemolytic activity of Dexa-GP NPs, Dexa-GP/ES100 NPs, and Dexa-GP/ES/Pu NCs at drug concentrations of 25-100 $\mu\text{g/ml}$ demonstrated that all formulations were safer and negate the potential of blood toxicity. At all concentrations, hemolysis was less than 2% for Dexa-GP/ES NPs and less than 1% for Dexa-GP and Dexa-GP/ES/Pu NCs (Figure 3.12 A, B). The presence of pullulan in the enteric coat further enhanced the safety profile of the nanosystem.

3.10.2. Cellular biocompatibility (MTT)

MTT cellular viability assessment of Dexa-GP, and Dexa-GP/ES/Pu NCs on elicited macrophages and murine-colon cells after 24 and 48 hours demonstrated the non-toxic, biocompatible nature of the drug loaded formulations. Dexa free state exhibited lesser cell viability than encapsulated within polymeric nanosystems. Dexa drug have

significantly reduced cell viability when compared with normal control. Whilst, both nanosystems have proved to be bio-safer with >80% macrophage viability and >70% colon-cell viability at various concentrations of the drug after 24 and 48 hours and found to differ insignificantly from the normal control. Dexa-GP/ES/Pu NCs, at various concentrations, have shown macrophage cell viability of about 88-95% and 83-91% (Figure 3.12 C, D) and colon-cell viability of 77-86% and 74-83% after 24 and 48 hours, respectively (Figure 3.12 E, F).

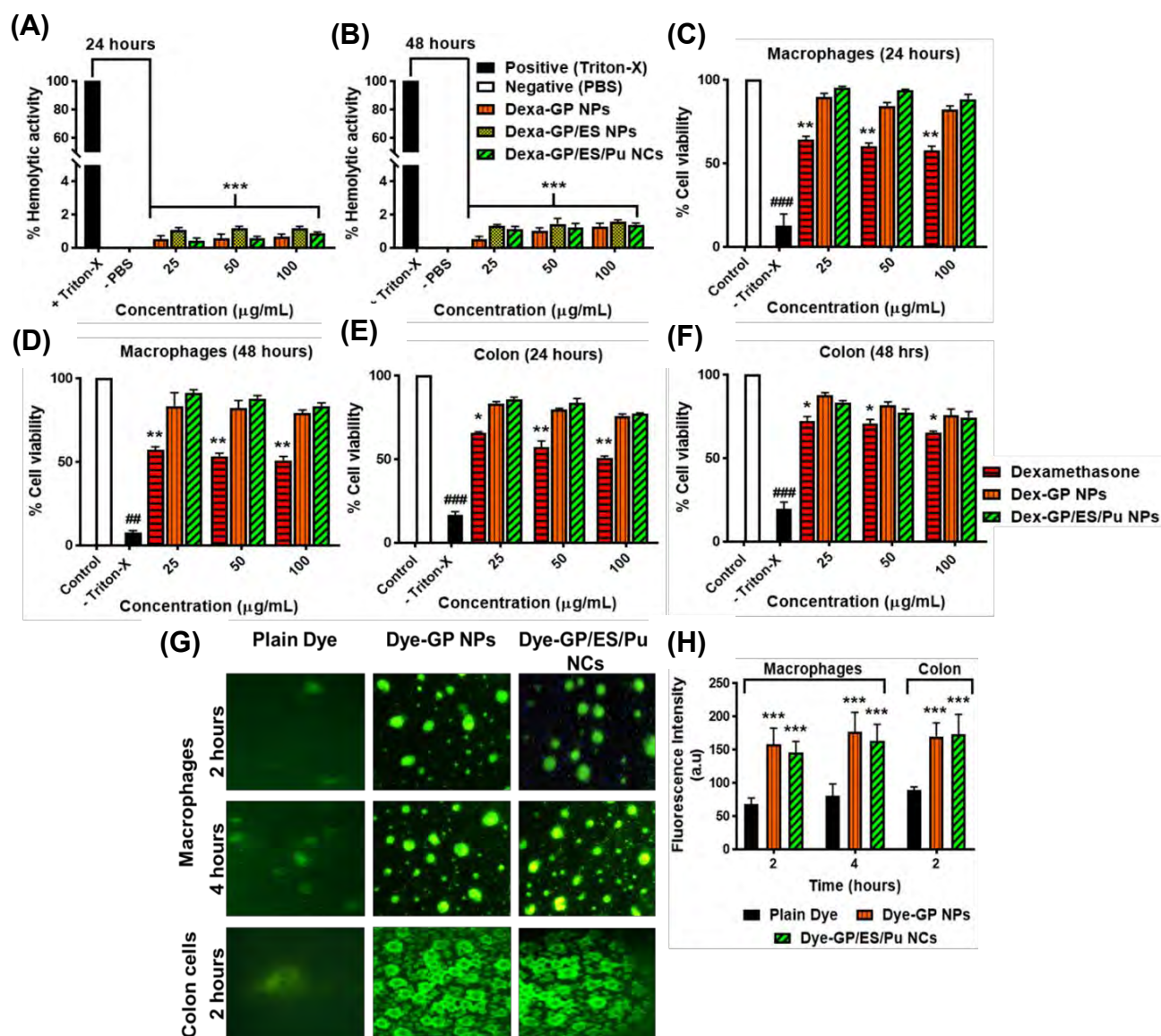


Figure 3. 12:: Cellular biocompatibility and uptake assay of DEXA-GP/ES/Pu NCs and galactose-based nano-formulations; Hemolytic activity of nanoformulations after 24 hours (A) and 48 hours (B); Macrophage cell viability assay after 24 hours (C) and 48 hours (D); Colon cell viability assay after 24 hours (E) and 48 hours (F); Macrophage and colon cells uptake of dye-labelled nanoformulation(s) (G);

Fluorescence intensity of the dye-labelled nanoformulation uptaken by the macrophage and colon cells (H)

3.10.3. Cell uptake studies

Fluorescein loaded GP NPs and GP/ES/Pu NCs were incubated with murine-derived macrophages to visualize the cellular endocytosis of nanocargoes loaded with a fluorescent dye (Figure 3.12 G, H). Free dye was used as a control. Dye loaded GP NPs have shown fluorescence after 2 and 4 hours of incubation; similarly, GP/ES/Pu NCs have shown fluorescence after 2 and 4 hours but maximum uptake intensity after 4 hours (Figure 3.12 G, H). Because ES/Pu coat dissolution or disintegration over time exposed the underneath GP core, which have more binding affinity for the MGL-2 macrophage-surface receptor leading to increased cellular uptake after 4 hours.

In murine-derived colon cells, both types of nanoparticles had enhanced uptake by the colon cell membranes (Figure 3.12 G, H). The increased uptake was based on the fact that particles around 200 nm are easily uptaken by the epithelial cells under enhanced epithelial permeability and retention effect (eEPR) (Yang and Merlin, 2019).

3.11. In vitro Permeation and Retention Assay

In vitro permeation assay was performed to evaluate permeation and retention effect of Rho-GP/ES/Pu NCs across goat intestine, over 8 hours in PBS (pH 7.4) at 37°C (Figure 3. 13 A-D). The greatest retention was observed after 4 hours of Rho-GP/ES/Pu NCs incubation (Figure 3. 13 A, B). In comparison with free Rhodamine-B control, it was obvious that nanocargoes exhibited significantly higher retention, lower permeation, and high retention to permeation ratio at all time points and incur sustained release characteristics, as manifested through increased concentration and fluorescence of dye in the intestine with lesser permeability into the buffer (Figure 3. 13 B-D). Rhodamine-B encapsulation within the nanocarrier system retained it within the intestinal tissue for a long time. This experiment further demonstrated enhanced local retention of the GP/ES/Pu NCs in the intestine.

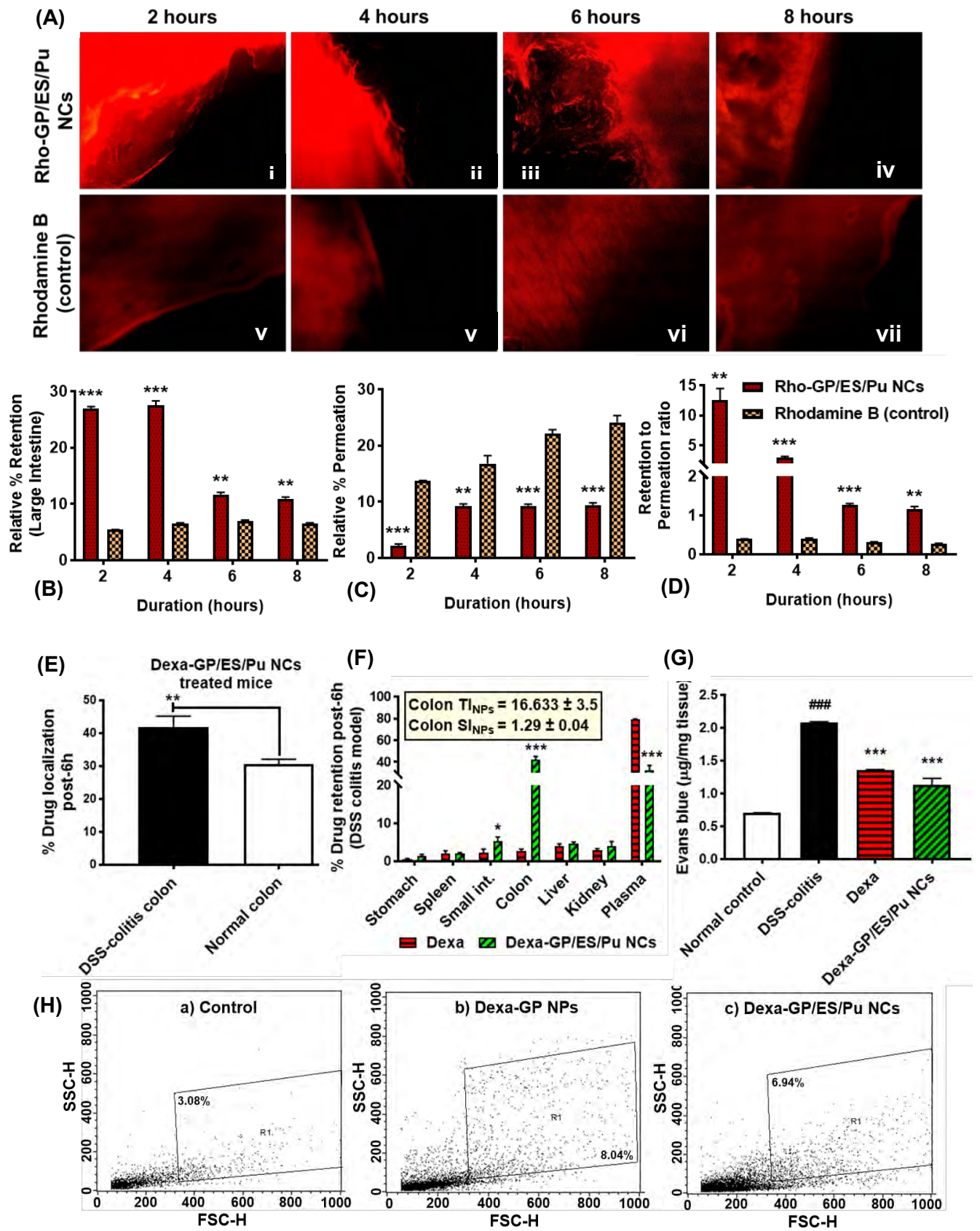


Figure 3. 13: Ex vivo permeation and retention assay of Rho-GP/ES/Pu NCs, in vivo biodistribution studies and vascular integrity assessment; A. Cross section of goat intestine illuminating under dye released from Rho-GP/ES/Pu NCs retention (i-iv) and free Rho dye control (v-viii) over 8 hours; B. Relative %age retention in the large intestine; C. Relative % age permeation across intestine into the buffer (pH 7.4); D. Retention to permeation ratio of the Rho-GP/ES/Pu NCs and free dye for 8 hours; E. % age drug localization after 6 hours of administration of Dexa-GP/ES/Pu NCs to the inflamed (DSS-induced colitis) and normal mice; F. % age drug retention or biodistribution to the vital organs after 6 hours of administration of Dexa-GP/ES/Pu NCs; G. Vascular integrity test: Evans blue permeation across vessels into the inflamed colon; H. Flowcytometry to analyze fluorescein loaded GP/ES/Pu NCs uptake by the colon-derived macrophages, untreated control (a), GP treated (b), GP/ES/Pu NCs treated (c)

3.12. Animal Studies

UC was induced in the BALB/c mice by administering DSS (3% w/v) in drinking water for 7 days and thereafter mice were divided into different groups.

3.12.1. Nanocargoes targeting ability

3.12.1.1. *Nanocargoes targeting index and localization capacity in the inflamed colon*

Dexa-GP/ES/Pu NCs localization in the healthy and DSS-induced inflamed mice after 6 hours of oral administration was investigated. The drug was released from the nanocargoes in a sustained fashion, thus retained at the colon for a prolonged time. Therefore, estimation of drug concentration at colon was an indirect measure of nanocargoes localization. It was found that the % drug retention in the inflamed colon was significantly higher ($p < 0.01^{**}$) than the drug concentration in the healthy colon (Figure 3. 13 E), because of altered pathophysiology in the inflammation including the eEPR effect, immune cells uptake, mucus, etc. that contributed towards nanocargoes localization.

Further, nanocargoes' drug targeting capability and biodistribution were assessed through drug quantification in the GIT regions and the vital organs. After 6 hours of Dexa-GP/ES/Pu NCs administration to the DSS-induced colitis mice, the highest amount of drug was accumulated at the colon (~41%), followed by plasma (~32%). Other organs (stomach, spleen, small intestine, liver, kidney) have only a small portion of the drug after nanocargoes intake (Figure 3. 13 F). While the free drug, given to the control group, failed to get localized in the colon (~2.6%), and majorly found in the plasma (~79%). The nanocargoes led colon targeting index was calculated to be 16.633

± 3.5 , and selectivity index 1.29 ± 0.04 , which indicated the site-specificity and drug targeting ability of the nanocarriers (Figure 3. 13 F). Thus, we postulate that the dual microbial-pH sensitive enteric layer on nanocargoes gets dissolved in colon microenvironment, slowly disclosing the underneath drug containing GP core which binds to MGL-2 receptors on colonic macrophages and releases the payload thereof in a sustained manner.

3.12.1.2. Flow cytometry

FCS analysis was performed to elucidate uptake of fluorescein loaded GP/ES/Pu NCs by the macrophages derived from inflamed colon lamina propria. The analysis showed a right shift in the forward scattering (FSC-H-FITC) and upward shift of the SSC-H plot, constituting the R1 area (Figure 3. 13 H). The scattering depicted changes in the morphology and size of the macrophage cells which highlighted the cellular uptake of nanocargoes. A control group of untreated macrophage cells was run in parallel. It was noted that GP NPs have slightly more internalization than GP/ES/Pu NCs because the galactose ligand in the GP NPs was exposed, therefore directly binds to MGL-2 receptor of macrophages. However, GP/ES/Pu NCs uncover underneath GP core over time and have more lasting uptake potential.

3.12.2. Oral Delivery of Dexamethasone-GP/ES/Pu NCs for Therapeutic Intervention of DSS Induced Colitis

3.12.2.1. Assessment of progression and intervention of colitis through morphological parameters and mortality rate

Scheme of experimental design to investigate therapeutic effects of nanoformulation is mentioned in Figure 3. 14 A. Progression of disease was monitored on daily basis. DSS induced colitis group had developed signs of disease, manifested through significant bodyweight decline ($p < 0.001^{####}$), and highest DAI scores (10.00 ± 0.23 , $p < 0.001^{####}$) as compared to the normal control (DAI = 0.2 ± 0.12) (Figure 3. 14 B, C). In the end, treatment with Dexamethasone-GP/ES/Pu NCs recovered mice body weight up to 93.45% and lowered DAI score to 3.4 ± 0.41 , as compared to DSS-colitis mice ($p < 0.001^{***}$) (Figure 3. 14 B, C). Further, the distress monitoring revealed that colitis induced significant stress to the mice ($p < 0.001^{####}$) compared to normal; and treatment with both Dexamethasone ($p < 0.05^*$) and Dexamethasone-GP/ES/Pu NCs ($p < 0.01^{**}$) alleviated the anxious symptoms of the colitis mice (Figure 3. 14 D). Further, Dexamethasone-GP/ES/Pu NCs treated mice had an

improved survival rate (80%), in comparison to untreated colitis mice (40%) (Figure 3. 14 E).

Weight evaluation of stomach, heart, liver, kidney, and lung depicted that DSS induced colitis did not impinge on these organs and thus treatment has no effect on these vital organs (Figure 3. 14 F). Colon weight to length ratio, colon length and spleen weight index demonstrated that Dexa-GP/ES/Pu NCs recovered the inflammation indices of colitis mice towards normal values with a decline in colon weight to length ratio, increase in colon length, and reduction in splenic weight (Figure 3. 14 F-I). It was observed that small intestine weight was significantly restored by the nanocargoes ($p < 0.05^*$) (Figure 3. 14 F), while the length was recovered to a little extent (Figure 3. 14 H). Assessment of morphological parameters have demonstrated the improvement with the course of nanocargoes treatment.

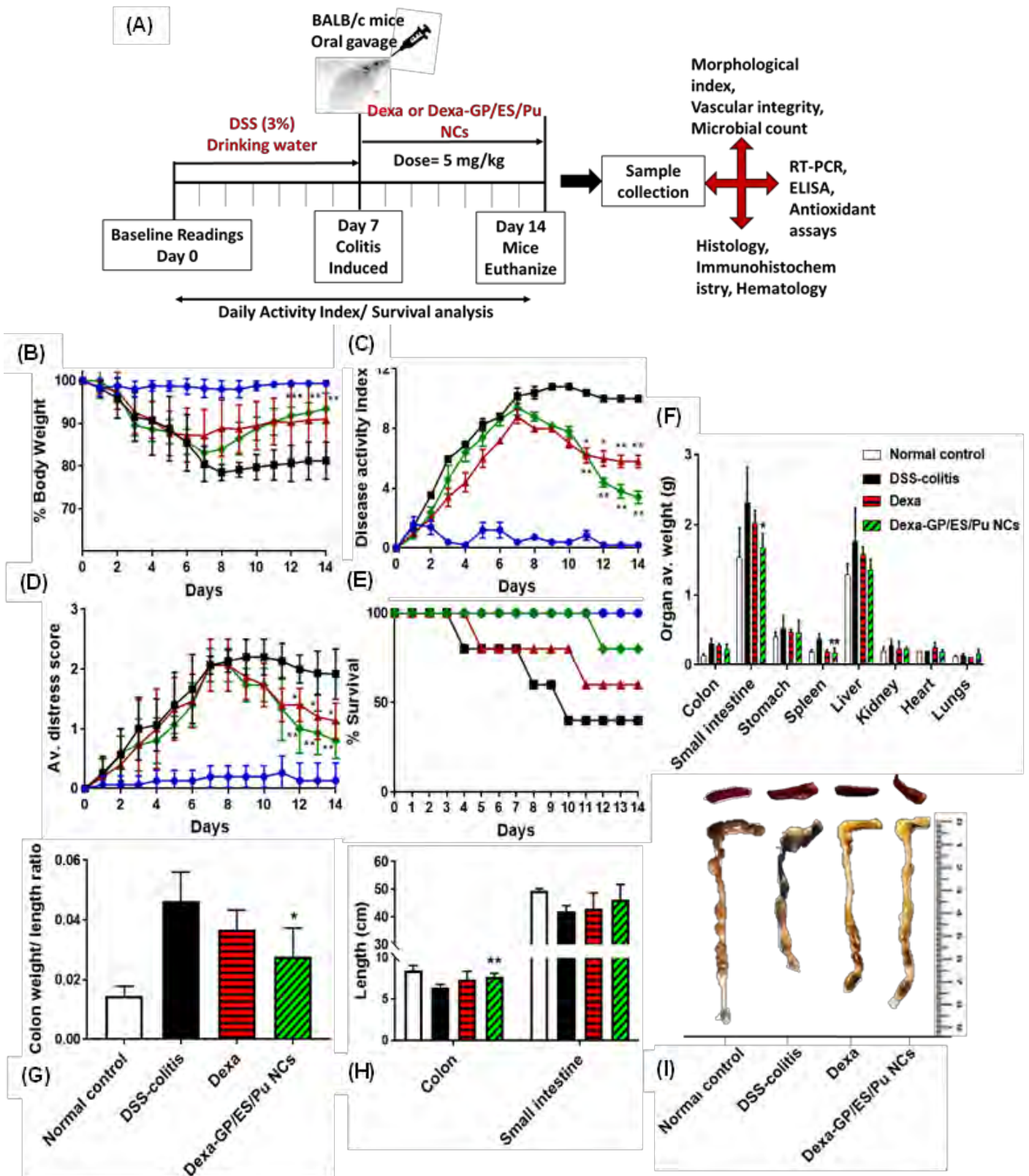


Figure 3. 14: Therapeutic evaluation of Dexa-GP/ES/Pu NCs through morphologic and physical parameters; Scheme of in vivo study design (A), body weight assessment (B), DAI scores (C), distress scores (D) and mortality (E), vital organs weight assessment (F), colon weight to length ratio (G), length of intestines (H), pictorial representation of colon and spleen (I)

3.12.2.2. Evaluation of colonic vascular integrity

Colon inflammation preceded structural and functional damage to the vascular endothelium by influencing several mediators and activators (Yang and Merlin, 2019). Therefore, estimation of Evans blue permeation across the endothelial membrane to the colon indicated the extent of inflammation. Findings demonstrated that the highest amount of Evans blue was concentrated in the DSS induced colitis mice, and treatment with Dexa and Dexa-GP/ES/Pu NCs have markedly decreased the dye permeation at the colon ($p < 0.001^{***}$) (Figure 3. 13 G). Thus, treatment aided in the restoration of endothelial integrity of the inflamed colon, because of recovery of epithelial integrity and chemokine factors.

3.12.2.3. Histopathological assessment

Histo-morphologic assessment enumerated loss of epithelial integrity, crypts distortion, and immune cells infiltration with a cumulative damage score. DSS-induced colitis produced severe histological destruction (score: 11.66 ± 0.192 , $p < 0.001^{###}$ Vs normal) (Figure 3.15 A, B). Dexa restored the total colon damage to a histo-score of 7 ± 0.33 ($p < 0.01^{**}$), while Dexa-GP/ES/Pu NCs have substantially alleviated the inflamed colon to a score of 4.33 ± 0.385 ($p < 0.001^{***}$) (Figure 3.15 A, B). The histopathological analysis of the small intestine depicted some signs of inflammation with an altered villi-crypt ratio in the DSS-colitis groups; the spleen has major marks of distortion, especially in the central white pulp region (Figure 3.15 A). Treatment with Dexa-GP/ES/Pu NCs has recovered inflammation-associated disruptions in the small intestine and spleen (Figure 3.15 A).

3.12.2.4. Immunohistochemistry

Since DSS-induced colitis uplifted the expression of inflammatory proteins and activated the signaling pathways like MAPK and NF- κ B (Hwang *et al.*, 2019). Therefore, the therapeutic efficacy of the anti-COX encapsulated drug (Dexa) inside the nanoformulation was investigated through immunohistochemical analysis of inflammatory signaling proteins. Findings indicated down-regulated expression of NF- κ B proteins by the Dexa (~41%) and Dexa-GP/ES/Pu NCs (~21%) and decreased expression of COX-2 protein on treatment with Dexa (~50%) and Dexa-GP/ES/Pu NCs (~33%) (Figure 3.15 C-E).

3.12.2.5. *ATR-FTIR analysis of the colon tissues*

The ATR-FTIR spectra obtained from pat dried colon tissues of different groups have been shown in Figure 3.15 F. While differentiating regions of FTIR spectrum, the sub-ranges representing N-H stretch of proteins are present in 3200-3300 cm^{-1} . And amide I and amide II correspond to 1640 cm^{-1} and 1540 cm^{-1} , respectively. Lipidic domains are peaking around 2850-2960 cm^{-1} and 1390-1457 cm^{-1} . The nucleic acid peak can be visualized at 1239 cm^{-1} , while carbohydrates are assigned to 1034-1100 cm^{-1} (Figure 3.15 F). The findings were consistent with the literature (ANDRONIE *et al.*, 2011; Li *et al.*, 2017; Bangaoil *et al.*, 2020). The major peaks positions are almost the same in the normal and colitis tissues, however, the differences in peak intensity, transmittance, and shape reflect the deviations (Li *et al.*, 2017). The structure and composition disruptions in the major biomolecules including proteins, lipids, nucleic acids, carbohydrates have an impact on the relative intensity exhibited by the functional groups of each biomolecule.

Analysis of spectra demonstrated that the intensity of the peaks representing -NH- of proteins (3265-3278 cm^{-1}) have minimum diversions in the colitis group from the normal. While DSS-colitis tissues have increased lipid peaks transmittance with decreased intensity, as depicted from lipidic -CH- stretch (2959-2961 cm^{-1}) and the fingerprint -COO-/CH- bands at 1457 cm^{-1} , and 1395-1399 cm^{-1} , compared to the normal control. Dexamethasone improved the lipidic content a little, while Dexamethasone-GP/ES/Pu NCs restored the peak ratio towards normal (Figure 3.15 F, G). Further, the protein amide I (1636.3 cm^{-1}) and amide II (1541.3 cm^{-1}) alterations in the DSS-colitis mice depicted changes in the protein content as well. Treatment with Dexamethasone-GP/ES/Pu NCs completely recovered protein amide band alterations. Nucleic acid intensity peaks at 1237-1239 cm^{-1} are lessened which showed increased transmittance but decreased absorbance in the DSS-colitis group, compared to the normal (Figure 3.15 F, G). The finding is interesting because it is contrary to the colon cancer FTIR analysis, where nucleic acids abundant production intensified the nucleic acid peak and absorbance (Li *et al.*, 2017). Further, carbohydrate bands at 1034 cm^{-1} are seemed to be altered in DSS-colitis because of distortions of glycoproteins (like mucin) of the colon (Figure 3.15 F, G). The treatment with Dexamethasone-GP/ES/Pu NCs found to be fruitful in balancing all biomolecular FTIR peaks representing protein amides, lipids, nucleic acid content, and carbohydrates because alleviation of inflammation by the drug loaded nanocargoes

through sustained mechanistic actions heal the mucosal injury with restoration of proteins and glycoproteins enzymes and receptors, lipidic structures and DNA/RNA and mucin levels.

3.12.2.6. Evaluation of colon microbial content

DSS induction had disturbed the microbial flora of the gut because of severe epithelial and luminal distortions. The bacteria log CFU/mL in the fecal culture of DSS-colitis mice exceeds 1.3 folds than that of normal healthy mice ($p < 0.001$). Dexa and Dexa-GP/ES/Pu NCs treated mice have decreased fecal CFU to 3.49 ± 0.025 ($p < 0.01$ vs DSS) and 3.17 ± 0.029 ($p < 0.001$ vs DSS), respectively, demonstrating the effect of treatment in restoring the natural microbiome (Figure 3.15 H).

3.12.2.7. Effect on blood sugar levels

Locally acting corticosteroid like Dexa promotes gluconeogenesis and sugar transport, thus, elevating blood sugar levels (Thiesen *et al.*, 2003). Therefore, measurement of sugar concentration in the blood is an indirect parameter to assess the enhanced function of Dexa after being released from the nanocargoes at the colon (Ali *et al.*, 2014). Both Dexa and Dexa-GP/ES/Pu NCs elevated the sugar content of the blood at the end of the experiment, however, a greater increase was observed with the encapsulated drug inside the nanocargoes (Figure 3.15 I).

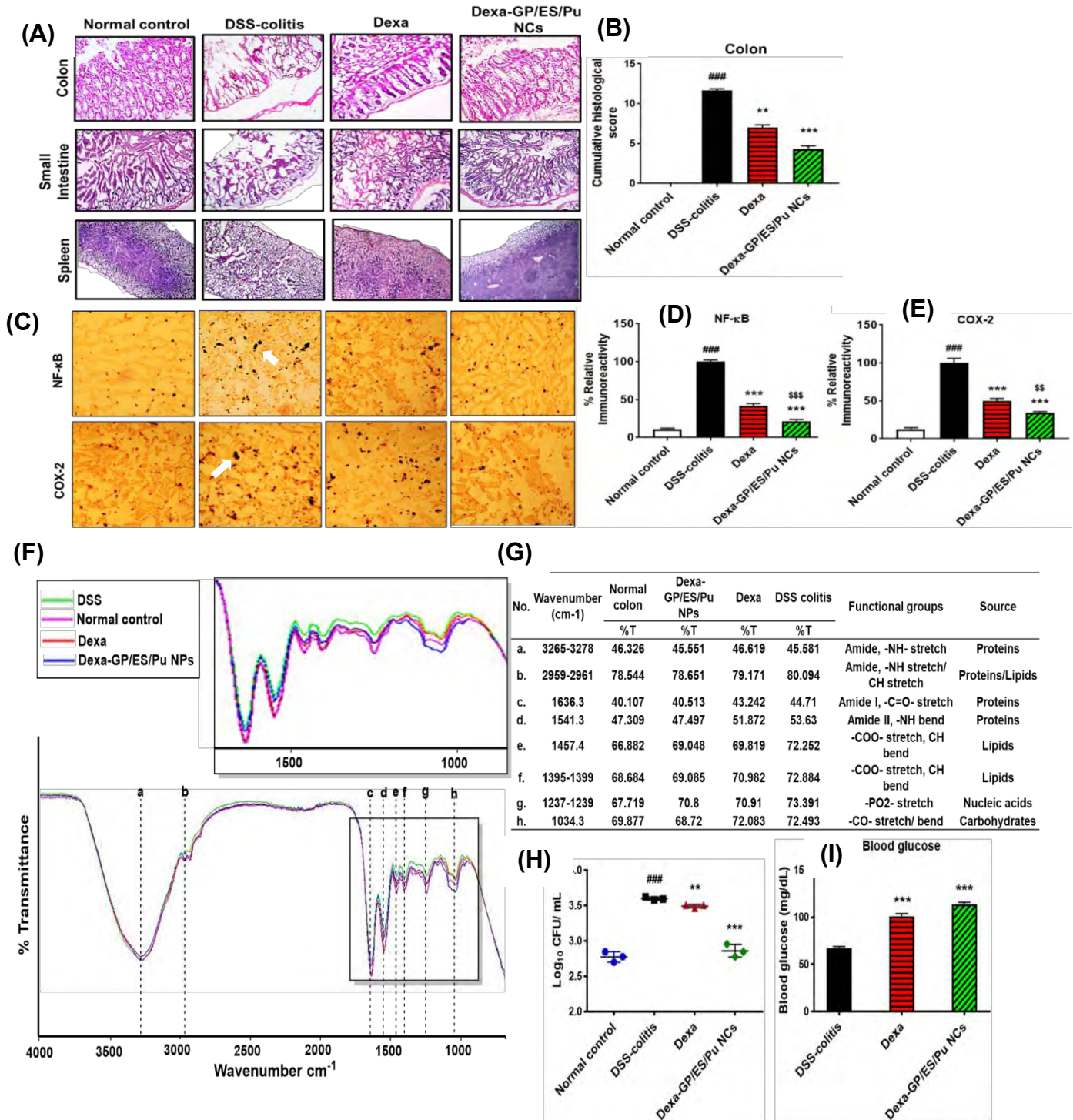


Figure 3. 15: Histopathology, immunoreactivity, ATR-FTIR, colon feces microbial count and blood glucose evaluation to determine therapeutic efficiency of Dexa-GP/ES/Pu NCs; A. Histology of colon, small intestine, and spleen from the representatives of normal control, DSS-colitis, Dexa and Dexa-GP/ES/Pu NCs treated mice groups; B. Colon cumulative histopathological score; C. Expression of NF- κ B and COX-2 at the colon tissues in the normal control, DSS-colitis, Dexa and Dexa-GP/ES/Pu NCs treated groups by immunohistochemistry; D. % Relative immunoreactivity of NF- κ B; E. Relative

immunoreactivity of COX-2; F. ATR-FTIR spectra of colon tissues excised from normal control, DSS-colitis, Dexa and Dexa-GP/ES/Pu NCs treated groups; G. Descriptive analysis of ATR-FTIR peaks with %transmittance at a particular wavenumber (cm^{-1}) and functional groups; H. Microbial colony forming units (logCFU/mL) from the fecal suspension obtained from different groups under investigation; I. Blood glucose levels of the mice of different groups under study

3.12.2.8. RT-PCR analysis for the expression of regulatory, inflammatory, and mechanistic proteins

iNOS is an inflammatory marker and elevated in response to free radicals and oxidative species, DSS augmented the expression of colonic iNOS. The iNOS production was significantly diminished by Dexa-GP/ES/Pu NCs treatment ($p < 0.05$) (Figure 3.16 a1), because of suppression of inflammatory pathways NF- κ B and COX-2 (Al-Harbi *et al.*, 2016). Loss of epithelial integrity is a clear manifestation of UC. E-cadherin is one of the tight junction proteins expressed on the intestinal epithelium; its expression significantly deteriorated in DSS-induced colitis model ($p < 0.001^{***}$), compared to the normal control. It was found that Dexa-GP/ES/Pu NCs led treatment of the DSS-induced colitis mice resumed the E-cadherins levels up to a marked extent ($p < 0.05$) (Figure 3.16 a2). Nanocargoes specific delivery of Dexa improved epithelial barrier functions by downregulation of pro-inflammatory cytokines particularly TNF- α (Boivin *et al.*, 2007).

3.12.2.9. Pro-inflammatory cytokines detection through ELISA

Estimation of pro-inflammatory cytokines demonstrated that the levels of IL-6 and TNF- α in the DSS-induced colitis mice considerably diminished with the treatment of both Dexa ($p < 0.01^{**}$) and Dexa-GP/ES/Pu NCs ($p < 0.001^{***}$) (Figure 3.16 b1-b2). A decrease in IL-6 and TNF- α is directly linked to the downregulation of the NF- κ B pathway (Liu *et al.*, 2017). Thus, the strategy seems to be effective against neutralizing the pro-inflammatory mediators through the enhanced effect of the drug release from Dexa-GP/ES/Pu NCs at the inflamed area of the colon.

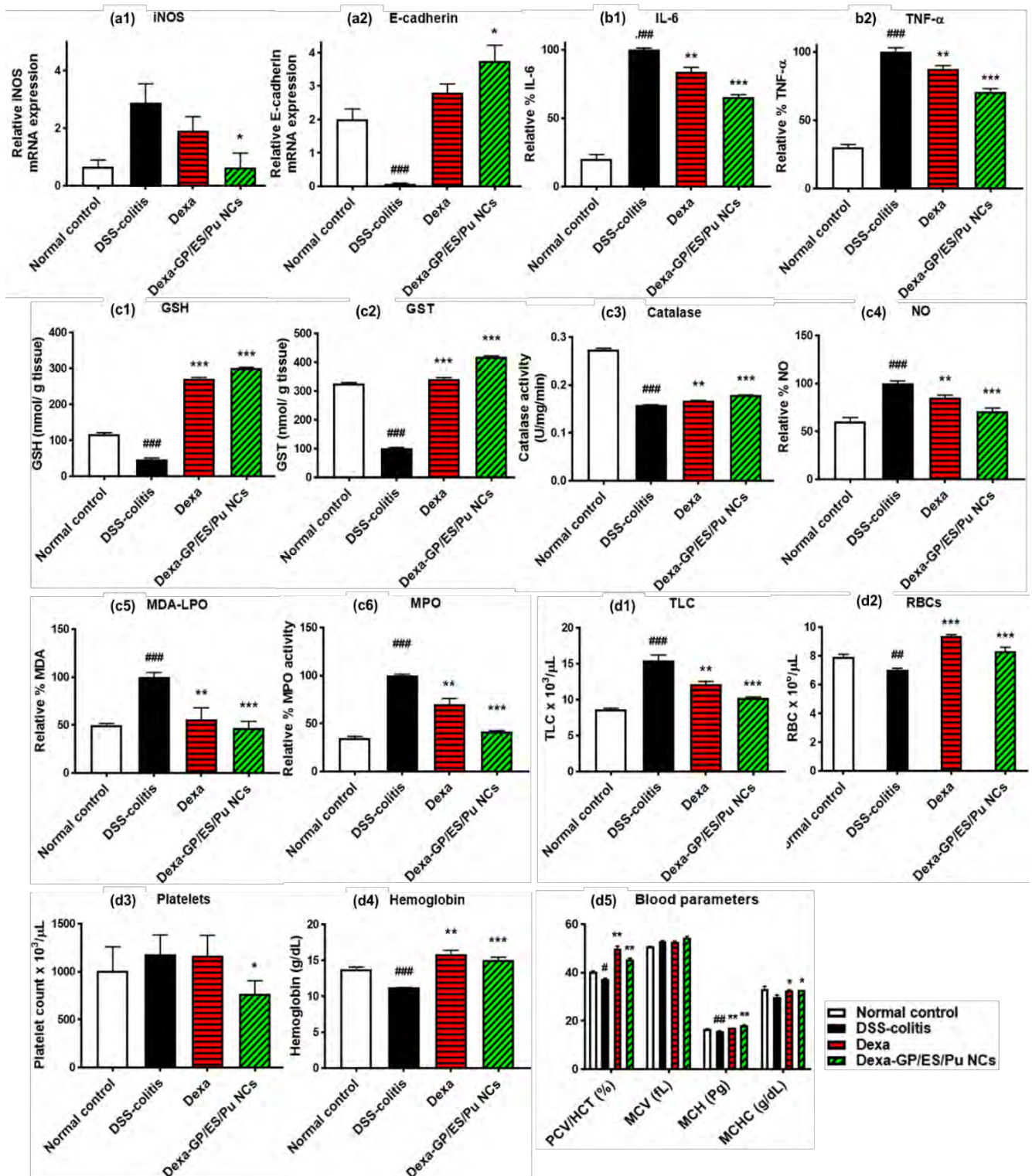


Figure 3. 16: RT-PCR, ELISA, antioxidant assays and blood indices to determine inflammation severity and Dexa-GP/ES/Pu NCs treatment effects; Relative mRNA expression of iNOS (a1) and E-cadherin (a2) from the colon tissues of different groups under study; Relative %age of pro-inflammatory cytokines IL-6 (b1) and TNF- α (b2) in the colon tissues of comparative groups; Concentration of antioxidants GSH (c1), GST (c2), catalase (c3), and oxidants NO (c4), MDA (c5) and MPO (c6) in the excised colon tissues from normal control, DSS-colitis, Dexa and Dexa-GP/ES/Pu NCs treated mice; Levels of

hematological parameters TLC (d1), RBC (d2), Platelets (d3), Hemoglobin (d4), PCV/HCT, MCV, MCH and MCHC (d5) in normal control, DSS-colitis, Dexa and Dexa-GP/ES/Pu NCs treated mice

3.12.2.10. Biochemical antioxidant assays

Inflammation is proceeded by oxidative burst and production of free reactive oxygen species which in turn overcomes the antioxidant scavenging system and damages the cells and the barriers. Likewise, DSS elevated the reactive oxygen species and decline the antioxidant protective enzymes of the intestine ($p < 0.001$ Vs normal). Levels of antioxidants including GSH ($p < 0.001$), GST ($p < 0.001$), catalase ($p < 0.001$) were increased by Dexa-GP/ES/Pu NCs (Figure 3.16 c1-c3), while the oxidative species like NO ($p < 0.001$), and MDA ($p < 0.001$) were significantly reduced by the nanoformulation (Figure 3.16 c4-c5). Dexa-GP/ES/Pu NCs reduced oxidative stress that diminished NF- κ B activity and thus improved GSH, GST, and catalase levels. Furthermore, Dexa and Dexa-GP/ES/Pu NCs treatment of DSS induced colitis mice considerably declined MPO activity by 69.7% ($p < 0.01$) and 41.3% ($p < 0.001$) (Figure 3.16 c6), respectively. In UC, increased immune cells accumulation especially neutrophil releases MPO enzyme catalyzes productivity of oxidative species to aggravate the inflammation (Chami *et al.*, 2018). Therefore, a decline in MPO activity by Dexa-GP/ES/Pu treatment indicated a decrease in neutrophil number at the inflamed tissues and thus demonstrated tissue recovery.

3.12.2.11. Assessment of hematological parameters

Evaluation of CBC facilitates in diagnosing the induction and severity of UC and the therapeutic effect of the treatment. DSS-induced colitis rose the levels of TLC to $15.4 \times 10^3 \pm 0.8 \times 10^3$ ($p < 0.001$), compared to the normal values of $8.6 \times 10^3 \pm 0.2 \times 10^3$. Treatment of colitis with Dexa and Dexa-GP/ES/Pu NCs reduced TLC to $12.13 \times 10^3 \pm 0.42 \times 10^3$ ($p < 0.01$) and $10.2 \times 10^3 \pm 0.2 \times 10^3$ ($p < 0.001$), respectively (Figure 3.16 d1). The RBC levels were decreased by DSS ($p < 0.01$ Vs normal control), which were resumed by both Dexa ($p < 0.001$) and Dexa-GP/ES/Pu NCs ($p < 0.001$) treatment (Figure 3.16 d2). The platelet count was slightly elevated in the DSS colitis group, which was decreased by Dexa-GP/ES/Pu NCs ($p < 0.05$ Vs DSS) (Figure 3.16 d3). The other blood parameters including Hemoglobin (Hb), packed cell volume/hematocrit (PCV/HCT), mean corpuscular volume (MCV), mean corpuscular hemoglobin (MCH) and mean corpuscular hemoglobin concentration (MCHC) were modified with DSS-induction

and successfully normalized with Dexa and Dexa-GP/ES/Pu NCs treatment (Figure 3.16 d4-d5). Mostly, Dexa-GP/ES/Pu NCs showed superior efficacy in regulating the blood biochemical values as compared to Dexa only (Figure 3.16 d1-d5). Blood tests are considered when diagnosing IBD, mostly immune cells elevated in inflammation and RBCs decline in colitis because of anemia and other parameters also disturbed. Restoration of TLCs, RBCs, hemoglobin, etc. indicated recovery from DSS-induced inflammation.

3.12.2.12. *In vivo biocompatibility and toxicity studies of Dexa-GP/ES/Pu NCs*

Dexa-GP/ES/Pu NCs were tested in healthy mice to investigate acute toxicity and in vivo biocompatibility. During the 7-day course of administration, the mortality rate was 0%, with no symptoms of allergy, lethargy, anxiety, and pain. The pattern of food and water intake did not vary. The daily weight assessment (Figure 3.17 A) showed negligible weight loss in the 7 days ($p=N.S$ Vs control). After 7 days, mice were euthanized, and major organs were isolated. Organ weight (stomach, small intestine, colon, spleen, liver, kidney, heart, and lung), small intestine and colon length, and colon weight to length ratio did not differ from the control (Figure 3.17 B-D). Moreover, feces collected at the end were tested for the bacterial count. The total bacterial log CFU/mL was parallel to the control (Figure 3.17 E), demonstrating that nanocargoes are safe for the natural colon microbiome. In fact, pullulan in the composition of nanoparticle not only improves the colon targeting ability but additionally serve as a probiotic and is beneficial to rectify the colitis-led microbiome disturbances. The biochemical investigation of the blood revealed normal concentrations of RBCs, WBCs, and other blood parameters (Figure 3.17 F, G). Further, the histopathological analysis of the organs had minimal deviations from the control (Figure 3.17 H).

The findings emphasized that Dexa-GP/ES/Pu NCs are non-toxic, biocompatible, and safe in living systems. Further, the apoptotic analysis of colon tissues using Annexin-V and propidium iodide demonstrated that Dexa-GP/ES/Pu NCs exposure resulted in 78.63% live cells as compared to 94.31% live cells in the control (Figure 3.17 I). The in vivo viability percentage mimics the MTT based In vitro cell viability range for the colon cells (Figure 3.12 E, F).

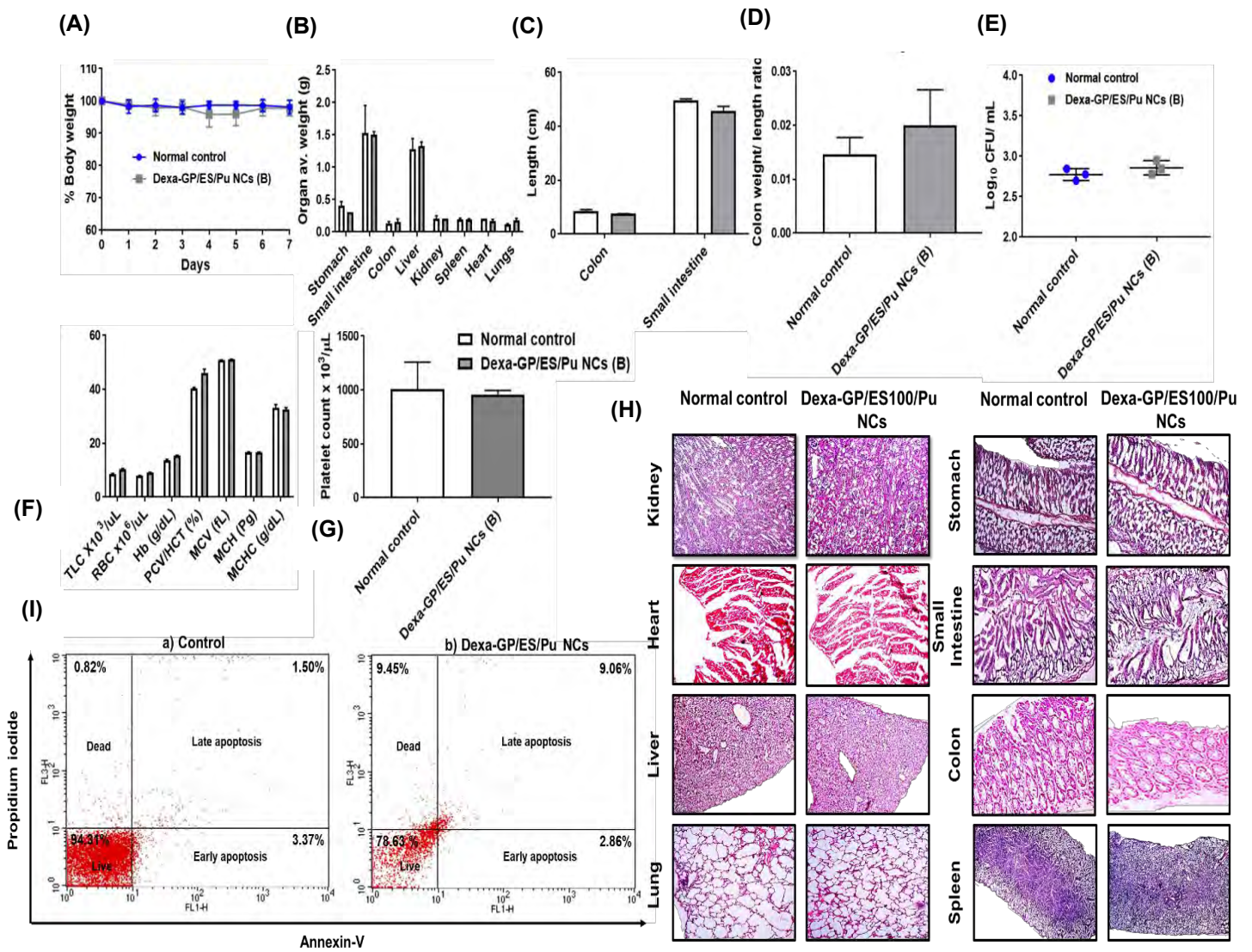


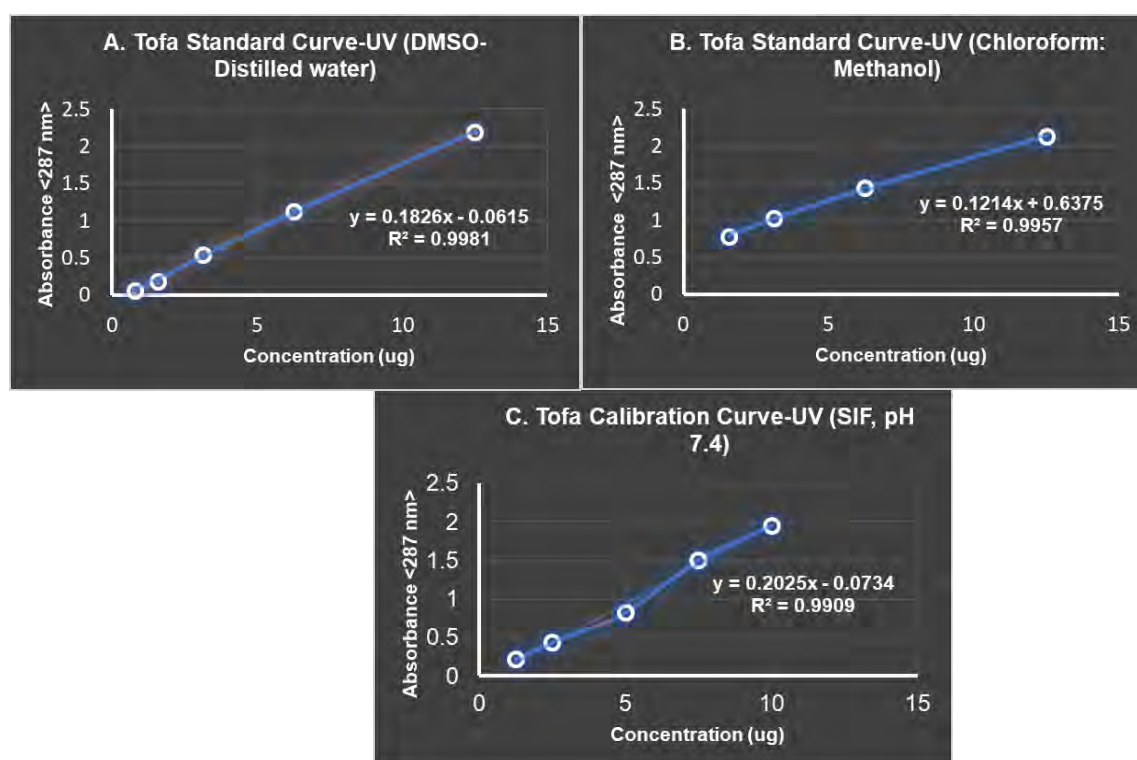
Figure 3. 17: Assessment of in vivo biocompatibility and toxicology during and after 7 days of administration Dexa-GP/ES/Pu to the healthy mice (n=3): A. % Bodyweight, B. Average organ weight (g), C. Intestine lengths (cm), D. Colon weight to length ratio, E. Fecal microbial growth (log CFU/mL), F. Hematological analysis, G. Platelet count, H. Histopathological investigations of vital organs (kidney, heart, liver, lung, stomach, small intestine, colon, and spleen), I. Colon cells apoptosis study with Annexin-V/Propidium iodide in the untreated normal healthy control and Dexa-GP/ES/Pu NCs treated healthy mice

PART-II (SECTION A)

Tofa-P/tfr NCs

3.13. Preparation of Tofa-P/tfr NCs

At first, UV and HPLC methods were developed to quantify the drug. The UV calibration curve of Tofa in DMSO: distilled water (0.1:1), chloroform: methanol (1:1), and SIF (pH 7.4) were obtained with regression of co-efficient R^2 values of 0.9981, 0.9957 and 0.9909, respectively (Figure 3.18 A-C). Tofa calibration curve was obtained using HPLC methods with linearity of 0.9994 and 0.9998 from methods 1 and 2, respectively (Figure 3.18 I-II).



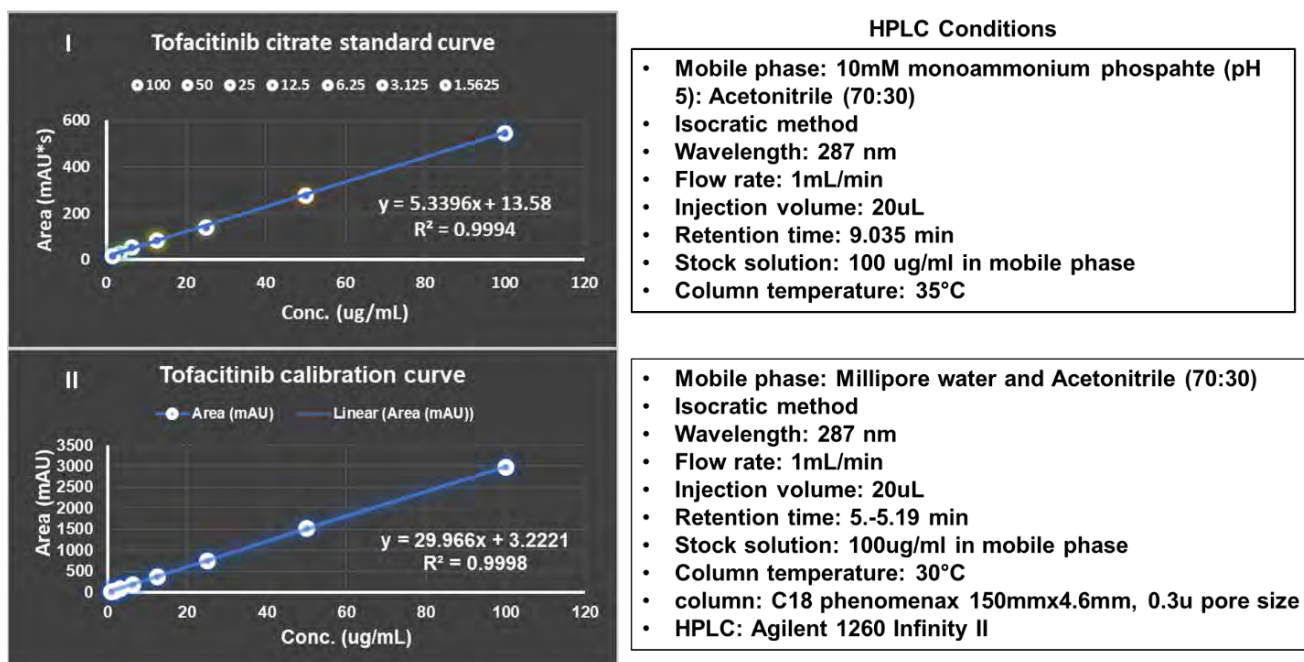


Figure 3. 18: Tofacitinib citrate (Tofa) calibration curves with various solvents using UV spectrophotometer (A-C) and HPLC calibration curves (I-II)

3.14. Preparation of Tofa-P/tfr NCs

The Tofa-P/tfr NCs preparation method was screened in the preliminary studies and the O/W emulsion method with physical adsorption of tfr in the external phases was selected. Moreover, different organic solvents were tried and chloroform: methanol (1:1) produced the most stable and uniform sized nano-formulation.

All three methods (mentioned in Method section 2.5 i-iii) formed stable nano-suspension with good particle size (<200 nm). However, method **ii** was selected because of maximum tfr adsorption from a relatively simple and cost-effective method. In comparison to method **i**, this method had relatively more tfr adsorption and decreased the number of steps. When compared to chemical conjugation, this method is safer and environment friendly with no use of toxic materials like EDC and NHS. Further, the tfr adsorption was good. All three methods were also tested to prepare drug-loaded P/tfr NCs. The tedious method of chemical conjugation always resulted in lesser drug entrapment efficiency. Together, with these considerations, tfr physical adsorption during emulsification (method **ii**) was selected for further optimization.

The QbD analysis indicated the critical variables among CMAs and CPPs afflicting the CQAs. The interactions between QTPP and CQAs determine the impact of each QTPP

on outcomes (Table 3.16) and each independent CPP/CMA on outcomes (CQAs) (Table 3. 17). Ishikawa diagram displayed all parameters that should be considered while developing nano-formulation (Figure 3. 19 A). The most influencing independent variable screened by risk assessment were tfr concentration, drug concentration, and surfactant concentration (Table 3. 17, Figure 3. 19 B). Homogenization speed is also prominent, but we have already adjusted it during preliminary trials. The critical dependent variables (CQAs) were particle size, tfr adsorption, and drug entrapment (Table 3.16, Table 3. 17, Figure 3.19 C). Afterward, 3^3 Box-Behnken design was applied to study the effect of selected variables and to formulate the optimum nano-formulation with desired features.

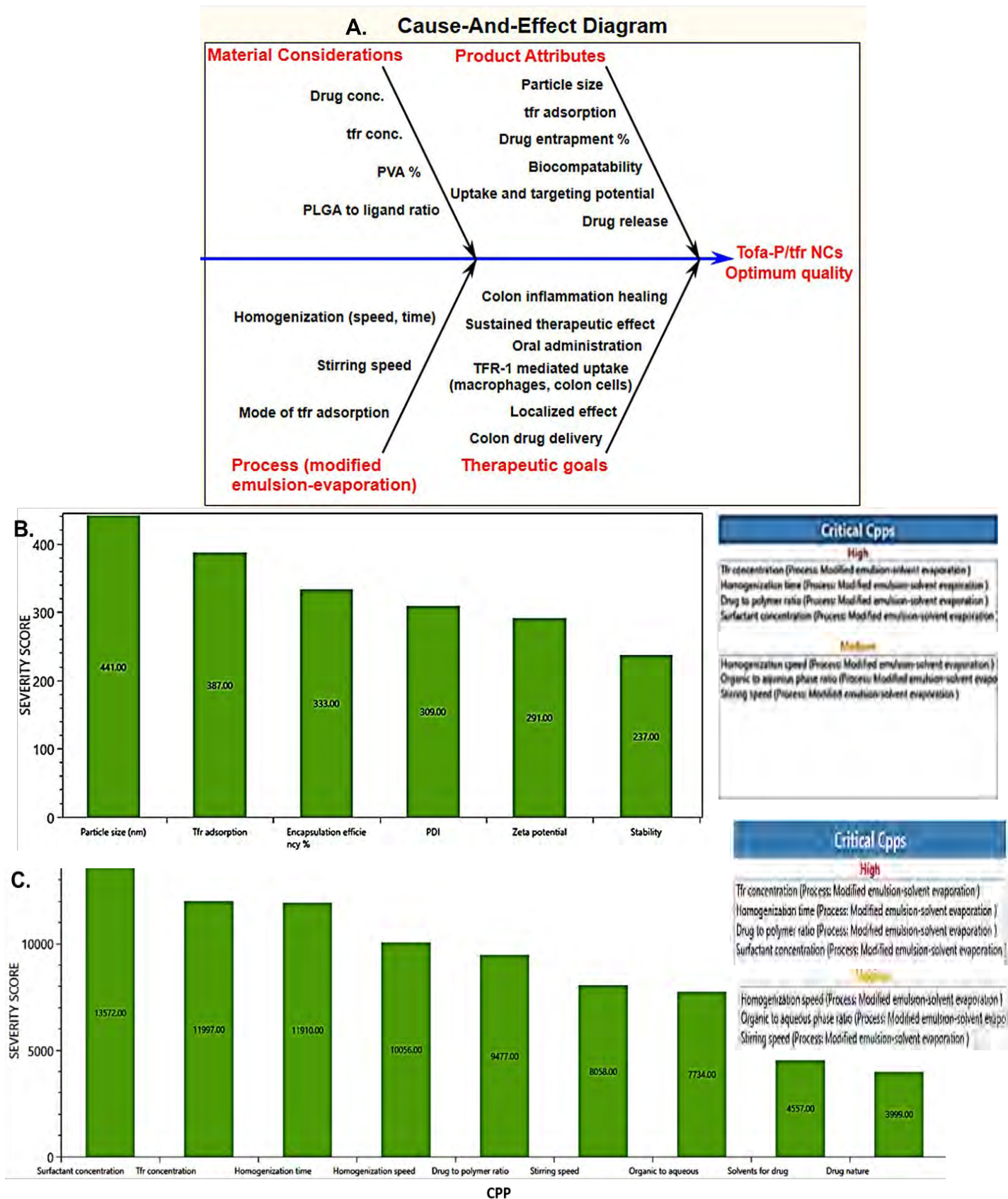


Figure 3. 19: QbD analysis: Cause and effect Ishikawa diagram for Tofa-P/tfr NCs (A); Screening of critical process parameters (B), and critical quality attributes (C) through risk-based assessment of severity scores

Table 3. 16: QbD-risk assessment of the impact of QTPPs on CQAs for Tofa-P/tfr NCs

| CQA/QTPP | Route of administration | Site of activity | Therapeutic indication | Dissolution profile | Physicochemical stability | Product characteristics | Dosage form design |
|--------------------|-------------------------|------------------|------------------------|---------------------|---------------------------|-------------------------|--------------------|
| Particle size (nm) | Low | High | High | High | High | High | High |
| Zeta potential | Low | Medium | Low | Low | High | High | High |
| EE % | Medium | Low | High | Medium | High | High | High |
| Tfr adsorption | Low | High | High | Medium | High | High | High |
| PDI | Medium | Low | Low | Medium | High | High | High |
| Stability | Low | Medium | Low | Low | High | High | Medium |

Table 3. 17: QbD-risk assessment of the impact of CPPs/CMA on CQAs for Tofa-P/tfr NCs

| Process: | Modified emulsion-solvent evaporation | | | | | | | | |
|--------------------|---------------------------------------|-----------|---------------------|----------------------|-------------|-----------------------|------------------|--------------------------------|----------------|
| CPP/CMA | Solvents to solubilize drug | Tfr conc. | Homogenization time | Homogenization speed | Drug nature | Drug to polymer ratio | Surfactant conc. | Organic to aqueous phase ratio | Stirring speed |
| CQA | | | | | | | | | |
| Particle size (nm) | Medium | High | High | High | Low | High | High | Medium | High |
| Zeta potential | Low | High | Low | Low | Low | Medium | Medium | Low | Low |
| EE % | High | Medium | High | High | High | High | Low | Medium | Medium |
| Tfr adsorption | Low | High | Medium | Medium | Low | Low | High | High | Medium |
| PDI | Low | Medium | High | Medium | Low | Medium | High | Medium | Medium |
| Stability | Low | Low | Medium | Medium | Medium | Medium | High | Medium | Medium |

3.14.1. DOE: Box-Behnken design (3³)

A 3³ Box-Behnken design was considered to generate 15 runs of different combinations of independent variables. The model provides a good estimation of the effect of each independent variable (tfr concentration, drug concentration, and PVA concentration) on each dependent variable (particle size, drug entrapment, and tfr adsorption). Coefficient of regression (R^2) for particle size, drug entrapment, and tfr adsorption was 0.986, 0.988, and 0.996, respectively. Good R^2 values indicated the goodness of fit of the design. Table 3. 18 represented 3³ Box-Behnken design for the set of independent variables affecting response variables.

Effect of independent variables on particle size (nm) (X): Different combinations of independent variables generated the particle size of Tofa-P/tfr NCs in the range of 205.2-250.4 nm (Table 3. 18) The polynomial equation representing the inter-relationship between independent variables and particle size (X) is mentioned in Equation 15:

$$X = 223.99 - 35.1A + 2.56B + 12.77C - 3.9AB - 2.95AC + 4.74BC - 9.8A^2 + 1.85B^2 - 2.73C^2 \dots\dots\dots 15$$

The multi-variable effect on particle size is obvious from the equation. The variables with a positive sign have a synergistic effect, while the negative sign has an agonist effect. ANOVA indicated that the tfr concentration (A) ($p < 0.01$) and PVA concentration (C) ($p < 0.01$) have a significant impact on the size, while drug concentration (B) have a minimal role. The formula depicted that the tfr concentration (A) have a negative effect on the size, indicating an increase in tfr concentration decreased particle size. Therefore, a higher tfr concentration is favorable in achieving lower particle size. It might be due to the reduction in surface charge on higher tfr concentration that resulted in bigger particles. The effect is prominently observed in the response surface plot (Figure 3. 20) and Pareto charts (Figure 3. 21 A).

The quadratic effect of tfr concentration is also prominent. Secondly, an increase in surfactant concentration increases particle size, because it increases the medium viscosity which lowered the effect of shear force to split the droplets into smaller sizes. The surface response plot (Figure 3. 20) and Pareto charts (Figure 3. 21 A) demonstrate the effect of surfactant concentration and drug concentration on the size. Drug concentration has a slightly positive effect but is not significant ($p = \text{NS}$).

Drug entrapment (%) (Y): Equation 16 describes the second-order equation for the effect of independent variables on drug entrapment (Y):

$$Y = 69.18 + 1.06A + 18.48B + 0.74C + 1.39AB - 0.76AC - 0.18BC - 0.028A^2 + 0.937B^2 + 1.23C^2 \dots\dots\dots 16$$

ANOVA indicated that drug concentration have a significant impact on drug entrapment ($p < 0.001$). An increase in drug concentration (B) have a direct effect on entrapment efficiency (Y). The tfr concentration (A) and PVA concentration (C) have a negligible effect on drug entrapment. Surface response plots (Figure 3. 20) and Pareto charts (Figure 3. 21 B) visually represented the inter-related effects.

Tfr adsorption (mg) (Z): 3^3 Box-Behnken design produced various combinations of independent variables that resulted in Tofa-P/tfr NCs with tfr adsorption in the range of 0.69-0.89 (Table 3. 18). Equation 17 demonstrates the relationship of studied variables on tfr adsorption:

$$Z = 0.76 + 0.18A + 0.013B + 0.019C + 0.002AB - 0.00015AC + 0.0071BC - 0.08A^2 + 0.0008B^2 + 0.0022C^2 \dots\dots 17$$

The foremost affecting variable is tfr concentration which positively impacts tfr adsorption ($p < 0.001$). However, the quadratic relation, A^2 , is negatively correlated, possibly because too much concentration may saturate the porous polymeric surfaces of the nanocarriers reduced the adsorption capacity of the polymeric surfaces. Drug concentration (B) have minimal impact on tfr adsorption. The PVA concentration (C) affects the adsorption rate and capacity of nanocarriers ($p < 0.05$), because it is the main constituent of the outer aqueous phase with tfr. Therefore, a higher surfactant may emulsify greater and improve the tfr protein adsorption during nanocarrier formation. Surface plots (Figure 3. 20) and Pareto charts (Figure 3. 21 C) represented the influence of variables on tfr adsorption.

Table 3. 18: 3^3 Box-Behnken Experimental design generating different runs to produce desired values of the dependent variables (output)

| Runs | Independent Variables | | | Dependent variables/ Output | | |
|------|-----------------------|--------------------|------------------|-----------------------------|------------------------|------------------------|
| | A. Tfr conc. (mg) | B. Drug conc. (mg) | C. PVA conc. (%) | X. Particle size (nm) | Y. Drug entrapment (%) | Z. tfr adsorption (mg) |
| 1 | 0.500000 | 0.500000 | 2.000000 | 241.00 | 59.94 | 0.68 |
| 2 | 1.000000 | 0.500000 | 2.000000 | 208.00 | 61.46 | 0.87 |
| 3 | 0.500000 | 2.000000 | 2.000000 | 245.10 | 77.00 | 0.70 |
| 4 | 1.000000 | 2.000000 | 2.000000 | 205.20 | 80.38 | 0.89 |
| 5 | 0.500000 | 1.000000 | 1.000000 | 240.00 | 65.24 | 0.69 |
| 6 | 1.000000 | 1.000000 | 1.000000 | 210.50 | 65.23 | 0.86 |
| 7 | 0.500000 | 1.000000 | 3.000000 | 250.40 | 68.17 | 0.70 |
| 8 | 1.000000 | 1.000000 | 3.000000 | 215.00 | 66.63 | 0.873 |
| 9 | 0.750000 | 0.500000 | 1.000000 | 209.00 | 59.39 | 0.69 |
| 10 | 0.750000 | 2.000000 | 1.000000 | 210.00 | 78.09 | 0.69 |
| 11 | 0.750000 | 0.500000 | 3.000000 | 222.00 | 58.50 | 0.71 |
| 12 | 0.750000 | 2.000000 | 3.000000 | 230.00 | 77.75 | 0.72 |
| 13 | 0.750000 | 1.000000 | 2.000000 | 216.30 | 67.67 | 0.70 |
| 14 | 0.750000 | 1.000000 | 2.000000 | 215.00 | 67.00 | 0.70 |
| 15 | 0.750000 | 1.000000 | 2.000000 | 218.00 | 67.90 | 0.71 |

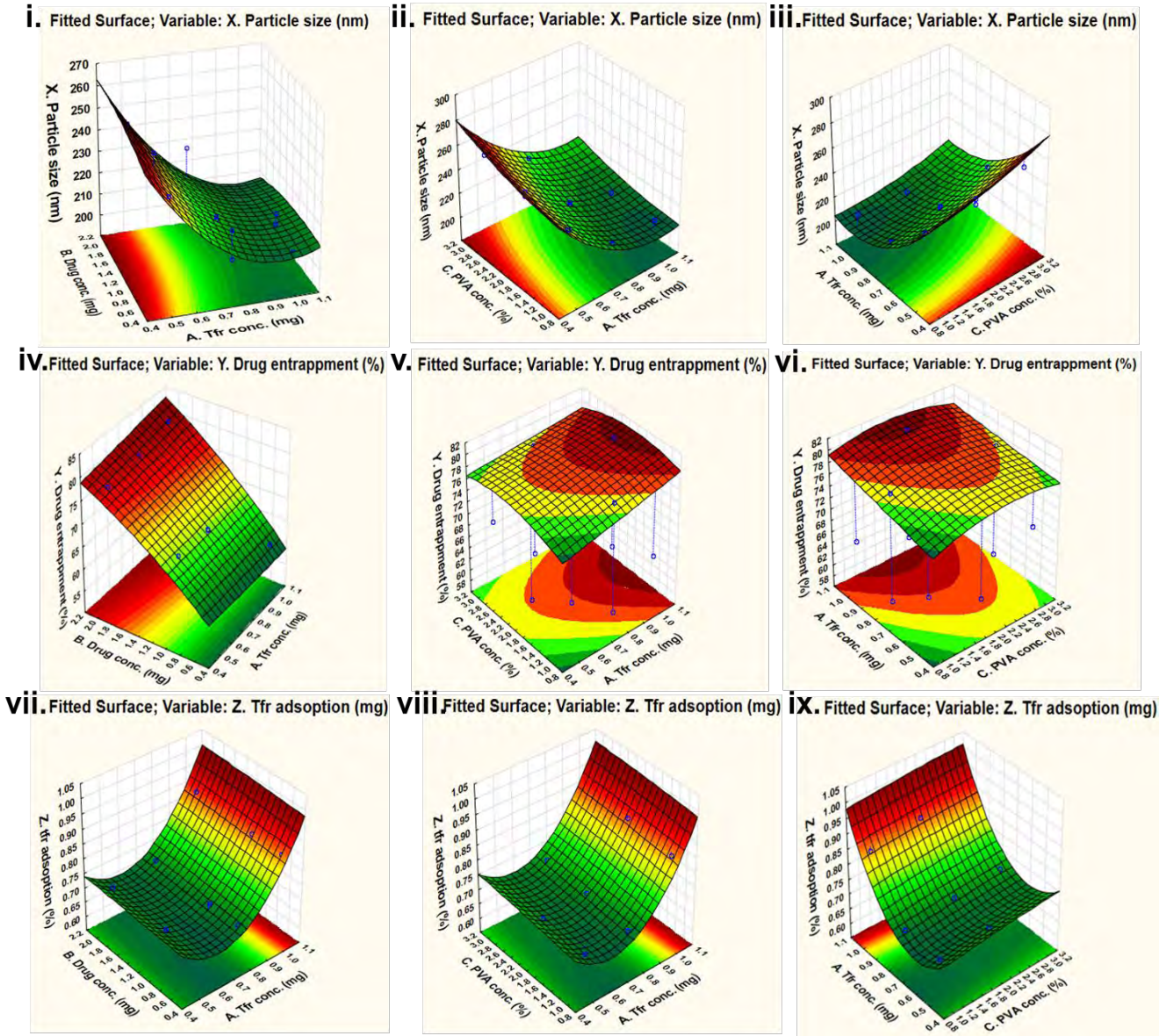


Figure 3. 20: Surface-response plots for the study of effects of independent variables on dependent variables (outcomes) under 3^3 Box-Behnken DOE

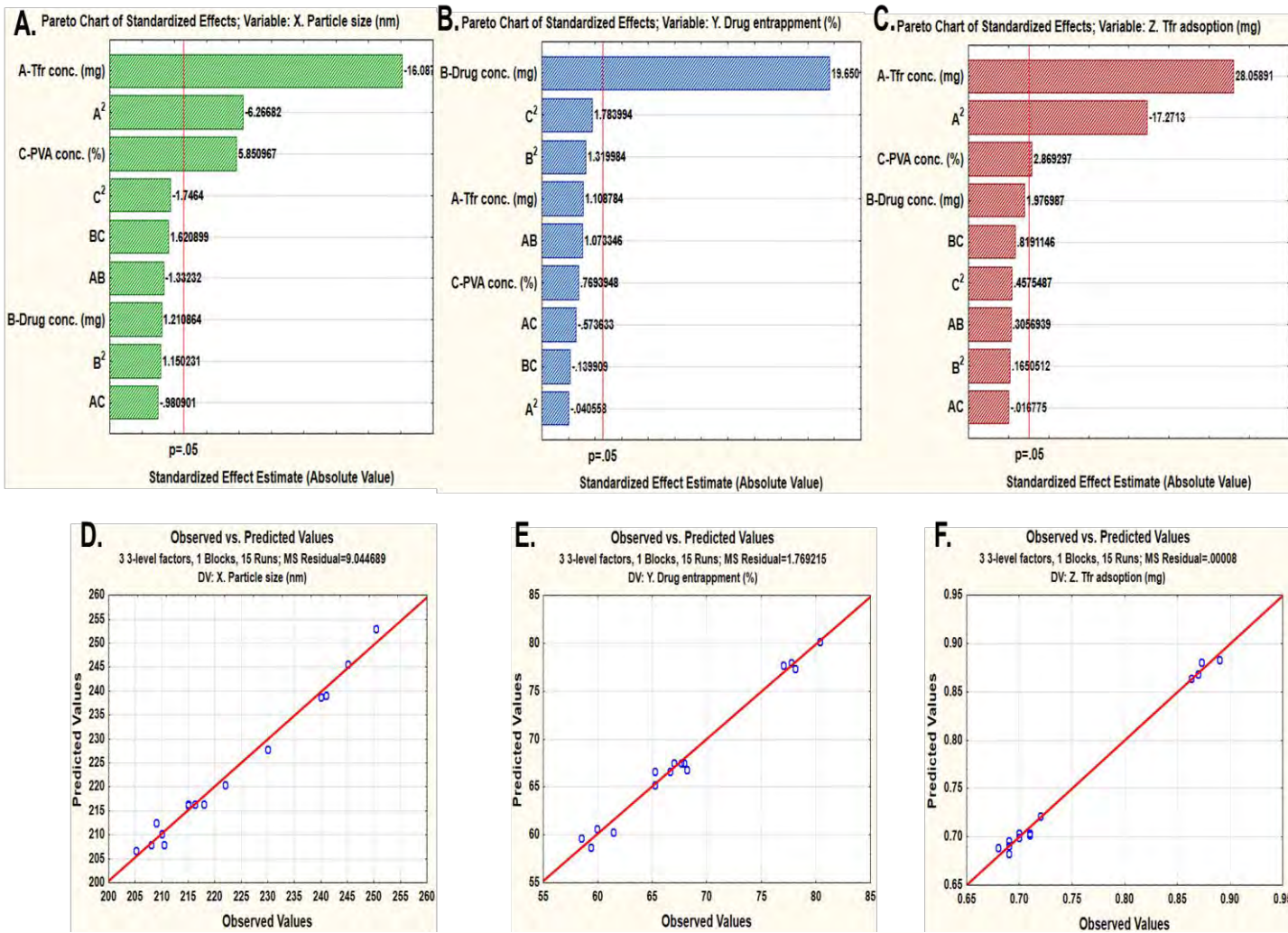


Figure 3. 21: A-C: Pareto charts of standardized effects on dependent variables (X, Y, Z); D-F: Difference between the predicted and experimental values of dependent variables using 3³ Box-Behnken design

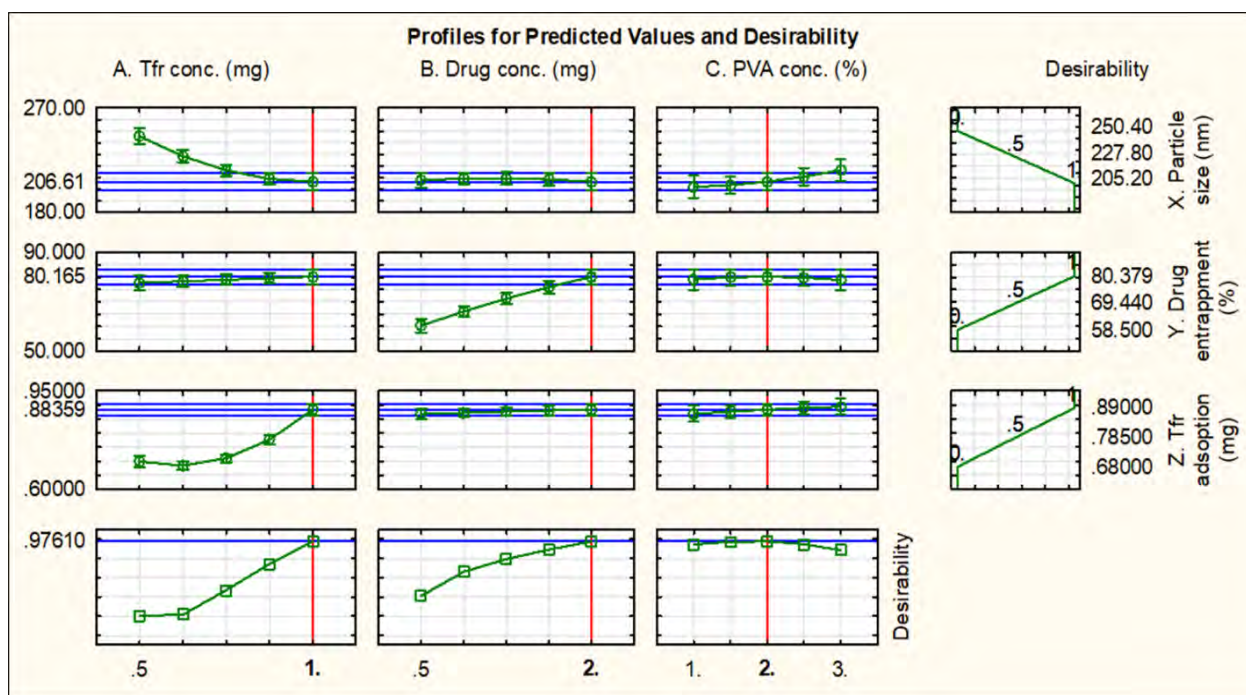


Figure 3. 22: Desirability profile to obtain the desired values of dependent variables (outcomes) from an appropriate combination of independent variables

3.14.2. 3³ Box-Behnken design validation

The model generated predicted dependent variable values that were found to be in good agreement with the experimental values with little residual values (Figure 3. 21 D-F). Further, the desirability profile was obtained using STATISTICA[®] 10.0 (Figure 3. 22) which depicted the best combination of variables to produce the desired outcomes i.e., minimum particle size and maximum drug entrapment and tfr adsorption. The optimum set of independent variables included tfr concentration (1 mg), drug concentration (2 mg) and PVA concentration (2%) that produced desirable outcomes to proceed further for characterization.

3.15. Physicochemical Characteristics and tfr Adsorption

The optimum set of independent variables was replicated thrice to produce Tofa-P/tfr NCs of desirable outcomes. The formed Tofa-P/tfr NCs have an average particle size of $208.0 \text{ nm} \pm 0.136 \text{ nm}$, the zeta potential of $-8.64 \text{ mV} \pm 1.735 \text{ mV}$, and PDI of 0.121 ± 0.004 (Table 3. 19, Figure 3. 23 A, B). The size distribution and surface morphology by SEM analysis was found to be uniform, and circular with a smooth surface (Figure 3. 23 B). It was noticed size was increased with the addition of tfr compared to Tofa-PLGA NCs (Table 3. 19). Moreover, the zeta potential was declined because of the

cationic nature of proteinaceous tfr onto the anionic PLGA (Table 3. 19). The findings are consistent with the literature (Chang *et al.*, 2012). The Tofa-P/tfr NCs met the required criteria of size around 200 nm, PDI<0.3, and negative zeta potential. The nanocarriers of these properties can easily be up taken by the epithelial and immune cells of the colon and retained at the site for a long with fewer chances of diarrhea mediated clearance in colitis. Further, the drug entrapment efficiency was $80.97\% \pm 0.79\%$, and entrapped drug content was $62.40 \mu\text{g}/\text{mg} \pm 5.37 \mu\text{g}/\text{mg}$ (Table 3. 19). The concentration of tfr was varied with the final set of selected variables, and it was found that the highest adsorption occurred with the highest tfr amount (Figure 3. 23 C). The adsorbed tfr on the surface of nanocarriers was $0.886 \text{ mg} \pm 0.015 \text{ mg}$ as measured through nanodrop (280/260nm) and $0.872 \text{ mg} \pm 0.089 \text{ mg}$ by Bradford's assay (Figure 3. 23 D). The amount adsorbed followed the experimental values of Box-Behnken trial runs.

Table 3. 19: Physicochemical characteristics of Tofa-PLGA NCs and Tofa-P/tfr NCs (mean \pm SD, n=3)

| Formulation | Particle size (nm) | Zeta potential (mV) | PDI | EE% | DL ($\mu\text{g}/\text{mg}$ NCs) | % Yield |
|----------------|--------------------|---------------------|-------------------|------------------|-----------------------------------|-------------------|
| Tofa-PLGA NCs | 122.87 \pm 1.47 | -11.09 \pm 0.39 | 0.075 \pm 0.064 | 81.50 \pm 1.59 | 65.59 \pm 1.53 | 87.17 \pm 1.041 |
| Tofa-P/tfr NCs | 208.0 \pm 1.36 | -8.64 \pm 1.735 | 0.121 \pm 0.004 | 80.97 \pm 0.79 | 62.40 \pm 5.37 | 89.08 \pm 0.88 |

3.15.1. TGA

TGA analysis of drug, Tofa-PLGA NCs, and Tofa-P/tfr NCs revealed their degradative pattern on rising temperatures. The TG graph depicted a sharp degradation peak of the drug at 230-240°C. Tofa melts around the same temperature (Bashir *et al.*, 2021). It is followed by a shallow decline till the end. While the pattern of Tofa-PLGA NPs and Tofa-P/tfr are alike and have a slight shift after 400°C; about 66% and 59% of the nanocarrier consumed till 450°C, respectively (Figure 3. 23 E).

3.15.2. DSC

The DSC thermogram of Tofa exhibited a sharp endotherm at 215°C, representing its melting point because of crystalline content (Figure 3. 23 F). While the thermograms of PLGA polymer and Tofa-P/tfr NCs were devoid of any sharp endotherm. The flattened curve of the nanocarrier indicated that Tofa entrapped within the Tofa-P/tfr NCs in the amorphous form rather than crystalline. Only a small endotherm at 109°C was prominent in Tofa-P/tfr NPs (Figure 3. 23 F), which might be representative of tfr

adsorbed on the surface (Jose *et al.*, 2019). A starting downward curvature ($\sim 10\text{-}15^\circ\text{C}$) was due to an abrupt change of temperature from freezing to 10°C .

3.15.3. ATR-FTIR

ATR-FTIR spectra of PLGA, Tofa, tfr and Tofa-P/tfr NCs are represented in Figure 3.23 G. The spectrum of PLGA consisting of peaks at 3470 cm^{-1} (-OH), 2998 cm^{-1} and 2952 cm^{-1} (-CH₂), 1742 cm^{-1} (C=O), 1422 cm^{-1} (C-OH in-plane), 1381 cm^{-1} (-CH₃), 1161 cm^{-1} (esteric C-O), and 1082 cm^{-1} (alcoholic C-O) (Figure 3. 23 G). The drug Tofa had major FTIR peaks at 3375 cm^{-1} , 3129 cm^{-1} , 1731 cm^{-1} , 1615 cm^{-1} , 1340 cm^{-1} , 1207 cm^{-1} and 842 cm^{-1} corresponding to -NH stretching band, C=C, C=O, secondary C=C stretch, C-N, C-O stretch, and -C-H respectively (Figure 3. 23 G). FTIR spectrum of tfr had an amine (-NH-) stretch at 3278 cm^{-1} , with an amide band at 1638 cm^{-1} , similar to literature report (Pooja *et al.*, 2015). The other peaks are visible at 2961 cm^{-1} (-CH₂), 2187 cm^{-1} (C \equiv N), 1507 cm^{-1} (CH₂/CH₃), and 1386 cm^{-1} (CH), 1235 cm^{-1} , and 1071 cm^{-1} (C-O) (Figure 3. 23 G). While Tofa-P/tfr NCs FTIR pattern had a prominent -NH - stretch at 3274 cm^{-1} , shallower than tfr corresponding peak, and an amide band at 1632 cm^{-1} that confirmed the coating of tfr on PLGA NCs. The other peaks at 2937 cm^{-1} , 2430 cm^{-1} , 1735 cm^{-1} , 1446 cm^{-1} , 1215 cm^{-1} and 1161 cm^{-1} represented -CH₂, either C \equiv N or C \equiv C, C=O, C-H bend, C-O, and esteric C-O respectively (Figure 3. 23 G). The unique peak at 2430 cm^{-1} have an appearance only in the nanocarrier, either due to adsorption of tfr onto the surface that resulted in bond formation or because of some impurities. The drug peaks were not prominent in the nanocarrier spectra, indicating complete entrapment of Tofa inside the polymeric structure and the absence of any surface-bound drug.

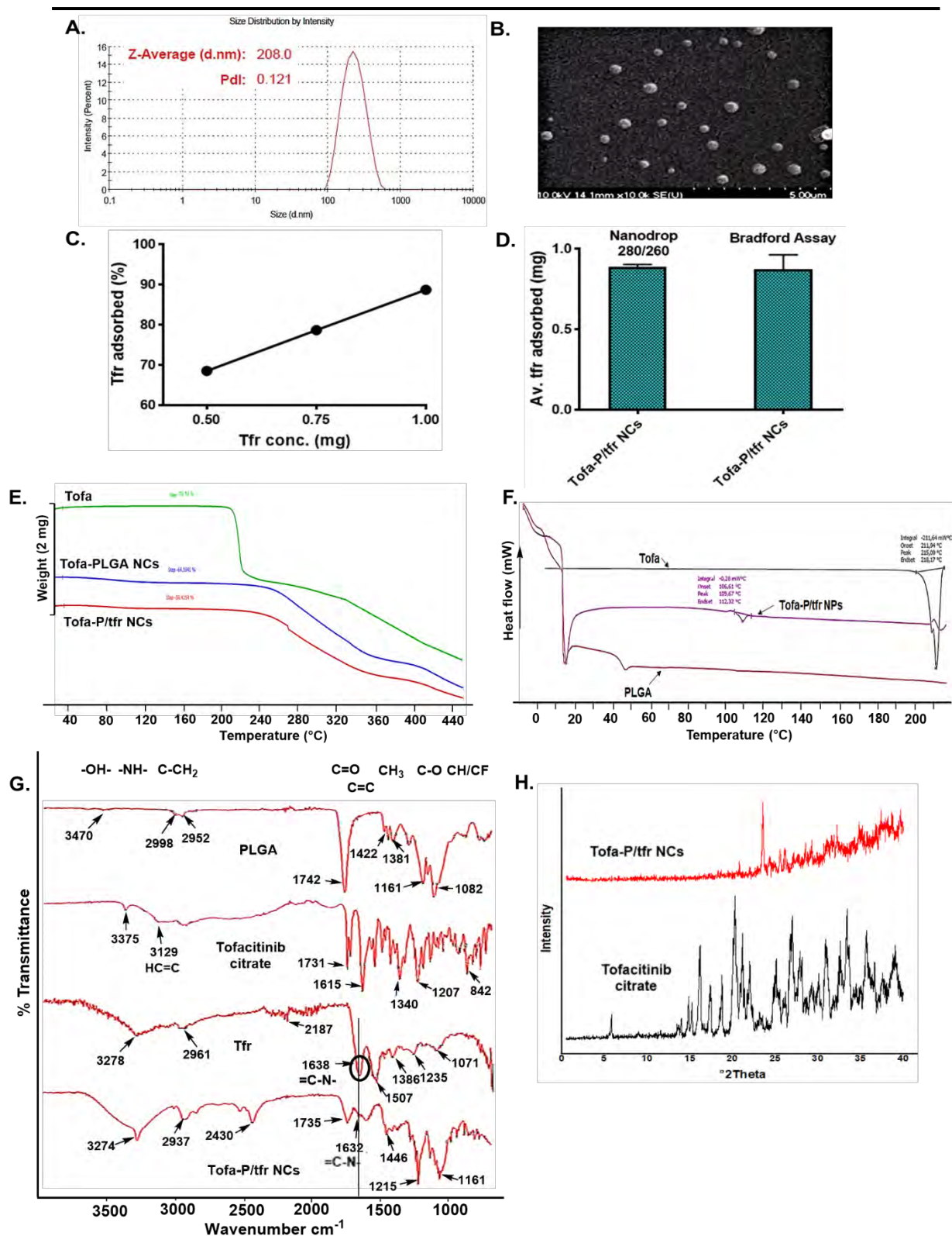


Figure 3. 23: Physicochemical characterization of Tofa-P/tfr NCs. A) Particle size, B) SEM images of Tofa-P/tfr NCs, (C) Effect of tfr concentration on %Tfr adsorbed, D) The concentration of adsorbed tfr on the nanocarrier, measured by Nanodrop and Bradford's assay, E) TGA thermograms of nanocarriers, F) DSC thermogram of nanocarrier and drug, G) ATR-FTIR spectra of drug, polymer and nanocarrier, H) XPRD spectra of drug and nanocarrier

3.15.4. XPRD

The XPRD spectra of Tofa and Tofa-P/tfr NCs has been shown in Figure 3. 23 H. Tofa exhibited crystalline nature, as depicted by prominent peaks starting from around 14-40 2°-Theta, indicating its crystalline nature. Whereas Tofa-P/tfr NCs have a relatively smoothed pattern, with a little peak around 24 2°-Theta, that may be because of tfr content in it (Figure 3. 23 H). The absence of drug peaks represented the conversion of the crystalline nature of the drug into an amorphous form inside the polymeric nanocarrier.

3.16. In Vitro Drug Release Studies

Drug release study conducted at pH 1.2 (0-2 hours) and pH 7.4 (2-72 hours) demonstrated a biphasic pattern for Tofa-PLGA NCs and Tofa-P/tfr NSh. Both types of nanocarriers showed an initial burst release of the drug followed by a sustained release pattern (Figure 3.24 A). Tofa-P/tfr NCs released up to $76.99\% \pm 2.68\%$ of drug, and Tofa PLGA NCs released $80.04\% \pm 2.322\%$ drug till 72 hours (Figure 3.24 A). Overall, the two release profiles had an insignificant difference, when compared using one-way ANOVA. However, the time points at 1.5 and 2 hours at pH 1.2 have major differences between the two profiles. Tofa-P/tfr NSh controlled the burst release of the drug at these time points significantly ($p < 0.01$), possibly because of the lesser amount of loosely entangled surface-bound drug than PLGA NCs. Drug release kinetics assessment showed that Tofa-P/tfr NSh followed both Korsmeyer-Peppas ($R^2=1.000$) and Peppas-Sahlin model ($R^2=1.000$) at pH 1.2 (Table 3. 20). The trend was the same at pH 7.4, with a Korsmeyer R^2 value of 0.9934 and very near Peppas-Sahlin R^2 of 0.9969 (Table 3. 20). The mechanism of drug release was Fickian diffusion, both at pH 1.2 and 7.4, since Korsmeyer's $n < 0.43$ (Zuo *et al.*, 2014) and Peppas-Sahlin m value approaches n at respective pHs profiles.

3.17. Mucin Binding Study

Mucins are glycoproteins, produced by intestinal epithelial cells in the mucus to protect it against pathogens and injuries. Its interaction with nanocarriers is of special interest because it determines the fate of nanocarrier mobility across the intestine epithelial cells, and time of residence in the mucus, clearance rate, etc. some polymeric nanocarriers with mucoadhesive nature stick to the site of action over a long period while some nanocarrier with opposite charge have least interaction with mucin and

reached reach the epithelial cells easily (Zeeshan *et al.*, 2019a). We assessed the ability of formed nanocarriers to interact with mucin. The size distribution analysis indicated Tofa-P/tfr NCs-mucin formulation interacted at some point with two overlapping peaks between 235-605 nm with a mean particle size of 521.6 nm (Figure 3.24 B).

It was noticed that bare PLGA NCs have the least interaction with mucin ($5.73\% \pm 0.78\%$) because of anionic nature, while the addition of tfr in Tofa-P/tfr NCs enhanced the mucin binding up to $40\% \pm 0.078\%$ ($p < 0.001^{***}$ vs PLGA NCs) (Figure 3.24 C). Tfr decreased the surface charge of nanocarriers (Figure 3.24) that facilitated interaction between mucin and Tofa-P/tfr NCs. Further, the viscosity increased when Tofa-P/tfr NCs interacted with mucin as compared to mucin or formulation only at all shear rates (Figure 3.24 D).

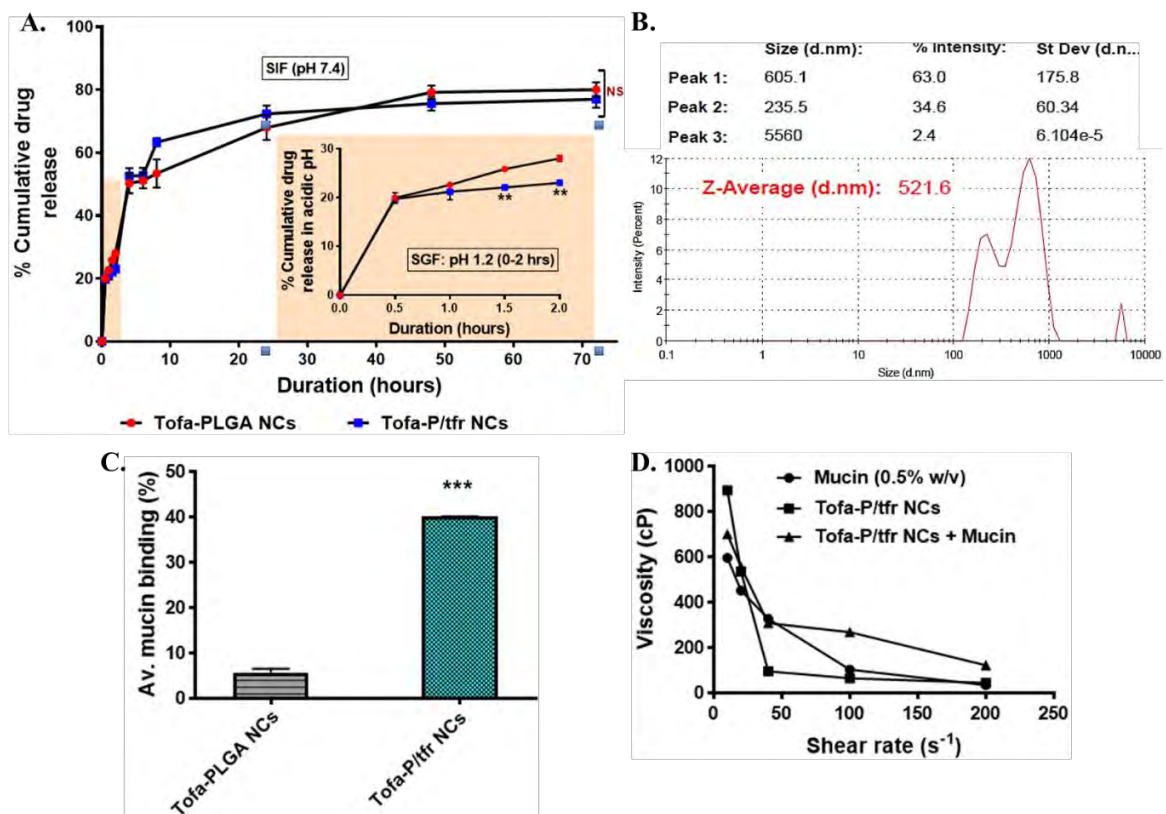


Figure 3. 24: Tofa-P/tfr NCs drug release studies and mucin interaction studies; A) In vitro drug release study in SGF (pH 1.2) and SIF (pH 7.4), n=3; B) Size distribution analysis of mucin-nanocarrier complex, C) Nanocarrier-mucin binding (%), D) Rheological investigation of mucin-nanocarrier complex.

Table 3. 20: Drug release kinetics of Tofa-P/tfr NCs in SGF at pH 1.2 (stomach) and SIF at pH 7.4 (colon)

| Tofa-P/tfr NCs (pH 1.2; 0-2 hours) | | | | | | |
|--|-------------------|--------------------|----------------|--------------------------------|----------------------|--|
| Parameter | Zero order | First order | Higuchi | Korsmeyer-peppas | Hixon-Crowell | Peppas-Sahlin |
| R_obs-pre | 0.7893 | 0.8156 | 0.9317 | 1.0000 | 0.8069 | 1.0000 |
| Rsqr | 0.3719 | 0.4721 | 0.8680 | 0.9999 | 0.4399 | 0.9999 |
| RMSE | 7.6890 | 7.0493 | 4.0696 | 0.0992 | 7.2610 | 0.1179 |
| AIC | 29.3294 | 28.4607 | 23.5285 | -13.6150 | 28.7567 | -11.9164 |
| MSC | -1.4836 | -1.3099 | -0.3234 | 7.1053 | -1.3691 | 6.7656 |
| Other | k0= 14.708 | k1=0.173 | kH=16.352 | kKp=21.251, n= 0.110 | Khc=0.055 | k1= 14.205, k2= 7.042, m= 0.082 |
| Tofa-P/tfr NCs (pH 7.4; 2-72 hours) | | | | | | |
| Parameter | Zero order | First order | Higuchi | Korsmeyer-peppas | Hixon-Crowell | Peppas-Sahlin |
| R_obs-pre | 0.6489 | 0.9449 | 0.8223 | 0.9934 | 0.8320 | 0.9969 |
| Rsqr | -1.0910 | 0.5816 | 0.6762 | 0.9868 | 0.1668 | 0.9938 |
| RMSE | 38.7260 | 17.3222 | 16.6924 | 3.3662 | 24.4461 | 2.5898 |
| AIC | 65.7335 | 54.4701 | 54.6754 | 32.2592 | 59.2929 | 29.0264 |
| MSC | -2.3499 | -0.7409 | -0.7702 | 2.4321 | -1.4298 | 2.8940 |
| Other | k0= 1.460 | k1= 0.126 | kH=7.393 | kKp=44.821, n= 0.134 | Khc= 0.019 | k1= 42.522, k2= - 5.883 , m=0.315 |

3.18. In Vitro Biocompatibility and Toxicity Studies

3.18.1. Hemolysis assay

RBCs hemolysis study established hemocompatibility of Tofa-PLGA NCs and Tofa-P/tfr NCs in a concentration from 25-100 $\mu\text{g/mL}$. Both formulations have negligible differences from PBS treated RBCs, while significant variations from the Triton-X group ($p < 0.001$ at all conc.) (Figure 3. 25 A). Triton-X was used because it is a known hemotoxic agent. Hence, Tofa-P/tfr NCs proved to be non-toxic to RBCs and thus safe if entered the bloodstream.

3.18.2. Cellular biocompatibility (MTT assay)

Cellular viability of peritoneum derived macrophages and murine-derived colon cells was assessed after incubation of formulation at a concentration of 25, 50, and 100 $\mu\text{g/mL}$ for 24 and 48 hours. Tofa-P/tfr NCs proved to be non-toxic to macrophages at all concentrations after 24 and 48 hours (Figure 3. 25 B, C), with statistically indifferent results from the normal PBS control cells. Triton-X is a toxic agent, that served as a negative control, which decreased macrophage viability pronouncedly after 24 and 48 hours ($p < 0.001$ vs normal). Likewise, an MTT assay was performed to assess cellular biocompatibility with colon cells. After 24 hours, Tofa-P/tfr NCs at a concentration of 25, 50, and 100 $\mu\text{g/mL}$ exhibited colon cell viability of about 83.45%,

67.92%, and 58.83%, respectively. 25-50 $\mu\text{g/mL}$ was found to be safe for the cells, however, 100 $\mu\text{g/mL}$ have reduced the living viability ($p < 0.05^*$ vs PBS normal control) (Figure 3. 25 D, E). Therefore, the dose should be carefully adjusted for colon drug delivery purpose in IBD. The same trend was also observed after 48 hours; however, the viability remains greater than 50% at 100 $\mu\text{g/mL}$. Higher doses ($>100 \mu\text{g/mL}$) are suggested for combating colon cancers.

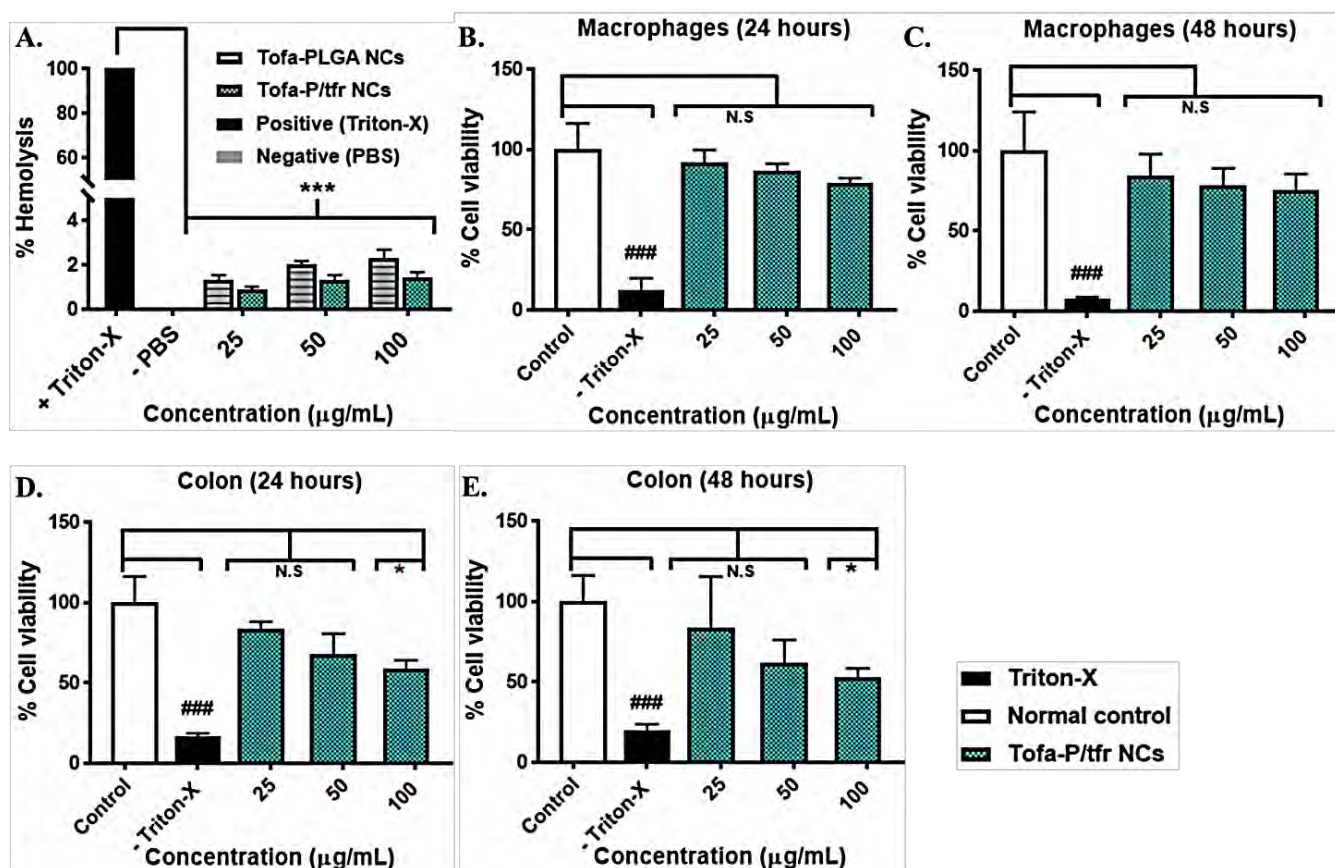


Figure 3. 25: In vitro hemolysis and cellular biocompatibility assays of Tofa-P/tfr NCs; Hemolytic activity drug loaded nanocarrier at various concentrations ($n=3$) (A); % Cell viability of murine derived macrophages after incubation with nano-formulation after 24 hours (B) and 48 hours (C); % Cell viability of murine derived colon cells after incubation with nano-formulation after 24 hours (D) and 48 hours (E)

3.18.3. Cellular uptake study-colon and macrophages

3.18.3.1. Colon uptake study

Fluorescein dye loaded P/tfr NCs were prepared to visualize uptake of nanocarriers by the colon cells. After 2 hours of incubation, colon cells heavily internalized Dye-P/tfr NCs with mean fluorescence intensity of 160.92 ± 35.28 a.u. ($p < 10^{-10}$ ****), compared to the plain dye intensity of 38.68 ± 14.38 a.u. (Figure 3. 26). Untreated colon cells served as a control.

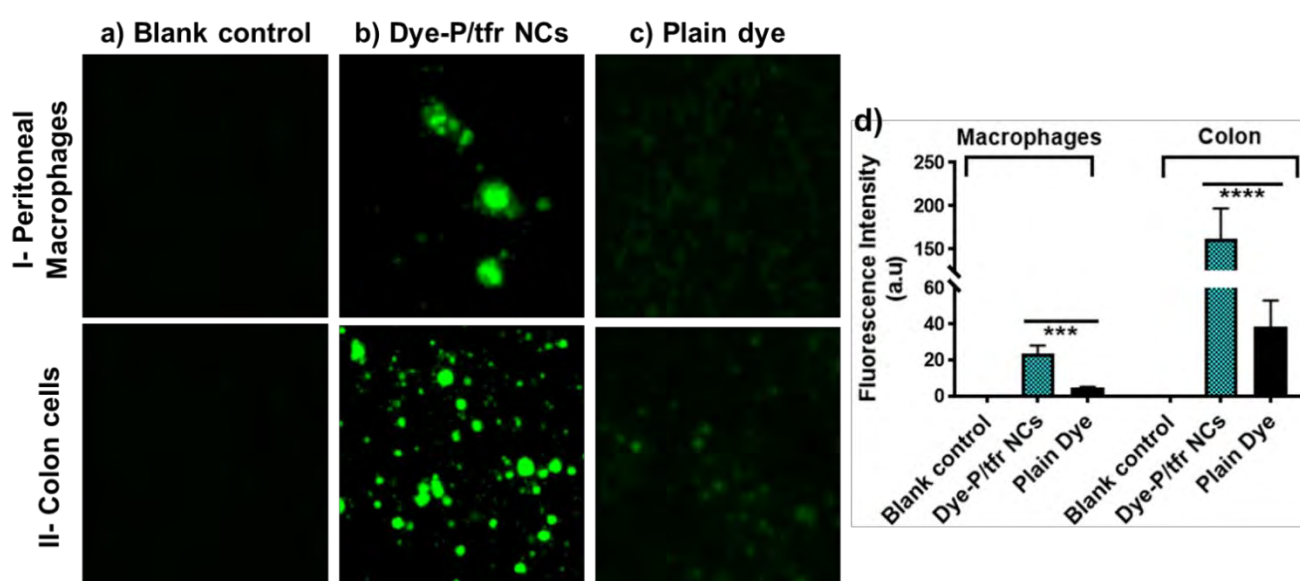


Figure 3. 26: a-c: Cellular uptake of dye-loaded P/tfr NCs by murine-macrophages (I) and colon cells (II); d: Emitted fluorescence intensity by the engulfed dye-loaded nanocarriers

3.18.3.2. Macrophage uptake and CD71 (TFR-1) inhibition assay

At first, a preliminary uptake experiment was conducted with peritoneal macrophages. Dye-P/tfr NCs was up taken up to fluorescence units of 23.59 ± 4.47 ($p < 0.001$ ***), compared to the plain dye (5.17 ± 0.13) after 2 hours (Figure 3. 26).

Next, the tfr-based assay involved THP-1 cell line-derived macrophages that expressed surface receptor TFR-1 or CD71 (Genin *et al.*, 2015; Andreesen *et al.*, 1984). Coumarin-6 dye-loaded P/tfr NCs were developed and incubated with macrophage cell lines. As a check, coumarin-6 loaded PLGA NCs were also prepared. After 2 hours of incubation, Dye-P/tfr NCs have shown significant uptake (147.83 ± 26.29 a.u., $p < 0.001$ ###), compared to plain dye (42.88 ± 13.35 a.u.) (Figure 3. 27). However, the internalization was competitively inhibited when the formulation was incubated with

anti-Tfr-1 antibody (Tfr-Ab) (102.07 ± 19.02 a.u., $p < 0.001^{***}$ vs P/tfr NCs (Figure 3.27) because the antibody binds to the CD71 receptor before its binding to Dye-P/tfr NCs. Therefore, the engulfment of Dye-P/tfr NCs in the presence of Tfr-Ab was only governed by a size-mediated mechanism. On the other hand, Dye-PLGA NCs were uptaken by the tfr-independent mechanism, therefore, a negligible difference was observed in the uptake of Dye-PLGA NCs and Dye-PLGA NCs+Tfr-Ab ($p = \text{NS}$) (Figure 3.27).

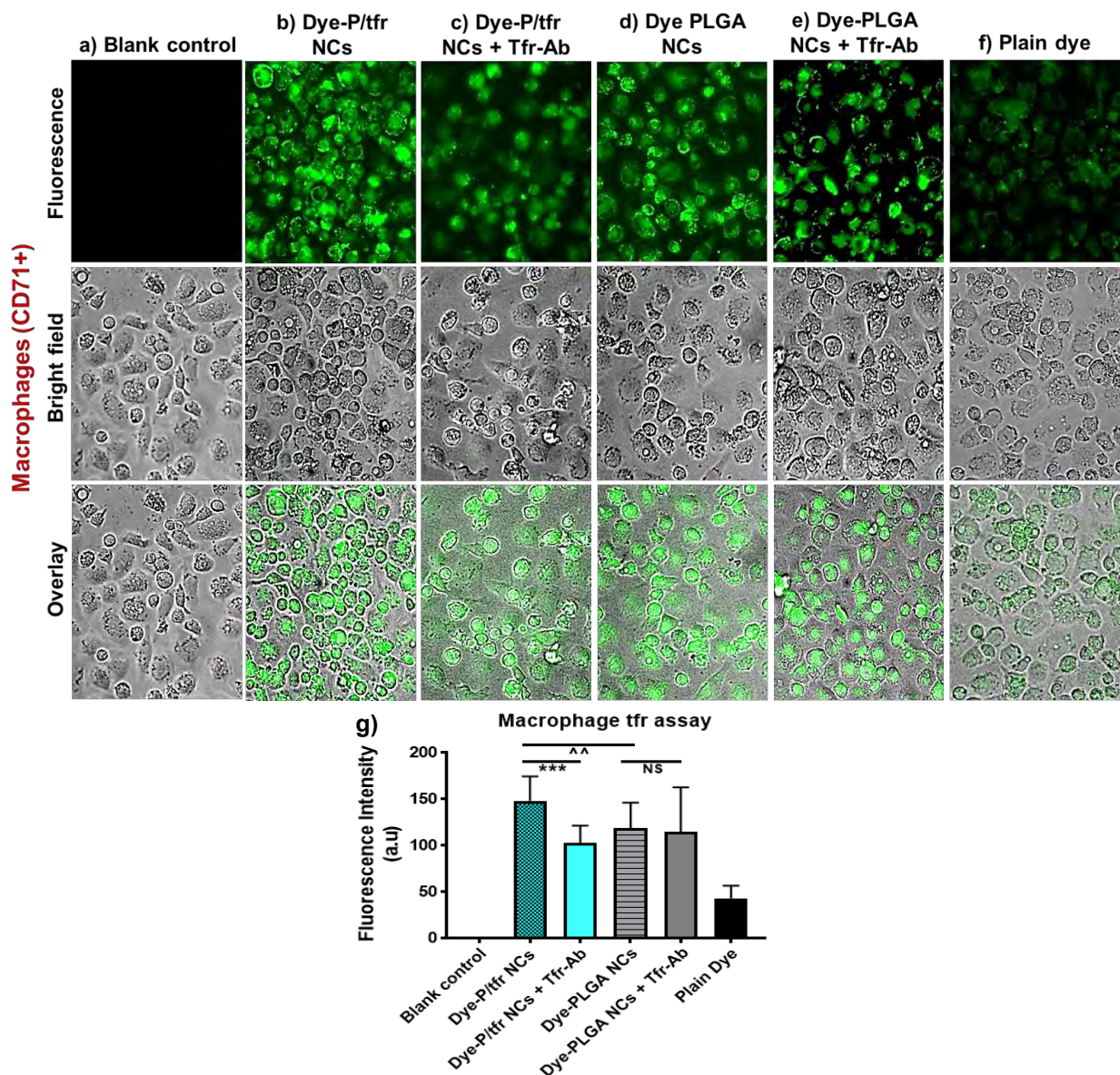


Figure 3. 27: Uptake of dye loaded PLGA NCs and P/tfr NCs in the absence and presence of anti-TFR-1 antibody (a-f) and the emitted fluorescence intensity (g)

3.19. Stability Studies

The effect of storage conditions on physicochemical and morphological properties of freeze-dried Tofa-P/tfr NCs was investigated. The freeze-dried nanocarriers were found to be in the appropriate limits of particle size, zeta potential, PDI, entrapment efficiency, and tfr adsorption after 1 and 6 months (Table 3. 21). However, care should be taken in case of liquid nanosuspension. The properties of liquid nanosuspension remained the same for a long at refrigerated temperature, but the amount of tfr adsorption declined over time.

Table 3. 21: Effect of storage conditions on freeze-dried Tofa-P/tfr NCs (mean \pm SD, n=3)

| Lyophilized Tofa-P/tfr NCs | Initial | | After 6 months | |
|----------------------------|------------------------------|------------------------------|--------------------------|--------------------------|
| | 4°C | 25°C | 4°C | 25°C |
| Particle size (nm) | 208 \pm 1.36 | 208 \pm 1.36 | 210.5 \pm 3.87 | 216.6 \pm 1.02 |
| Zeta potential (mV) | -8.64 \pm 1.73 | -8.64 \pm 1.74 | -8.1 \pm 0.53 | -7.97 \pm 2.89 |
| PDI | 0.121 \pm 0.004 | 0.121 \pm 0.004 | 0.121 \pm 1.25 | 0.136 \pm 1.24 |
| EE% | 80.97 \pm 0.79 | 80.97 \pm 0.80 | 77.92 \pm 2.59 | 76.92 \pm 2.27 |
| tfr adsorption | 0.886 \pm 0.015 (88.6%) | 0.886 \pm 0.015 (88.6%) | 0.79 \pm 0.15 (79%) | 0.71 \pm 0.23 (71%) |

3.20. Animal Studies

The animal model of colon inflammation was developed by 3% DSS induction for 7 days.

3.21. In Vivo Nanocarrier Targeting Ability

To understand nanocarrier targeting potential, and biodistribution, the released drug was estimated in the colon and the other vital organs. It was obvious that the highest concentration was found in the colon (15.97% \pm 0.49%) (Figure 3.28 I), because of the higher uptake by the distorted epithelial cells and recruited macrophages expressing TFR-1 receptor in the DSS inflamed colon. The stomach, small intestine, and spleen have a <2% accumulation of drug (Figure 3.28 I). While liver and kidney shared about ~0.6% drug content, indicative of delayed elimination and more retention at the targeted site after 6 hours of Tofa-P/tfr NCs administration.

Further, the flowcytometry colon-macrophage uptake investigations after oral administration of dye-loaded nanocarriers demonstrated deviations in the forward

scattered plot (FSC-H) (Figure 3.28 II). Statistics estimated about 19.73% gated area with a major shift. The shift indicated changes in the size and structure of the cells, attributed to the engulfment of nanocarriers (Patel *et al.*, 2016a; Alwani *et al.*, 2016). Therefore, Tofa-P/tfr NCs have the potential to target macrophages during colon inflammation.

3.22. Therapeutic Evaluation of Tofa-P/tfr NCs in DSS-Induced Colitis

3.22.1. Morphological parameters assessment to determine colitis severity and the treatment efficacy

DSS induced colon inflammation reduces the weight of the mice, as a sign of disease progression (Park *et al.*, 2015). The DSS afflicted mice have continuously declining body weight from Day 1-14, and the weight loss is more prominent after the 7th day of induction, compared to the normal mice ($p < 0.001^{###}$, Figure 3.28 III). Treatment with Tofa and Tofa-P/tfr NCs restored the bodyweight of the mice up to $87.81\% \pm 4.95\%$ ($p = \text{NS}$) and $91.36\% \pm 3.91\%$ ($p < 0.01^{**}$), respectively (Figure 3.28 III). The nanocarriers have a more pronounced effect on weight recovery than Tofa. Further, the DAI score was calculated that represented the sum of average body weight loss, rectal bleeding, and protrusion and stool consistency. The DSS group has the highest DAI score (10.6 ± 0.12), depicting the disease severity ($p < 0.001^{###}$ vs normal) at the end (Figure 3.28 IV). While Tofa has a DAI score of 6.2 ± 0.42 ($p < 0.01^{**}$) and Tofa-P/tfr NCs has a 4.8 ± 0.35 score ($p < 0.001^{***}$) at the end of the experiment (Figure 3.28 IV).

The colitis morphological investigations revealed that DSS mediated colon weight increase ($p < 0.001^{##}$), length shortening ($p < 0.05^{\#}$), high colon weight to length ratio ($p < 0.001^{###}$) and increase in splenic weight ($p < 0.001^{###}$), compared to normal control (Figure 3.28 V-VII). The other vital organs (liver, lungs, heart, kidney, stomach) were not affected by the disease (Figure 3.28 VII). Small intestine length shortened ($p < 0.05^{\#}$ vs normal), possibly because of some deteriorating influence of DSS on the small intestine when passing through GIT after oral intake. Tofa-P/tfr NCs recovered colon weight ($p < 0.05^*$), length ($p < 0.05^*$), weight-length ratio ($p < 0.05^*$), spleen weight ($p < 0.01^{**}$) and small intestine length ($p < 0.05^*$) significantly (Figure 3.28 V-VII). The nano-formulation have no impact on the weights of vital organs while treating colon inflammation ($p = \text{NS}$) (Figure 3.28 VII).

The survival analysis during disease progression and therapy (day 0-14) indicated about 60% and 80% of the mice in Tofa and Tofa-P/tfr NCs group survived till the end. Overall, the survival rate improved up to 40% and 60% by the respective treatment of colitis mice (survival=20%) (Figure 3.28 VIII).

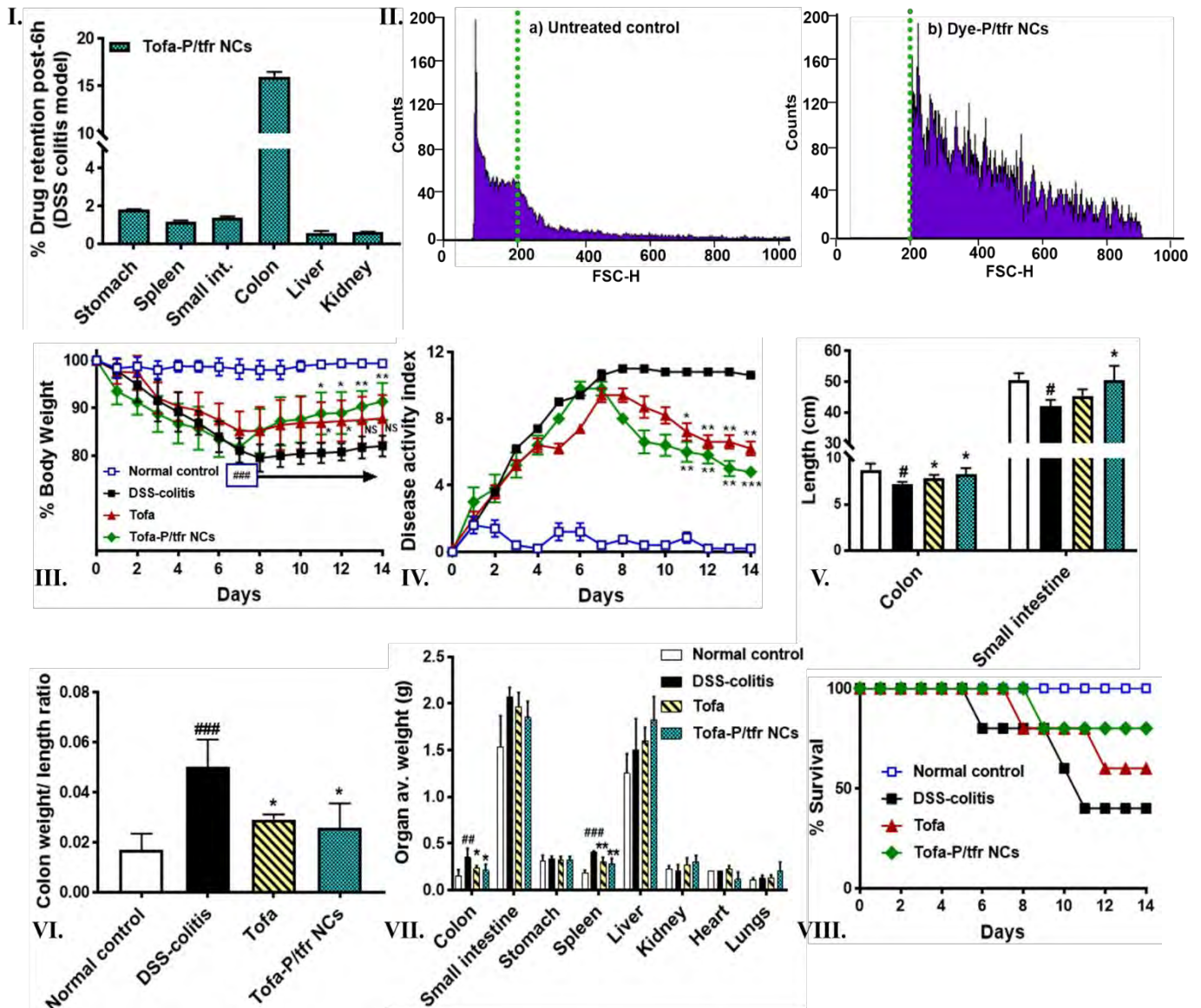


Figure 3. 28: Tofa-P/tfr NCs in vivo biodistribution, colon-macrophages uptake and therapeutic assessment through morphological and physical parameters; I: Biodistribution studies in the DSS-induced colitis mice (n=3); II: Uptake of nanocarriers by colon-macrophages after oral administration in the DSS-induced mice; III: Therapeutic action determination: Assessment of daily body weight during course of induction and therapy by nanocarriers, IV: Disease activity index from Day 0-14, V: Assessment of intestinal length to determine inflammation severity, VI: Colon weight/length index, VII: Effect of colitis and treatment on the weight of organs, VIII: % Survival analysis of the normal, DSS-colitis, Tofa and Tofa-P/tfr NCs groups from Day 0-14 (n=5/ group)

3.22.2. Histopathological investigations

The representative histological images from the normal, DSS-colitis, Tofa, and Tofa-P/tfr NCs groups are shown in Figure 3.29 a-e. DSS group had the highest score of 12 because of severe inflammation appeared as loss of epithelial integrity, infiltration of immune cells, and crypts damage ($p < 0.001^{###}$ vs normal, Figure 3.29 b). The histo-damage score was reduced by Tofa (7.33 ± 0.38 , $p < 0.01^{**}$) and Tofa-P/tfr NCs (4.67 ± 0.38 , $p < 0.001^{***}$) treatment of colitis mice (Figure 3.29 c-e). The therapeutic action is again more promising when the drug is delivered via novel nano-formulation ($p < 0.05^{\wedge}$). Tofa is an immunosuppressive drug that suppressed immune cells and retarded pro-inflammatory cytokines which in turn decreased epithelial and crypt distortion (D'Amico *et al.*, 2019). Its therapeutic action was strengthened when delivered through a nanocarrier that prevent its pre-degradation and localized the therapeutic effect to the colon with improved efficacy and lesser side effects for a long.

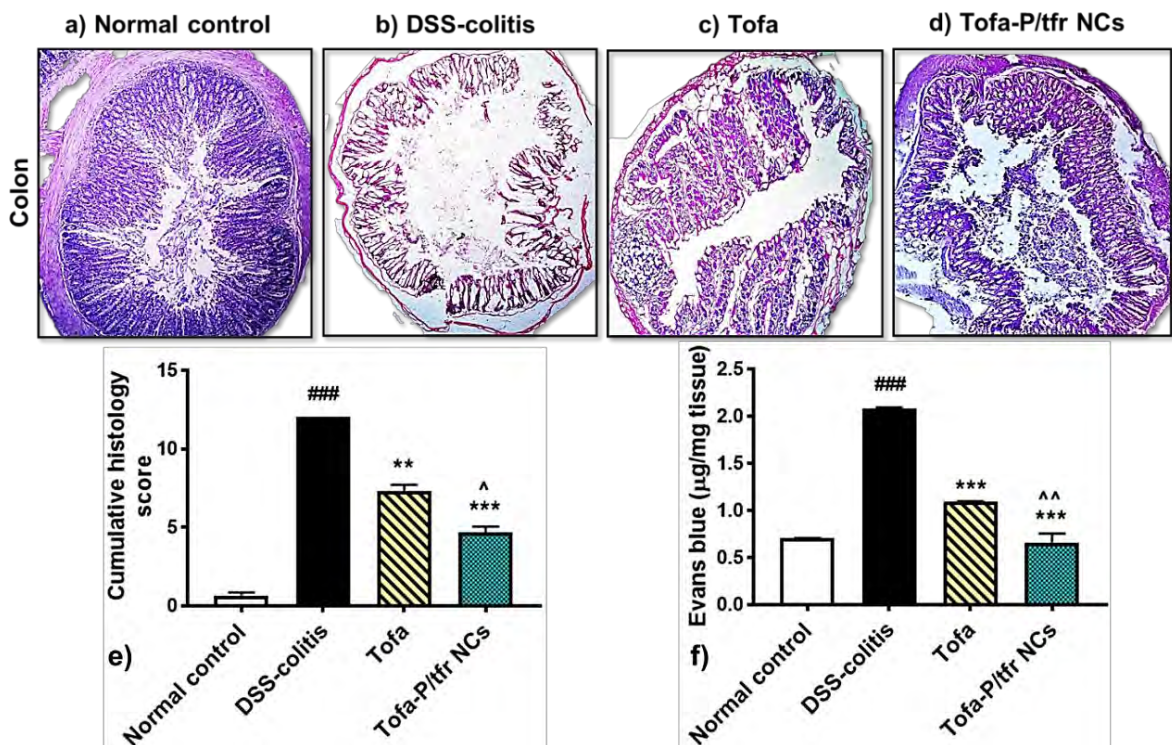


Figure 3. 29: Histological and vascular integrity evaluation of the colon excised from normal, DSS-colitis, Tofa and Tofa-P/tfr NCs treated groups; Histological images of the respective groups (a-d), Histological scoring of the respective groups (e) (n=3); Evaluation of vascular integrity by Evans blue assay in the normal, DSS-colitis, Tofa and Tofa-P/tfr NCs treated groups (f) (n=3)

3.22.3. Vascular function test

Further, vascular endothelial permeation was analyzed through Evan's blue assay. The concentration of Evan's dye in the colon of DSS induced mice was higher than the colon of normal mice ($p < 0.001^{###}$, Figure 3.29 f). The leaky vasculature favored more dye to permeate across endothelium to inflamed colon from systemic circulation (Radu and Chernoff, 2013). Treatment with Tofa ($p < 0.001^{***}$) and Tofa-P/tfr NCs ($p < 0.001^{***}$) recovered the vascular integrity through a reduction in inflammatory mediators and toxic signals. Though Tofa-P/tfr NCs ($p < 0.01^{^^}$ vs Tofa) have a greater effect in vasculature healing than plain Tofa (Figure 3.29 f).

3.22.4. RT-PCR analysis to determine mechanistic and therapeutic effects on ameliorating inflammation and recovering barrier function

Tofa acts by inhibiting JAK proteins (JAK1,3) which prevents phosphorylation of STAT proteins and downregulates the inflammatory mediators (D'Amico *et al.*, 2019). We assessed Tofa activity while measuring STAT-1 expression through RT-PCR. Findings suggested DSS overly expressed STAT-1 ($p < 0.05^{\#}$ vs normal), which was diminished by Tofa ($p = \text{NS}$) and markedly reduced by Tofa-P-tfr NCs ($p < 0.05^*$, Figure 3. 30 A). The relative downregulation was greater with Tofa-P-tfr NCs treatment (Figure 3. 30 A). Furthermore, UC had increased the expression of the TFR-1 receptor, because of the heavy recruitment of TFR-1 expressing macrophages (Liu *et al.*, 2021). TFR-1 is also present on colon epithelial cells which were upregulated in the inflammation (Liu *et al.*, 2021). Therefore, tfr as a ligand on polymeric nanocarriers facilitated macrophage and colon targeting in UC (Harel *et al.*, 2011). RT-PCR analysis demonstrated higher TFR-1 levels in DSS-colitis mice ($p < 0.05^{\#}$ vs normal, Figure 3. 30 B) which facilitates our rationale of targeting. TFR-1 expression was inhibited non-significantly by Tofa ($p = \text{NS}$) and significantly by the course of treatment with Tofa-P-tfr NCs ($p < 0.05^*$) (Figure 3. 30 B) because Tofa within nanocarrier has a more therapeutic effect which extensively diminished inflammatory events with immune cells suppression and conversion of macrophages towards anti-inflammatory phenotype (Texler *et al.*, 2022; Aung *et al.*, 2021).

The compromised epithelial and endothelial membrane integrity are major hallmarks in colitis (Park *et al.*, 2015). We have examined epithelial membrane function through the expression of tight junction protein, E-cadherin (Schnoor, 2015). The expression

levels were pronouncedly lowered in the colitis induced mice (0.083 ± 0.015 , $p < 0.001^{###}$), as compared to the normal (1.99 ± 0.32) (Figure 3. 30 C). E-cadherin expression was restored by Tofa to 0.32 ± 0.45 ($p = \text{NS}$) and by Tofa-P/tfr NCs to 0.34 ± 0.39 ($p = \text{NS}$), but not to statistically significant values (Figure 3. 30 C).

RT-PCR expression of iNOS further proved its high levels in DSS-colitis (Figure 3. 30 D), which was decreased by Tofa to a little extent but not significantly, however, reduced significantly by Tofa-P/tfr NCs ($p < 0.05^*$) (Figure 3. 30 D). Tofa mediated STAT inhibition further inhibited the NF- κ B pathway that ultimately lowered the iNOS levels (Sharma *et al.*, 2020; Ma *et al.*, 2015). In short, the imbalance between antioxidants and oxidative species was leveled by the treatment of nanocarrier.

3.22.5. Evaluation of pro-inflammatory cytokines

Moreover, DSS profoundly elevated the levels of the pro-inflammatory cytokine ($p < 0.001^{###}$ vs normal). JAK/STAT inhibition by the released drug from the Tofa-P/tfr NCs markedly decreased the levels of pro-inflammatory cytokines including IL-6 ($p < 0.001^{***}$) and TNF- α ($p < 0.001^{***}$) (Figure 3. 30 E-F). The therapeutic effects of Tofa-P/tfr NCs in reducing IL-6 ($p < 0.05^{\wedge}$) and TNF- α ($p < 0.001^{\wedge\wedge}$) levels were more pronounced compared to Tofa alone (Figure 3. 30 E-F).

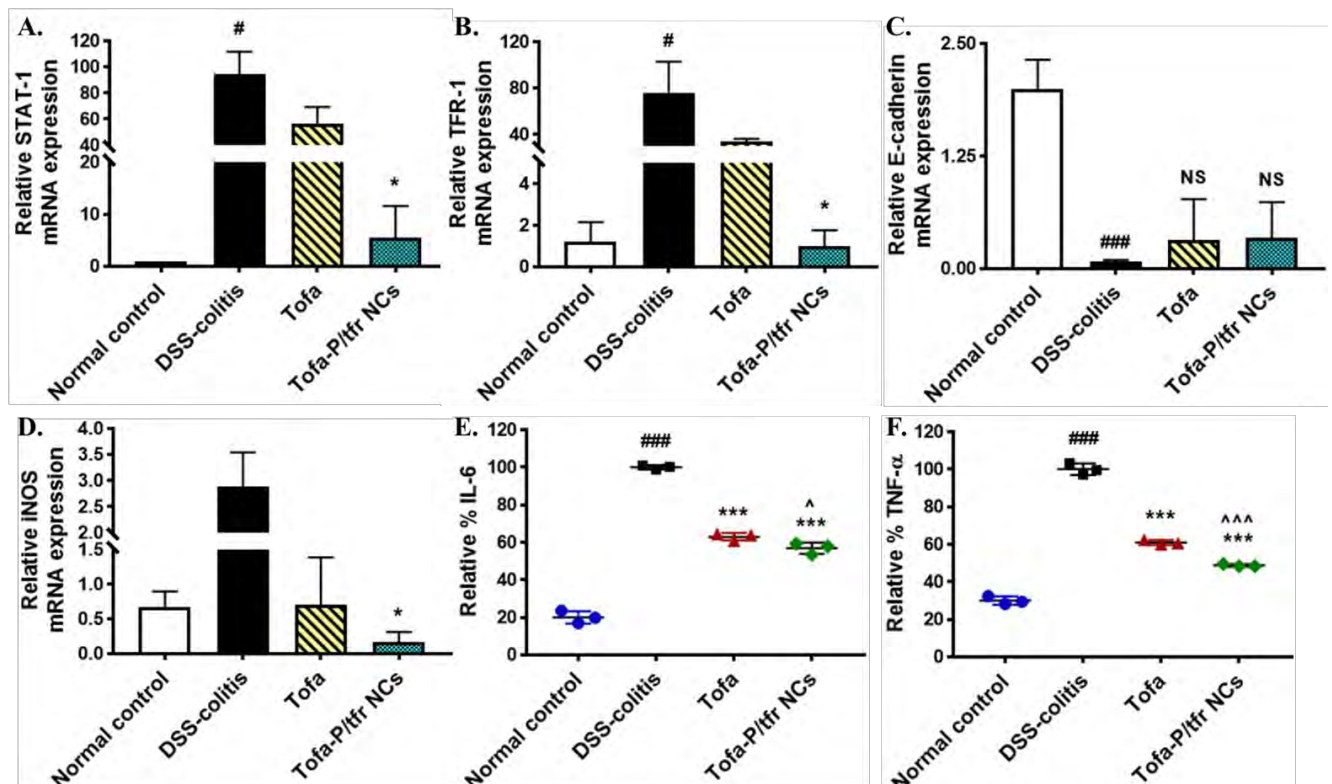


Figure 3. 30: RT-PCR expression of STAT-1 (A), TFR-1 (B), E-cadherin (C) and iNOS (D); And levels of proinflammatory cytokines, IL-6 (E) and TNF- α (F) from the colon tissue excised from normal, DSS-colitis, Tofa and Tofa-P/tfr NCs groups (n=5)

3.22.6. Assessment of colon antioxidant protection

Furthermore, inflammation generated reactive oxygen species that weakens the antioxidant protection of the colon tissue with the excessive generation of free radicals (Zeeshan *et al.*, 2019b). The DSS-colitis mice have lower concentrations of antioxidants (GSH, GST, catalase) (Figure 3.31 A-C) and escalated amounts of oxidants (NO, MDA) (Figure 3.31 D, E). Tofa free drug improved the levels of GSH (128.53 ± 1.87 nmol/g tissue) ($p < 0.001^{***}$), GST (152.60 ± 10.64 nmol/g tissue) ($p < 0.01^{**}$), and catalase (0.17 ± 0.003 U/mg/min) ($p < 0.05^*$), and reduced NO, MDA to $41.25 \pm 2.53\%$ ($p < 0.001^{***}$) and $49.46 \pm 9.31\%$ ($p < 0.01^{**}$), respectively (Figure 3.31).

Tofa-P/tfr NCs markedly normalized the levels of NO and MDA to $18.17 \pm 2.84\%$ ($p < 0.001^{***}$) and $39.48 \pm 2.03\%$ ($p < 0.001^{***}$), respectively (Figure 3.31) and elevated antioxidants including GSH, GST and catalase to 134.14 ± 5.61 nmol/g tissue ($p < 0.001^{***}$), 346.88 ± 5.41 nmol/g tissue ($p < 0.001^{***}$) and 0.186 ± 0.0035 U/mg/min ($p < 0.01^{**}$), respectively (Figure 3.31) via Tofa led JAK/STAT mechanism that alleviated severity of inflammation.

Furthermore, neutrophil infiltration was assessed from MPO activity that indicated an uprise of MPO in DSS induced colitis ($p < 0.001^{###}$, Figure 3.31 F), treatment with Tofa and Tofa-P/tfr NCs sharply decreased levels up to $64.44\% \pm 7.34\%$ ($p < 0.01^{**}$) and $46.22\% \pm 2.78\%$ ($p < 0.001^{***}$), respectively (Figure 3.31 F). Again, the drug inside the nanocarrier was found to be more precise in action ($p < 0.05^{\wedge}$) than the plain drug.

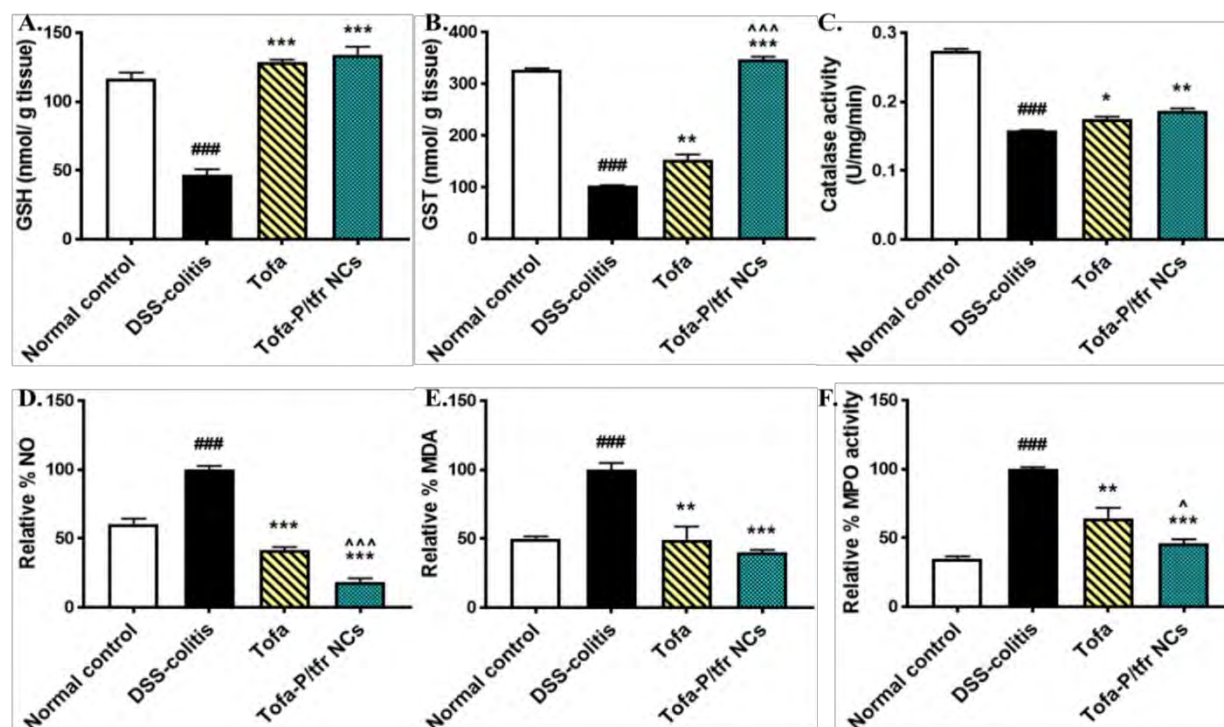


Figure 3. 31: Antioxidant protection evaluated through quantification of antioxidants in the colon tissue excised from normal, DSS-colitis, Tofa and Tofa-P/tfr NCs groups (n=5), Antioxidant GSH (A), GST (B) and Catalase (C), and oxidative species NO (D), MDA (E) and neutrophil marker MPO (F)

3.22.7. Evaluation of blood indices and RFTs

To evaluate the effect of formulation on blood parameters, the collected blood from the mice of each group (n=3) demonstrated elevated concentrations of total leukocyte count (TLC) due to inflammation in the DSS-induced colitis ($p < 0.001^{###}$ vs normal, Figure 3. 32 A). TLC count was diminished by the Tofa-P/tfr NCs to a large extent ($p < 0.001^{***}$), suggesting alleviation of colitis (Figure 3. 32 A). The RBCs count, Hemoglobin (Hb) levels and packed cell volume/hematocrit (PCV/HCT) were lowered in the DSS-colitis group (RBCs: $p < 0.01^{##}$, Hb: $p < 0.001^{###}$, PCV/HCT: $p < 0.05^{\#}$ vs normal). Tofa-P/tfr NCs treatment of the DSS-inflamed mice restored RBCs count ($p < 0.01^{**}$), Hb ($p < 0.05^*$) and PCV ($p < 0.05^*$) significantly (Figure 3. 32 A). The other altered parameters like mean corpuscular volume (MCV) and mean corpuscular hemoglobin (MCH) were restored by Tofa-P/tfr NCs therapy (Figure 3. 32 A). Next, blood serum was collected to detect renal function. RFT indices including serum urea, serum creatinine, and serum uric acid were within the normal range for both Tofa and Tofa-P/tfr NCs groups (Figure 3. 32 B) and complied with the normal group. C-reactive protein (CRP) is another indicator of inflammation (Masoodi *et al.*, 2011). The values

of CRP for the Tofa treated group was $3.2 \text{ mg/L} \pm 0.2 \text{ mg/L}$ and for the Tofa-P/tfr NCs treated group was $3.00 \text{ mg/L} \pm 0.1 \text{ mg/L}$ (Figure 3. 32 C). The reference range for inflammation is >6 , therefore, both groups have CRP within the normal limits.

3.22.8. Investigation of colon microbiome

The colon microbiome is an essential element of the digestive tract, which gets altered with inflammation. The collected feces from the bowel of all groups were cultured on growth media to determine the growth rate of bacteria. The DSS-induced colitis group have significantly elevated $\log_{10}\text{CFU/mL}$ ($p < 0.001^{###}$) compared to the normal (Figure 3. 32 D). The treatment with Tofa reduced the elevated growth but not to a marked extent, while Tofa-P/tfr NCs balanced bacterial $\log_{10}\text{CFU/mL}$ significantly ($p < 0.01^{**}$, Figure 3. 32 D). This assay ensured that the nanocarriers have minimal damage to the natural microbiome and through enhanced amelioration of inflammation, it recovered bacterial growth to normal limits.

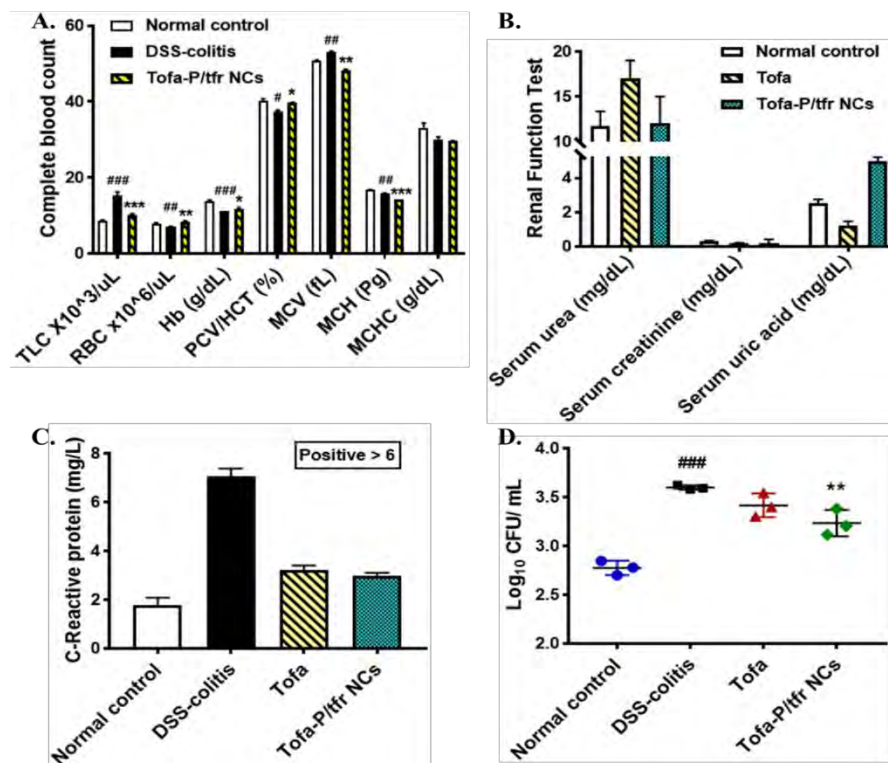


Figure 3. 32: Elucidation of the effect of therapy on blood parameters, renal function, inflammatory blood marker, and colon feces microbial content; Assessment of blood cells count (A), Assessment of drug and drug loaded nanocarrier effect on renal function (B), Determination of C-reactive proteins (CRP) levels to know inflammation severity (C), Microbial growth on the colon-feces culture, taken from Normal control, DSS-colitis, Tofa, and Tofa-P/tfr NCs groups (D)

PART-II (SECTION B)

Tofa-LP/tfr NSh and Tofa-LP/tfr/ES NSh

Graphical Abstract:

pH sensitive tfr anchored lipid-PLGA nanoshells (Tofa-LP/tfr/ES NSh) handles multilevel barriers for colon-specific targeting in the UC and successfully localizes and cure the inflamed colon tissue (Figure 3. 33)

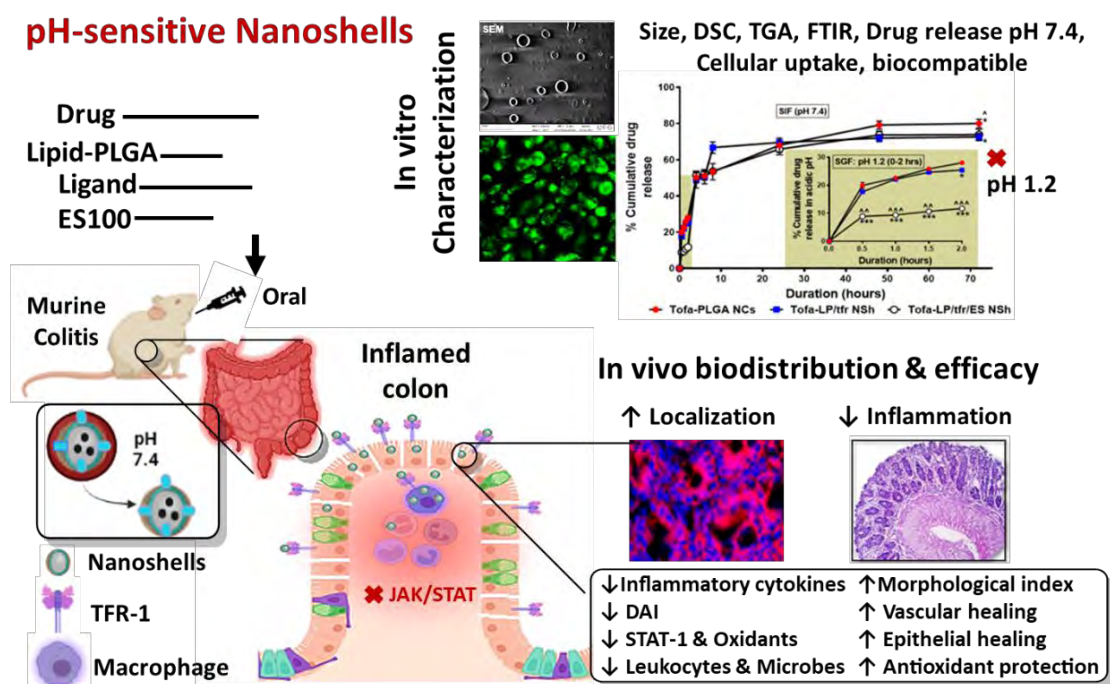


Figure 3. 33: pH sensitive nanoshells (Tofa-LP/tfr/ES NSh) target colon tissues to mitigate inflammation

3.23. Preparation and Physicochemical Characterization of Tofa-LP/tfr NSh and Tofa-LP/tfr/ES NSh

Both Tofa-LP/tfr NSh and Tofa-LP/tfr/ES NSh were prepared with good stability. The ratio of phospholipon 90G to PLGA concentration was studied and 1:4 produced optimum quality nanoshells.

Tofa-LP/tfr NSh and Tofa-LP/tfr/ES NSh have a particle size of $258.3 \text{ nm} \pm 3.4 \text{ nm}$ and $281.8 \text{ nm} \pm 6.33 \text{ nm}$, respectively (Table 3. 22, Figure 3. 34 A). Both have negative zeta potential, the later pH-sensitive has more anionic charge because of more anionic ES100 coating with carboxylic groups (Table 3. 22). Further, the physicochemical properties of Tofa-LP NSh (without tfr) were also elucidated. The findings revealed

that the tfr adsorption increased the particle size of Tofa-LP/tfr NSh and decreased the zeta potential because tfr is cationic and it decreased the zeta potential of the nanoshells. Likewise, Tofa-LP/ES NSh have more negative zeta potential (-38.6 ± 0.87) than Tofa-LP/tfr/ES (-30.7 ± 0.17), because of the presence of tfr content (Figure 3. 34 A, Table 3. 22).

The PDI of both Tofa-LP/tfr NSh and Tofa-LP/tfr/ES NSh was less than 0.3 (Table 3. 22), indicating a homogenous monodispersed system. The SEM analysis revealed spherical and smooth surface morphology of Tofa-LP/tfr NSh and Tofa-LP/tfr/ES NSh and the particle size range complied with zeta sizer findings. The interior seemed to be darker than the outer layer, possibly because of inside lipidic content and the outer polymeric layer that constituted a core-shell spherical nanostructure (Figure 3. 34 B). Next, the adsorption of tfr on Tofa-LP/tfr NSh was 0.85 ± 0.046 (85%) and on Tofa-LP/tfr/ES NSh 0.703 ± 0.015 (70%), by the Nanodrop measurements. And Bradford's assay estimated about 0.87 ± 0.09 (87%) and 0.84 ± 0.11 (84%) tfr adsorption on Tofa-LP/tfr NSh and Tofa-LP/tfr/ES NSh, respectively (Figure 3. 34 C).

The drug encapsulation was found to be about 84% and 91% and the total drug loading (DL) was 62.54 ± 1.37 and 27.26 ± 1.55 with Tofa-LP/tfr NSh and Tofa-LP/tfr/ES NSh, respectively (Table 3. 22).

Table 3. 22: Physicochemical characteristics of drug-loaded nanoshells (mean \pm SD, n=3)

| Formulation | Particle size (nm) | Zeta potential (mV) | PDI | EE% | DL | % Yield |
|--------------------|--------------------|---------------------|-------------------|------------------|-------------------|------------------|
| Tofa-LP NSh | 244.5 ± 4.41 | -13.7 ± 3.25 | 0.22 ± 0.01 | 82.29 ± 1.93 | 54.13 ± 1.51 | 88.82 ± 1.05 |
| Tofa-LP/tfr NSh | 258.3 ± 3.4 | -7.97 ± 1.12 | 0.287 ± 0.016 | 84.42 ± 1.85 | 62.54 ± 1.37 | 88.07 ± 1.47 |
| Tofa-LP/ES NSh | 270.2 ± 4.91 | -38.6 ± 0.87 | 0.11 ± 0.041 | 88.89 ± 1.89 | 29.83 ± 1.003 | 91.1 ± 1.12 |
| Tofa-LP/tfr/ES NSh | 281.8 ± 6.33 | -30.7 ± 0.17 | 0.16 ± 0.098 | 91.31 ± 5.18 | 27.26 ± 1.55 | 90.34 ± 1.12 |

3.23.1. TGA

TGA analysis revealed that Tofa degradation started around 230-240°C with a sharp mass loss curve corresponding to the melting point of Tofa (Bashir *et al.*, 2021), followed by a steep curve where the decline continues till 450°C (Figure 3. 34 D). About 79.56% Tofa degraded till the end of a run. While Tofa-PLGA NCs, Tofa-P/tfr NCs, Tofa-LP/tfr NSh and Tofa-LP/tfr/ES NSh did not have sharp peaks at 240°C that

represented encapsulation of drug within the nanocarrier and absence of any surface-bound drug. For all nanocarriers, the peak drop started around 280°C that continued till 450°C. Tofa-LP/tfr NSh and Tofa-LP/tfr/ES NSh peak decline were smoother, with 69% and 71% till the end (Figure 3. 34 D). The addition of ES100 incurred a slight decline in the start indicated moisture loss, followed by major degradation after 280°C.

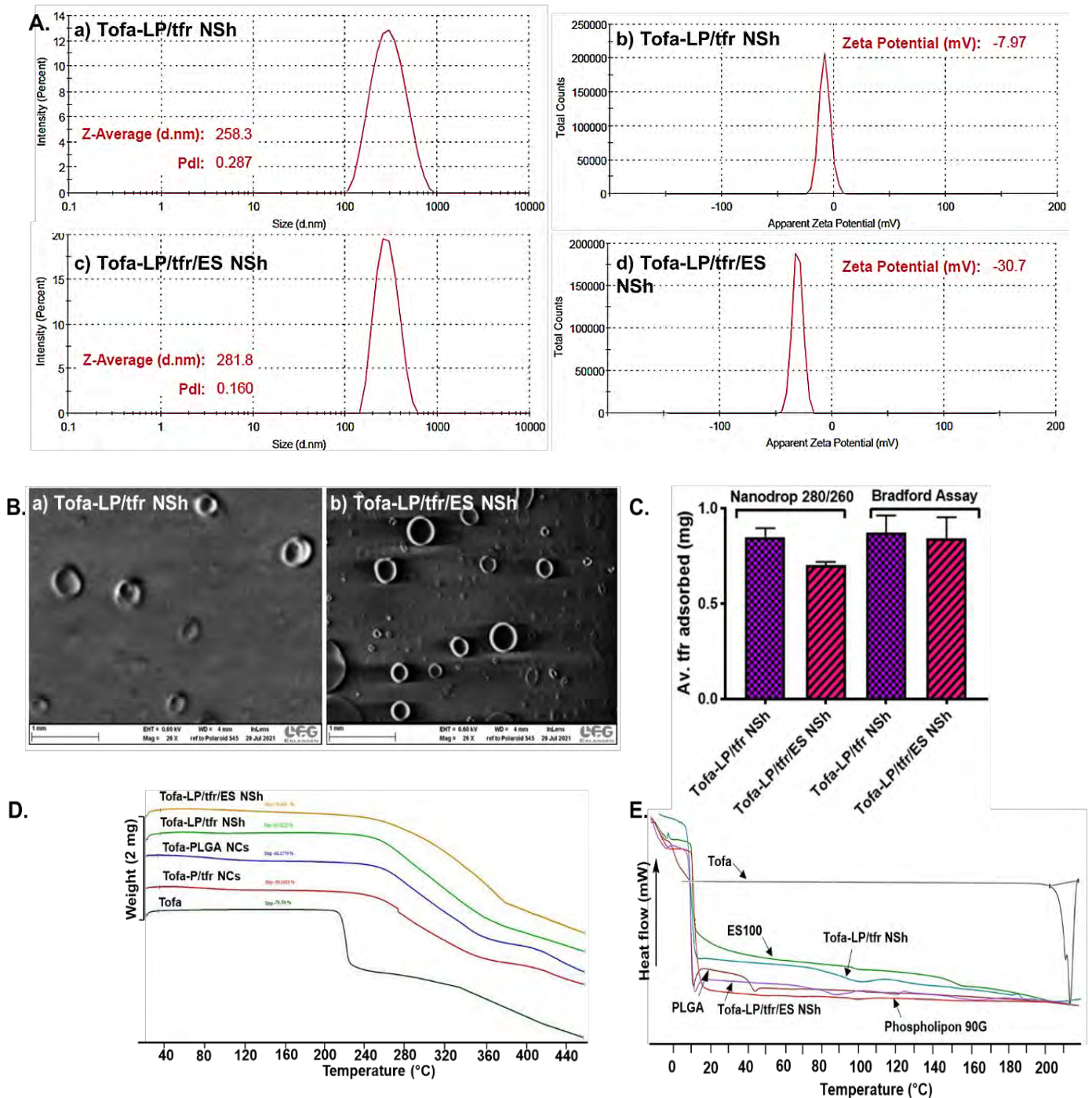


Figure 3. 34: Physicochemical properties of Tofa-LP/tfr NSh and Tofa-LP/tfr/ES NSh. A: Particle size and zeta potential analysis of Tofa-LP/tfr NSh (a, b) and of Tofa-LP/tfr/ES NSh (c, d); B: SEM images

of Tofa-LP/tfr NSh (a) and Tofa-LP/tfr/ES NSh (b); C: Quantitative analysis of tfr adsorption on Tofa-LP/tfr NSh and Tofa-LP/tfr/ES NSh; D: TGA and, E: DSC thermograms of drug and nanoshells

3.23.2. DSC

The DSC thermograms of the Tofa loaded nano-formulations are devoid of any sharp melting endotherm, whereas Tofa exhibited a sharp melting curve at 215°C that corresponds to its crystalline content (Figure 3. 34 E). It was depicted from the thermograms of drug-loaded nanocarriers that Tofa was dispersed in the highly amorphous form inside the nanocarriers (Figure 3. 34 E) and additionally confirmed the absence of any surface-bound drug. Further, a starting down peak (around 11°C) was observed in the case of polymer and nanocarriers, possibly because of a sudden change of temperature from freezing to 10-15°C.

3.23.3. ATR-FTIR

ATR-FTIR spectra of Tofa, polymers, phospholipon-90G, tfr, Tofa-LP NSh, Tofa-LP/tfr NSh, Tofa-P/tfr NSh and Tofa-LP/tfr/ES NSh are presented in Figure 3. 35 A, B. The polymers (PLGA and ES100) spectra have their characteristic peaks. Tofa FTIR spectrum had the peaks including 3375 cm^{-1} (-NH-), 3129 cm^{-1} (C=C), 1731 cm^{-1} (C=O), 1615 cm^{-1} (C=C), 1340 cm^{-1} (C-N), 1207 cm^{-1} (C-O) and 842 cm^{-1} (C-H) (Figure 3. 35 A). Tfr spectrum represented major peaks at 3274 cm^{-1} (-NH-) and 1638 cm^{-1} (O=C-NH) (Figure 3. 35), consistent with the literature (Pooja *et al.*, 2015). Tofa-LP NSh had bands mimicking PLGA and phospholipon-90G spectra (Figure 3. 35 B). While Tofa-LP/tfr NSh has an additional characteristic amide band of tfr at 1632 cm^{-1} that demonstrated coating of tfr on LP core. In Tofa-LP/tfr NSh, the primary amine peak is less prominent (Figure 3. 35 B). However, this amine peak (3274 cm^{-1}) can be seen in Tofa-P/tfr NSh (Figure 3. 35 B). Tofa-LP/tfr/ES NSh have representative peaks of PLGA, ES100, phospholipon-90G with a very weak amide band at 1632 cm^{-1} , mostly hidden because of coating of ES100 onto the surface of LP/tfr core (Figure 3. 35 A, B). Moreover, the concentration of tfr is very less compared to ES100, therefore, it is difficult to appear in the spectra prominently. The drug peak is also not obvious either because of complete drug encapsulation or of a very less concentration ratio compared to the polymers.

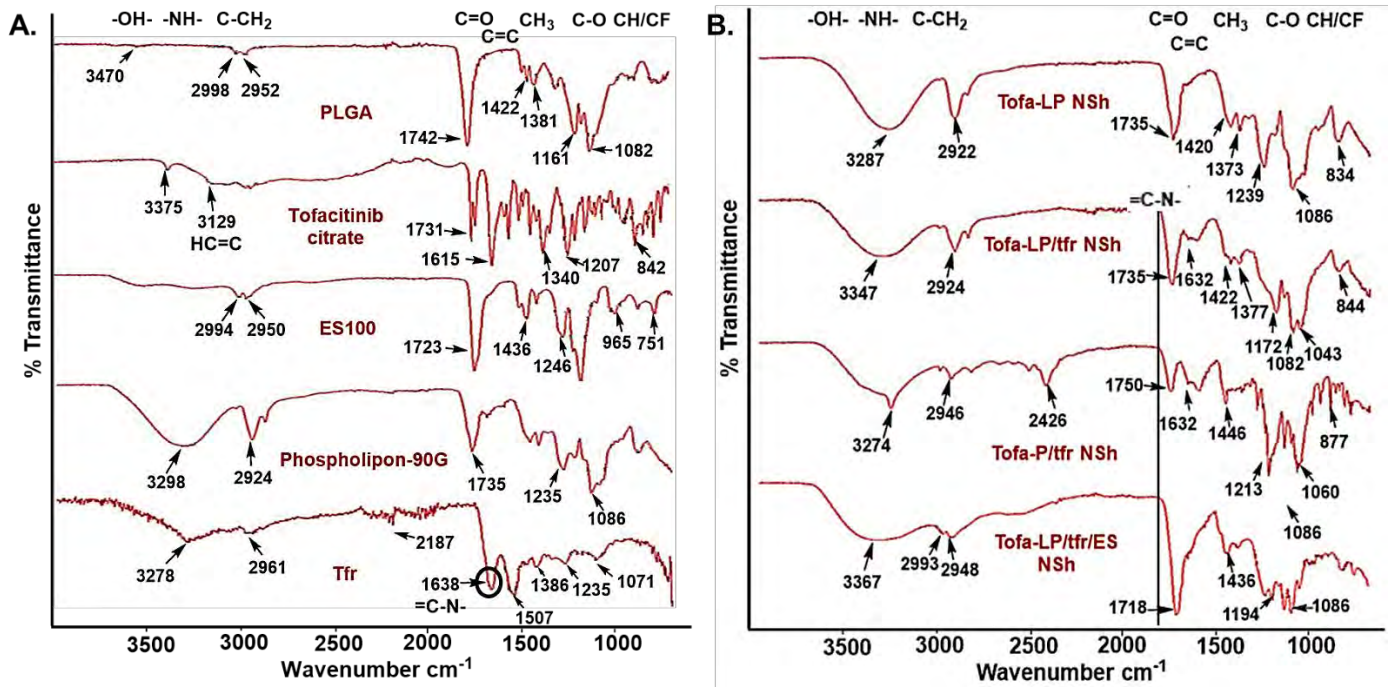


Figure 3.35: ATR-FTIR spectra of drug, excipients and nanoshells

3.24. In Vitro Drug Release Studies

To assess the drug release behavior of Tofa-PLGA NCs, Tofa-LP/tfr NSh and Tofa-LP/tfr/ES NSh, the study was conducted at pH 1.2 and 7.4. The pH values were selected according to the pH values of the stomach and colon (Ali *et al.*, 2014). Tofa-LP/tfr NSh released Tofa up to $25.44\% \pm 0.423$ at acidic pH (0-2 hours), and $72.57\% \pm 2.054\%$ at colon pH (pH 7.4, 2-72 hours). While Tofa-LP/tfr/ES NSh delivered $11.69\% \pm 0.285\%$ drug at pH 1.2 and $73.85\% \pm 3.02\%$ at pH 7.4 (

Figure 3.36 A). A control group of Tofa-PLGA NCs have released up to $28.03\% \pm 0.626\%$ and $80.04\% \pm 2.322\%$ at acidic and pH 7.4, respectively. It was observed that the drug release by Tofa-LP/tfr/ES NSh at all time points of acidic pH was significantly lowered than that of Tofa-PLGA NCs (0-2 hour: $p < 0.001^{***}$) and Tofa-LP/tfr NSh (0.5, 1.5th hour: $p < 0.01^{\wedge\wedge}$ and at 1 and 2 hours: $p < 0.001^{\wedge\wedge}$) (

Figure 3.36 A), because of the presence of pH-sensitive ES100 coat that retard dose dumping at acidic upper parts of GIT (Zeeshan *et al.*, 2019a). Overall, the drug release pattern differed between Tofa-LP/tfr NSh and Tofa-PLGA NCs ($p < 0.05^*$) from 0-72 hours and the difference also existed between the drug release profiles of Tofa-LP/tfr/ES NSh and Tofa-PLGA NCs ($p < 0.05^*$). Moreover, the release patterns of Tofa-LP/tfr NSh and Tofa-LP/tfr/ES NSh varied from each other ($p < 0.05^{\wedge}$).

Further, the drug release kinetics evaluation by the mathematical models (DDsolver) demonstrated that the best-fitted model for Tofa-LP/tfr NSh was Peppas-Sahlin, both at acidic pH ($R^2=0.9999$) and pH 7.4 ($R^2=0.9885$) (Table 3. 23). Tofa-LP/tfr/ES NSh had the best relevance to both Korsmeyer-Peppas ($R^2=0.9976$) and Peppas-Sahlin ($R^2=0.9977$) at pH 1.2. Similarly, the best-adapted models at pH 7.4, were both Korsmeyer-Peppas ($R^2=0.9981$) and Peppas-Sahlin ($R^2=0.9983$) for Tofa-LP/tfr/ES NSh (Table 3. 24). The other parameters including highest MSC, lowest AIC, and RMSE were also considered to select the best model (Zuo *et al.*, 2014).

Korsmeyer's n and Peppas m values predicted the mechanism of drug release from the system (Zhang *et al.*, 2010). Tofa-LP/tfr NSh mechanism of drug release suggested by the Korsmeyer's n value was Fickian diffusion at acidic pH and pH 7.4, though the m value at pH 1.2 was 0.5, suggestive of little deviation from the pattern (Table 3. 23). Likewise, Tofa-LP/tfr/ES NSh released the drug through Fickian diffusion mechanism at pH 1.2 ($n=0.206$, $m=0.155$), and by the similar mechanism at pH 7.4 ($n=0.143$, $m=0.25$) (Table 3. 24).

3.25. Mucin Binding Study

Mucin-nanoshell interaction was studied to determine the mucoadhesive properties of the nanoshells. Tofa-LP/tfr NSh have $53.00\% \pm 0.181129\%$ mucin binding, while Tofa-LP/tfr/ES NSh have $35.79\% \pm 0.09\%$ binding (Figure 3.36 B). Tofa-LP/tfr NSh had increased binding than Tofa-PLGA NCs ($p<0.001$) because of lipid and tfr content that decreased the anionic character and improved mucus-binding. Tofa-LP/tfr/ES NSh still have increased binding than Tofa-PLGA NCs ($p<0.001$). However, the presence of the ES100 coat decreased the binding efficiency of Tofa-LP/tfr/ES NSh, as compared to Tofa-LP/tfr NSh (Figure 3.36 B). Further, the viscosity appeared almost parallel for both Tofa-LP/tfr NSh and Tofa-LP/tfr NSh-mucin, with a slight increase in Tofa-LP/tfr NSh-mucin viscosity at a shear rate below $50s^{-1}$ (Figure 3.36 C). The viscosity of Tofa-LP/tfr/ES NSh-mucin complex was always greater than that of mucin or Tofa-LP/tfr/ES NSh alone (Figure 3.36 D). The possible reason might be the very low viscosity of formulation that increases on binding with mucin.

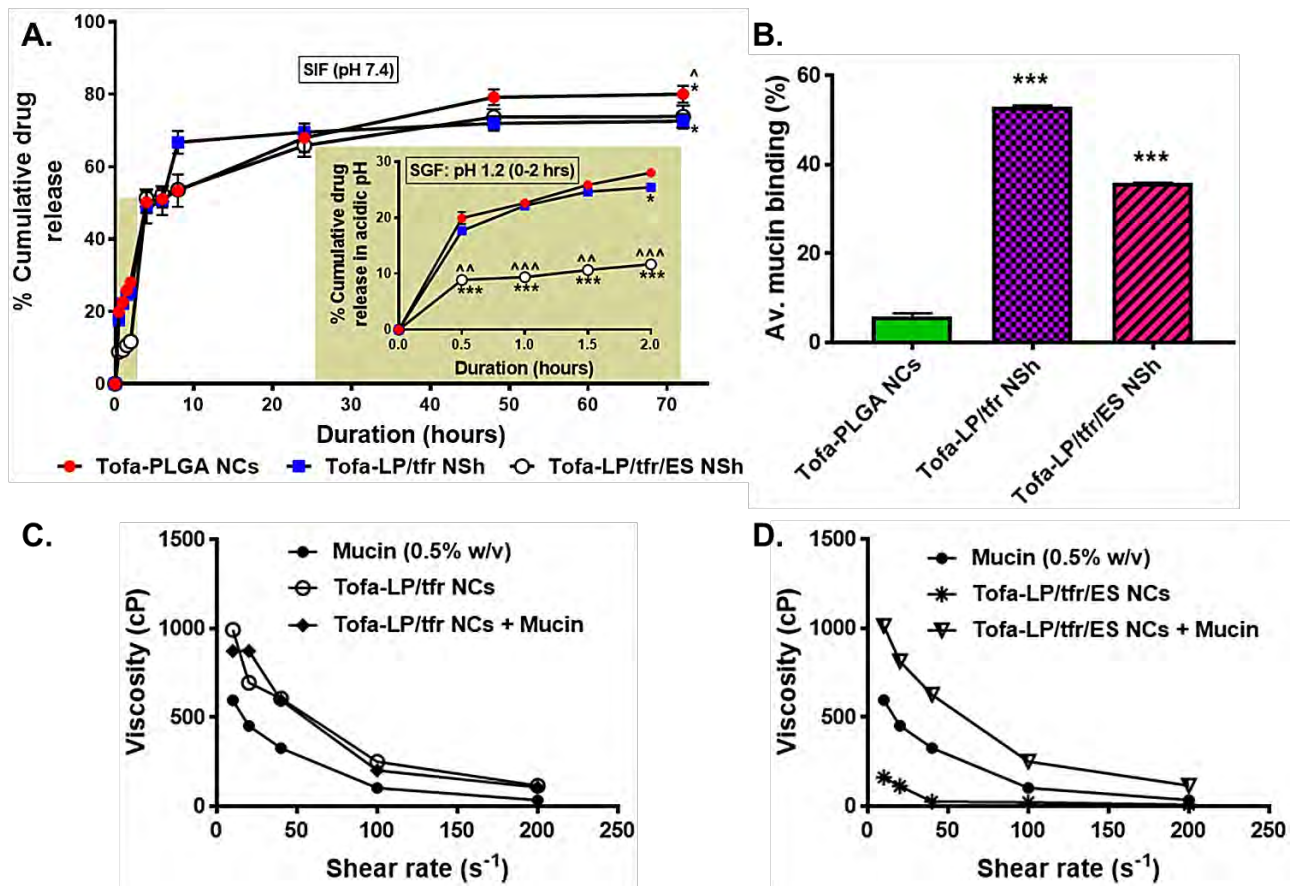


Figure 3.36: of Tofa-LP/tfr NSH and of Tofa-LP/tfr/ES NSH drug release and mucin binding studies; A: % Cumulative drug release at SGF (pH 1.2) and SIF (pH 7.4), B: % Mucin-nanoshells binding investigation, C: Effect of mucin binding on the viscosity of Tofa-LP/tfr NSH, D: Effect of mucin binding on viscosity of Tofa-LP/tfr/ES NSH

Table 3. 23: Drug release kinetics of Tofa-LP/tfr NSh at pH 1.2 and 7.4

| Tofa-LP/tfr NSh (pH 1.2; 0-2 hours) | | | | | | | Tofa-LP/tfr NSh (pH 7.4; 2-72 hours) | | | | | |
|-------------------------------------|------------|-------------|-----------|---------------------|---------------|----------------------------|--------------------------------------|-------------|---------|---------------------|---------------|-------------------------------|
| Parameter | Zero order | First order | Higuchi | Korsmeyer-peppas | Hixon-Crowell | Peppas-Sahlin | Zero order | First order | Higuchi | Korsmeyer-peppas | Hixon-Crowell | Peppas-Sahlin |
| R obs-pre | 0.8715 | 0.8957 | 0.9762 | 0.9989 | 0.8878 | 1.0000 | 0.6122 | 0.9263 | 0.7928 | 0.9814 | 0.8041 | 0.9885 |
| R² | 0.6043 | 0.6928 | 0.9529 | 0.9977 | 0.6649 | 0.9999 | -1.1905 | 0.4350 | 0.6286 | 0.9631 | 0.0173 | 0.9771 |
| RMSE | 6.6051 | 5.8199 | 2.6305 | 0.5804 | 6.0780 | 0.1198 | 38.3427 | 19.4727 | 17.2956 | 5.4485 | 25.6811 | 4.8039 |
| AIC | 27.8099 | 26.5443 | 19.1650 | 4.0521 | 26.9783 | -11.7509 | 65.5942 | 56.1085 | 55.1724 | 39.0009 | 59.9829 | 37.6762 |
| MSC | -0.7941 | -0.5410 | 0.9348 | 3.9574 | -0.6278 | 7.1180 | -2.3855 | -1.0304 | -0.8967 | 1.4135 | -1.5839 | 1.6028 |
| Other | k0=15.846 | k1=0.188 | kH=18.542 | kKp=21.692, n=0.262 | Khc=0.059 | k1= 32.7, k2=-10.43, m=0.5 | k0=1.391 | k1=0.121 | kH=6.89 | kKp=44.742, n=0.123 | Khc= 0.018 | k1=40.175, k2=-5.487, m=0.339 |

Table 3. 24: Drug release kinetics of Tofa-LP/tfr/ES NSh at pH 1.2 and 7.4

| Tofa-LP/tfr/ES NSh (pH 1.2; 0-2 hours) | | | | | | | Tofa-LP/tfr/ES NSh (pH 7.4; 2-72 hours) | | | | | |
|--|------------|-------------|----------|--------------------|---------------|----------------------------|---|-------------|----------|----------------------|---------------|-----------------------------|
| Parameter | Zero order | First order | Higuchi | Korsmeyer-peppas | Hixon-Crowell | Peppas-Sahlin | Zero order | First order | Higuchi | Korsmeyer-peppas | Hixon-Crowell | Peppas-Sahlin |
| R obs-pre | 0.8511 | 0.8606 | 0.9629 | 0.9976 | 0.8574 | 0.9977 | 0.6795 | 0.9154 | 0.8429 | 0.9981 | 0.8372 | 0.9983 |
| R² | 0.5415 | 0.5793 | 0.9272 | 0.9951 | 0.5669 | 0.9953 | -0.9883 | 0.3887 | 0.7104 | 0.9963 | 0.0773 | 0.9966 |
| RMSE | 3.1634 | 3.0300 | 1.4554 | 0.3758 | 3.0743 | 0.4527 | 35.6783 | 19.7835 | 14.9153 | 1.6954 | 24.3053 | 2.0759 |
| AIC | 20.4479 | 20.0172 | 13.2460 | -0.2934 | 20.1621 | 1.5396 | 64.5859 | 56.3302 | 53.0995 | 22.6570 | 59.2120 | 25.9155 |
| MSC | -1.0313 | -0.9452 | 0.4090 | 3.1169 | -0.9742 | 2.7503 | -2.2840 | -1.1046 | -0.6431 | 3.7059 | -1.5163 | 3.2404 |
| Other | k0=7.093 | k1=0.076 | kH=8.137 | kKp=9.888, n=0.206 | Khc=0.025 | k1= 6.59, k2=3.29, m=0.155 | k0=1.392 | k1=0.101 | kH=7.158 | kKp=41.1412, n=0.143 | Khc= 0.018 | k1=43.598, k2=-6.19, m=0.25 |

3.26. In Vitro Biocompatibility and Toxicity Studies

3.26.1. Hemolysis assay

Hemolysis assay described minimal toxicity of Tofa-LP/tfr NSh and Tofa-LP/tfr/ES NSh on blood cells at various concentrations (Figure 3. 37 A). There was no significant difference in the viability of PBS treated and formulations' treated RBCs. The difference only existed between Tofa-LP/tfr NSh and Triton-X control ($p < 0.001$). Likewise, Tofa-LP/tfr/ES NSh differed markedly from the Triton-X hemolysis agent at all concentrations ($p < 0.001$) (Figure 3. 37 A). Therefore, both formulations can be administered into the body with the least toxicity if entered systemic circulation.

3.27. Cellular biocompatibility

3.27.1.1. *MTT assay (colon, macrophages)*

MTT assay was performed to study the effect of Tofa-LP/tfr NSh and Tofa-LP/tfr/ES NSh on the viability of murine-derived macrophages and colon cells. Both nano-formulations at various concentrations were found to be inert and biocompatible with macrophages and colon cells after 24 and 48 hours (Figure 3. 37 B-E). PBS treated macrophages and colon cells served as a normal control for respective experiments. Triton-X served as a negative control with pronounced cellular toxicity ($p < 0.001$ vs PBS control). Hence, Tofa-LP/tfr NSh and Tofa-LP/tfr/ES NSh can be considered as a safe and non-toxic strategy for colon targeting in UC.

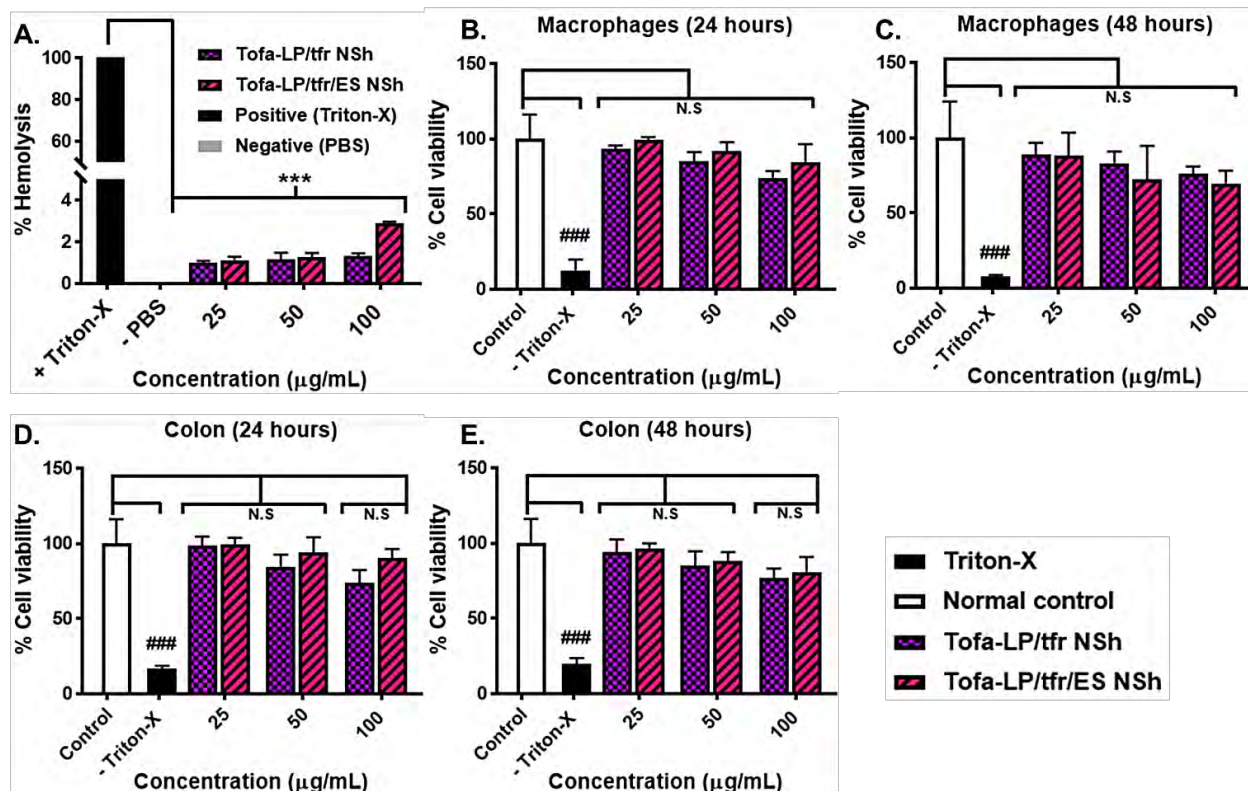


Figure 3. 37: In vitro hemolysis and cellular biocompatibility studies of Tofa-LP/tfr NSh and Tofa-LP/tfr/ES NSh; % Hemolytic activity exhibited by nanoshells (A), Effect of nanoshells on the viability of macrophages after 24 hours (B) and 48 hours (C), Effect of nanoshells on the colon cell viability after 24 hours (D) and 48 hours (E)

3.27.1.2. *Caco-2* apoptosis study (7-AAD, PI)

The dyes PI and 7-AAD are known to be viability dyes because these are impermeable to the membranes of viable cells, thus, excluded from the live viable cells (Zembruski *et al.*, 2012; Riccardi and Nicoletti, 2006). When the cell dies, the dye crossed the disintegrated membrane and binds to DNA and dead cells can be detected by fluorescence. Both dyes can be detected at FL-3 (red) channels of flowcytometry. We have treated *caco-2* cells with the nano-formulations and after 6 hours assess the viability using PI and 7-AAD, separately. The upper compartment is for 7-AAD+ or PI+ cells (dead cells), while the lower indicated viable cells (7-AAD- or PI-). The FACS analysis with 7-AAD dye indicated that both nano-formulations have higher biocompatibility, with $\geq 90\%$ viable *caco-2* cells after 6 hours (Figure 3. 38 I). Similarly, both nanoshells have $\geq 90\%$ *caco-2* viability, with PI dye assessment after 6 hours (Figure 3. 38 II). The difference from untreated healthy cells control (negative) is insignificant.

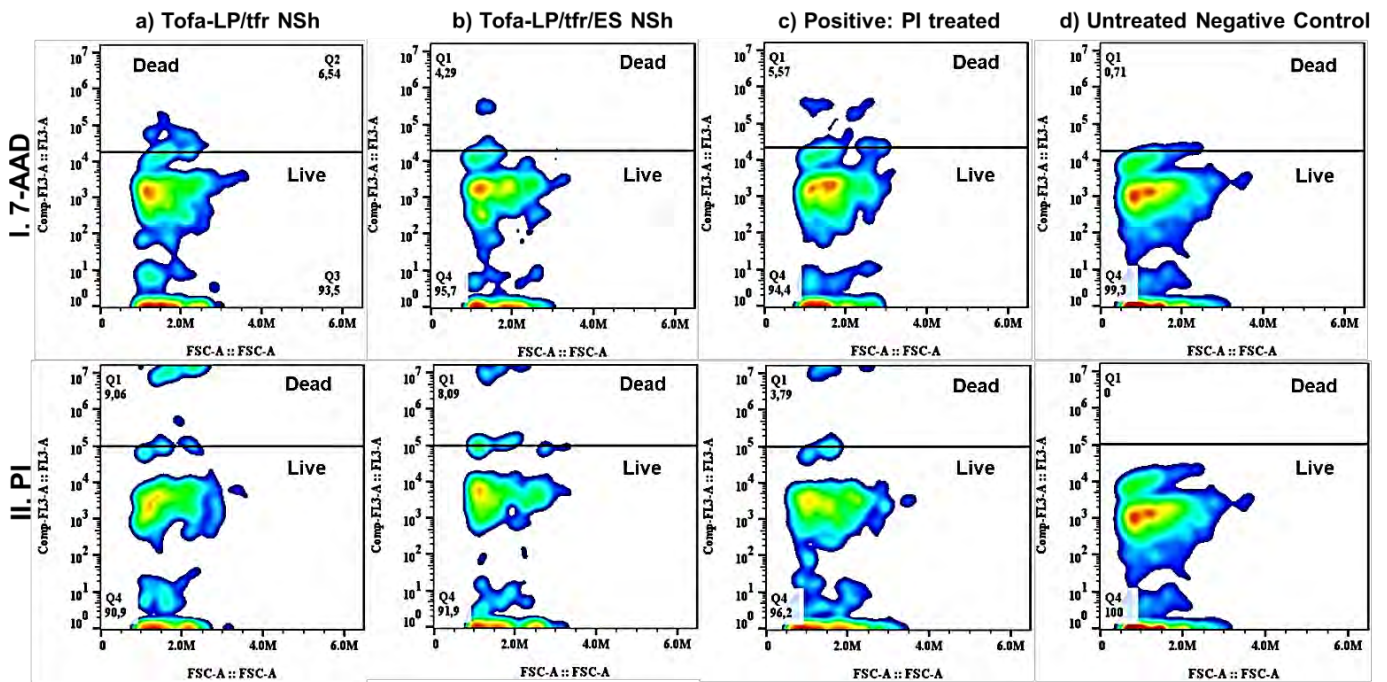


Figure 3.38: Evaluation of Caco-2 apoptosis by the Tofa-LP/tfr NSh and Tofa-LP/tfr/ES NSh, as indicated by 7-AAD (I) and PI (II) viability dyes

3.28. Caco-2 Uptake Studies

Coumarin-6 dye loaded LP/tfr NSh and Coumarin-6 dye loaded LP/tfr/ES NSh were prepared to observe uptake of nanoshells by the Caco-2 cells. Dye-LP/tfr NSh have exhibited 69.32 ± 20.24 a.u. ($p < 0.001^{***}$ vs plain dye) uptake after 2 hours and 72.94 ± 33.02 ($p < 0.001^{***}$ vs plain dye) after 4 hours of incubation with Caco-2 cells (Figure 3.39 I). While Dye-LP/tfr/ES NSh have 60.32 ± 17.00 a.u. ($p < 0.001^{***}$ vs plain dye) and 74.28 ± 23.22 ($p < 0.001^{***}$ vs plain dye) internalization after 2 and 4 hours of incubation (Figure 3.39 I). The two nano-formulations have an insignificant difference after 2 and 4 hours ($p = \text{NS}$). Additionally, FACS analysis was conducted in parallel. The histogram revealed about 93% and 96.4% engulfment of Dye-LP/tfr NSh after 2- and 4-hours incubation (Figure 3.39 II). And for Dye-LP/tfr/ES NSh, the uptake was about 84.2% and 96.5% after 2- and 4-hours incubation with Caco-2 cells (Figure 3.39 II).

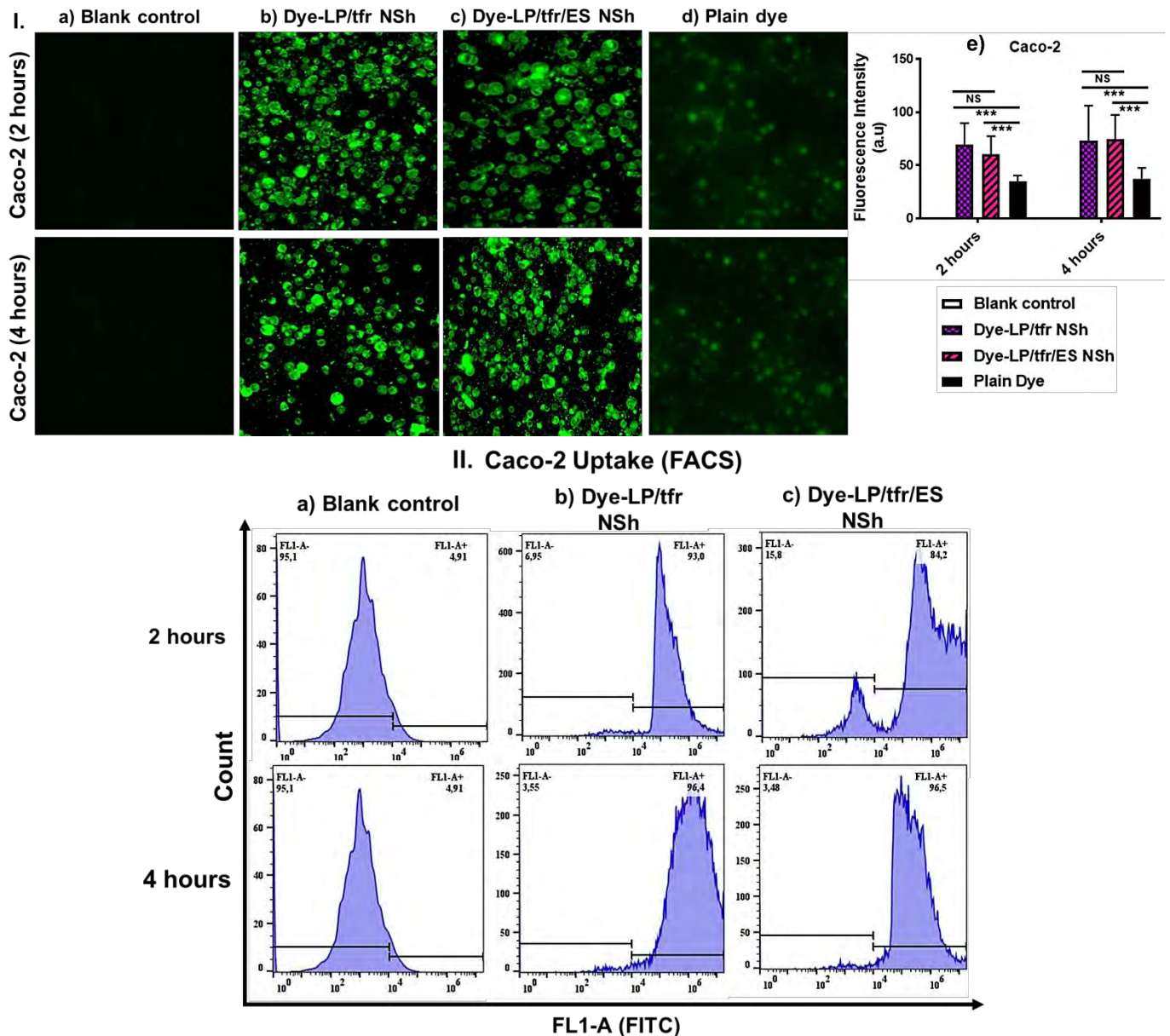


Figure 3. 39: Caco-2 uptake investigations of nanoshells by dye fluorescence and FACS analysis; I. Cellular uptake of Dye loaded LP/tfr NSh and LP/tfr/ES NSh by the Caco-2 cells after 2 and 4 hours of incubation by fluorescence microscopy (a-e); II. FACS analysis of Caco-2 uptake of Dye loaded LP/tfr NSh and LP/tfr/ES NSh

3.29. Macrophage Assays

3.29.1. Macrophage uptake

THP-1 monocytes were converted into macrophages (Figure 3. 40 I). The derived macrophages were incubated with Dye-LP/tfr NSh and Dye-LP/tfr/ES NSh formulations. The derived macrophages have TFR-1 (CD71) receptor expressed on their surface (Andreesen *et al.*, 1984). Both Dye-LP/tfr NSh ($p < 10^{-10}$ ##### vs plain dye)

and Dye-LP/tfr/ES NSh ($p < 10^{-10}$ ##### vs plain dye) have extensive uptake after 2 hours (Figure 3. 40 IIa-g). When Tfr-Ab was added to the cell line before incubation of nano-formulations, then the uptake of both Dye-LP/tfr NSh and Dye-LP/tfr/ES NSh was competitively inhibited by the CD71 receptor occupying antibody (Figure 3. 40 IIc, e, g). The uptake of Dye-LP/tfr NSh + Tfr-Ab ($p < 0.001$ ***) and Dye-LP/tfr/ES NSh + Tfr-Ab ($p < 0.01$ ***) was significantly lowered than Dye-LP/tfr NSh and Dye-LP/tfr/ES NSh, respectively (Figure 3. 40 IIa-g). And the mechanism involved for the internalization of nano-formulations in the presence of Tfr-Ab was not CD71 mediated, rather it might be general size mediated uptake of nano-formulations.

3.29.2. Macrophage JAK/STAT inhibition assay

Macrophages were activated into M1 pro-inflammatory macrophages (Figure 3. 40 I). Elicited macrophages with LPS and IF- γ have activated JAK/STAT pathway (Orecchioni *et al.*, 2019). Activated macrophages treated with PBS only have higher expression of JAK-1 and STAT-1 (Figure 3. 40 III, IV). The macrophages were treated with Tofa-LP/tfr NSh and Tofa-LP/tfr/ES NSh to investigate their effects on JAK-1 and STAT-1 expression. RT-PCT analysis indicated that JAK-1 was suppressed by Tofa-LP/tfr NSh ($p < 0.01$ **) and Tofa-LP/tfr/ES NSh ($p < 0.001$ ***) significantly (Figure 3. 40 III). While Tofa drug diminished it to some extent but not significant ($p = \text{NS}$). Similarly, STAT-1 was inhibited by Tofa-LP/tfr NSh ($p < 0.05$ *) and Tofa-LP/tfr/ES NSh ($p < 0.05$ *) markedly, but non-significantly by Tofa alone (Figure 3. 40 IV).

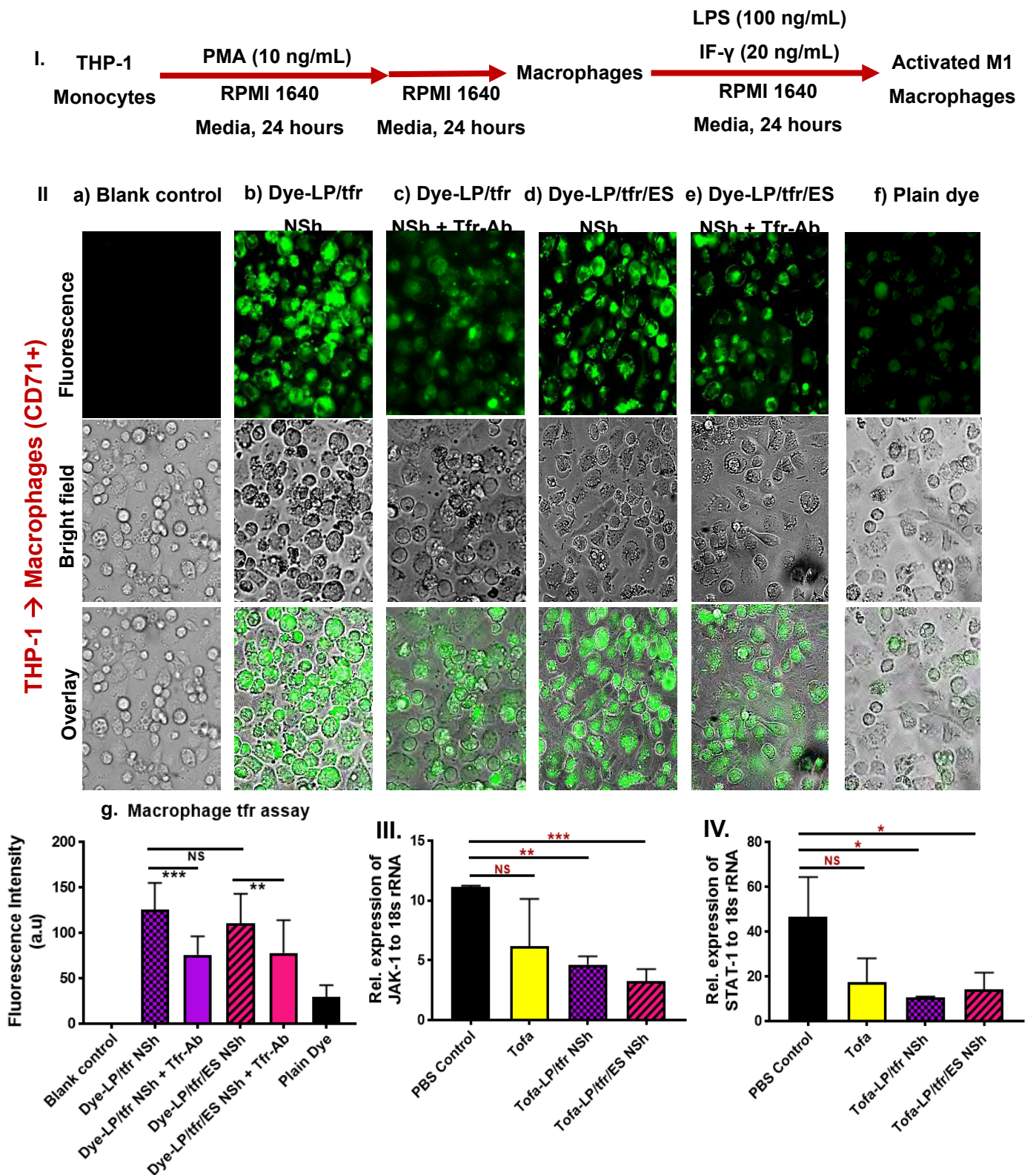


Figure 3. 40: In vitro THP-1 derived macrophages uptake assay and JAK/STAT inhibition assay; I: Scheme to convert activated macrophages from THP-1 monocytes, II: Cellular uptake of Dye loaded LP/tfr NSh and LP/tfr/ES NSh by THP-1 derived macrophages (a-f) and respective fluorescence intensity (g), III: Evaluation of expression of JAK-1 and, IV: STAT-1 by the activated macrophages and nanoshells' treated macrophages

3.30. Stability Studies

On storage, the Tofa-LP/tfr/ES NSh have minor changes in physicochemical properties with some increase in size and other minor changes. However, it retained the criteria of suitability (Table 3. 25).

Table 3. 25: Effect of storage conditions on physicochemical properties of Tofa-LP/tfr/ES NSh (mean \pm SD, n=3)

| Tofa-LP/tfr/ES NSh | Initial | | After 1 month | | After 6 months | |
|----------------------------|------------------|------------------|------------------|-------------------|-------------------|------------------|
| | 4°C | 25°C | 4°C | 25°C | 4°C | 25°C |
| Particle size (nm) | 281.3 \pm 6.33 | 281.3 \pm 6.34 | 283 \pm 4.86 | 285.5 \pm 7.05 | 284.23 \pm 4.99 | 289.2 \pm 5.12 |
| Zeta potential (mV) | -26.7 \pm 2.2 | -26.7 \pm 2.3 | -24.9 \pm 2.25 | -24.5 \pm 3.1 | -24.5 \pm 3.0 | -19.5 \pm 3.1 |
| PDI | 0.16 \pm 0.098 | 0.16 \pm 0.099 | 0.175 \pm 0.09 | 0.189 \pm 0.015 | 0.216 \pm 0.099 | 0.218 \pm 0.25 |
| EE% | 91.31 \pm 5.18 | 91.31 \pm 5.19 | 90.55 \pm 3.50 | 90.87 \pm 2.14 | 89.82 \pm 2.80 | 88.52 \pm 3.15 |

3.31. Animal Studies

The DSS-colitis model was successfully established in all male BALB/c mice with 7-day intake of DSS in drinking water, except for the normal healthy group.

3.32. Preliminary In Vivo Studies

3.32.1. Nanoshell's colon targeting ability and localization

The targeting potential of Tofa-LP/tfr NSh and Tofa-LP/tfr/ES NSh was determined by the quantification of the released drug in the colon and vital organs, post 6 hours administration to the DSS-colitis mice. Tofa-LP/tfr NSh and Tofa-LP/tfr/ES NSh accumulated about 17.94 \pm 0.17% and 32.79% \pm 3.49% drug at the inflamed colon (Figure 3. 41 I). The drug content localized in the colon by Tofa-LP/tfr/ES NSh ($p < 0.01^{**}$) was greater than Tofa-LP/tfr NSh, similarly, the stomach drug concentration by Tofa-LP/tfr/ES NSh ($p < 0.01^{**}$) was smaller than Tofa-LP/tfr NSh (Figure 3. 41 I). It highlighted the role of pH-sensitive coat that enhanced colon drug delivery and protects the drug dumping at the stomach. The spleen had <2% for both nanocarriers and the small intestine had lesser drug share by Tofa-LP/tfr/ES NSh ($p < 0.01^{**}$), compared to Tofa-LP/tfr NSh (Figure 3. 41 I). The kidney and liver have minimal drug content from both types of nanoshells. However, Tofa-LP/tfr/ES NSh group has more drug in the liver than Tofa-LP/tfr NSh (Figure 3. 41 I), maybe because of increased drug absorption. Further, it has been observed in a comparative study that

Tofa-LP/tfr/ES NSh had released more drug in the DSS-inflamed colon than the healthy colon (Figure 3. 41 II), illuminating the role of pH-sensitive nanoshells in colon inflammation.

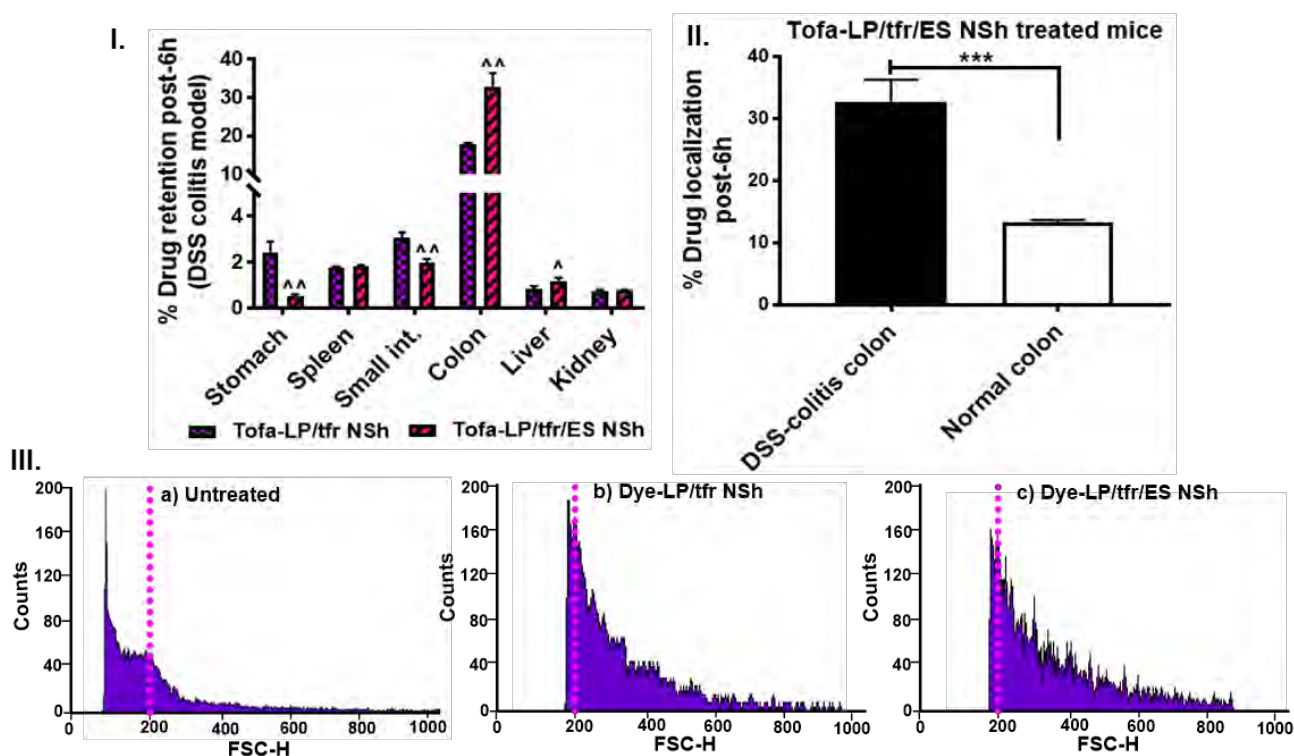


Figure 3. 41: Preliminary in vivo nanoshells localization and retention studies and colon-macrophages uptake; I: Relative drug retention by Tofa-LP/tfr NSh and Tofa-LP/tfr/ES NSh in the DSS-induced mice, II: Drug localization in the normal healthy and DSS-induced colitis mice after 6 hours of Tofa-LP/tfr/ES NSh oral administration, III: Uptake by the colon-macrophages after oral administration of nanoshells to the DSS-colitis mice (n=3)

3.32.2. Flow cytometry uptake study

The in vivo macrophage uptake determination by flowcytometry suggested increased uptake of dye-LP/tfr NSh and dye-LP/tfr/ES NSh by the colon derived macrophages, compared to untreated controls (Figure 3. 41 III). A deviation in the forward scattered plot (FSC-H) indicated changes in morphology, size, and structural dimensions of the macrophages (Patel *et al.*, 2016a; Alwani *et al.*, 2016). About 9.04% and 8.39% area was shifted from the marked area by the dye-LP/tfr NSh and dye-LP/tfr/ES NSh groups, respectively (Figure 3. 41 III). The shift represented intake of nanoshells by colon recruited macrophages.

3.32.3. In vivo visualization of biodistribution of nanoshells

Co-6 dye-loaded LP/tfr NSh and LP/tfr/ES NSh were given orally to the healthy and DSS-induced colitis mice to observe in vivo biodistribution inside the gut. After 18 hours, the whole GIT was excised and observed under Maestro In Vivo Imaging System (CRI, Inc., Woburn, MA) for the fluorescence generated from the dye-loaded nanoshells. It was observed that Co-6- LP/tfr NSh majorly localized in the upper part of the small intestine in the healthy mice (a) and the mid part of the small intestine in the DSS-mice (c) (Figure 3. 42 Ia, c). Some dye emissions can be observed from the colonic region attributed to some localized concentrations in the colon as well. Whereas Co-6- LP/tfr/ES NSh have major red fluorescent emission from the colon area of both the healthy (b) and DSS-induced mice (d) (Figure 3. 42 Ib, d). In DSS-colitis mice, the Co-6- LP/tfr/ES NSh have accumulation in the cecum and colon, with very lesser spots in the small intestine.

Further, the colon tissue from healthy and DSS-colitis groups treated with Co-6- LP/tfr/ES NSh were visualized under the confocal microscope to study tissue-level localization. Co-6 either entrapped or released from the nanoshell was detected under red signal, DAPI was stained to locate cell nucleus, and the overlay image gave a full picture. It was obvious from confocal images that the nanoshells have a higher accumulation in the DSS-inflamed colon than the healthy colon (Figure 3. 42 II).

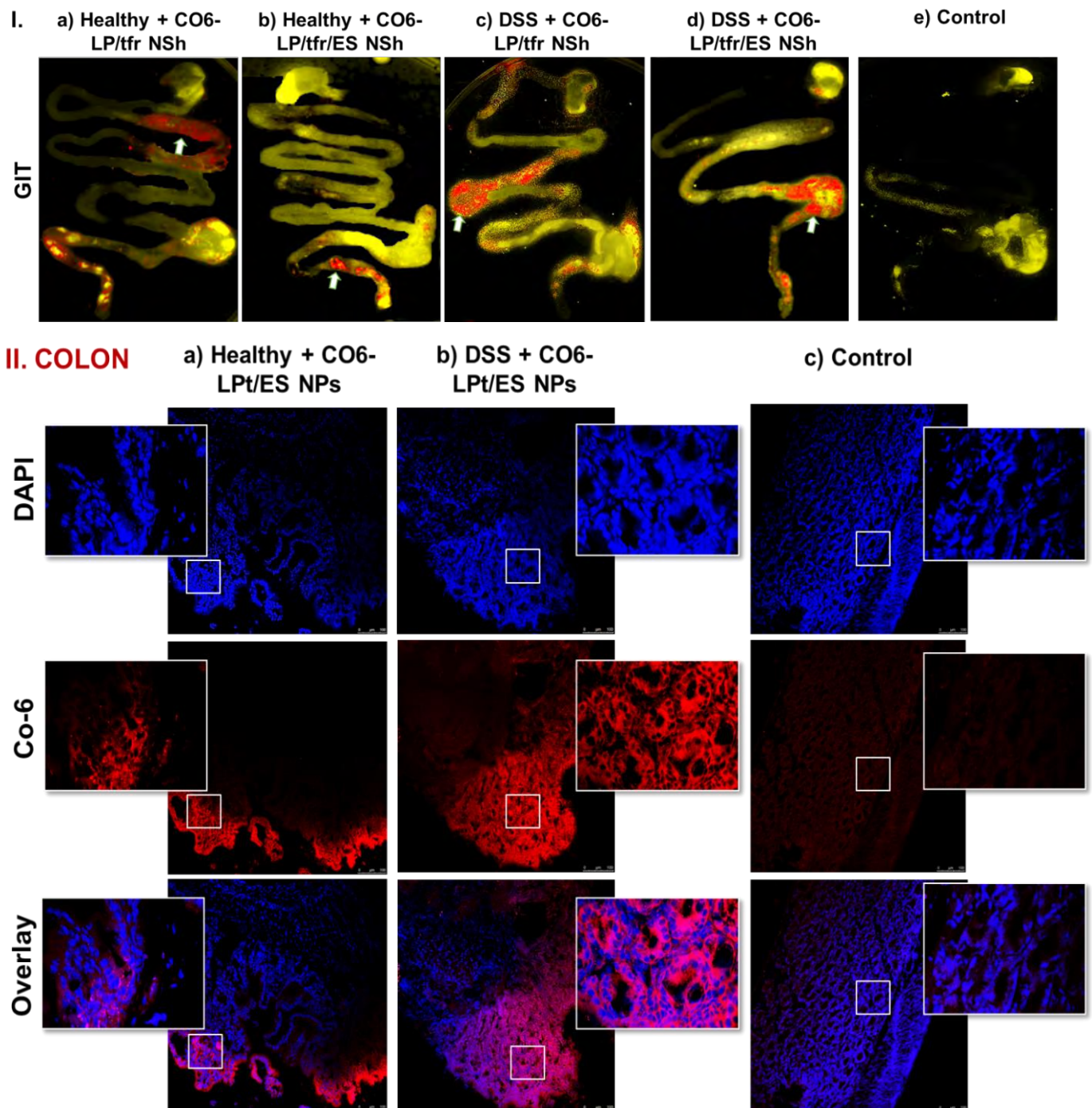


Figure 3. 42: Nanoshells in vivo biodistribution imaging studies; I: Nanoshells biodistribution inside the GIT post 18 hours oral administration to the healthy and DSS-inflamed mice, II: Confocal microscopic images of the excised colon from healthy and DSS-induced mice, treated with dye loaded LP/tfr/ES NSh (DAPI: blue channel, Co-6: red channel)

3.33. In Vivo Therapeutic Efficacy Investigations

3.33.1. Morphological assessment of colitis severity and treatment efficacy

One of the major manifestations of UC is bodyweight reduction. In our experiment, DSS significantly lowered the weight of the mice from day 1-14. Tofa-LP/tfr NSh recovered the bodyweight of the mice afflicted with DSS-induced colitis, and Tofa-LP/tfr/ES NSh also restored the mice weight (Figure 3. 43 A). Further, the DAI score is the index of disease activity, therefore, the colitis mice have the highest DAI score on Day 8-9, with a little recovery of DAI on the 14th day because of the self-healing properties of the tissues (Figure 3. 43 B). But still, the DSS-DAI score was highest among all groups. Treatment with the nanoformulations retrieved the DAI score near the normal values, for instance, Tofa-LP/tfr NSh and Tofa-LP/tfr/ES NSh have the DAI score of 4.6 ± 0.42 and 3.6 ± 0.53 , respectively on the 14th day (Figure 3. 43 B).

Furthermore, the physical evaluation of DSS-induced colitis mice indicated a significant loss in the length of the colon ($p < 0.01###$) and small intestine ($p < 0.05\#$), with an increase in weight of the colon ($p < 0.01###$) and spleen ($p < 0.001####$), compared to the normal (Figure 3. 43 C, D). The resultant increase in colon weight to length ratio is another index of disease severity of the DSS mice ($p < 0.001####$ vs normal) (Figure 3. 43 E). The other excised organs including the heart, kidney, liver, lungs, and stomach had a negligible effect on colitis (Figure 3. 43 D). Colon length ($p < 0.05^*$), colon weight to length ratio ($p < 0.01^{**}$), and spleen weight ($p < 0.01^{**}$) were resumed by the treatment with Tofa-LP/tfr NSh (Figure 3. 43 C-E). Likewise, Tofa-LP/tfr/ES NSh recovered the inflammation indices including colon length ($p < 0.001^{***}$), colon weight to length ratio ($p < 0.001^{***}$), weight to length ratio ($p < 0.001^{***}$) and splenic weight ($p < 0.001^{***}$) significantly (Figure 3. 43 C-E). The length of the small intestine was restored by Tofa-LP/tfr NSh ($p < 0.05^*$) and Tofa-LP/tfr/ES NSh ($p < 0.001^{**}$) therapy (Figure 3. 43 C). The vital organs have no toxic effects by the treatment with nano-formulations (Figure 3. 43 D).

The survival analysis of the all groups indicated that only 20% of mice survived in the DSS induced colitis group till the end of the experiment, while Tofa-LP/tfr NSh and Tofa-LP/tfr/ES NSh have about 80% and 100% survival rate, respectively (Figure 3. 43 F).

3.33.2. Histopathological reversal of colitis

DSS caused significant damage to the architecture of the colon, as evident from the histopathological score of 12 ($p < 0.001$ ###), compared to the normal mice score of 0.67 (Figure 3. 43 G-H). Tofa drug restored the features ($p < 0.01$ **). While Tofa-LP/tfr NSh ($p < 0.001$ ***) and Tofa-LP/tfr/ES NSh ($p < 0.001$ ***) more significantly lessened the histological damage because of significant healing of epithelial membrane, crypt's structure restructuring and decreased the number of immune cells infiltrates (Figure 3. 43 G-H). Tofa-LP/tfr/ES NSh have significantly greater healing than the plain drug Tofa ($p < 0.05$ ^), whereas Tofa-LP/tfr NSh did not differ markedly.

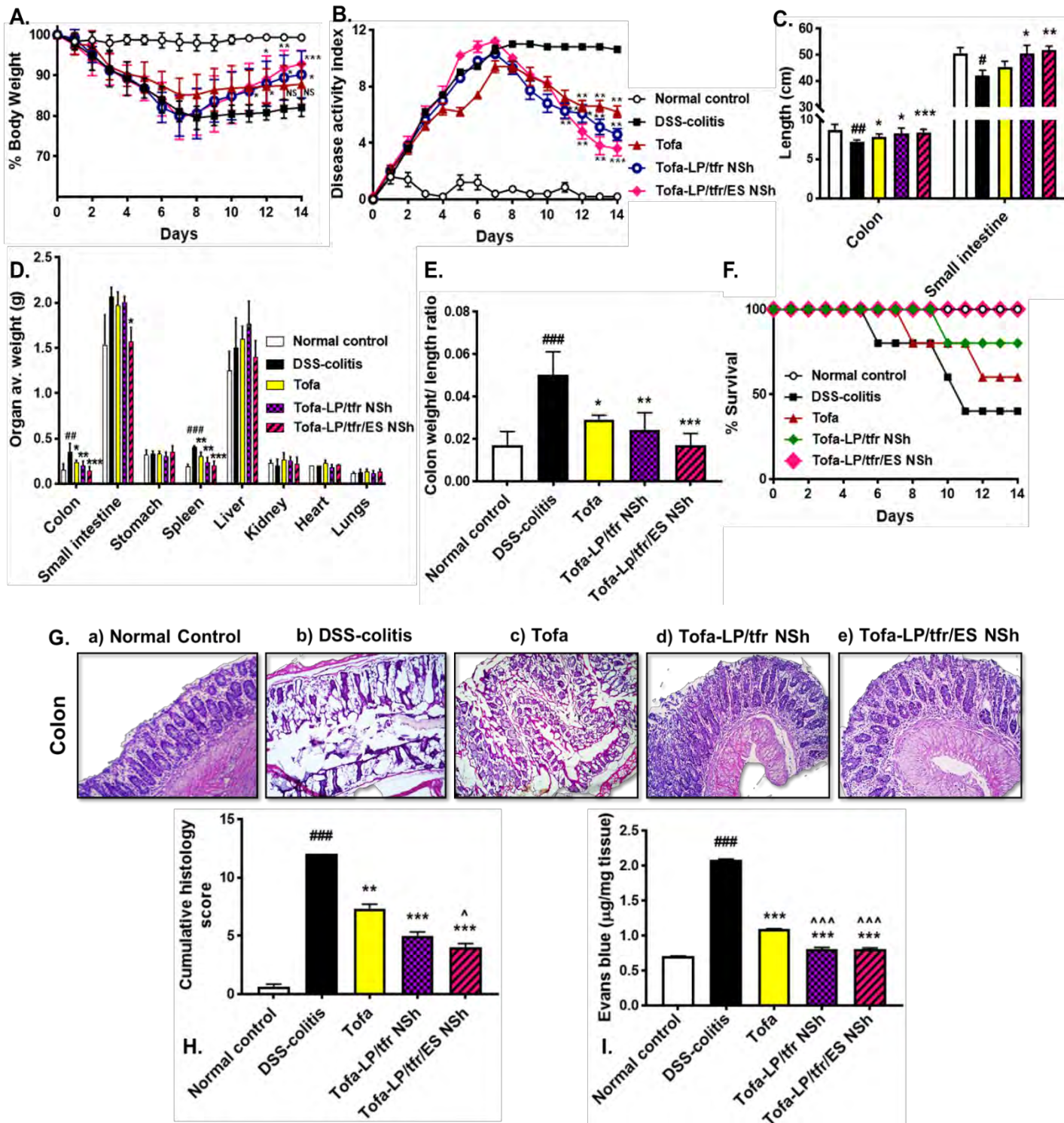


Figure 3. 43: Therapeutic evaluation of Tofa loaded nanoshells' treatment efficacy through morphological, physical, histological and vascular integrity assessment; Bodyweight (%) (A), DAI score (B), Intestine length (C), Organ's weight (D), Colon weight to length ratio (E), and % survival analysis (n=5) (F), Histological images (Ga-e), Cumulative histo-score (n=5) (H), and vascular integrity assessment by the permeated Evans blue dye by the normal, DSS-colitis, Tofa, Tofa-LP/tfr NSh and Tofa-LP/tfr/ES NSh treated groups (n=3)

3.33.3. Assessment of vascular integrity

Colon vasculature intactness was assessed through the amount of Evans blue permeated across the blood vessels to the colon tissue (Radu and Chernoff, 2013). Since the vessels became leaky in inflammation, therefore, DSS-colitis have the highest amount of dye content ($2.087 \pm 0.0062 \mu\text{g}/\text{mg}$ tissue, $p < 0.001###$) compared to the normal (0.71 ± 0.0013) (Figure 3. 43 I). Tofa, Tofa-LP/tfr NSh and Tofa-LP/tfr/ES NSh significantly recovered the endothelial membrane, as demonstrated by the decline in Evans blue concentration in the colon tissues to $1.091 \pm 0.0079 \mu\text{g}/\text{mg}$, $0.81 \pm 0.020 \mu\text{g}/\text{mg}$ and $0.802 \pm 0.019 \mu\text{g}/\text{mg}$, respectively (Figure 3. 43 I). Both nanoshells have superior efficacy than plain drug Tofa ($p < 0.001^^^$, Figure 3. 43 I).

3.33.4. RT-PCR analysis for the expression of inflammatory (iNOS), mechanistic (STAT-1), epithelial membrane (E-cadherin), and receptor-oriented proteins (TFR-1)

JAK/STAT is the pathway that aggravates inflammation in colitis (Salas *et al.*, 2020), and Tofa acts by inhibiting JAK/STAT pathway, therefore, we have studied STAT-1 expression. RT-PCR expression of STAT-1 was down-regulated by the treatment groups, which was elevated in DSS mice ($p < 0.05\#$ vs normal). Tofa-LP/tfr/ES NSh lowered the levels most significantly ($p < 0.05^*$), followed by Tofa-LP/tfr NSh ($p < 0.05^*$) and Tofa ($p = \text{NS}$) (Figure 3. 44 A).

Since recruitment of immune cells particularly macrophages rose in the inflammation, therefore, TFR-1 or CD71 receptors on the surface of macrophages and colon cells became an ideal target for IBD. The expression of TFR-1 increased in DSS colitis mice ($p < 0.05\#$ vs normal). However, the expression was significantly diminished in the Tofa-LP/tfr NSh ($p < 0.05^*$) and Tofa-LP/tfr/ES NSh ($p < 0.05^*$) treated groups (Figure 3. 44 B). Plain drug have an insignificant effect. The encapsulated drug was released from the nanoshells in a sustained manner with an enhanced activity that reversed inflammatory events and suppressed the immune cells that ultimately decreased TFR-1 expression. It seems to be interesting that our rationale of TFR-1 targeting automatically worked in the case of colon inflammation with decreased targeting efficacy to the normal tissue.

Colitis leads to severe damage of epithelial linings, as evident from decreased levels of tight junction protein, E-cadherin, in the DSS inflamed mice ($p < 0.001$ ### vs normal, Figure 3. 44 C). The expression of tight junction gate proteins was slightly restored by Tofa ($p = \text{NS}$), and pronouncedly recovered by Tofa-LP/tfr NSh ($p < 0.05^*$) and Tofa-LP/tfr/ES NSh ($p < 0.05^*$) (Figure 3. 44 C).

Furthermore, the JAK/STAT mechanism is also linked to NF- κ B, therefore, it aided to reduce the levels of iNOS either by a direct or indirect mechanism. The increase of iNOS in the DSS induced colitis mice was decreased by Tofa ($p = \text{NS}$), Tofa-LP/tfr NSh ($p < 0.05^*$), and Tofa-LP/tfr/ES NSh to ($p < 0.05^*$) (Figure 3. 44 D). iNOS is a key mediator of inflammation that generated free oxygen species to produce a potent inflammatory response. Declined iNOS concentrations in the nanoshells' treated groups indicated prominent healing and recovery.

3.33.5. Pro-inflammatory cytokines assessment

The inhibition of the JAK/STAT pathway and subsequent NF- κ B blockade decreased the pro-inflammatory cytokines storm. Therefore, the concentrations of IL-6 in the serum were lowered by Tofa ($p < 0.001^{***}$), Tofa-LP/tfr NSh ($p < 0.001^{***}$), and Tofa-LP/tfr/ES NSh ($p < 0.001^{***}$) (Figure 3. 44 E). Furthermore, TNF- α was declined by all treatment groups ($p < 0.001^{***}$), especially by Tofa-LP/tfr/ES NSh (Figure 3. 44 F).

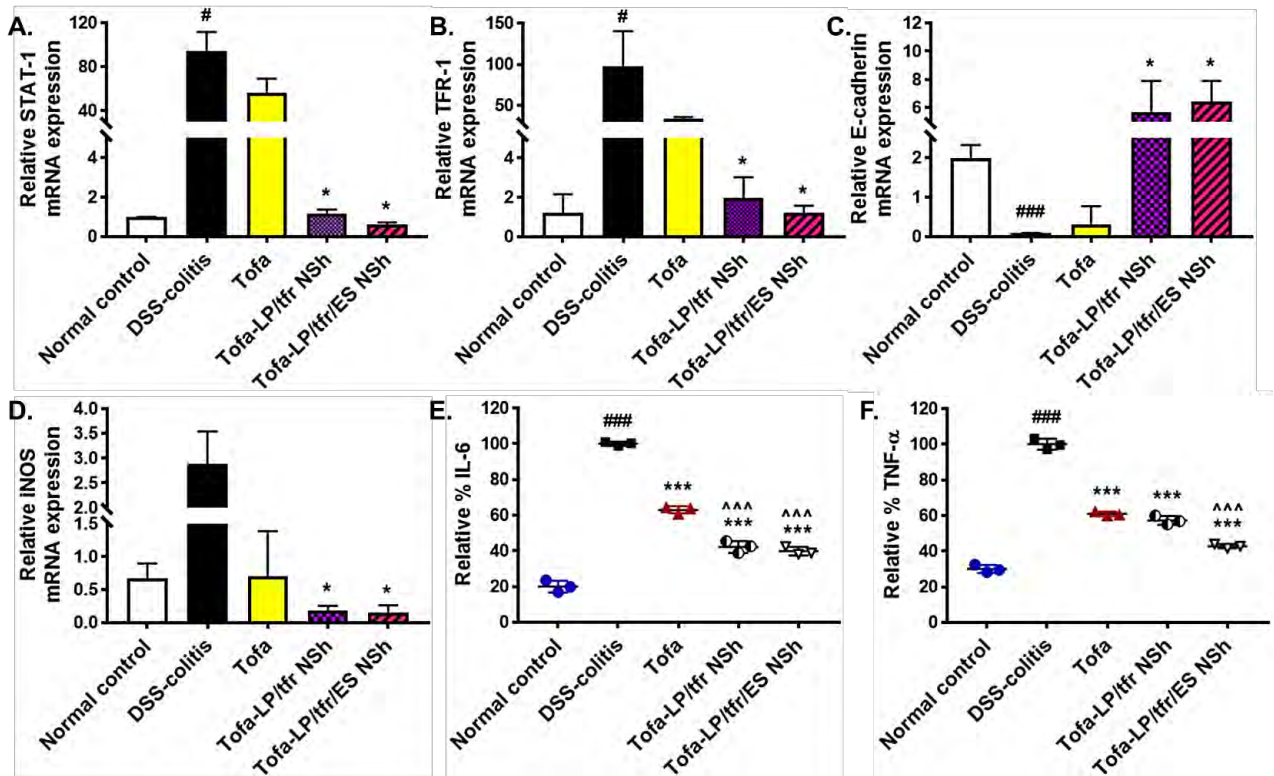


Figure 3. 44: RT-PCR expression of STAT-1 (A), TFR-1 (B), E-cadherin (C) and iNOS (D); And levels of proinflammatory cytokines, IL-6 (E) and TNF- α (F) from the colon tissue excised from normal, DSS-colitis, Tofa and Tofa-LP/tfr NSH and Tofa-LP/tfr/ES NSH groups (n=5)

3.33.6. Antioxidant protection by the nanoshell delivered drug to the colon

3.33.6.1. Immunohistochemistry for antioxidant markers

Nrf2 is known to play an essential role in the cellular detoxification mechanism by expressing various enzymes and proteins with antioxidant properties including GSH, and HO-1. HO-1 scavenges free oxidative radicals and lowered oxidative stress in inflammation (Saha *et al.*, 2020).

Here, we investigate the expression of Nrf2 and HO-1 in the excised colon tissues of each group through immunohistochemistry. The findings demonstrated low expression of the respective markers (Nrf2, HO-1) in the DSS inflamed colon ($p < 0.001$ ### vs normal, Figure 3. 45 I-II). HO-1 expression was upregulated by Tofa ($p < 0.01$ **), Tofa-P/tfr nanocarrier (NCs) ($p < 0.01$ **), Tofa-LP/tfr NSH ($p < 0.01$ **), and Tofa-LP/tfr/ES NSH ($p < 0.001$ ***) (Figure 3. 45 Ia-g). The highest expression was observed in the Tofa-LP/tfr/ES NSH treated group (Figure 3. 45 Ig). Nrf2 was also upregulated by the treatment groups, but mostly by the Tofa-LP/tfr/ES NSH group (Figure 3. 45 II).

Tofa downregulates phosphorylated JAK/STAT via Nrf2 translocation to the nucleus in inflammatory and neurodegenerative diseases (Ma *et al.*, 2015; Guo *et al.*, 2016), therefore the resultant Nrf2 up-regulation alleviates the inflammation. Further, JAK/STAT inhibition, in turn, downregulated NF- κ B pathways that is also responsible for Nrf2 enhanced function by encapsulating Tofa (Sharma *et al.*, 2020).

3.33.6.2. *Biochemical antioxidant assays*

The excessive production of reactive oxygen species and lack of antioxidant enzymes weakened the natural cellular protection in colitis. The assessment of antioxidants GSH, GST, and catalase enzyme indicated a sharp decline in DSS induced colitis (Figure 3. 45 A-C), whereas the oxidative species like MDA and NO were enhanced pronouncedly in colitis (Figure 3. 45 D, E). Tofa increased antioxidants and lowered down oxidants (Figure 3. 45 A-E). The treatment with Tofa-LP/tfr NSh elevated GSH ($p < 0.001^{***}$), GST ($p < 0.001^{***}$) and catalase ($p < 0.001^{***}$) and decreased NO ($p < 0.001^{***}$) and MDA ($p < 0.001^{***}$) (Figure 3. 45 A-E). Likewise, Tofa-LP/tfr/ES NSh rose sharply GSH ($p < 0.001^{***}$), GST ($p < 0.001^{***}$) and catalase ($p < 0.001^{***}$), while significantly levelled down NO ($p < 0.001^{***}$) and MDA levels ($p < 0.001^{***}$) (Figure 3. 45 A-E). Furthermore, neutrophil marker MPO increased up to many times in DSS induced colitis ($p < 0.001^{###}$ vs normal, Figure 3. 45 F). The MPO activity was most prominently lowered by Tofa-LP/tfr/ES NSh treatment ($p < 0.001^{***}$, Figure 3. 45 F), as a result of extended drug-mediated immunosuppression.

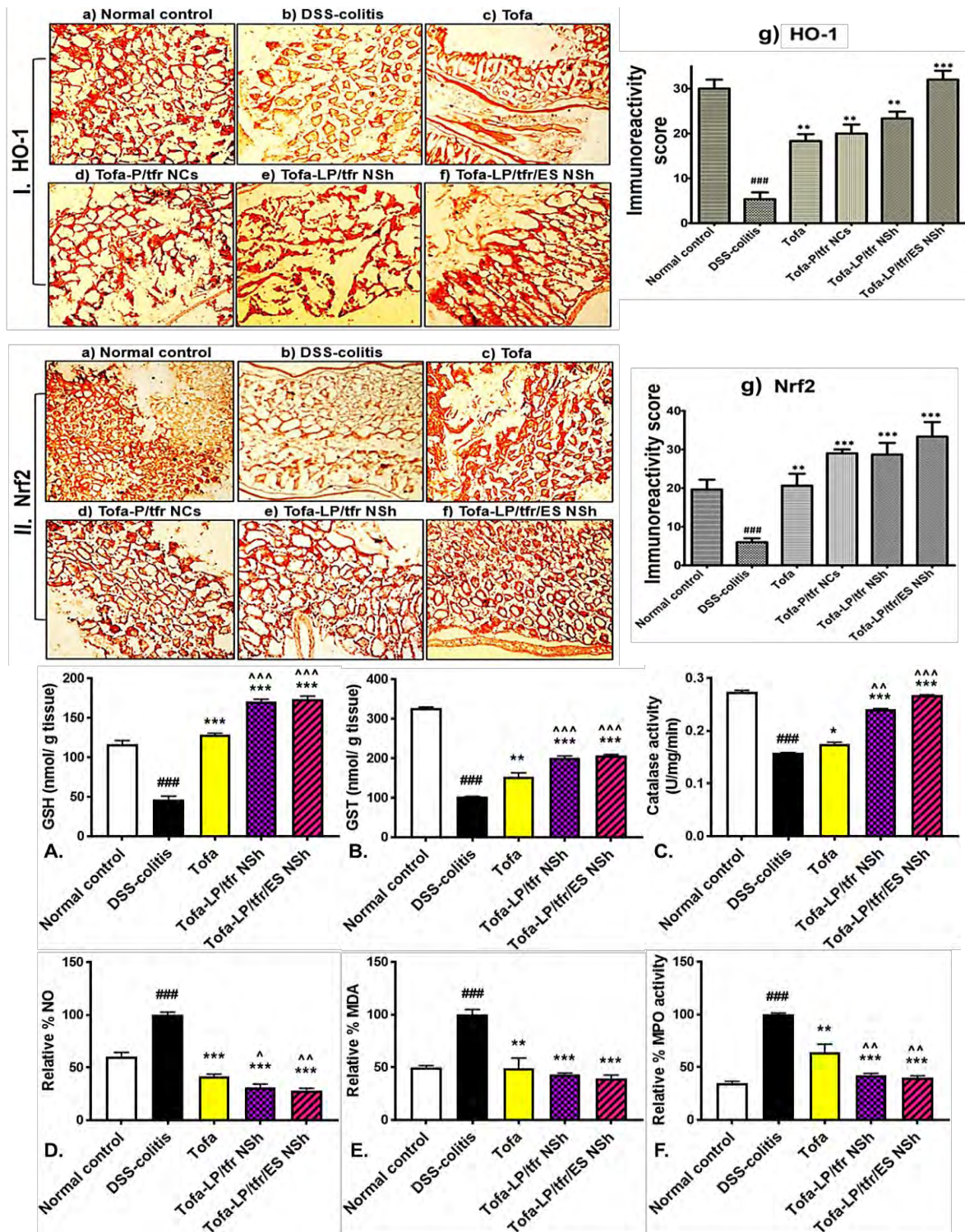


Figure 3. 45: Tofa-LP/tfr NSH and Tofa-LP/tfr/ES NSH mediated in vivo antioxidant protection analysis through immunohistochemistry and biochemical antioxidant assays; Assessment of antioxidant markers expression, HO-1 (I) and Nrf-2 (II) by immunohistochemistry of the excised colon tissues from normal, DSS-colitis, Tofa and Tofa-LP/tfr NSH and Tofa-LP/tfr/ES NSH groups; Biochemical assays to determine antioxidant protection through quantification of antioxidants GSH (A), GST (B) and Catalase (C), and oxidative species NO (D), MDA (E) and neutrophil marker MPO (F) in the colon tissue excised from normal, DSS-colitis, Tofa and Tofa-LP/tfr NSH and Tofa-LP/tfr/ES NSH groups (n=5)

3.33.7. Evaluation of bloodborne indices

Blood was collected to evaluate the course of therapy of colitis through various indices. The total leukocyte count (TLC) was found to be pronouncedly higher in the colitis mice ($15.4 \times 10^3/\mu\text{L} \pm 0.8 \times 10^3/\mu\text{L}$, $p < 0.001###$) than the normal control ($8.6 \times 10^3/\mu\text{L} \pm 0.2 \times 10^3/\mu\text{L}$) (Figure 3. 46 A). The count was considerably reduced by Tofa-LP/tfr NSh to $6.73 \times 10^3/\mu\text{L} \pm 0.75 \times 10^3/\mu\text{L}$ ($p < 0.001***$) and by Tofa-LP/tfr/ES NSh to $5.57 \times 10^3/\mu\text{L} \pm 0.21 \times 10^3/\mu\text{L}$ ($p < 0.001***$) (Figure 3. 46 A). The RBC count was decreased by DSS induction ($p < 0.01##$ vs normal), which was restored by Tofa-LP/tfr NSh ($p < 0.01**$) and more by Tofa-LP/tfr/ES NSh ($p < 0.001***$) (Figure 3. 46 A). The Hemoglobin (Hb), packed cell volume/hematocrit (PCV/HCT), and mean corpuscular hemoglobin (MCH) were also recovered towards normal values by both Tofa-LP/tfr NSh and Tofa-LP/tfr/ES NSh (Figure 3. 46 A).

The RFT parameters like serum urea concentration were found in the normal range of 12-45 mg/dL, serum creatine up to 1.2 mg/dL, and serum uric acid < 7 for both Tofa-LP/tfr NSh and Tofa-LP/tfr/ES NSh (Figure 3. 46 B). Further, CRP values were lesser than 6 for both Tofa-LP/tfr NSh and Tofa-LP/tfr/ES NSh (Figure 3. 46 C), indicating no inflammation.

3.33.8. Assessment of feces microbial growth

The natural microbiome of the colon is disturbed in colitis. Therefore, we estimated the bacterial growth of the feces taken from the bowel of each group. Findings indicated increased bacterial growth in the DSS-induced colitis mice ($p < 0.001###$ vs normal, Figure 3. 46 D). Treatment with the plain drug had a negligible effect on the growth rate, while bacterial $\log_{10}\text{CFU/mL}$ was reduced predominantly with Tofa-LP/tfr NSh ($p < 0.01**$) and Tofa-LP/tfr/ES NSh ($p < 0.001***$) treatment (Figure 3. 46 D).

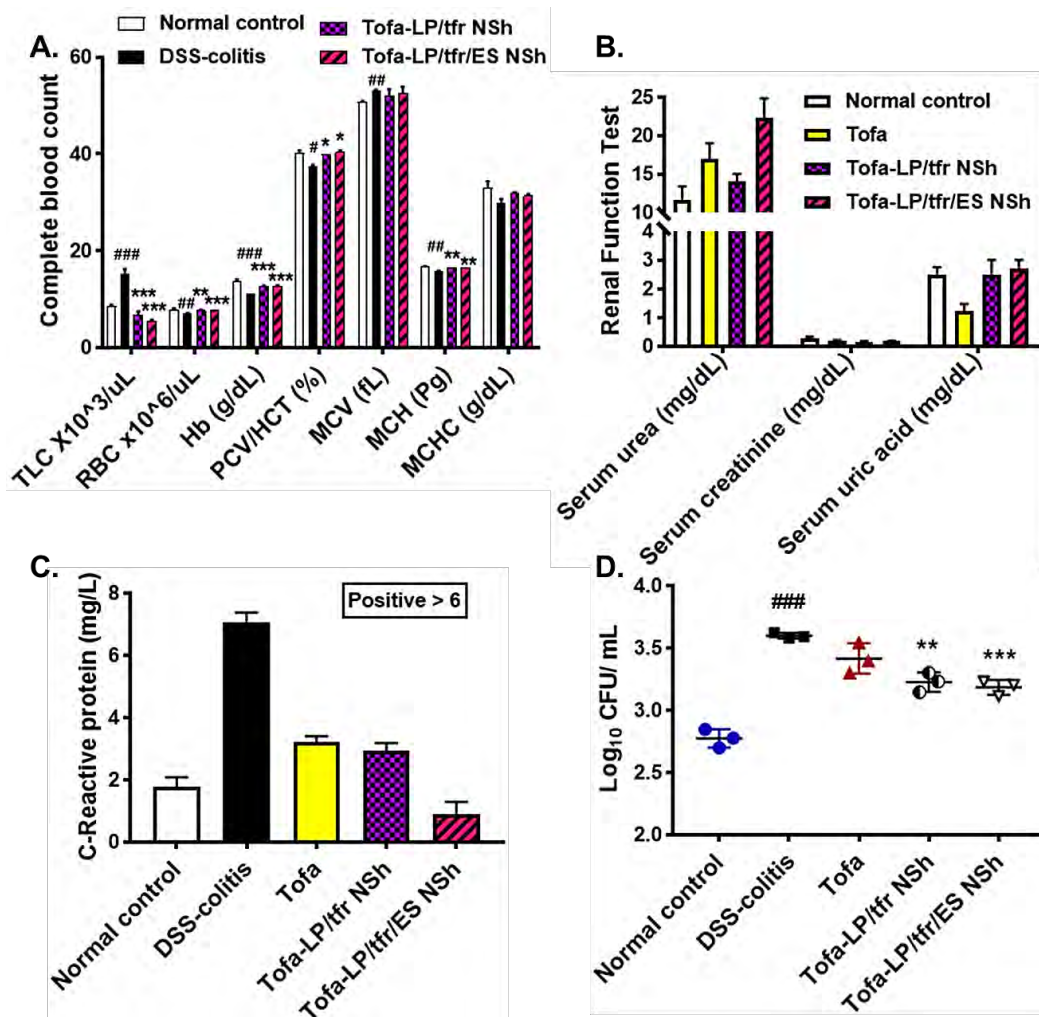


Figure 3. 46: Elucidation of the effect of therapy on the blood cells count (A), renal function (B), C-reactive proteins (CRP) (C), and colony-forming units from the feces of Normal control, DSS-colitis, Tofa, and Tofa-P/tfr NCs groups (D)

3.33.9. In vivo biocompatibility evaluation of Tofa-LP/tfr/ES NSh

Tofa-LP/tfr/ES NSh was administered to healthy mice for 7-days to study the effects of acute toxicity. The mice have a normal food intake pattern, sleep cycle with no signs of distress and allergy. The daily body weight measurements indicated negligible changes from day 0-4 and 6-7, only a deviation was observed at day 5 (Figure 3. 47 A). Multiple confounding factors might be responsible for this deviation and more detailed investigations are required. Further, the gross investigations demonstrated no effect on weights of organs, intestine length, and colon weight to length ratio (Figure 3. 47 B-D). The colon microbial flora remained intact and same growth rate as that of healthy mice (Figure 3. 47 E). Colon tissue apoptotic study revealed about 85% viable live cells compared to 94% live cells in the healthy untreated controls (Figure 3. 47 F). Though

the nanoshells still proved to be safe, however, long-term investigations will further establish the safety profile.

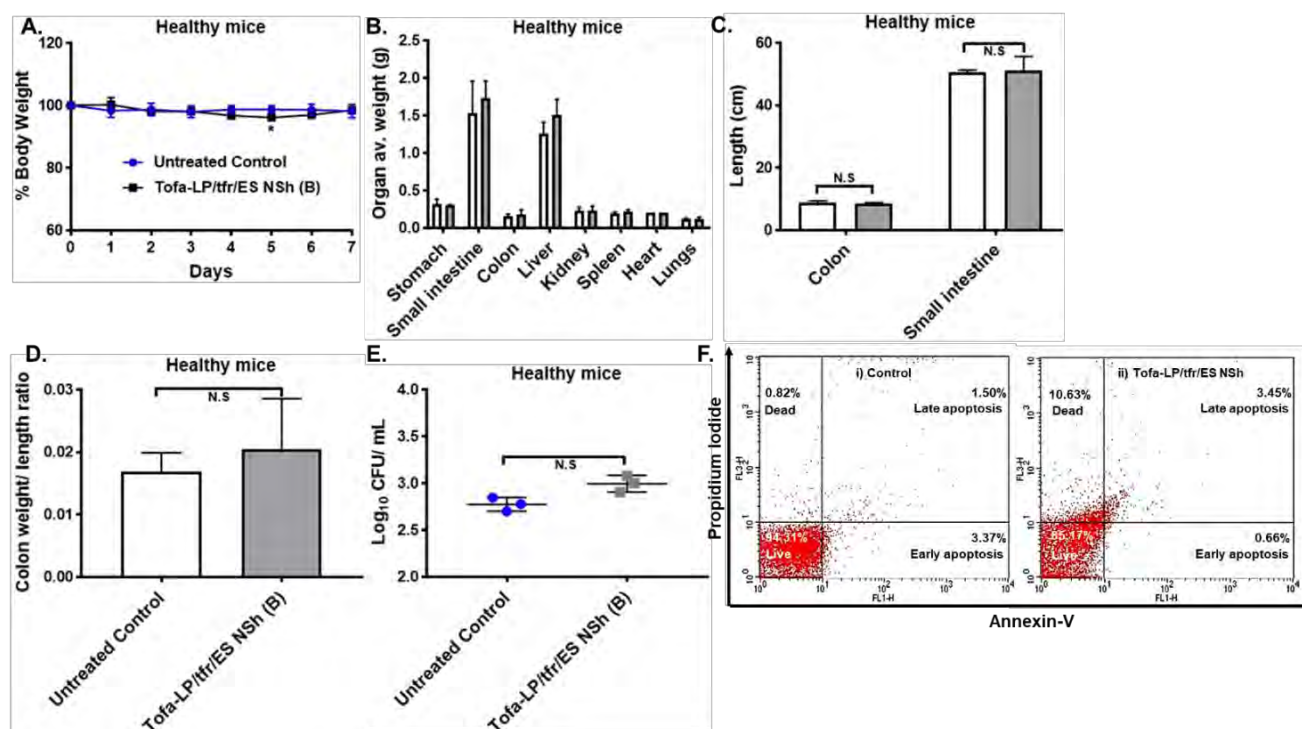


Figure 3. 47: In vivo biocompatibility evaluation of Tofa-LP/tfr/ES NSh through morphological, microbial, and apoptotic parameters; % Body weight (A), Weight of vital organs (B), Intestinal length (C), Colon weight to length ratio (D), Fecal microbial content (E) and Colon apoptosis by the nanoformulation using Annexin-V and PI dyes after 7-day administration to the healthy mice (n=3)

PART-III

TAC-P/Lys NCs and TAC-P/Lys/ES-L100 NCs

3.34. Preparation and Optimization of TAC-P/Lys NCs and TAC- P/Lys/ES-L100 NCs

HPLC calibration curve of TAC was developed under standard conditions with linearity ($R^2=0.995$) and robustness (Figure 3. 48).

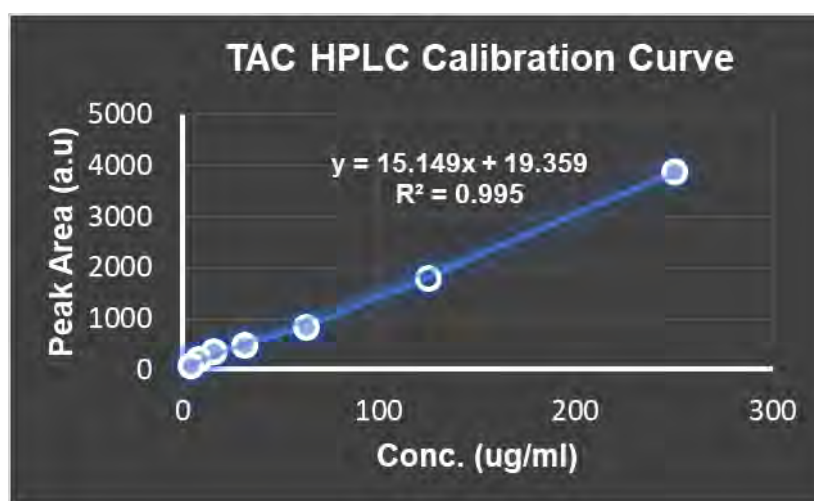


Figure 3. 48: HPLC Calibration Curve of TAC

The process parameters including probe sonication time, surfactant concentrations and ES100-EL100 ratios were the most influencing on particle size. Probe sonication for 90 seconds had reduced particle size with enough shear stress, 2% PVA surfactant produced desired size distribution and further increase in concentration increased the size. ES100-EL100 1:1 ratio dissolved reasonably in the solvent and worked best for coating, other ratio disturbed stability. That's why these parameters were kept fixed and nanocarriers were developed by using these ranges.

The obtained TAC-P/Lys NCs and TAC- PLGA/Lys/ES-L100 NCs have a particle size of $108.3 \text{ nm} \pm 0.964 \text{ nm}$ and $240.4 \text{ nm} \pm 4.586 \text{ nm}$, respectively (Figure 3. 49 I-III). The pH-sensitive coat increases the size, but it is still $<300 \text{ nm}$ which is necessary for uptake by the cells (Zeeshan *et al.*, 2019a). Additionally, the coat disintegrates at colonic pH, exposing the underneath core with diminished size. The zeta potential of TAC-P/Lys NCs was negative, while TAC-P/Lys/ES-L100 have a more negative potential of $-29.2 \text{ mV} \pm 0.935 \text{ mV}$ (Figure 3. 49 I-III), because of the anionic Eudragit

S/L mixture with free carboxyl groups that makes the surface more negatively charged. Since particles repel due to more ionic charge, therefore, it facilitates towards more stable nanosuspension. The PDI of both formulations complied with the range of monodispersed homogeneously distributed nanocarrier (Figure 3. 49 III). Further, the SEM and TEM analysis indicated the homogenous distributed, spherical-shaped, smooth surface topology of both nanocarriers. The ES-L100 coated formulation has a more whitish tinge on the outside than the interior of the particles, indicating the presence of a coat (Figure 3. 49 IV-V). The encapsulation efficiency of TAC-P/Lys NCs and TAC- PLGA/Lys/ES-L100 NCs was found to be $89.07\% \pm 4.76\%$ and $92.26\% \pm 0.021\%$ (Figure 3. 49 VI), and the drug content was $59.38 \mu\text{g}/\text{mg} \pm 3.18 \mu\text{g}/\text{mg}$ and $26.36 \mu\text{g}/\text{mg} \pm 0.06 \mu\text{g}/\text{mg}$, respectively (Figure 3. 49 VI). DSC thermogram of drug-loaded nanocarriers demonstrated thermal stability over a range of temperature from -10°C to 220°C . The drug had a sharp melting point at 130°C , which indicated its crystalline nature. The peak was absent in the drug-loaded nanocarriers because of the conversion of the drug into an amorphous form inside the nanocarriers (Figure 3. 49 VII).

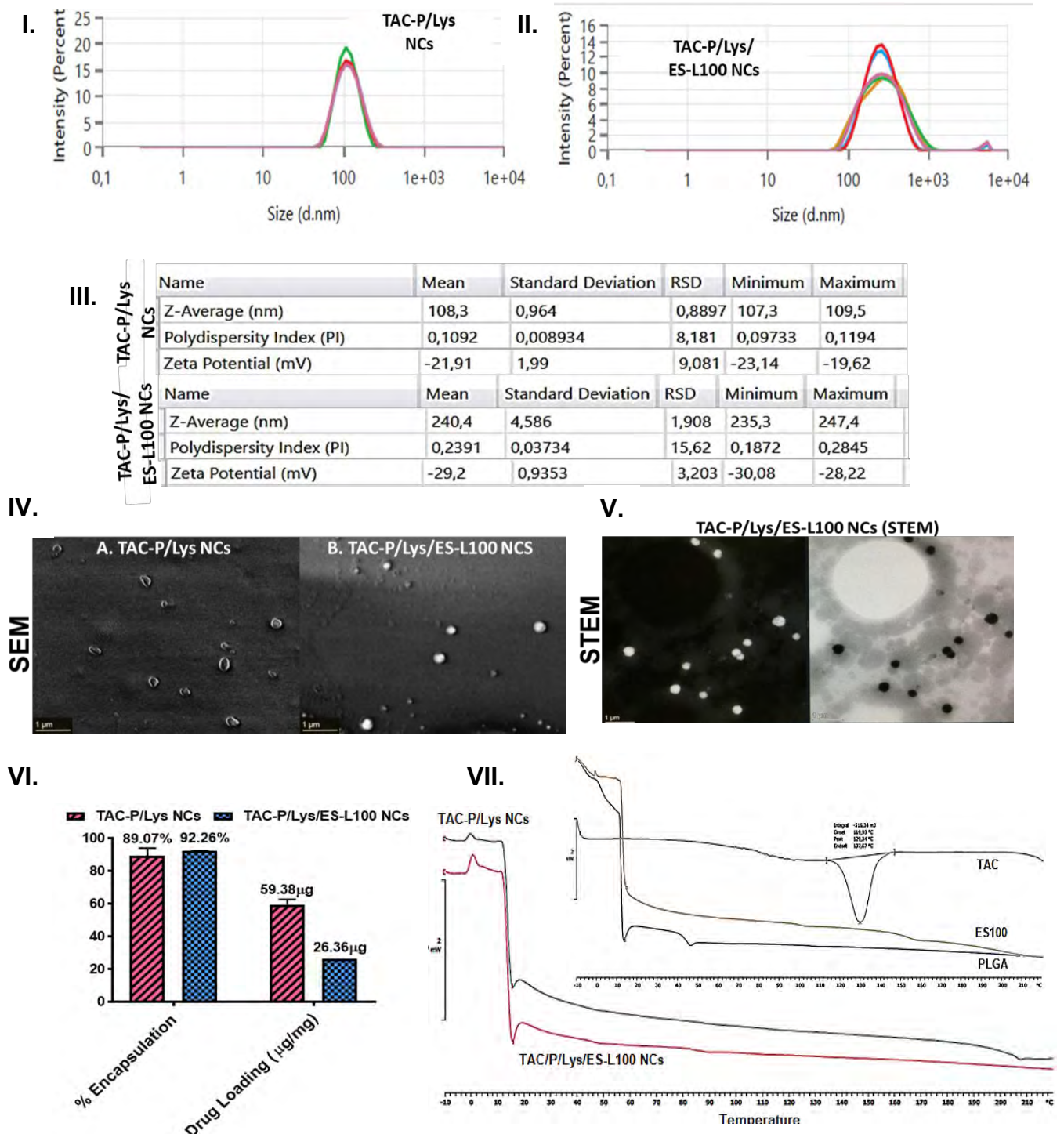


Figure 3. 49: Physicochemical properties of TAC-P/Lys NCs and TAC-P/Lys/ES-L100 NCs (mean \pm SD, n=3); I: Particle size of TAC-P/Lys NCs, II: Particle size of TAC-P/Lys/ES-L100 NCs, III: Physicochemical parameters of TAC loaded nanocarriers, IV: SEM images of TAC-P/Lys NCs (A) and TAC-P/Lys/ES-L100 NCs (B), V: STEM images of TAC-P/Lys/ES-L100 NCs, VI: % Encapsulation and drug loading of nanocarriers, VII: DSC thermograms of drug (TAC), excipients and nanocarriers

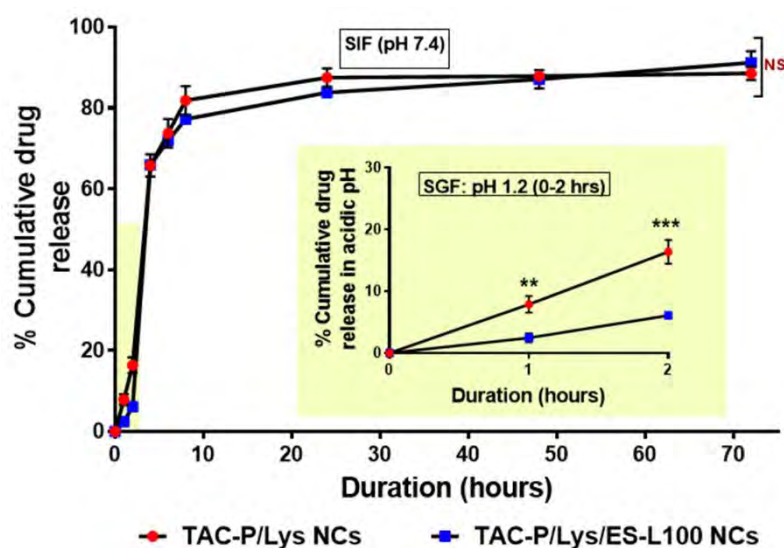


Figure 3. 50: In vitro drug release of TAC-P/Lys NCs and TAC-P/Lys/ES-L100 NCs in SGF at pH 1.2 and SIF at pH 7.4

3.35. Drug Release Studies and Kinetics

In vitro drug release studies of TAC-P/Lys NCs and TAC-P/Lys/ES-L100 NCs were performed at SGF (pH 1.2) and SIF (pH 7.4), according to the physiological pH values and our rationale. TAC-P/Lys NCs have retarded burst release of drug at pH 1.2, as exhibited by TAC-PLGA NCs. L-Lysine adsorption has controlled the release rate, therefore, it aided against stomach degradation of the drug (Figure 3. 50). Further, TAC-P/Lys/ES-L100 NCs have dual pH-sensitive polymers that induced more control over drug release at acidic pH. The burst release effect at pH 1.2 was more lessened by TAC-P/Lys/ES-L100 NCs than without ES-L100 coat (Figure 3. 50). The combination of pH-sensitive polymers in the nanocarriers prevented offsite targeting in other regions of GIT. The drug release in SIF (pH 7.4) from both nanocarriers was parallel to each other with a sustained release character (Figure 3. 50).

The drug release kinetics indicated that TAC-P/Lys NCs followed the Korsmeyer-Peppas model at pH 1.2 and pH 7.4. The mode of drug release was non-Fickian diffusion ($n > 0.5$) at pH 1.2 and Fickian diffusion ($n < 0.5$) at pH 7.4 (Table 3.26). TAC-P/Lys/ES-L100 NCs were best fitted to Korsmeyer-Peppas at pH 1.2 and pH 7.4, respectively. The n -value indicated non-Fickian diffusion of drug release at pH 1.2 and

Fickian diffusion at pH 7.4 to be the mechanism of drug release from TAC-P/Lys/ES-L100 NCs (Table 3.26)

Table 3. 26: Drug release kinetic modeling of TAC-P/Lys NCs and TAC-P/Lys/ES-L100 NCs at pH 1.2 and 7.4

| TAC-P/Lys NCs (pH 1.2; 0-2 hours) | | | | | | TAC-P/Lys NCs (pH 7.4; 2-72 hours) | | | | |
|---|-----------------------|-----------------------|------------------------|----------------------------------|------------------------|--|-----------------------|------------------------|----------------------------------|------------------------|
| Parameter | Zero order | First order | Higuchi | Korsmeyer-peppas | Hixon-Crowell | Zero order | First order | Higuchi | Korsmeyer-peppas | Hixon-Crowell |
| R_{obs-pre} | 0.9998 | 0.9989 | 0.967 | 1.000 | 0.993 | 0.545 | 0.987 | 0.74 | 0.9921 | 0.76 |
| Rsqr | 0.9994 | 0.9974 | 0.932 | 1.000 | 0.984 | -1.573 | 0.924 | -0.0102 | 0.9843 | 0.044 |
| RMSE | 0.195 | 0.419 | 2.138 | 0.000 | 0.383 | 50.90 | 8.75 | 31.89 | 4.3619 | 31.036 |
| AIC | -5.74 | -1.145 | 8.64 | Perfect fit | -1.685 | 69.56 | 44.91 | 63.02 | 35.89 | 62.63 |
| MSC | 6.145 | 4.615 | 1.353 | Perfect fit | 2.924 | -2.82 | 0.7014 | -1.885 | 1.99 | -1.83 |
| Other | k ₀ =8.138 | k ₁ =0.088 | k _H =10.359 | k _{Kp} =7.89, n=1.055 | K _{hc} =0.029 | k ₀ =1.719 | k ₁ =0.236 | k _H =14.402 | k _{Kp} =63.859, n=0.084 | K _{hc} =0.021 |
| TAC-P/Lys/ES-L100 NCs (pH 1.2; 0-2 hours) | | | | | | TAC-P/Lys/ES-L100 NCs (pH 7.4; 2-72 hours) | | | | |
| Parameter | Zero order | First order | Higuchi | Korsmeyer-peppas | Hixon-Crowell | Zero order | First order | Higuchi | Korsmeyer-peppas | Hixon-Crowell |
| R_{obs-pre} | 0.994 | 0.9931 | 0.942 | 1.0000 | 0.993 | 0.593 | 0.982 | 0.7757 | 0.9979 | 0.7825 |
| Rsqr | 0.986 | 0.9836 | 0.88 | 1.0000 | 0.984 | -1.416 | 0.902 | 0.09 | 0.9959 | 0.1139 |
| RMSE | 0.364 | 0.3918 | 1.060 | 0.000 | 0.383 | 48.67 | 9.800 | 29.8 | 2.1988 | 29.478 |
| AIC | -1.983 | -1.5427 | 4.430 | -203.94 | -1.685 | 65.73 | 46.49 | 62.097 | 26.296 | 61.914 |
| MSC | 3.024 | 2.876 | 0.886 | 70.344 | 2.924 | -2.345 | 0.476 | -1.753 | 3.3617 | -1.7265 |
| Other | k ₀ =2.929 | k ₁ =0.03 | k _H =3.693 | k _{Kp} =2.4681, n=1.302 | K _{hc} =0.01 | k ₀ =1.460 | k ₁ =0.221 | k _H =14.289 | k _{Kp} =60.319, n=0.098 | K _{hc} =0.021 |

3.36. In Vitro Cell-Based Studies

3.36.1. Caco-2 viability assay with 7-AAD and PI staining

To elucidate the toxicity potential of TAC-P/Lys NCs and TAC-P/Lys/ES-L100 NCs on Caco-2 cells, the cell viability assays with 7-AAD and PI were performed. After 6 hours of incubation, TAC-P/Lys NCs and TAC-P/Lys/ES-L100 NCs have Caco-2 viability of about 90.3% and 91.6% with 7-AAD dye; and about 92.3% and 93.4% with PI dye, respectively (Figure 3.51 I). Only viability dye (7-AAD or PI) treated cells served as a positive control, while untreated cells as a negative control. Thus, the nanocarriers proved to be non-toxic and biocompatible with the cells. After 24 hours of incubation, TAC-P/Lys NCs had the caco-2 viability of about 90.3% and TAC-P/Lys/ES-L100 NCs had 91.6% cellular viability, as assessed by the 7-AAD dye. The

PI dye test additionally confirmed the findings, with 92.3% and 93.4% viable caco-2 cells on 24 hours incubation with TAC-P/Lys NCs and TAC-P/Lys/ES-L100 NCs, respectively (Figure 3.51 II).

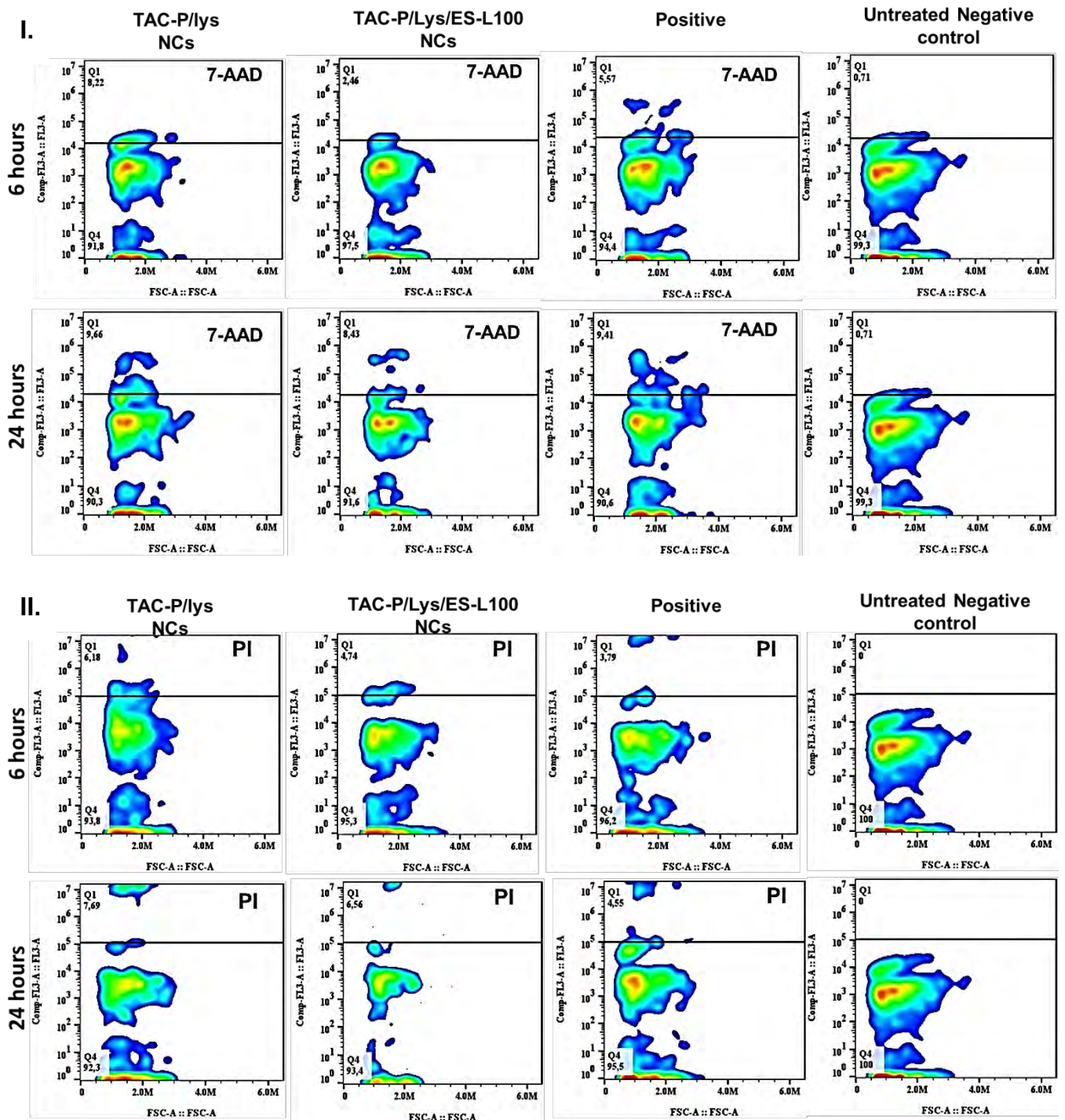


Figure 3. 51: Effect of TAC loaded nanocarriers on caco-2 viability after 6 and 24 hours of incubation using 7-AAD (I) and PI (II) dyes

3.36.2. Caco-2 uptake

Coumarin-6 dye-loaded nanocarriers were prepared and assessed for the uptake potential by the Caco-2 cells. The cellular internalization of TAC-P/Lys NCs and TAC-P/Lys/ES-L100 NCs was pronounced with mean fluorescence intensity of about 140.56 a.u. \pm 43.09 a.u. ($p < 10^{-5}$ *****) and 105.37 a.u. \pm 30.78 a.u. ($p < 10^{-5}$ *****), compared to the plain dye (43.52 a.u. \pm 6.15 a.u.) (Figure 3. 52 I). Therefore, both nanocarriers can retain at the colon inflamed tissue due to extensive uptake by the cells. However, TAC-P/Lys NCs ($p < 0.01$ ^^) have more uptake than TAC-P/Lys/ES-L100 NCs (Figure 3. 52 I), because of their comparatively lower size.

3.36.3. Macrophage uptake studies

THP-1 monocytes were successfully converted into macrophages, as evident from morphology and expression of surface markers. Both TAC-P/Lys NCs and TAC-P/Lys/ES-L100 NCs were predominantly engulfed by the macrophages, emitting mean fluorescence intensity of 93.36 a.u. \pm 37.44 a.u. ($p < 10^{-5}$ *****), and 99.35 a.u. \pm 30.97 a.u. ($p < 10^{-5}$ *****), respectively after 2 hours of incubation (Figure 3. 52 II). The two groups of nanocarriers have an insignificant difference in the uptake by the macrophages (Figure 3. 52 II).

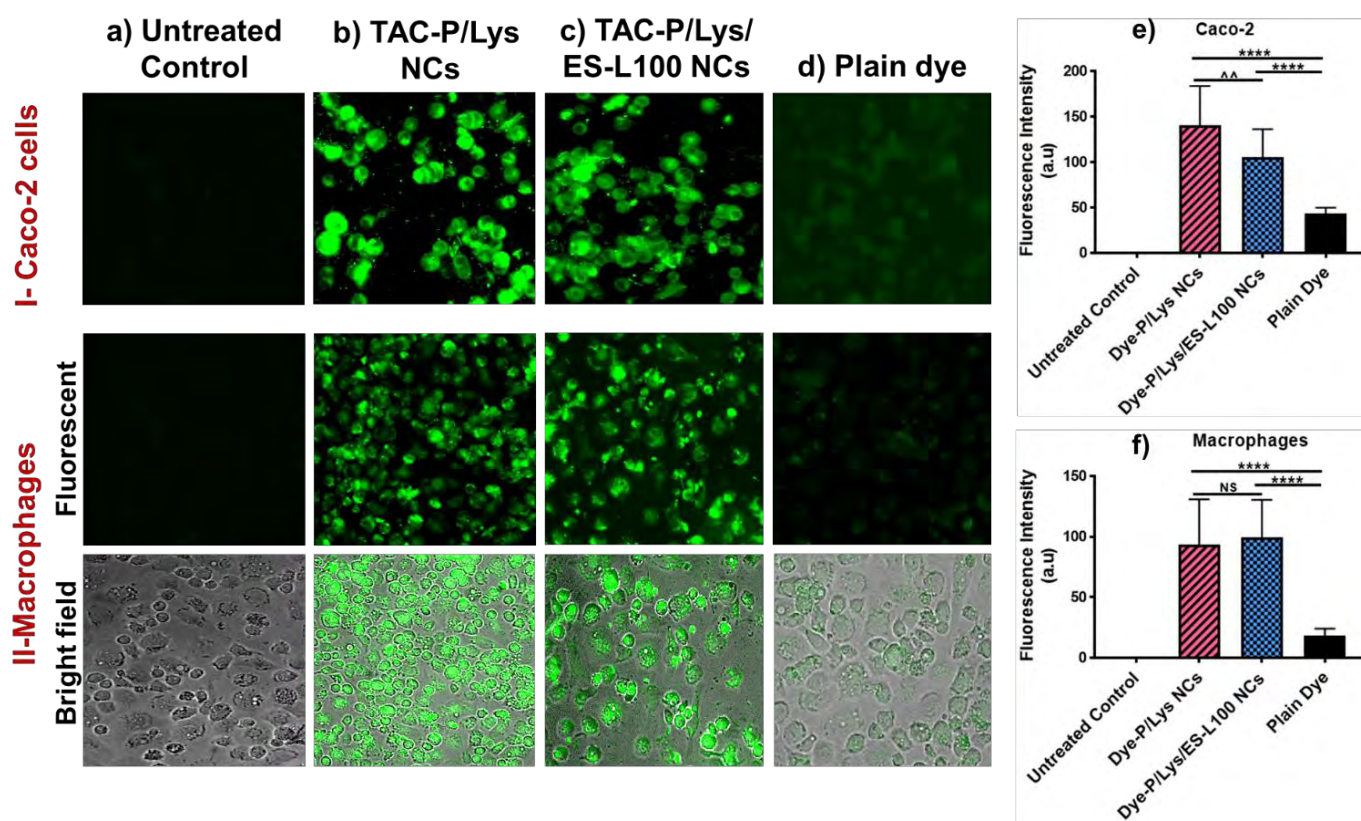


Figure 3. 52: TAC based nanocarriers uptake by Caco-2 cells (I) and THP-1 derived macrophages (II)

3.37. Animal Studies

OXA induced colitis model was considered because it is a T helper cell type 2 (Th2) mediated process. Stimulated T-cells produced abundant cytokines that exacerbate inflammation. Since TAC is a T-cell suppressor drug, therefore, this model is suitable for the study of the therapeutic effects of the drug and its nanocarriers.

3.37.1. Development of OXA-induced colitis and Therapeutic evaluation of nanocarriers through morphological indices

Mice were experimentally divided into 5 groups. The first one was the normal control, the second was OXA-colitis with no treatment, and the last three groups were treated with TAC, TAC-P/Lys NCs, and TAC-P/Lys/ES-L100, respectively. The experimental study design is depicted in Figure 3.53 I. To assess the degree of inflammation during therapy, a mini endoscopy was performed to assess the inflammation indices like diarrhea, rectal bleeding, mucus production, angiogenesis, etc. on a wide window. The MEICS score was based on the inflammation indices, mentioned in Table 2. 8. OXA-colitis have excessive mucous production, granularity, translucency, etc. (Figure 3.53 II), with a significantly higher MEICS score than the normal control (9.5 ± 0.7 vs $1.0 \pm$

1.0, $p < 0.01###$, Figure II-III). TAC reduced the score up to 6 ± 3 , but not significantly ($p = \text{NS}$) (Figure 3.53 II-III). While TAC-P/Lys NCs and TAC-P/Lys/ES-L100 significantly declined the disease severity and inflammation indices to MEICS score of 4.25 ± 0.96 ($p < 0.01**$) and 3.25 ± 1.66 ($p < 0.01**$), respectively (Figure 3.53 II-III). The bodyweight of the mice was monitored from day 1-5 of the treatment. We have noticed that OXA-colitis mice continuously lose weight till the third day after induction and slightly gained weight on the 4th day (Figure 3.53 IV). Therefore, we have euthanized all the mice groups on the 4th day. While treatment with TAC drug, TAC-P/Lys NCs and TAC-P/Lys/ES-L100 have an initial weight decline which was stabilized afterward with the weight recovery of up to $88.92\% \pm 3.65\%$ ($p = \text{NS}$), $89.97\% \pm 3.78\%$, ($p < 0.05*$) and $90.98\% \pm 2.26\%$ ($p < 0.05*$), respectively, at the end of the experiment (Figure 3.53 IV). The MEICS and body weight loss were resumed by TAC-P/Lys/ES-L100 greater than the counterpart treatments. Both nanocarriers worked better than the plain drug. And ES-L100 coated nanocarriers proved to be superior in recovering the MEICS and body weight than uncoated nanocarriers (Figure 3.53 II-IV).

Colon length was decreased by OXA induction ($p < 0.05\#$ vs normal) (Figure 3.53 V-VI). TAC restored the length up to $7.50 \text{ cm} \pm 0.71 \text{ cm}$ ($p = \text{NS}$), TAC-P/Lys NCs up to $7.75 \text{ cm} \pm 0.957 \text{ cm}$ ($p < 0.05*$) and TAC-P/Lys/ES-L100 NCs up to $8.5 \text{ cm} \pm 0.5 \text{ cm}$ ($p < 0.05*$) (Figure 3.53 V-VI). Therefore, colon weight to length ratio, disturbed by colitis ($p < 0.01###$ vs normal), was regained towards normality by the treatment groups, in the order TAC-P/Lys/ES-L100 NCs > TAC-P/Lys NCs > TAC drug (Figure 3.53 VII).

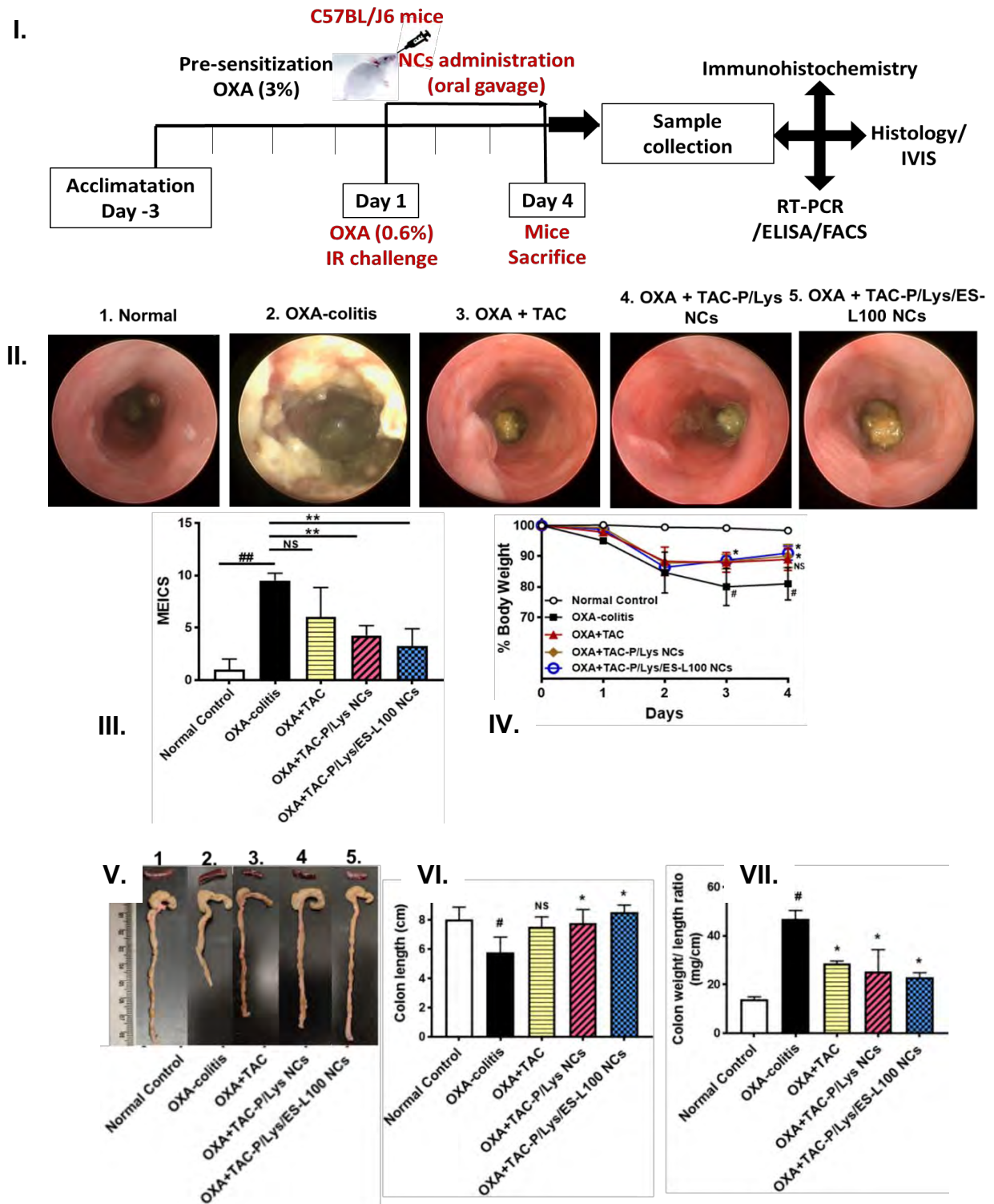


Figure 3. 53: Therapeutic evaluation of TAC nanocarriers in the OXA-colitis mice through endoscopic and morphological parameters; I. Scheme of experimental design, II. Endoscopic evaluation of colon for the assessment of inflammation, III. MEICS score, IV. Body weight of mice during induction and treatment, V-VI. colon length and VII. Colon weight to length index (n=4/group)

3.37.2. Histopathological analysis

The exacerbation of inflammation in OXA induced mice led to damage of colon crypts, compromised epithelial membrane integrity, recruited immune cells burdened the tissue with heavy payloads of pro-inflammatory markers and mediators. All the tissue damage can be visualized through histological observations (Figure 3. 54 I). The normal control had preserved tissue architecture. The OXA-colitis mice have the highest histological score (11.33 ± 0.19 , $p < 0.001####$), compared to the lowest score of normal control (0.67 ± 0.193 , Figure 3. 52 I-II).

Histological analysis of mice from TAC, TAC-P/Lys NCs and TAC-P/Lys/ES-L100 have the cumulative histo-scores of 7.33 ± 0.38 ($p < 0.01**$), 5.67 ± 0.19 ($p < 0.001***$), and 4.67 ± 0.38 ($p < 0.001***$), respectively (Figure 3. 52 I-II). Both nanocarriers restored inflammation severity greater than the plain drug.

The healing was more prominent with ES-L100 nanocarriers than the other groups. The TAC-P/Lys/ES-L100 NCs treatment had recovered the histological features and mucosal distortions towards the normal. Thus, it pleaded the point that the enteric coat delivered more amount of drug specifically to the colon and restored the inflammation associated damage.

The histological features of the small intestine have a mild effect of colitis, while the stomach remains unaffected (Figure 3. 52 III-IV). Therefore, treatment groups have a negligible effect on the small intestine and stomach (Figure 3. 52 III-IV).

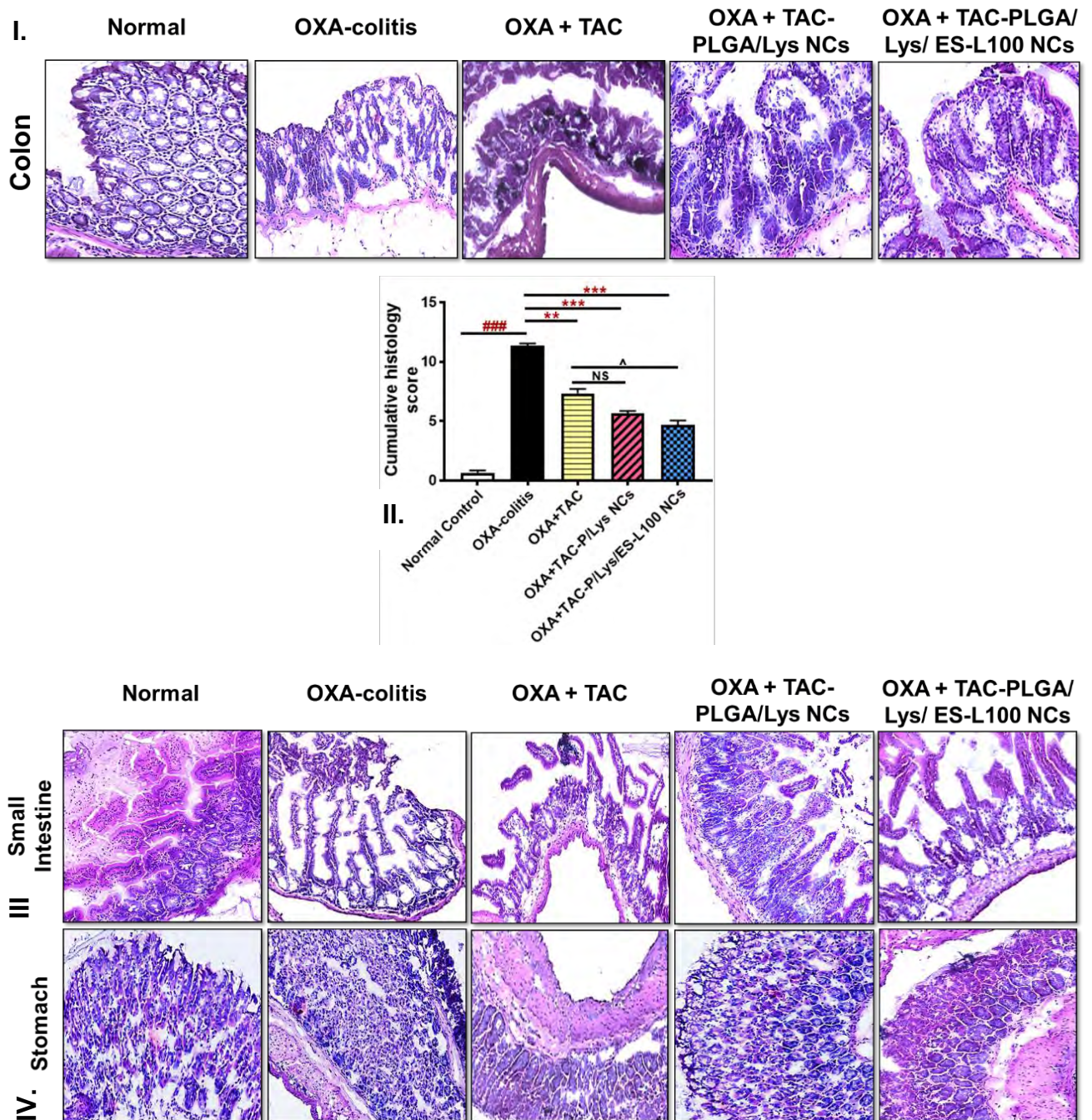


Figure 3. 54: Histopathological investigation of OXA-colitis group and the treatment groups; I. Colon, II. Colon histoscore, III. Small intestine, IV. Stomach

3.37.3. IVIS imaging to assess myeloperoxidase (MPO) activity

MPO is a heme-containing peroxidase enzyme and has a progressive role in the initiation and progression of inflammation. It is abundantly present in the granulocytes, mostly expressed in the neutrophils, therefore, it regulated neutrophil function. MPO catalyzed the reactions generating reactive oxygen species that aggravate the inflammation (Aratani, 2018). Here, we have elucidated MPO activity, as a marker of

neutrophil infiltration that increased during inflamed conditions. The live mice imaging to detect MPO levels using IVIS is a unique alternative to existing methods (Ali *et al.*, 2014). Injected luminol is a redox-sensitive dye, which emitted blue luminescence (wavelength= 425 nm) on exposure to the oxidizing agent. IVIS imaging detected bioluminescence signals of oxidative species from mice of each group. The scale of luminescence demonstrated the intensity of the signals and inflammation (Figure 3.55). The highest signal was received from the OXA-colitis group that indicated colitis severity (Figure 3.5. The mice treated with plain TAC have comparatively lesser signals than OXA-colitis, which is a sign of little healing. Whereas very weak luminescence was detected from TAC-P/Lys NCs and TAC-P/Lys/ES-L100 NCs treated mice (Figure 3.55) indicating lowered MPO activity. Both nanocarriers were efficient in combating MPO levels and free oxidative species that in turn revealed lesser granulocyte in the colon and amelioration of colon inflammation.

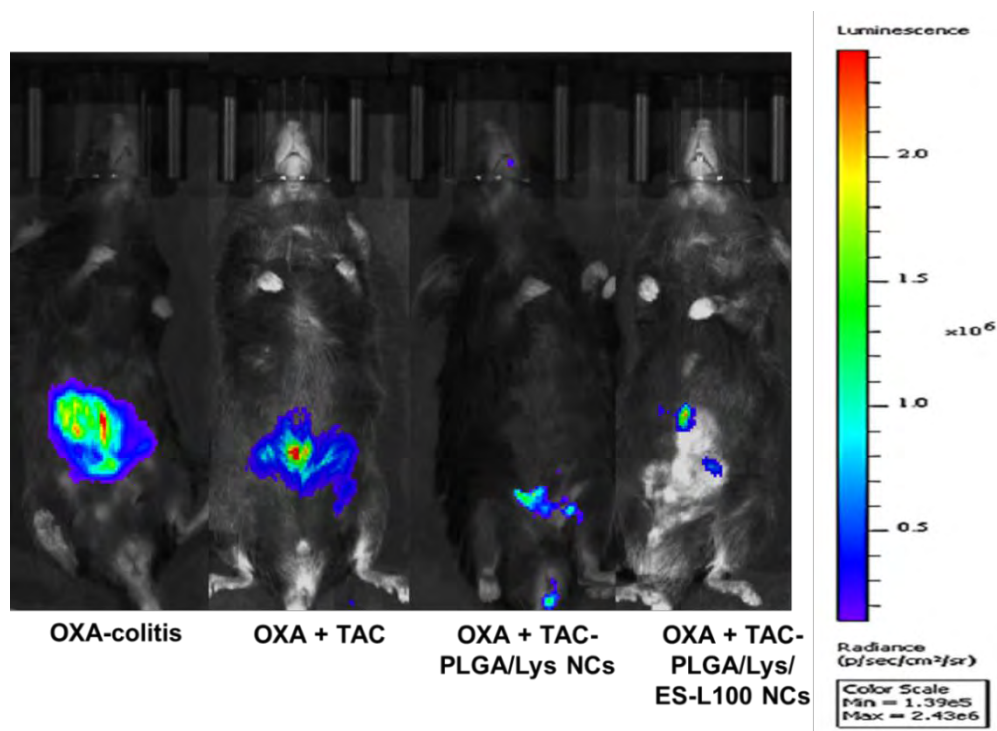


Figure 3. 55: Effect of TAC based nanocarriers on the MPO activity in the OXA-colitis, assessed by IVIS system

3.37.4. Evaluation of treatment mediated pITK suppression to mediate protection against OXA-colitis by Immunohistochemistry and flowcytometry

ITK plays a major role in inflammation and auto-immune disorder (Lechner *et al.*, 2020). TAC being an immunosuppressive drug mediates its action through calcineurin

and NFATc inhibition and T-cell suppression (Wu *et al.*, 2020). In the T-cells, ITK is activated to phosphorylated ITK (pITK) by T-cell receptor signaling and Lck (Lechner *et al.*, 2021). pITK activated several inflammatory pathways like MAPK, NF- κ B, NFATc, etc. (Gallagher *et al.*, 2020).

In the previous study, the OXA-colitis model demonstrated elevated mRNA levels of ITK and active production of pITK by the mucosal CD4⁺ T-cells (Lechner *et al.*, 2021). Here, we have assessed pITK expression levels in the T-cells of the colon and spleen to know OXA-induced disease activity and the drug action.

Colon tissues were stained for CD3⁺ T-cells (green) and pITK (red) and with DAPI to locate cellular nuclei through immunohistochemistry (Figure 3. 56 I). The OXA-colitis expressed heavy levels of pITK in the colon tissues and CD3⁺pITK⁺ cells i.e., the T-cells with pITK expression. The expression of both pITK⁺ colon cells and CD3⁺pITK⁺ cells was decreased by all treatment groups (Figure 3. 56 I-II). Oxa-colitis have about 54 ± 6.56 CD3⁺pITK⁺ cells (Figure 3. 56 I-II). While TAC, TAC-P/Lys NCs and TAC-P/Lys/ES-L100 NCs declined CD3⁺pITK⁺ cells to 13.67 ± 2.52 ($p < 0.01^{**}$), 8.67 ± 2.08 ($p < 0.001^{***}$) and 6.67 ± 1.53 ($p < 0.001^{***}$), respectively (Figure 3. 56 I-II). TAC-P/Lys/ES-L100 NCs significantly differed from plain TAC ($p < 0.05^{\wedge}$), while TAC-P/Lys NCs have insignificant differences with the plain drug ($p = \text{NS}$). The two types of nanocarriers did not have statistically significant differences.

Further, the CD4⁺ T-cells were harvested from the spleen of all experimental groups and run under flowcytometer. The OXA-colitis group had markedly increased levels of CD4⁺pITK⁺ cells ($p < 0.001^{##}$ vs normal, Figure 3. 56 III-IV). TAC treatment reduced the levels of CD4⁺pITK⁺ cells ($p < 0.05^*$), while CD4⁺pITK⁺ cells were more significantly lowered by TAC-P/Lys NCs ($p < 0.01^{**}$) and TAC-P/Lys/ES-L100 NCs ($p < 0.001^{**}$), respectively (Figure 3. 56 III-IV).

The efficiency of TAC-P/Lys NCs and TAC-P/Lys/ES-L100 NCs in leveling the pITK expressions in the T-cells is prominent from these experiments (Figure 3. 56). Thus, we can say that the action of TAC inside the nanocarriers was enhanced by safe and site-directed delivery of the drug to the inflamed tissues.

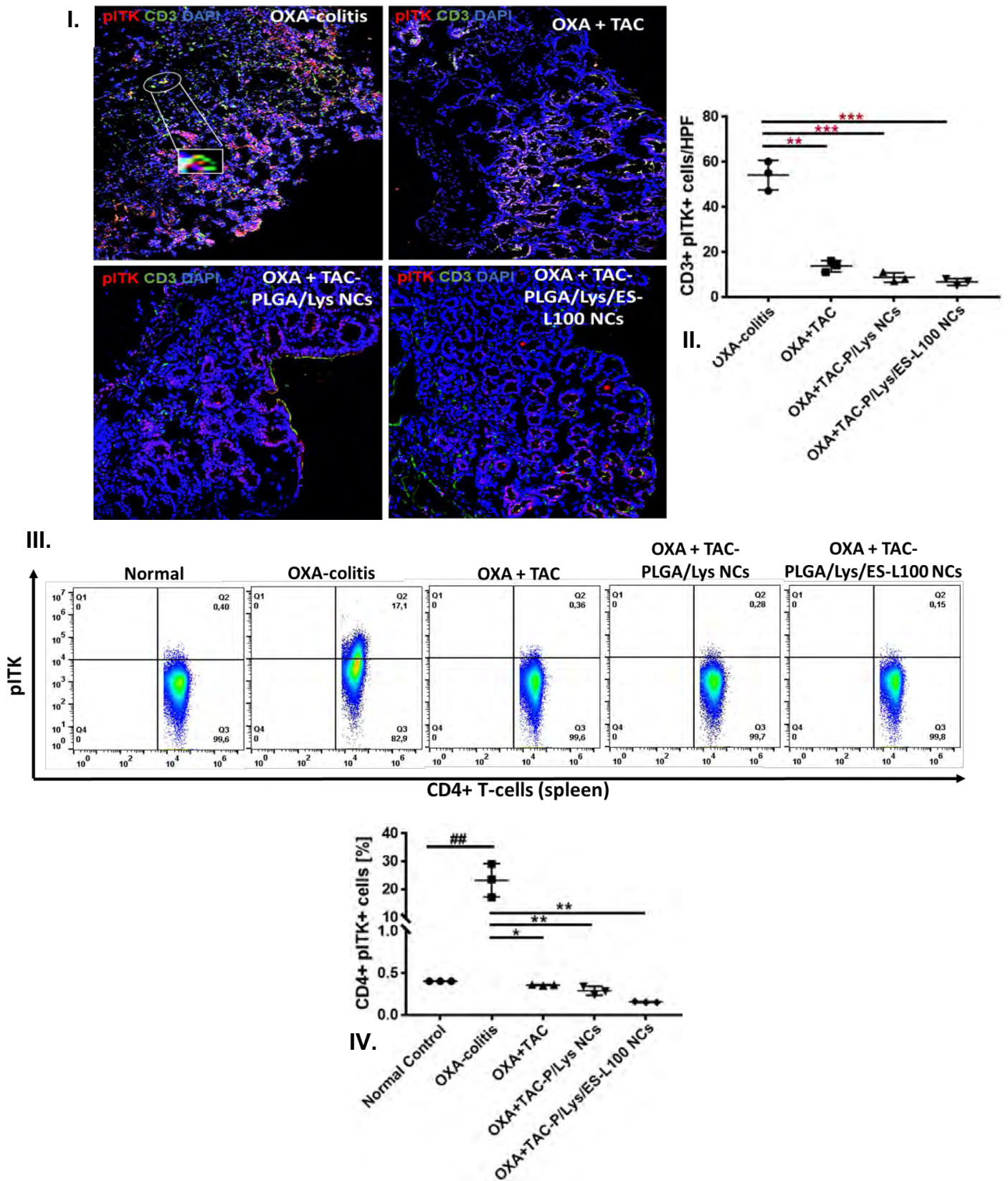


Figure 3. 56: Evaluation of inflammatory mediator pITK in the T-cells through immunoreactivity and flowcytometry; I. Immunohistochemistry images, II. Immunoreactivity score (CD3+pITK+ cells), III. Flowcytometry and IV. FACS score (CD4+pITK+) for pITK expression

3.37.5. Investigation of RT-PCR expression of inflammatory proteins and epithelial barrier proteins and ELISA for pro-Inflammatory mediator analysis

TAC worked by binding to intracellular immunophilin, and this complex inhibits calcineurin. Calcineurin is involved in the regulation of nuclear factor of activated T-cells (NFATc), which relocates to the nucleus and increased the expression of IL-2 producing genes. TAC inhibits the dephosphorylation of NFATc-1 and thus retarded T-cells signal transduction and IL-2 transcription and several cytokines production (Wu *et al.*, 2020; Murakami *et al.*, 2021; Bendickova *et al.*, 2017). Calcineurin also activates NF- κ B, therefore its inhibition retarded NF- κ B activation. Further, inhibition of T-cell receptor signaling, in turn, decreases activation or phosphorylation of ITK. pITK driven NF- κ B and NFATc activations were further minimized (Lechner *et al.*, 2021; Gallagher *et al.*, 2020).

OXA-colitis have the highest expression of pITK ($p < 0.001###$, Figure 3. 57 A), NFATc-1 ($p < 0.01##$, Figure 3. 57 B) and NF- κ B ($p < 0.001###$, Figure 3. 57 C), compared to the normal controls. TAC declined pITK ($p < 0.001***$), NFATc-1 ($p < 0.01**$) and NF- κ B ($p < 0.01**$) (Figure 3. 57 A-C), when treated OXA induced mice. TAC-P/Lys NCs reduced the expression of pITK ($p < 0.001***$), NFATc-1 ($p < 0.01**$) and NF- κ B ($p < 0.001***$) (Figure 3. 57 A-C). And TAC-P/Lys/ES-L100 NCs lowered the levels of pITK ($p < 10^{-5}****$, Figure 3. 57 A), NFATc-1 ($p < 10^{-5}****$, Figure 3. 57 B) and NF- κ B ($p < 10^{-5}****$, Figure 3. 57 C), significantly. The ES-L100 coated nanocarriers proved to be colon-specific drug delivery, therefore, pronouncedly recovered the levels of pITK, NFATc-1, and NF- κ B more than the plain TAC and TAC-P/Lys NCs.

Ocln-1 is a tight junction protein that regulates the integrity of the colon epithelial cell membrane. Inflammation compromised barrier integrity and thus downregulated the levels of ocln-1 in humans (Yamamoto-Furusho *et al.*, 2012). However, animal OXA models have a little discussion about this topic, as per our knowledge. Here we observed that normal colons have a higher expression of ocln-1 proteins (Figure 3. 57 D). The colitis induction with OXA declined ocln-1 levels but was not significant ($p = \text{NS}$ vs control, Figure 3. 57 D). All treatment groups either the plain drug or nanocarriers leveled up ocln-1, but not to a significant extent ($p = \text{NS}$, Figure 3. 57 D).

In OXA induced colitis, enhanced activity of Th2 cells results in a burst of cytokines (Boirivant *et al.*, 1998). The storm of pro-inflammatory cytokines was counterbalanced by the enormous production of transforming growth factor (TGF- β) (Feagins, 2010). The RT-PCR analysis demonstrated the up-regulation of TGF- β in the colon tissues of the OXA-colitis group, the levels were markedly higher than the normal control ($p < 0.001###$, Figure 3. 57 E). TGF- β was significantly downregulated by TAC ($p < 0.01**$), TAC-P/Lys NCs ($p < 0.01**$) and much more decreased by TAC-P/Lys/ES-L100 NCs ($p < 0.001***$) (Figure 3. 57 E). It was reported that TAC mechanistically decreased TGF- β levels by the SMAD signaling pathway (Ren *et al.*, 2020).

Next, VEGF-A is an essential mediator for angiogenesis. Since compromised endothelial integrity and angiogenesis are the major hallmarks in colitis (Mateescu *et al.*, 2017), therefore we have assessed the expression of VEGF-A in the experimental groups. The colitis group had a higher amount of VEGF-A ($p < 0.001###$) than the normal (Figure 3. 57 F). TAC has decreased VEGF-A levels ($p < 0.01**$), while protein expression was predominantly lessened by TAC-P/Lys NCs ($p < 0.001***$) and TAC-P/Lys/ES-L100 NCs ($p < 0.001***$) treatments (Figure 3. 57 F). The VEGF-A and angiogenesis may be lowered because of alleviation of inflammation or because of anti-VEGF action of TAC or TAC-loaded nanocarriers (Chen *et al.*, 2018).

IL-6 is a major pro-inflammatory cytokine, the levels increased in OXA-colitis mice ($p < 0.01##$ vs Normal, Figure 3. 57 G). Treatment groups, TAC-P/Lys NCs ($p < 0.001***$) and TAC-P/Lys/ES-L100 NCs ($p < 0.001***$) declined IL-6 levels significantly (Figure 3. 57 G) that indicated recovery from inflammation.

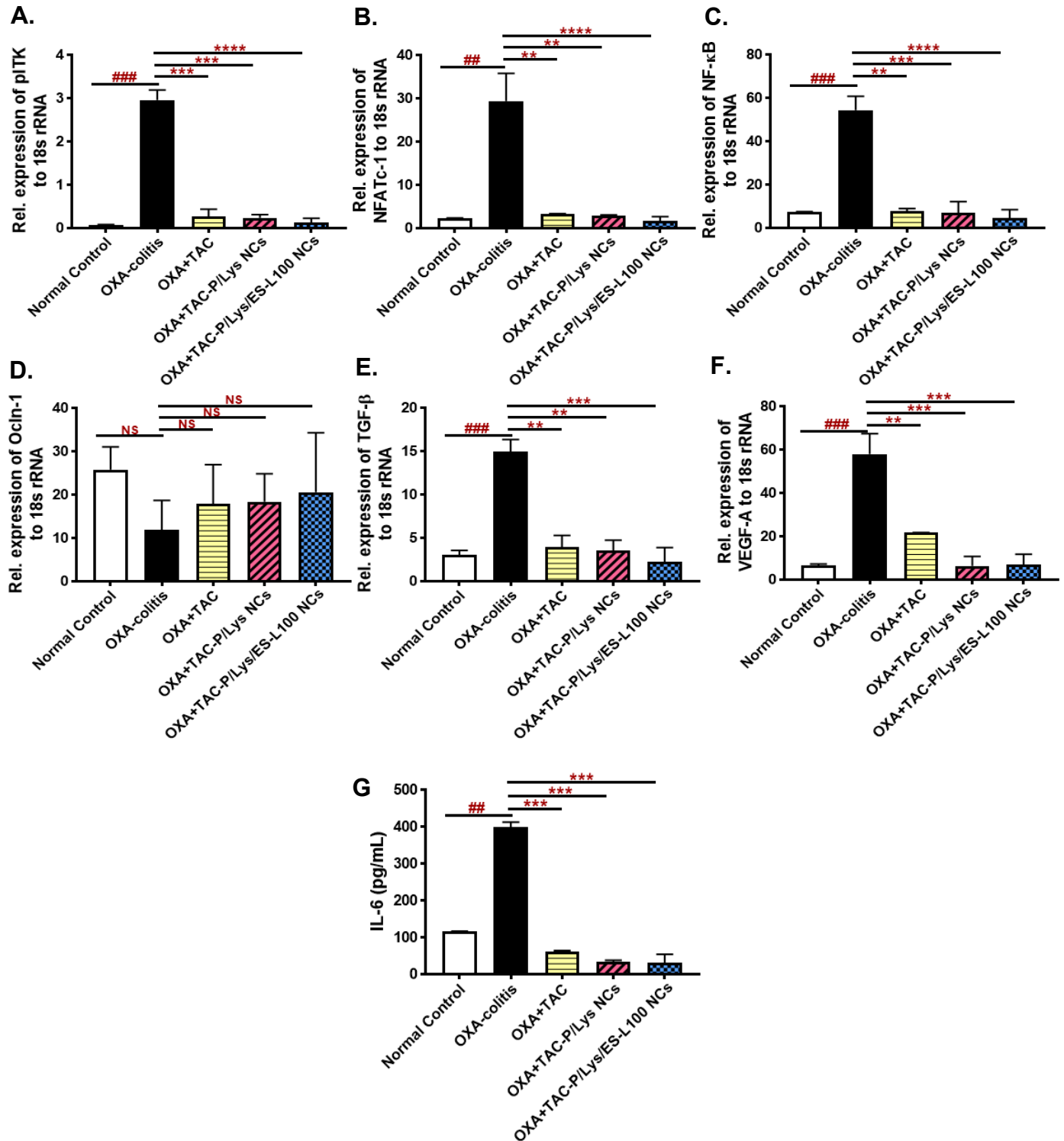


Figure 3. 57: RT-PCR analysis of inflammation mediator proteins (pITK, NFATc-1, NF-κB, TGF-β), tight junction protein (Ocln-1), angiogenesis factor (VEGF-A), and ELISA analysis of pro-inflammatory IL-6 expression

3.37.6. Assessment of pro-inflammatory M1-macrophages by flowcytometry

Collected spleen tissues from all experimental groups were smashed and processed to harvest macrophages. Macrophages were first identified using macrophage-specific markers F4/80 and CD11b. Then, we assessed the proportion of pro-inflammatory M1-macrophages in the whole macrophage population by M1-specific marker CD38. The findings suggested the highest proportion of M1 macrophages in the OXA-colitis group ($53.53\% \pm 7.79\%$, $p < 0.01$ vs normal), whereas normal control had a share of about ($20.46\% \pm 2.35\%$) (Figure 3. 58 I-II). The TAC drug, TAC-P/Lys NCs and TAC-P/Lys/ES-L100 NCs treatment of the OXA-inflamed mice have lowered the pro-inflammatory macrophages to $26.7\% \pm 0.00$ ($p < 0.05^*$), $23.7\% \pm 11.82\%$ ($p < 0.05^*$) and $23.58\% \pm 0.93\%$ ($p < 0.05^*$), respectively (Figure 3. 58 I-II). One representative image from each group is shown in Figure 3. 58 I-II. Overall, the two nano-formulation have insignificant differences ($p = \text{NS}$). The TAC-P/Lys/ES-L100 NCs have a lesser number of M1-macrophages than the pure drug ($p < 0.05^{\wedge}$).

The suppression of pro-inflammatory M1-macrophages suggests that the treatment groups played role in the amelioration of colon inflammation, thus, decreasing the macrophage count recruited at the tissue.

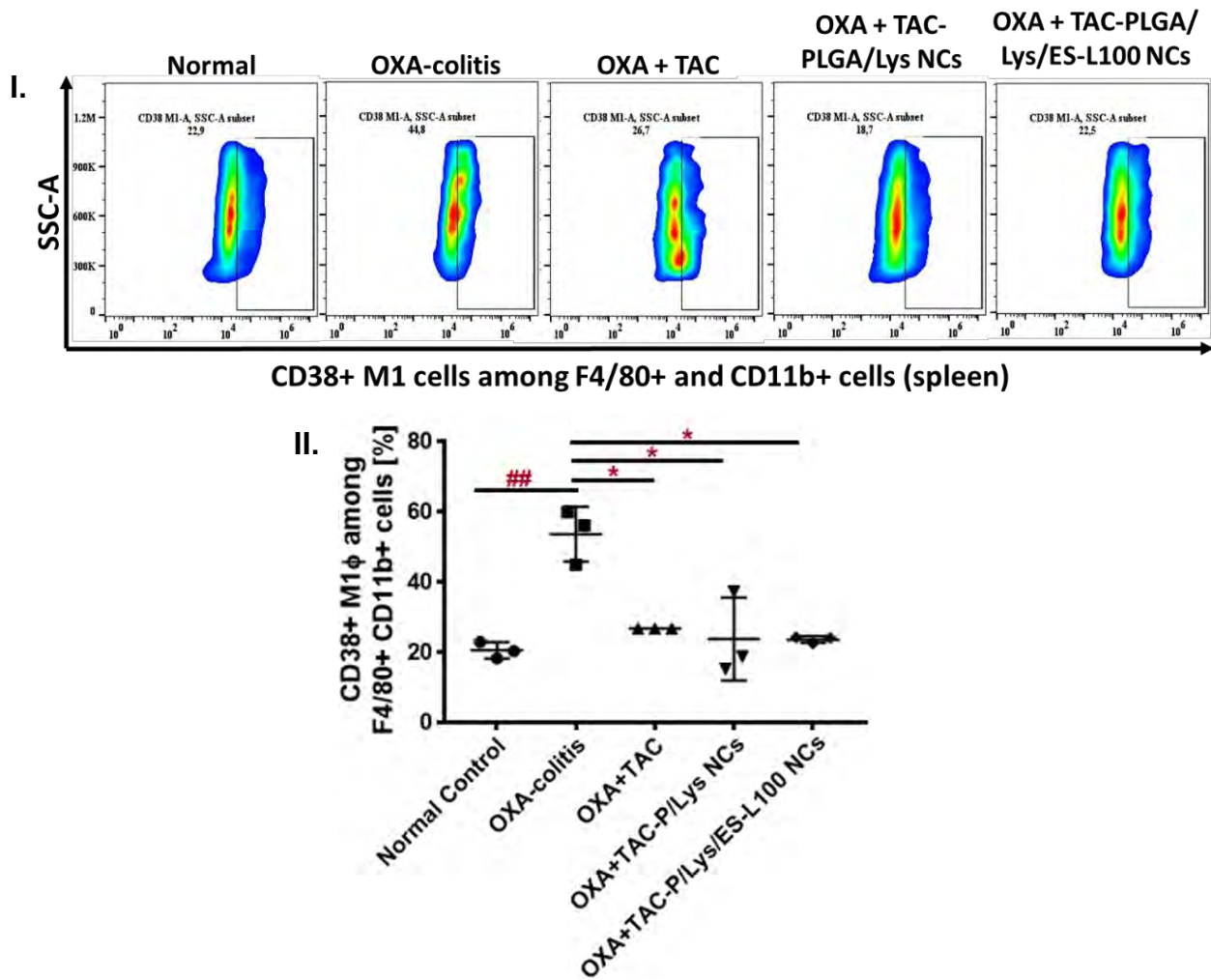


Figure 3. 58: Assessment of pro-inflammatory M1- macrophages expressing CD38 surface marker in the treatment and disease groups through flowcytometer (n=3)

CHAPTER 4

DISCUSSION

4. DISCUSSION

IBD is a big term defining inflammation of the intestine. UC is one of its major types that afflicts the large intestine mainly the colon. Various murine models have been studied for IBD including chemically induced models, genetically modified models, T-cell transfer models (Waldner and Neurath, 2009). Among chemically induced murine models, various inducers like TNBS, DSS, and OXA were successful in the induction of inflammation (Waldner and Neurath, 2009). Mostly, IBD therapeutics failed in the long-term management of the symptoms and mucosal healing of the colon. The unique pathophysiological barriers like stomach pH, bile acids, GIT degradative enzymes, heavy mucus, efflux pumps, and severe diarrhea cause flushing of drugs out the bowel with lesser therapeutic effect (Zeeshan *et al.*, 2019a; Hua *et al.*, 2015). High doses caused tolerance and resistance against the drug in IBD patients. Various strategies have been designed and evaluated in murine models of IBD to combat potential barriers and improve therapeutic efficacy.

In the modern era, development in nanotechnology devised several nanomaterials and nanocarriers for better therapeutics in many diseases. For IBD, the nanocarriers made of a wide array of materials like polymeric, metallic, magnetic, dendritic, lipidic, etc. have been investigated (Yang *et al.*, 2020).

In this regard, pH-sensitive polymeric nanocarriers have achieved great success in animal models. For instance, Eudragit based polymers especially ES100 have a threshold pH of ≥ 7 , which corresponds to colonic pH. Therefore, ES100 based nanocarriers specifically deliver the drug to the colon (Zu *et al.*, 2021; Zeeshan *et al.*, 2019b; Naeem *et al.*, 2018a; Zeeshan *et al.*, 2019a). Another polymer from the Eudragit family, EL100, degraded at a pH ≥ 6 . It is mostly used for small intestine drug delivery. However, the combination of ES100 and EL100 can be employed to counter the pH-mediated fluctuations at the inflamed colon.

Further, microbial enzyme-sensitive polymers are considered for stimuli-sensitive drug delivery to the colon. Since the colon is a plethora of resident bacteria that secreted enzymes (Dieterich *et al.*, 2018). Therefore, the natural polymers degraded by these bacterial enzymes and not by the GIT enzymes are favorable for targeting the colon only. Pullulan is a versatile polymer used for many biological activities, biocompatible

implants, and drug delivery purposes (Singh *et al.*, 2021). Recently, researchers investigated its role to target the colon (Lima *et al.*, 2017). It is a unique material that only delivers the drug to the colon against enzyme responsive stimuli but also served as a probiotic and beneficial effect on colon health (Liang *et al.*, 2019; Lima *et al.*, 2017).

On the other hand, advancement in research led to the development of ligand-anchored nanocarriers that specifically binds to the targeted receptors. These receptors or moieties are heavily overexpressed in the colon inflammation on the surface of epithelial cells and immune cells (Liu *et al.*, 2021). Recently, macrophages are the target cells in IBD, because of the recruitment of a large number of macrophages and conversion of resident monocytes into macrophages at the inflamed colon (Jones *et al.*, 2018). As a result of cytokines storm, the expression of various receptors increases several times in the inflammation.

In this regard, various ligand-bound polymeric nanoparticles were fabricated to overcome the limitations of bare polymeric nanocarriers and actively target the macrophage-receptors associated with inflammation and deliver the drug to the targeted site to execute its therapeutic function (Xiao *et al.*, 2018; Zhang *et al.*, 2013). For instance, sugar-based ligands including mannose, galactose, N-acetylglucosamine, fucose, and glucose have considerable targeting affinity to calcium type (C-type) lectin receptors expressed over macrophage surface, thus sugar bound nanocarriers demonstrated promising macrophage targeting ability (Zhang *et al.*, 2013; Hatami *et al.*, 2019; Shepherd *et al.*, 1981; Mukhtar *et al.*, 2020). One of the C-type lectin receptors expressed on the macrophage surface is the MGL-2/CD301b receptor, which is specifically involved in the recognition, binding, and uptake of D-galactose and N-acetylgalactosamine moieties, found on both endogenous and exogenous substances (Denda-Nagai *et al.*, 2010). Previously, galactose anchored nanoparticles were fabricated to improve oral systemic drug delivery (Siu *et al.*, 2018), to target inflamed GIT in conjunction with different polymers (Zhang *et al.*, 2013), and embedded in hydrogels (Xiao *et al.*, 2018).

Likewise, transferrin receptors (TFR-1/CD71) are present abundantly on colon epithelial cells and the recruited immune cells specifically macrophages at the colon during inflammation (Liu *et al.*, 2021; Harel *et al.*, 2011). The overexpression of the

receptor can be exploited for ligand-receptor mediated drug delivery purpose and to combat the activated inflammatory pathways in the macrophages and epithelial cells of the colon (Harel *et al.*, 2011). In this regard, holo-human transferrin (tfr) was anchored to the surface of nanocarriers and proved to be efficacious in various allied diseases like colorectal cancer (Sardoiwala *et al.*, 2020; Varshosaz *et al.*, 2017). However, the tfr-PLGA rationale was not tried for targeting in UC, as per our knowledge. The transferrin anchored PLGA nanocarriers (PLGA/tfr NCs) have more control over drug release than simple PLGA nanocarriers, which incur some stability against dose dumping at acidic pH (Scheeren *et al.*, 2020). Further, the upregulated TFR-1 receptors are the target for tfr ligand-based nanocarrier (Liu *et al.*, 2021), where PLGA-tfr nanocarriers bind, engulfed by the cells, and release the payload to mediate its mechanistic action. Therefore, receptor-mediated uptake of PLGA/tfr nanocarriers enables prolonged localized stay at the inflamed colon, whereby releasing the drug in a sustained manner, and overcomes diarrhea-led clearance.

Large variations in the disease condition, state of disease (active vs remission), genetic susceptibility, and inter-and intra-variations among individuals altered the colon microenvironment. Therefore, it is very difficult to translate the concept into larger animals or humans. To address the issues, various combinations of strategies are devised to work in a pliable inflammatory environment.

In the present thesis work, we have developed three different strategies based on stimuli sensitive and ligand anchored nanocarriers for multi-level targeting of the inflamed colon tissue.

In the first work (part-I), we developed D-galactose conjugated PLGA (GAL-PLGA) nanocarriers for specific targeting of MGL-2 receptors on the macrophages recruited at the inflamed colon. At first, GAL-PLGA polymer was synthesized through a simplified esterification reaction, and then nanoparticles were fabricated using QbD based approach and DOE. QbD approach enabled us to prepare the best quality nanoparticles with desirable attributes. These DEXA-GAL-PLGA NPs were tested with physicochemical, in vitro cell-based, and preliminary in vivo techniques and found to be suitable. Macrophages at the inflamed site facilitated uptake of galactose bound PLGA nanocarrier with prolonged adherence and therapeutic efficacy, meanwhile, enhanced stability against dose dumping effect at GIT variations of pH and enzymes.

Moreover, the GAL-PLGA nanoparticles incorporated all qualities of a nanosized PLGA carrier with ease in uptake and incurred sustained drug release characteristics (Zeeshan *et al.*, 2019a). D-galactose is a sugar and non-toxic, contrary to several ligands reported to be harmful (Bozich *et al.*, 2014), therefore the GAL-PLGA nano-system is inert to the living tissues.

Further, these nanoparticles were enveloped inside dual stimuli sensitive coat i.e., pH + microbial enzyme responsive coat for therapeutic evaluation in a murine colitis model. Therefore, Dexa-GP/ES/Pu NCs were prepared with the aim to specifically target the colon under the influence of pH and pullulanase microbiome enzyme. And once the nanocarriers reached the colon, then the outer coat dissolves exposing the underneath core which have D-galactose ligand that binds to MGL-2 macrophage receptors and overcomes the extracellular and intracellular challenges like heavy mucus, efflux pumps, reactive oxygen species, intracellular pH, etc. (Yang *et al.*, 2020; Zeeshan *et al.*, 2019a). Whereby PLGA induced sustained drug release character for long-term action. The physicochemical techniques confirmed size uniformity and desirable attributes with sustained drug release at pH 7.4 and minimal at pH 1.2. Cell-based assays demonstrated hemocompatibility and cell compatibility to colon cells and macrophages. The macrophages have extensive uptake of Dexa-GP/ES/Pu NCs, which was competitively inhibited in the presence of D-galactose in the media. The nanocarrier showed good retention in the excised intestine tissue. Further, the DSS-induced colitis model was established in the mice and assessed through various inflammation indices. The Dexa-GP/ES/Pu NCs showed a good targeting ratio and exhibited superb therapeutic efficacy in the DSS-colitis model. Daily parameters, clinical activity index, histology, biochemical antioxidant assays, RT-PCR analysis of tight junction proteins and inflammatory markers, hematological parameters confirmed that the inflammation was reduced and treated by Dexa-GP/ES/Pu NCs. Immunohistochemistry demonstrated enhanced Dexa activity as manifested from declined COX-2 and NF- κ B levels. Further, all materials used in the synthesis are inert, and in vivo toxicology assessment in the healthy mice showed negligible signs of toxicity. Therefore, the novel Dexa loaded GP/ES/Pu NCs can be able to cross the pathophysiological barriers at both organ and tissue levels in the GIT with higher

therapeutic efficiency, biocompatibility, and improved targeting and retention properties required for the therapeutic success in UC.

The second strategy (Part-II) aimed to encapsulate a JAK/STAT inhibitor, Tofacitinib citrate (Tofa) inside advanced nanocarriers. In section-A, nanocarriers made up of PLGA and tfr were developed using modified emulsion-evaporation and adsorption methods. Tfr was adsorbed to the PLGA surface during the formation of nanocarriers. Tofa-P/tfr NCs can target TFR-1 receptors on macrophages and colon epithelial cells in IBD. The nanocarriers were designed using the QbD approach and 3³ Box-Behnken DOE. The optimal formulation have the best attributes and good drug encapsulation that are pre-requisite to target the inflamed colon. The nanocarriers were characterized through physicochemical, in vitro, cell-based, and in vivo studies in the DSS-induced colitis model. The nanocarriers met the prerequisite of physicochemical properties and drug release at pH 7.4. In vitro cell-based biocompatibility and extensive uptake by colon and macrophages were observed with competitive inhibition with antibodies during macrophage uptake. Nanocarriers have good targeting potential in the inflamed mice, as indicated by biodistribution studies in the mice. Further, the therapeutic role is established in the DSS-colitis model by balancing the morphological, histopathological, biochemical, microbial indices, and pro-inflammatory cytokines levels. The epithelial and vascular membrane integrity was also recovered, and the drug mechanistic action was enhanced when delivered inside nanocarriers. Thus, the drug-loaded P/tfr NCs are promising in mediating site-specific drug delivery to the colon via overexpressed TFR-1 receptor and have a good potential for ameliorating colitis for a prolonged duration.

In section B, the nanocarriers were further improved for enhanced biocompatibility, drug loading, and site-specific targeting. Therefore, the drug-loaded lipid-PLGA mixture was covered with tfr and the whole core was coated under pH-sensitive polymer, ES100. Therefore, the unique pH-sensitive lipid-polymer hybrid nanocarriers were named nanoshells. The nanoshells can target the colon in relevance to pH, where the nanocore targets the TFR-1 receptor and thus have enhanced uptake and residence at colon cells and macrophages. Thus, the drug was released in a sustained manner from the lipid-PLGA matrix and have a prolonged therapeutic effect. Uncoated Tofa-LP/P/tfr NSh and coated Tofa-LP/P/tfr/ES NSh were successfully fabricated and characterized with good physicochemical properties. The drug release profile of coated nanoshells

was more suitable than the uncoated one because of minimal release at pH 1.2. In vitro cell-based assays and caco-2 apoptosis studies confirmed biocompatibility and tfr-based uptake in the macrophages. The Tofa loaded nanoshells inhibited JAK-1 and STAT-1 in the elicited macrophages, confirming improved drug action against inflammatory pathways. In vivo biodistribution studies confirmed enhanced accumulation of nanoshells in the inflamed colon compared to the healthy. In vivo therapeutic efficacy against DSS induced colitis was established by improved clinical, histological, biochemical, hematological, morphological, and microbial indices. And toxicological investigations in the healthy mice suggested minimal toxicity potential in the living system.

The nanocarriers developed in Part I and Part II were tested in the DSS induced colitis model because of its toxicity towards colon epithelial cells that resembles human UC conditions. The model is favorable to investigate the therapeutic effects of nano-formulations on mucosal healing and barrier function (Solomon *et al.*, 2010).

OXA induced colitis is typically referred to increase T-cells recruitment at the inflamed colon, therefore, the OXA induced colitis model is particularly important to investigate the therapeutic effects of the drugs that suppress T-cells or related pathways (Weigmann and Neurath, 2016). TAC is an immunosuppressant that inhibits T-cells activation and progression (Matsuoka *et al.*, 2015); therefore, we have assessed the therapeutic efficacy of TAC loaded nanocarriers (Part III) in the OXA induced colitis.

The third strategy (Part-III) aimed to utilize a novel stabilizer, and drug release controlling amino-acid i.e., L-Lysine. Nowadays, L-Lysine containing polymeric nanocarriers are investigated for colon drug delivery purposes as well. Tacrolimus (TAC) was loaded as a drug. TAC-loaded PLGA/Lys NCs were developed and coated with dual pH-sensitive coat including ES100 and EL100 polymeric combinations. The designed TAC-P/Lys NCs and TAC-P/Lys/ES-L100 NCs were prepared through modified emulsion evaporation and coating techniques. Both nanocarriers have good physicochemical properties and coated have good drug release patterns with retardation of drug release at pH 1.2. Caco-2 cells and macrophages have good uptake. Oxazolone (OXA) induced colitis model was developed. Both nanocarriers demonstrated enhanced drug activity as manifested from the amelioration of inflammation, TAC-P/Lys/ES-L100 NCs found to be more efficacious than their counterpart. The endoscopy score,

body weight, MPO activity, pro-inflammatory cytokines expression revealed mitigation of inflammation. Further, anti-pITK is involved in the T-cells regulation and promotes inflammatory events. The expression of pITK was explored through different techniques including FACs, RT-PCR, and immunohistochemistry. Downregulation of pITK in the colon and spleen T-cells indicated enhanced drug action when delivered inside the nanocarrier. The expression of other aligned major inflammatory pathway proteins (NFATc-1, NF- κ B) was also downregulated that confirmed success of the strategy. Further, the pro-inflammatory IL-6, angiogenesis factor VEGF-A and TGF- β levels were declined by the nanocarrier treatment. Additionally, TAC-P/Lys/ES-L100 NCs healed the inflamed colon, as exhibited by lower proinflammatory M1 macrophages count.

In short, all three strategies served as a unique solution to various problems in the way of colon targeting during inflammation. Dexamethasone loaded galactosylated nanocarriers are a good choice for initial IBD therapy. Tofacitinib loaded TfR based nanoshells can be used for moderate to severe colitis cases especially steroid-refractory cases since the presence of TfR-1 on colon epithelial cells and immune cells makes the rationale suitable to target abundantly expressed TfR-1 on the cells. TAC loaded nanocarriers are also good for steroid-refractory, moderate to severe colitis cases, and extensively inhibit pITK mediated activation of T-cells in the inflammation.

5. CONCLUSIONS

In conclusion, all three strategies targeted and delivered the drug to the inflamed colon with dual stimuli sensitive and biomolecule anchored polymeric nanocarriers and successful in ameliorating colon inflammation with enhanced drug therapeutic efficacy.

The key points are:

- GAL-PLGA polymer was synthesized by simple esterification reaction, optimized by systematic design-based approach.
- QbD based approach screened out the independent variables and their influence on CQAs of the nano-formulation and the selected variables were studied and adjusted using Box-Behnken design. The optimized GAL-PLGA nanoparticles have appropriate attributes (size, zeta potential, EE%, PDI), are necessary for colon targeting, and are found to be biocompatible and have good targeting efficiency to the colon in the inflammation.
- GAL-PLGA nanoparticles were further subjected to coating with a dual ES100/Pu coat to mediate stimuli-sensitive colon targeting. The coated Dexa-GP/ES/Pu NCs have all attributes that are prerequisites to target colon because of dual stimuli sensitive coat and ligand anchored core and demonstrated efficient results in the DSS-induced colitis model.
- Tofa-P/tfr NCs were synthesized using QbD and Box-Behnken design that optimizes the formulation variables to produce nanoformulation with the best characteristics.
- Further, Tofa-LP/tfr NSh and Tofa-LP/tfr/ES NSh have enhanced properties because of lipidic content in the core that facilitates more drug content to be encapsulated, controlled drug release, and have some protective effects on intestine mucosa. The pH-sensitive nature enables more colon-specific action.
- All Tofa-P/tfr NCs, Tofa-LP/tfr NSh and Tofa-LP/tfr/ES NSh proved to be efficacious in restoring inflammation in the DSS-colitis model. However, the last one had the superior action because of multiple characteristics.

- TAC-P/Lys NCs and TAC-P/Lys/ES-L100 NCs were developed with optimal characteristics. The lysine content incurred control over drug release. Both types of nanocarriers have good uptake potential and biocompatibility. TAC-P/Lys/ES-L100 NCs have superior therapeutic efficacy and suppression of pITK levels in the T-cells in the OXA-colitis model as compared to TAC-P/Lys NCs

6. FUTURE PROSPECTIVE

- Exploration of the potential of excipients used in the development of nanocarriers for their role in combating inflammation of the intestine
- Evaluation of nano-formulations in the other animal models of intestinal inflammation
- The evaluation can be exceeded through detailed pharmacokinetics studies
- Detailed evaluation of the effect of the ligand on targeting receptors
- Utilizations of other ligands in developing stimuli sensitive-PLGA based nanocarriers and exploration of their colon targeting potential
- Exploration of ligand anchored nanocarriers especially tfr based nanocarriers in targeting colorectal cancer
- Investigation of novel stimuli sensitive polymers which can be employed for colon targeting purpose
- Large scale formulation development (for industrial scale-up)
- Testing of nano-formulations on the large animals
- Translation of the concepts into human studies

REFERENCES

REFERENCES

- Abraham C & Cho JH (2009). Inflammatory bowel disease. *N Engl J Med*, 361(21): 2066.
- Akhgari A, Garekani HA, Sadeghi F & Azimaie M (2005). Statistical optimization of indomethacin pellets coated with pH-dependent methacrylic polymers for possible colonic drug delivery. *Int J Pharm*, 305(1): 22-30.
- Al-Harbi NO, Imam F, Al-Harbi MM, Ansari MA, Zoheir KM, Korashy HM, Sayed-Ahmed MM, Attia SM, Shabanah OA & Ahmad SF (2016). Dexamethasone attenuates LPS-induced acute lung injury through inhibition of NF- κ B, COX-2, and pro-inflammatory mediators. *Immunol Invest*, 45(4): 349-369.
- Ali H, Weigmann B, Collnot E-M, Khan SA, Windbergs M & Lehr C-M (2016). Budesonide loaded PLGA nanoparticles for targeting the inflamed intestinal mucosa—Pharmaceutical characterization and fluorescence imaging. *Pharm Res*, 33(5): 1085-1092.
- Ali H, Weigmann B, Neurath MF, Collnot EM, Windbergs M & Lehr CM (2014). Budesonide loaded nanoparticles with pH-sensitive coating for improved mucosal targeting in mouse models of inflammatory bowel diseases. *J Control Release*, 183: 167-177.
- Alwani S, Kaur R, Michel D, Chitanda JM, Verrall RE, Karunakaran C & Badea I (2016). Lysine-functionalized nanodiamonds as gene carriers: development of stable colloidal dispersion for in vitro cellular uptake studies and siRNA delivery application. *Int J Nanomedicine*, 11: 687.
- Andreesen R, Osterholz J, Bodemann H, Bross K, Costabel U & Löhr G (1984). Expression of transferrin receptors and intracellular ferritin during terminal differentiation of human monocytes. *Blut*, 49(3): 195-202.
- ANDRONIE L, PÂNZARU SC, Cozar O & Domşa I (2011). FT-IR spectroscopy for human colon tissue diagnostic. *Rom. J. Biophys*, 21(2): 85-91.
- Annese V, Bassotti G, Napolitano G, Usai P, Andriulli A & Vantrappen G (2009). Gastrointestinal motility disorders in patients with inactive Crohn's disease. *Scand J Gastroenterol*.

- Anselmo AC, Langer RS & Jaklenec A (2016). Ph-responsive mucoadhesive polymeric encapsulated microorganisms. U.S. Patent Application No. 15/372,703.
- Antoni L, Nuding S, Wehkamp J & Stange EF (2014). Intestinal barrier in inflammatory bowel disease. *World J Gastroenterol*, 20(5): 1165-1179.
- Aratani Y (2018). Myeloperoxidase: its role for host defense, inflammation, and neutrophil function. *Arch Biochem Biophys*, 640: 47-52.
- Arifin WN & Zahiruddin WM (2017). Sample Size Calculation in Animal Studies Using Resource Equation Approach. *Malays J Med Sci*, 24(5): 101-105.
- Aung WW, Wang C, Xibei J, Horii M, Mizumaki K, Kano M, Okamura A, Kobayashi T & Matsushita T (2021). Immunomodulating role of the JAKs inhibitor tofacitinib in a mouse model of bleomycin-induced scleroderma. *J Dermatol Sci*, 101(3): 174-184.
- Badhana S, Garud N & Garud A (2013). Colon specific drug delivery of mesalamine using eudragit S100-coated chitosan microspheres for the treatment of ulcerative colitis. *Int. Curr. Pharm. J.*, 2(3): 42-48.
- Baker MJ, Trevisan J, Bassan P, Bhargava R, Butler HJ, Dorling KM, Fielden PR, Fogarty SW, Fullwood NJ & Heys KA (2014). Using Fourier transform IR spectroscopy to analyze biological materials. *Nat Protoc*, 9(8): 1771-1791.
- Bangaoil R, Santillan A, Angeles LM, Abanilla L, Lim Jr A, Ramos MC, Fellizar A, Guevarra Jr L & Albano PM (2020). ATR-FTIR spectroscopy as adjunct method to the microscopic examination of hematoxylin and eosin-stained tissues in diagnosing lung cancer. *PLoS One*, 15(5): e0233626.
- Barea M, Jenkins M, Gaber M & Bridson R (2010). Evaluation of liposomes coated with a pH responsive polymer. *Int J Pharm*, 402(1): 89-94.
- Bashir S, Aamir M, Sarfaraz RM, Hussain Z, Sarwer MU, Mahmood A, Akram MR & Qaisar MN (2021). Fabrication, characterization and in vitro release kinetics of tofacitinib-encapsulated polymeric nanoparticles: A promising implication in the treatment of rheumatoid arthritis. *Int J Polym Mater Polym Biomater*, 70(7): 449-458.
- Becker C, Fantini MC, Wirtz S, Nikolaev A, Kiesslich R, Lehr H-A, Galle PR & Neurath MF (2005). In vivo imaging of colitis and colon cancer development in mice using high resolution chromoendoscopy. *Gut*, 54(7): 950-954.

- Beloqui A, Coco R, Memvanga PB, Ucakar B, des Rieux A & Pr at V (2014). pH-sensitive nanoparticles for colonic delivery of curcumin in inflammatory bowel disease. *Int J Pharm*, 473(1): 203-212.
- Bendickova K, Tidu F & Fric J (2017). Calcineurin–NFAT signalling in myeloid leucocytes: new prospects and pitfalls in immunosuppressive therapy. *EMBO Mol Med*, 9(8): 990-999.
- Bernstein CN, Fried M, Krabshuis J, Cohen H, Eliakim R, Fedail S, Garry R, Goh K, Hamid S & Khan AG (2010). World Gastroenterology Organization Practice Guidelines for the diagnosis and management of IBD in 2010. *Inflamm Bowel Dis*, 16(1): 112-124.
- Bertoni S, Liu Z, Correia A, Martins JP, Rahikkala A, Fontana F, Kemell M, Liu D, Albertini B & Passerini N (2018). pH and Reactive Oxygen Species-Sequential Responsive Nano-in-Micro Composite for Targeted Therapy of Inflammatory Bowel Disease. *Adv Funct Mater*: 1806175.
- Bhatt PC, Verma A, Al-Abbasi FA, Anwar F, Kumar V & Panda BP (2017). Development of surface-engineered PLGA nanoparticulate-delivery system of Tet1-conjugated nattokinase enzyme for inhibition of A β 40 plaques in Alzheimer’s disease. *Int J Nanomedicine*, 12: 8749.
- Boirivant M, Fuss IJ, Chu A & Strober W (1998). Oxazolone colitis: a murine model of T helper cell type 2 colitis treatable with antibodies to interleukin 4. *J Exp Med*, 188(10): 1929-1939.
- Boivin MA, Ye D, Kennedy JC, Al-Sadi R, Shepela C & Ma TY (2007). Mechanism of glucocorticoid regulation of the intestinal tight junction barrier. *Am J Physiol Gastrointest Liver Physiol*, 292(2): G590-G598.
- Bozich JS, Lohse SE, Torelli MD, Murphy CJ, Hamers RJ & Klaper RD (2014). Surface chemistry, charge and ligand type impact the toxicity of gold nanoparticles to *Daphnia magna*. *Environmental Science: Nano*, 1(3): 260-270.
- Bradford MM (1976). A rapid and sensitive method for the quantitation of microgram quantities of protein utilizing the principle of protein-dye binding. *Anal Biochem*, 72(1): 248-254.

- Brand S (2009). Crohn's disease: Th1, Th17 or both? The change of a paradigm: new immunological and genetic insights implicate Th17 cells in the pathogenesis of Crohn's disease. *Gut*, 58(8): 1152-1167.
- Brunner M, Lackner E, Exler P, Fluiter H, Kletter K, Tschurlovits M, Dudczak R, EICHLER HG & Müller M (2006). 5-aminosalicylic acid release from a new controlled-release mesalazine formulation during gastrointestinal transit in healthy volunteers. *Aliment Pharmacol Ther*, 23(1): 137-144.
- Bruschi ML (2015). Mathematical models of drug release. *Strategies to modify the drug release from pharmaceutical systems*. Woodhead Publishing, 2015; 63-86.
- Buchman AL (2001). Side effects of corticosteroid therapy. *J Clin Gastroenterol*, 33(4): 289-294.
- Chami B, Martin NJ, Dennis JM & Witting PK (2018). Myeloperoxidase in the inflamed colon: A novel target for treating inflammatory bowel disease. *Arch Biochem and Biophys*, 645: 61-71.
- Chang J, Paillard A, Passirani C, Morille M, Benoit J-P, Betbeder D & Garcion E (2012). Transferrin adsorption onto PLGA nanoparticles governs their interaction with biological systems from blood circulation to brain cancer cells. *Pharm Res*, 29(6): 1495-1505.
- Chaves PDS, Frank LA, Frank AG, Pohlmann AR, Guterres SS & Beck RCR (2018). Mucoadhesive properties of Eudragit® RS100, Eudragit® S100, and Poly (ϵ -caprolactone) nanocapsules: Influence of the vehicle and the mucosal surface. *AAPS PharmSciTech*, 19(4): 1637-1646.
- Chen L, Zhong J, Li S, Li W, Wang B, Deng Y & Yuan J (2018). The long-term effect of tacrolimus on alkali burn-induced corneal neovascularization and inflammation surpasses that of anti-vascular endothelial growth factor. *Drug Des Devel Ther*, 12: 2959.
- Chen Q, Xiao B & Merlin D (2017). Nanotherapeutics for the treatment of inflammatory bowel disease. *Expert Rev Gastroenterol Hepatol*: 495-497.
- Chourasia M & Jain S (2004). Polysaccharides for colon targeted drug delivery. *Drug Deliv*, 11(2): 129-148.

- Chowdary Vadlamudi H, Prasanna Raju Y, Rubia Yasmeen B & Vulava J (2012). Anatomical, biochemical and physiological considerations of the colon in design and development of novel drug delivery systems. *Curr Drug Del*, 9(6): 556-565.
- Collnot E-M, Ali H & Lehr C-M (2012). Nano-and microparticulate drug carriers for targeting of the inflamed intestinal mucosa. *J Control Release*, 161(2): 235-246.
- Corbo C, Cromer WE, Molinaro R, Furman NET, Hartman KA, De Rosa E, Boada C, Wang X, Zawieja DC & Agostini M (2017). Engineered biomimetic nanovesicles show intrinsic anti-inflammatory properties for the treatment of inflammatory bowel diseases. *Nanoscale*, 9(38): 14581-14591.
- Crcarevska MS, Dodov MG & Goracinova K ((2008)). Chitosan coated Ca–alginate microparticles loaded with budesonide for delivery to the inflamed colonic mucosa. *Eur J Pharm Biopharm*, 68(3): 565-578.
- Crcarevska MS, Dodov MG, Petrussevska G, Gjorgoski I & Goracinova K (2009). Bioefficacy of budesonide loaded crosslinked polyelectrolyte microparticles in rat model of induced colitis. *J Drug Target*, 17(10): 788-802.
- D'Amico F, Parigi TL, Fiorino G, Peyrin-Biroulet L & Danese S (2019). Tofacitinib in the treatment of ulcerative colitis: efficacy and safety from clinical trials to real-world experience. *Therap Adv Gastroenterol*, 12: 1756284819848631-1756284819848631.
- D'souza AA & Devarajan PV (2015). Asialoglycoprotein receptor mediated hepatocyte targeting—Strategies and applications. *J Control Release*, 203: 126-139.
- Dalal C & Jana NR (2018). Galactose multivalency effect on the cell uptake mechanism of bioconjugated nanoparticles. *J Phys Chem C*, 122(44): 25651-25660.
- Danhier F, Ansorena E, Silva JM, Coco R, Le Breton A & Pr eat V (2012). PLGA-based nanoparticles: an overview of biomedical applications. *J Control Release*, 161(2): 505-522.
- Dassopoulos T, Sultan S, Falck–Ytter YT, Inadomi JM & Hanauer SB (2013). American Gastroenterological Association Institute Technical Review on the Use of Thiopurines, Methotrexate, and Anti–TNF- α Biologic Drugs for the Induction and Maintenance of Remission in Inflammatory Crohn's Disease. *Gastroenterology*, 145(6): 1464-1478. e5.

- de Arce Velasquez A, Ferreira LM, Stangarlin MFL, da Silva CdB, Rolim CMB & Cruz L (2014). Novel Pullulan–Eudragit® S100 blend microparticles for oral delivery of risedronate: Formulation, in vitro evaluation and tableting of blend microparticles. *Mater Sci Eng C*, 38: 212-217.
- Dell'Albani P, Santangelo R, Torrisi L, Nicoletti VG, de Vellis J & Giuffrida Stella AM (2001). JAK/STAT signaling pathway mediates cytokine-induced iNOS expression in primary astroglial cell cultures. *J Neurosci Res*, 65(5): 417-424.
- Denda-Nagai K, Aida S, Saba K, Suzuki K, Moriyama S, Oo-Puthinan S, Tsuiji M, Morikawa A, Kumamoto Y & Sugiura D (2010). Distribution and function of macrophage galactose-type c-type lectin 2 (MGL2/CD301b): efficient uptake and presentation of glycosylated antigens by dendritic cells. *J Biol Chem*, 285(25): 19193-19204.
- Dew M, Hughes P, Lee M, Evans B & Rhodes J (1982). An oral preparation to release drugs in the human colon. *Br J Clin Pharmacol*, 14(3): 405-408.
- Dew M, Ryder R, Evans N, Evans B & Rhodes J (1983). Colonic release of 5-amino salicylic acid from an oral preparation in active ulcerative colitis. *Br J Clin Pharmacol*, 16(2): 185-187.
- Dieterich W, Schink M & Zopf Y (2018). Microbiota in the gastrointestinal tract. *Medical Sciences*, 6(4): 116.
- Ding D, Kundukad B, Somasundar A, Vijayan S, Khan SA & Doyle PS (2018). Design of mucoadhesive PLGA microparticles for ocular drug delivery. *ACS Appl Bio Mater*, 1(3): 561-571.
- Djuris J, Ibric S & Djuric Z (2013). Quality-by-design in pharmaceutical development. *Computer-Aided Applications in Pharmaceutical Technology*. Woodhead Publishing; 1-16.
- Dong H, Tian L, Gao M, Xu H, Zhang C, Lv L, Zhang J, Wang C, Tian Y & Ma X (2017). Promising galactose-decorated biodegradable poloxamer 188-PLGA diblock copolymer nanoparticles of resibufogenin for enhancing liver cancer therapy. *Drug Deliv*, 24(1): 1302-1316.
- Dotan I, Hallak A, Arber N, Santo M, Alexandrowitz A, Knaani Y, Hershkovich R, Brazowski E & Halpern Z (2001). Low-dose low-molecular weight heparin

(enoxaparin) is effective as adjuvant treatment in active ulcerative colitis: an open trial. *Dig Dis Sci*, 46(10): 2239-2244.

Duan H, Lü S, Gao C, Bai X, Qin H, Wei Y, Wu Xa & Liu M (2016). Mucoadhesive microparticulates based on polysaccharide for target dual drug delivery of 5-aminosalicylic acid and curcumin to inflamed colon. *Colloids Surf B Biointerfaces*, 145: 510-519.

Dubey R, Dubey R, Omrey P, Vyas S & Jain S (2010). Development and characterization of colon specific drug delivery system bearing 5-ASA and camylofine dihydrochloride for the treatment of ulcerative colitis. *J Drug Target*, 18(8): 589-601.

Erben U, Loddenkemper C, Doerfel K, Spieckermann S, Haller D, Heimesaat MM, Zeitz M, Siegmund B & Kühl AA (2014). A guide to histomorphological evaluation of intestinal inflammation in mouse models. *Int J Clin Exp Pathol*, 7(8): 4557.

Ewe K, Schwartz S, Petersen S & Press AG (1999). Inflammation does not decrease intraluminal pH in chronic inflammatory bowel disease. *Dig Dis Sci*, 44(7): 1434-1439.

Executive. HaS. Occupational Exposure Limits: Health and Safety Executive. 2002 Sudbury.

Fallingborg J, Pedersen P & Jacobsen BA (1998). Small intestinal transit time and intraluminal pH in ileocecal resected patients with Crohn's disease. *Dig Dis Sci*, 43(4): 702-705.

Feagins LA (2010). Role of transforming growth factor- β in inflammatory bowel disease and colitis-associated colon cancer. *Inflamm Bowel Dis*, 16(11): 1963-1968.

Festing MF & Altman DG (2002). Guidelines for the design and statistical analysis of experiments using laboratory animals. *ILAR J*, 43(4): 244-258.

Fischer M, Siva S, Wo JM & Fadda HM (2017). Assessment of small intestinal transit times in ulcerative colitis and Crohn's disease patients with different disease activity using video capsule endoscopy. *AAPS PharmSciTech*, 18(2): 404-409.

Frasco MF, Almeida GM, Santos-Silva F, Pereira MdC & Coelho MA (2015). Transferrin surface-modified PLGA nanoparticles-mediated delivery of a proteasome inhibitor to human pancreatic cancer cells. *J Biomed Mater Res A*, 103(4): 1476-1484.

- Freire MCLC, Alexandrino F, Marcelino HR, Picciani PHdS, Genre J, Oliveira AGd & Egito ESTd (2017). Understanding drug release data through thermodynamic analysis. *Materials*, 10(6): 651.
- Fu K, Pack DW, Klibanov AM & Langer R (2000). Visual evidence of acidic environment within degrading poly (lactic-co-glycolic acid)(PLGA) microspheres. *Pharm Res*, 17(1): 100-106.
- Gallagher MP, Conley JM, Vangala P, Reboldi A, Garber M & Berg LJ (2020). The Tec kinase ITK differentially optimizes NFAT, NF- κ B, and MAPK signaling during early T cell activation to regulate graded gene induction. *bioRxiv*.
- Gammella E, Buratti P, Cairo G & Recalcati S (2017). The transferrin receptor: the cellular iron gate. *Metallomics*, 9(10): 1367-1375.
- Gao M, Xu H, Bao X, Zhang C, Guan X, Liu H, Lv L, Deng S, Gao D & Wang C (2016). Oleanolic acid-loaded PLGA-TPGS nanoparticles combined with heparin sodium-loaded PLGA-TPGS nanoparticles for enhancing chemotherapy to liver cancer. *Life Sci*, 165: 63-74.
- Genin M, Clement F, Fattaccioli A, Raes M & Michiels C (2015). M1 and M2 macrophages derived from THP-1 cells differentially modulate the response of cancer cells to etoposide. *BMC Cancer*, 15(1): 577.
- Godse R, Rathod M, De A & Shinde U (2021). Intravitreal galactose conjugated polymeric nanoparticles of etoposide for retinoblastoma. *J Drug Deliv Sci Technol*, 61: 102259.
- Goel S, Kaur T, Singh N & Jacob J (2021). Tunable macroporous D-galactose based hydrogels for controlled release of a hydrophilic drug. *Eur Polym J*, 150: 110409.
- Gugulothu D, Kulkarni A, Patravale V & Dandekar P (2014). pH-Sensitive Nanoparticles of Curcumin–Celecoxib Combination: Evaluating Drug Synergy in Ulcerative Colitis Model. *J Pharm Sci*, 103(2): 687-696.
- Guo C, Yang L, Wan C-X, Xia Y-Z, Zhang C, Chen M-H, Wang Z-D, Li Z-R, Li X-M & Geng Y-D (2016). Anti-neuroinflammatory effect of Sophoraflavanone G from *Sophora alopecuroides* in LPS-activated BV2 microglia by MAPK, JAK/STAT and Nrf2/HO-1 signaling pathways. *Phytomedicine*, 23(13): 1629-1637.

- Gupta S, Agarwal A, Gupta NK, Saraogi G, Agrawal H & Agrawal G (2013). Galactose decorated PLGA nanoparticles for hepatic delivery of acyclovir. *Drug Dev Ind Pharm*, 39(12): 1866-1873.
- Gupta VK, Beckert TE & Price JC (2001). A novel pH-and time-based multi-unit potential colonic drug delivery system. I. Development. *Int J Pharm*, 213(1): 83-91.
- Habig WH, Pabst MJ & Jakoby WB (1974). Glutathione S-transferases: the first enzymatic step in mercapturic acid formation. *J Biol Chem*, 249(22): 7130-7139.
- Hanauer SB (2006). Inflammatory bowel disease: epidemiology, pathogenesis, and therapeutic opportunities. *Inflamm Bowel Dis*, 12(5): S3-S9.
- Harel E, Rubinstein A, Nissan A, Khazanov E, Nadler Milbauer M, Barenholz Y & Tirosh B (2011). Enhanced transferrin receptor expression by proinflammatory cytokines in enterocytes as a means for local delivery of drugs to inflamed gut mucosa. *PLoS One*, 6(9): e24202-e24202.
- Hatami E, Mu Y, Shields DN, Chauhan SC, Kumar S, Cory TJ & Yallapu MM (2019). Mannose-decorated hybrid nanoparticles for enhanced macrophage targeting. *Biochem Biophys Rep*, 17: 197-207.
- Hebden Ja, Blackshaw P, Perkins A, Wilson C & Spiller R (2000). Limited exposure of the healthy distal colon to orally-dosed formulation is further exaggerated in active left-sided ulcerative colitis. *Aliment Pharmacol Ther*, 14(2): 155-162.
- Hendrickson BA, Gokhale R & Cho JH (2002). Clinical aspects and pathophysiology of inflammatory bowel disease. *Clin Microbiol Rev*, 15(1): 79-94.
- Hu G & Liu L 2015. Orally taken colon-targeted preparation for treatment of inflammatory bowel diseases and preparation method thereof. CN Patent No.103315959 B.
- Hu Z, Mawatari S, Shibata N, Takada K, Yoshikawa H, Arakawa A & Yosida Y (2000). Application of a biomagnetic measurement system (BMS) to the evaluation of gastrointestinal transit of intestinal pressure-controlled colon delivery capsules (PCDCs) in human subjects. *Pharm Res*, 17(2): 160-167.
- Hua S, Marks E, Schneider JJ & Keely S (2015). Advances in oral nano-delivery systems for colon targeted drug delivery in inflammatory bowel disease: selective

- targeting to diseased versus healthy tissue. *Nanomed Nanotechnol Biol Med*, 11(5): 1117-1132.
- Huang Y, Guo J & Gui S (2018). Orally targeted galactosylated chitosan poly (lactic-co-glycolic acid) nanoparticles loaded with TNF- α siRNA provide a novel strategy for the experimental treatment of ulcerative colitis. *Eur J Pharm Sci*, 125: 232-243.
- Hubrecht RC & Carter E (2019). The 3Rs and Humane Experimental Technique: Implementing Change. *Animals*, 9(10): 754.
- Hugot J-P, Chamaillard M, Zouali H, Lesage S, Cézard J-P, Belaiche J, Almer S, Tysk C, O'Morain CA & Gassull M (2001). Association of NOD2 leucine-rich repeat variants with susceptibility to Crohn's disease. *Nature*, 411(6837): 599-603.
- Hurtta M, Pitkänen I & Knuutinen J (2004). Melting behaviour of D-sucrose, D-glucose and D-fructose. *Carbohydr Res*, 339(13): 2267-2273.
- Hwang Y-J, Nam S-J, Chun W, Kim SI, Park SC, Kang CD & Lee SJ (2019). Anti-inflammatory effects of apocynin on dextran sulfate sodium-induced mouse colitis model. *PLoS One*, 14(5): e0217642.
- Ibekwe VC, Fadda HM, McConnell EL, Khela MK, Evans DF & Basit AW (2008). Interplay between intestinal pH, transit time and feed status on the in vivo performance of pH responsive ileo-colonic release systems. *Pharm Res*, 25(8): 1828-1835.
- Ibekwe VC, Liu F, Fadda HM, Khela MK, Evans DF, Parsons GE & Basit AW (2006). An investigation into the in vivo performance variability of pH responsive polymers for ileo-colonic drug delivery using gamma scintigraphy in humans. *J Pharm Sci*, 95(12): 2760-2766.
- Islam MA, Alam MR & Hannan MO (2012). Multiresponse optimization based on statistical response surface methodology and desirability function for the production of particleboard. *Compos B Eng*, 43(3): 861-868.
- Jain A, Kesharwani P, Garg NK, Jain A, Jain SA, Jain AK, Nirbhavane P, Ghanghoria R, Tyagi RK & Katare OP (2015). Galactose engineered solid lipid nanoparticles for targeted delivery of doxorubicin. *Colloids Surf B Biointerfaces*, 134: 47-58.
- Jain KK (2012). Nanopharmaceuticals. *The Handbook of Nanomedicine*. Springer; 171-234.

- Jain S & Datta M (2015). Oral extended release of dexamethasone: Montmorillonite–PLGA nanocomposites as a delivery vehicle. *Appl Clay Sci*, 104: 182-188.
- Jerkic M, Peter M, Ardelean D, Fine M, Konerding MA & Letarte M (2010). Dextran sulfate sodium leads to chronic colitis and pathological angiogenesis in Endoglin heterozygous mice. *Inflamm Bowel Dis*, 16(11): 1859-1870.
- Jones G-R, Bain CC, Fenton TM, Kelly A, Brown SL, Ivens AC, Travis MA, Cook PC & MacDonald AS (2018). Dynamics of colon monocyte and macrophage activation during colitis. *Front Immunol*, 9: 2764.
- Jose S, A CT, Sebastian R, H SM, A AN, Durazzo A, Lucarini M, Santini A & Souto EB (2019). Transferrin-Conjugated Docetaxel-PLGA Nanoparticles for Tumor Targeting: Influence on MCF-7 Cell Cycle. *Polymers*, 11(11): 1905.
- Jubeh TT, Barenholz Y & Rubinstein A (2004). Differential adhesion of normal and inflamed rat colonic mucosa by charged liposomes. *Pharm Res*, 21(3): 447-453.
- Kaplan GG (2015). The global burden of IBD: from 2015 to 2025. *Nat Rev Gastroenterol Hepatol*, 12(12): 720-727.
- Kashyap PC, Marcobal A, Ursell LK, Larauche M, Duboc H, Earle KA, Sonnenburg ED, Ferreyra JA, Higginbottom SK & Million M (2013). Complex interactions among diet, gastrointestinal transit, and gut microbiota in humanized mice. *Gastroenterology*, 144(5): 967-977.
- Katsuma M, Watanabe S, Kawai H, Takemura S, Masuda Y & Fukui M (2002). Studies on lactulose formulations for colon-specific drug delivery. *Int J Pharm*, 249(1): 33-43.
- Keely S, Feighery L, Campion DP, O'Brien L, Brayden DJ & Baird AW (2011). Chloride-led disruption of the intestinal mucous layer impedes Salmonella invasion: evidence for an 'enteric tear' mechanism. *Cell Physiol Biochem*, 28(4): 743-752.
- Khan A, Ullah MZ, Afridi R, Rasheed H, Khalid S, Ullah H, Ali H, AlSharari SD, Kim YS & Khan S (2019). Antinociceptive properties of 25-methoxy hispidol A, a triterpenoid isolated from *Poncirus trifoliata* (Rutaceae) through inhibition of NF- κ B signalling in mice. *Phytother Res*, 33(2): 327-341.

- Khan MZI, Prebeg Ž & Kurjaković N (1999). A pH-dependent colon targeted oral drug delivery system using methacrylic acid copolymers: I. Manipulation of drug release using Eudragit® L100-55 and Eudragit® S100 combinations. *J Control Release*, 58(2): 215-222.
- Knipe JM, Strong LE & Peppas NA (2016). Enzyme- and pH-responsive microencapsulated nanogels for oral delivery of siRNA to induce TNF- α knockdown in the intestine. *Biomacromolecules*, 17(3): 788-797.
- Kshirsagar SJ, Bhalekar MR, Patel JN, Mohapatra SK & Shewale NS (2012). Preparation and characterization of nanocapsules for colon-targeted drug delivery system. *Pharm Dev Technol*, 17(5): 607-613.
- Lamprecht A, Yamamoto H, Takeuchi H & Kawashima Y (2003). Microsphere design for the colonic delivery of 5-fluorouracil. *J Control Release*, 90(3): 313-322.
- Lamprecht A, Yamamoto H, Takeuchi H & Kawashima Y (2004). Design of pH-sensitive microspheres for the colonic delivery of the immunosuppressive drug tacrolimus. *Eur J Pharm Biopharm*, 58(1): 37-43.
- Lamprecht A, Yamamoto H, Takeuchi H & Kawashima Y (2005). A pH-sensitive microsphere system for the colon delivery of tacrolimus containing nanoparticles. *J Control Release*, 104(2): 337-346.
- Le Ray A-M, Gautier H, Bouler J-M, Weiss P & Merle C (2010). A new technological procedure using sucrose as porogen compound to manufacture porous biphasic calcium phosphate ceramics of appropriate micro- and macrostructure. *Ceram Int*, 36(1): 93-101.
- Lechner K, Mott S, Al-Saifi R, Knipfer L, Wirtz S, Atreya R, Vieth M, Rath T, Fraass T, Winter Z, August A, Luban J, Zimmermann VS, Weigmann B & Neurath MF (2021). Targeting of the Tec Kinase ITK Drives Resolution of T Cell-Mediated Colitis and Emerges as Potential Therapeutic Option in Ulcerative Colitis. *Gastroenterology*, 161(4): 1270-1287 e19.
- Lechner KS, Neurath MF & Weigmann B (2020). Role of the IL-2 inducible tyrosine kinase ITK and its inhibitors in disease pathogenesis. *J Mol Med (Berl)*, 98(10): 1385-1395.

- Li Q, Hao C, Kang X, Zhang J, Sun X, Wang W & Zeng H (2017). Colorectal cancer and colitis diagnosis using fourier transform infrared spectroscopy and an improved K-nearest-neighbour classifier. *Sensors*, 17(12): 2739.
- Liang Y, Zhao X, Ma PX, Guo B, Du Y & Han X (2019). pH-responsive injectable hydrogels with mucosal adhesiveness based on chitosan-grafted-dihydrocaffeic acid and oxidized pullulan for localized drug delivery. *J Colloid Interface Sci*, 536: 224-234.
- Lim D & Fairbanks AJ (2017). Selective anomeric acetylation of unprotected sugars in water. *Chem. Sci.*, 8(3): 1896-1900.
- Lima IAd, Pomin SP & Cavalcanti OA (2017). Development and characterization of pullulan-polymethacrylate free films as potential material for enteric drug release. *Braz. J. Pharm. Sci.*, 53.
- Lin Y, Yang X, Yue W, Xu X, Li B, Zou L & He R (2014). Chemerin aggravates DSS-induced colitis by suppressing M2 macrophage polarization. *Cell Mol Immunol*, 11(4): 355-366.
- Liu P, Gao C, Chen H, Vong CT, Wu X, Tang X, Wang S & Wang Y (2021). Receptor-mediated targeted drug delivery systems for treatment of inflammatory bowel disease: Opportunities and emerging strategies. *Acta Pharm Sin B*, 11(9): 2798-2818.
- Liu T, Zhang L, Joo D & Sun S-C (2017). NF- κ B signaling in inflammation. *Signal Transduct Target Ther*, 2(1): 17023.
- Lu B, Lv X & Le Y (2019). Chitosan-modified PLGA nanoparticles for control-released drug delivery. *Polymers*, 11(2): 304.
- Lu M & Varley AW (2013). Harvest and culture of mouse peritoneal macrophages. *Bio Protoc*, 3(22): 967-970.
- Ma C, Wang Y, Dong L, Li M & Cai W (2015). Anti-inflammatory effect of resveratrol through the suppression of NF- κ B and JAK/STAT signaling pathways. *Acta Biochim Biophys Sin*, 47(3): 207-213.
- Magalhães J, L Chaves L, C Vieira A, G Santos S, Pinheiro M & Reis S (2020). Optimization of Rifapentine-Loaded Lipid Nanoparticles Using a Quality-by-Design Strategy. *Pharmaceutics*, 12(1): 75.

- Makadia HK & Siegel SJ (2011). Poly lactic-co-glycolic acid (PLGA) as biodegradable controlled drug delivery carrier. *Polymers*, 3(3): 1377-1397.
- Makhlof A, Tozuka Y & Takeuchi H (2009). pH-Sensitive nanospheres for colon-specific drug delivery in experimentally induced colitis rat model. *Eur J Pharm Biopharm*, 72(1): 1-8.
- Mandracchia D, Trapani A, Perteghella S, Sorrenti M, Catenacci L, Torre ML, Trapani G & Tripodo G (2018). pH-sensitive inulin-based nanomicelles for intestinal site-specific and controlled release of celecoxib. *Carbohydr Polym*, 181: 570-578.
- Margarida Cardoso M, Peça IN, Raposo CD, Petrova KT, Teresa Barros M, Gardner R & Bicho A (2016). Doxorubicin-loaded galactose-conjugated poly (d, l-lactide-co-glycolide) nanoparticles as hepatocyte-targeting drug carrier. *J Microencapsul*, 33(4): 315-322.
- Maroni A, Moutaharrik S, Zema L & Gazzaniga A (2017). Enteric coatings for colonic drug delivery: state of the art. *Expert Opin Drug Deliv*, 14(9): 1027-1029.
- Masataka Katsuma, Watanabe S, Takemura S, Sako K, Sawada T, Masuda Y, Nakamura K, Fukui M, Connor AL & Wilding IR (2004). Scintigraphic evaluation of a novel colon-targeted delivery system (CODESTTM) in healthy volunteers. *J Pharm Sci*, 93(5): 1287-1299.
- Masoodi I, Tijjani BM, Wani H, Hassan NS, Khan AB & Hussain S (2011). Biomarkers in the management of ulcerative colitis: a brief review. *Ger Med Sci*, 9.
- Mateescu RB, Bastian AE, Nichita L, Marinescu M, Rouhani F, Voiosu AM, Benguş A, Tudoraşcu DR & Popp CG (2017). Vascular endothelial growth factor-key mediator of angiogenesis and promising therapeutical target in ulcerative colitis. *Rom J Morphol Embryol*, 58(4): 1339-1345.
- Matricon J, Barnich N & Ardid D (2010). Immunopathogenesis of inflammatory bowel disease. *Self/Nonself*, 1(4): 299-309.
- Matsuoka K, Saito E, Fujii T, Takenaka K, Kimura M, Nagahori M, Ohtsuka K & Watanabe M (2015). Tacrolimus for the Treatment of Ulcerative Colitis. *Intest Res*, 13(3): 219-226.
- McConnell EL, Liu F & Basit AW (2009). Colonic treatments and targets: issues and opportunities. *J Drug Target*, 17(5): 335-363.

- McConnell EL, Short MD & Basit AW (2008). An in vivo comparison of intestinal pH and bacteria as physiological trigger mechanisms for colonic targeting in man. *J Control Release*, 130(2): 154-160.
- McGuckin MA, Eri R, Simms LA, Florin TH & Radford-Smith G (2008). Intestinal barrier dysfunction in inflammatory bowel diseases. *Inflamm Bowel Dis*, 15(1): 100-113.
- Meissner Y, Pellequer Y & Lamprecht A (2006). Nanoparticles in inflammatory bowel disease: particle targeting versus pH-sensitive delivery. *Int J Pharm*, 316(1): 138-143.
- Merigo F, Brandolese A, Facchin S, Missaggia S, Bernardi P, Boschi F, D'Inca R, Savarino EV, Sbarbati A & Sturniolo GC (2018). Glucose transporter expression in the human colon. *World J Gastroenterol*, 24(7): 775.
- Miljković M (2010). Relative reactivity of hydroxyl groups in monosaccharides. *Carbohydrates*. Springer; 113-142.
- Mongia P, Khatik R, Raj R, Jain N & Pathak A (2014). pH-Sensitive Eudragit S-100 coated chitosan nanoparticles of 5-amino salicylic acid for colon delivery. *J Biomater Tissue Eng*, 4(9): 738-743.
- Moron MS, Depierre JW & Mannervik B (1979). Levels of glutathione, glutathione reductase and glutathione S-transferase activities in rat lung and liver. *Biochim Biophys Acta Gen Subj*, 582(1): 67-78.
- Mukhtar M, Zesshan M, Khan S, Shahnaz G, Khan SA, Sarwar HS, Pasha RA & Ali H (2020). Fabrication and optimization of pH-sensitive mannose-anchored nano-vehicle as a promising approach for macrophage uptake. *Appl Nanosci*, 1-15.
- Murakami Y, Fujiya M, Konishi H, Isozaki S, Sugiyama Y, Kobayashi Y, Sasaki T, Kunogi T, Takahashi K & Ando K (2021). The Optimal Dose of Tacrolimus in Combination Therapy with an Anti-TNF α Antibody in a Mouse Colitis Model. *Biol Pharm Bull*, 44(4): 564-570.
- Naeem M, Bae J, Oshi MA, Kim M-S, Moon HR, Lee BL, Im E, Jung Y & Yoo J-W (2018a). Colon-targeted delivery of cyclosporine A using dual-functional Eudragit® FS30D/PLGA nanoparticles ameliorates murine experimental colitis. *Int J Nanomedicine*, 13: 1225.

- Naeem M, Cao J, Choi M, Kim WS, Moon HR, Lee BL, Kim M-S, Jung Y & Yoo J-W (2015a). Enhanced therapeutic efficacy of budesonide in experimental colitis with enzyme/pH dual-sensitive polymeric nanoparticles. *Int J Nanomedicine*, 10: 4565.
- Naeem M, Choi M, Cao J, Lee Y, Ikram M, Yoon S, Lee J, Moon HR, Kim M-S & Jung Y (2015b). Colon-targeted delivery of budesonide using dual pH-and time-dependent polymeric nanoparticles for colitis therapy. *Drug Des Devel Ther*, 9: 3789.
- Naeem M, Kim W, Cao J, Jung Y & Yoo J-W (2014). Enzyme/pH dual sensitive polymeric nanoparticles for targeted drug delivery to the inflamed colon. *Colloids Surf B Biointerfaces*, 123: 271-278.
- Naeem M, Oshi MA, Kim J, Lee J, Cao J, Nurhasni H, Im E, Jung Y & Yoo J-W (2018b). pH-triggered surface charge-reversal nanoparticles alleviate experimental murine colitis via selective accumulation in inflamed colon regions. *Nanomed Nanotechnol Biol Med*, 14(3): 823-834.
- Naghavi M, Wang H, Lozano R, Davis A, Liang X, Zhou M, Vollset SE, Ozgoren AA, Abdalla S & Abd-Allah F (2015). Global, regional, and national age-sex specific all-cause and cause-specific mortality for 240 causes of death, 1990-2013: a systematic analysis for the Global Burden of Disease Study 2013. *Lancet*, 385(9963): 117-171.
- Nakase H, Okazaki K, Tabata Y, Uose S, Ohana M, Uchida K, Matsushima Y, Kawanami C, Oshima C & Ikada Y (2000). Development of an oral drug delivery system targeting immune-regulating cells in experimental inflammatory bowel disease: a new therapeutic strategy. *J Pharmacol Exp Ther*, 292(1): 15-21.
- Namdev N & Patidar R (2016). Design and evaluation of enteric coated egg albumin microspheres loaded with Mesalamine for colon-specific drug delivery. *World J Pharm Pharm Sci*, 8: 1765-78.
- Nejad ZM, Torabinejad B, Davachi SM, Zamanian A, Garakani SS, Najafi F & Nezafati N (2019). Synthesis, physicochemical, rheological and in-vitro characterization of double-crosslinked hyaluronic acid hydrogels containing dexamethasone and PLGA/dexamethasone nanoparticles as hybrid systems for specific medical applications. *Int J Biol Macromol*, 126: 193-208.
- Ng SC, Shi HY, Hamidi N, Underwood FE, Tang W, Benchimol EI, Panaccione R, Ghosh S, Wu JC & Chan FK (2017). Worldwide incidence and prevalence of

- inflammatory bowel disease in the 21st century: a systematic review of population-based studies. *Lancet*, 390(10114): 2769-2778.
- Nidhi, Rashid M, Kaur V, Hallan SS, Sharma S & Mishra N (2016). Microparticles as controlled drug delivery carrier for the treatment of ulcerative colitis: A brief review. *Saudi Pharm J*, 24(4): 458-472.
- Nugent S, Kumar D, Rampton D & Evans D (2001). Intestinal luminal pH in inflammatory bowel disease: possible determinants and implications for therapy with aminosalicylates and other drugs. *Gut*, 48(4): 571-577.
- Nunes T, Barreiro-de Acosta M, Marin-Jiménez I, Nos P & Sans M (2013). Oral locally active steroids in inflammatory bowel disease. *J Crohns Colitis*, 7(3): 183-191.
- Onishi H, Oosegi T & Machida Y (2008). Efficacy and toxicity of Eudragit-coated chitosan–succinyl-prednisolone conjugate microspheres using rats with 2, 4, 6-trinitrobenzenesulfonic acid-induced colitis. *Int J Pharm*, 358(1): 296-302.
- Orecchioni M, Ghosheh Y, Pramod AB & Ley K (2019). Macrophage Polarization: Different Gene Signatures in M1(LPS+) vs. Classically and M2(LPS–) vs. Alternatively Activated Macrophages. *Front Immunol*, 10.
- Organization WH (2010). *WHO guidelines on drawing blood: best practices in phlebotomy*, World Health Organization.
- Oshi MA, Naeem M, Bae J, Kim J, Lee J, Hasan N, Kim W, Im E, Jung Y & Yoo J-W (2018). Colon-targeted dexamethasone microcrystals with pH-sensitive chitosan/alginate/Eudragit S multilayers for the treatment of inflammatory bowel disease. *Carbohydr Polym*, 198: 434-442.
- Pallagi E, Ambrus R, Szabó-Révész P & Csóka I (2015). Adaptation of the quality by design concept in early pharmaceutical development of an intranasal nanosized formulation. *Int J Pharm*, 491(1-2): 384-92.
- Papa A, Danese S, Gasbarrini A & Gasbarrini G (2000). Potential therapeutic applications and mechanisms of action of heparin in inflammatory bowel disease. *Aliment Pharmacol Ther*, 14(11): 1403-1409.
- Park J-H, Cho H-J & Kim D-D (2017). Poly((D,L)lactic-glycolic)acid-star glucose nanoparticles for glucose transporter and hypoglycemia-mediated tumor targeting. *Int J Nanomedicine*, 12: 7453-7467.

- Park SY, Kang Z, Thapa P, Jin YS, Park JW, Lim HJ, Lee JY, Lee SW, Seo MH, Kim MS & Jeong SH (2019). Development of sorafenib loaded nanoparticles to improve oral bioavailability using a quality by design approach. *Int J Pharm*, 566: 229-238.
- Park YH, Kim N, Shim YK, Choi YJ, Nam RH, Choi YJ, Ham MH, Suh JH, Lee SM, Lee CM, Yoon H, Lee HS & Lee DH (2015). Adequate Dextran Sodium Sulfate-induced Colitis Model in Mice and Effective Outcome Measurement Method. *Journal of cancer prevention*, 20(4): 260-267.
- Patel K, Doddapaneni R, Sekar V, Chowdhury N & Singh M (2016a). Combination approach of YSA peptide anchored docetaxel stealth liposomes with oral antifibrotic agent for the treatment of lung cancer. *Mol Pharm*, 13(6): 2049-2058.
- Patel RR, Chaurasia S, Khan G, Chaubey P, Kumar N & Mishra B (2016b). Cromolyn sodium encapsulated PLGA nanoparticles: An attempt to improve intestinal permeation. *Int J Biol Macromol*, 83: 249-258.
- Peça IN, Petrova KT, Cardoso MM & Barros MT (2012). Preparation and characterization of polymeric nanoparticles composed of poly (dl-lactide-co-glycolide) and poly (dl-lactide-co-glycolide)-co-poly (ethylene glycol)-10%-Triblock end-capped with a galactose moiety. *React Funct Polym*, 72(10): 729-735.
- Pellequer. Yann, Meissner. Yvette, Ubrich. Nathalie & Alf L (2007). Epithelial heparin delivery via microspheres mitigates experimental colitis in mice. *J Pharmacol Exp Ther*, 321(2): 726-733.
- Pichai M & Ferguson LR (2012). Potential prospects of nanomedicine for targeted therapeutics in inflammatory bowel diseases. *World J Gastroenterol*, 18(23): 2895-2901.
- Pirro M, Rombouts Y, Stella A, Neyrolles O, Bulet-Schiltz O, van Vliet SJ, de Ru AH, Mohammed Y, Wuhler M & van Veelen PA (2020). Characterization of Macrophage Galactose-type Lectin (MGL) ligands in colorectal cancer cell lines. *Biochim Biophys Acta Gen Subj*, 1864(4): 129513.
- Podczec F, Mitchell CL, Newton JM, Evans D & Short MB (2007). The gastric emptying of food as measured by gamma-scintigraphy and electrical impedance tomography (EIT) and its influence on the gastric emptying of tablets of different dimensions. *J Pharm Pharmacol*, 59(11): 1527-1536.

- Pooja D, Kulhari H, Tunki L, Chinde S, Kuncha M, Grover P, Rachamalla SS & Sistla R (2015). Nanomedicines for targeted delivery of etoposide to non-small cell lung cancer using transferrin functionalized nanoparticles. *RSC Adv*, 5(61): 49122-49131.
- Prantera C & Marconi S (2013). Glucocorticosteroids in the treatment of inflammatory bowel disease and approaches to minimizing systemic activity. *Therap Adv Gastroenterol*, 6(2): 137-156.
- Pulli B, Ali M, Forghani R, Schob S, Hsieh KL, Wojtkiewicz G, Linnoila JJ & Chen JW (2013). Measuring myeloperoxidase activity in biological samples. *PLoS One*, 8(7): e67976.
- Radu M & Chernoff J (2013). An in vivo assay to test blood vessel permeability. *J Vis Exp*, (73): e50062-e50062.
- Rana S, Sharma S, Malik A, Kaur J, Prasad K, Sinha S & Singh K (2013). Small intestinal bacterial overgrowth and orocecal transit time in patients of inflammatory bowel disease. *Dig Dis Sci*, 58(9): 2594-2598.
- Ren Y, Jian X, Zhang Z, Ning Q, Kan B & Kong L (2020). Effects of tacrolimus on the TGF- β 1/SMAD signaling pathway in paraquat-exposed rat alveolar type II epithelial cells. *Mol Med Report*, 22(5): 3687-3694.
- Rhodes JM (2007). The role of *Escherichia coli* in inflammatory bowel disease. *Gut*, 56(5): 610-612.
- Riccardi C & Nicoletti I (2006). Analysis of apoptosis by propidium iodide staining and flow cytometry. *Nat Protoc*, 1(3): 1458-1461.
- Roldo M, Hornof M, Caliceti P & Bernkop-Schnürch A (2004). Mucoadhesive thiolated chitosans as platforms for oral controlled drug delivery: synthesis and in vitro evaluation. *Eur J Pharm Biopharm*, 57(1): 115-121.
- Rossi S, Vigani B, Sandri G, Bonferoni MC, Caramella CM & Ferrari F (2019). Recent advances in the mucus-interacting approach for vaginal drug delivery: From mucoadhesive to mucus-penetrating nanoparticles. *Expert Opin Drug Deliv*, 16(8): 777-781.
- Rowe RC, Sheskey PJ & Weller PJ (2009). *Handbook of pharmaceutical excipients*, Libros Digitales-Pharmaceutical Press.

- Saha S, Buttari B, Panieri E, Profumo E & Saso L (2020). An overview of Nrf2 signaling pathway and its role in inflammation. *Molecules*, 25(22): 5474.
- Salas A, Hernandez-Rocha C, Duijvestein M, Faubion W, McGovern D, Vermeire S, Vetrano S & Vande Casteele N (2020). JAK–STAT pathway targeting for the treatment of inflammatory bowel disease. *Nat Rev Gastroenterol Hepatol*, 17(6): 323-337.
- Saltan F & Akat H (2013). Synthesis and thermal degradation kinetics of D-(+)-GALACTOSE CONTAINING POLYMERS. *Polímeros*, 23(6): 697-704.
- Sana E, Zeeshan M, Ain QU, Khan AU, Hussain I, Khan S, Lepeltier E & Ali H (2021). Topical delivery of curcumin-loaded transfersomes gel ameliorated rheumatoid arthritis by inhibiting NF- κ B pathway. *Nanomedicine*, 16(10): 819-837.
- Sardoiwala MN, Kushwaha AC, Dev A, Shrimali N, Guchhait P, Karmakar S & Roy Choudhury S (2020). Hypericin-loaded transferrin nanoparticles induce PP2A-regulated BMI1 degradation in colorectal cancer-specific chemo-photodynamic therapy. *ACS Biomater Sci Eng*, 6(5): 3139-3153.
- Sareen R, Jain N, Rajkumari A & Dhar K (2016). pH triggered delivery of curcumin from Eudragit-coated chitosan microspheres for inflammatory bowel disease: characterization and pharmacodynamic evaluation. *Drug Deliv*, 23(1): 55-62.
- Sartor RB (2008). Microbial influences in inflammatory bowel diseases. *Gastroenterology*, 134(2): 577-594.
- Sartor RB (2010). Genetics and environmental interactions shape the intestinal microbiome to promote inflammatory bowel disease versus mucosal homeostasis. *Gastroenterology*, 139(6): 1816-1819.
- Sasaki Y, Hada R, Nakajima H, Fukuda S & Munakata A (1997). Improved localizing method of radiopill in measurement of entire gastrointestinal pH profiles: colonic luminal pH in normal subjects and patients with Crohn's disease. *Am J Gastroenterol*, 92(1).
- Scheeren LE, Nogueira-Librelo DR, Macedo LB, de Vargas JM, Mitjans M, Vinardell MP & Rolim CMB (2020). Transferrin-conjugated doxorubicin-loaded PLGA nanoparticles with pH-responsive behavior: a synergistic approach for cancer therapy. *J Nanopart Res*, 22(3): 72.

- Schmidt C, Lautenschlaeger C, Collnot E-M, Schumann M, Bojarski C, Schulzke J-D, Lehr C-M & Stallmach A (2013). Nano-and microscaled particles for drug targeting to inflamed intestinal mucosa—A first in vivo study in human patients. *J Control Release*, 165(2): 139-145.
- Schnoor M (2015). E-cadherin Is Important for the Maintenance of Intestinal Epithelial Homeostasis Under Basal and Inflammatory Conditions. *Dig Dis Sci*, 60(4): 816-818.
- Senthilkumar M, Amaresan N & Sankaranarayanan A (2021). Estimation of Catalase. *Plant-Microbe Interactions: Laboratory Techniques*. New York, NY: Springer US; 113-115.
- Shal B, Khan A, Khan AU, Ullah R, Ali G, Islam SU, Ali H, Seo E-K & Khan S (2021). Alleviation of Memory Deficit by Bergenin via the Regulation of Reelin and Nrf-2/NF- κ B Pathway in Transgenic Mouse Model. *Int J Mol Sci*, 22(12): 6603.
- Sharma N, Madan P & Lin S (2016). Effect of process and formulation variables on the preparation of parenteral paclitaxel-loaded biodegradable polymeric nanoparticles: A co-surfactant study. *Asian J Pharm Sci*, 11(3): 404-416.
- Sharma V, Kaur A & Singh TG (2020). Counteracting role of nuclear factor erythroid 2-related factor 2 pathway in Alzheimer's disease. *Biomed Pharmacother*, 129: 110373.
- Shefer A & Shefer S 2004. Oral controlled release system for targeted drug delivery into the cell and its nucleus for gene therapy, DNA vaccination, and administration of gene based drugs. US Patent No. 20040224019A1.
- Shefer A & Shefer SD 2010. pH triggered targeted controlled release systems for the delivery of pharmaceutical active ingredients. U.S. Patent No. 7,670,627.
- Shen Y, Li X, Dong D, Zhang B, Xue Y & Shang P (2018). Transferrin receptor 1 in cancer: a new sight for cancer therapy. *Am J Cancer Res*, 8(6): 916-931.
- Shepherd VL, Lee Y, Schlesinger PH & Stahl PD (1981). L-Fucose-terminated glycoconjugates are recognized by pinocytosis receptors on macrophages. *Proceedings of the National Academy of Sciences*, 78(2): 1019-1022.
- Simões A, Veiga F, Figueiras A & Vitorino C (2018). A practical framework for implementing Quality by Design to the development of topical drug products: Nanosystem-based dosage forms. *Int J Pharm*, 548(1): 385-399.

- Singh R & Saini G (2014). Pullulan as therapeutic tool in biomedical applications. *Advances in Industrial Biotechnology*. India: IK International Publishing House Pvt. Ltd; 263-91.
- Singh RS, Kaur N, Hassan M & Kennedy JF (2021). Pullulan in biomedical research and development-A review. *Int J Biol Macromol*, 166: 694-706.
- Singh RS, Kaur N, Rana V & Kennedy JF (2017). Pullulan: A novel molecule for biomedical applications. *Carbohydr Polym*, 171: 102-121.
- Sipos B, Szabó-Révész P, Csóka I, Pallagi E, Dobó DG, Bélteky P, Kónya Z, Deák Á, Janovák L & Katona G (2020). Quality by Design Based Formulation Study of Meloxicam-Loaded Polymeric Micelles for Intranasal Administration. *Pharmaceutics*, 12(8): 697.
- Siu FY, Ye S, Lin H & Li S (2018). Galactosylated PLGA nanoparticles for the oral delivery of resveratrol: enhanced bioavailability and in vitro anti-inflammatory activity. *Int J Nanomedicine*, 13: 4133.
- Sohail M, Mudassir, Minhas MU, Khan S, Hussain Z, de Matas M, Shah SA, Khan S, Kousar M & Ullah K (2019). Natural and synthetic polymer-based smart biomaterials for management of ulcerative colitis: a review of recent developments and future prospects. *Drug Deliv and Transl Res*, 9(2): 595-614.
- Sohail MF, Javed I, Hussain SZ, Sarwar S, Akhtar S, Nadhman A, Batool S, Bukhari NI, Saleem RSZ & Hussain I (2016). Folate grafted thiolated chitosan enveloped nanoliposomes with enhanced oral bioavailability and anticancer activity of docetaxel. *J Mater Chem B*, 4(37): 6240-6248.
- Solomon L, Mansor S, Mallon P, Donnelly E, Hoper M, Loughrey M, Kirk S & Gardiner K (2010). The dextran sulphate sodium (DSS) model of colitis: an overview. *Comp Clin Path*, 19(3): 235-239.
- Sproston NR & Ashworth JJ (2018). Role of C-reactive protein at sites of inflammation and infection. *Front Immunol*, 9: 754.
- Tacchini L, Gammella E, De Ponti C, Recalcati S & Cairo G (2008). Role of HIF-1 and NF- κ B transcription factors in the modulation of transferrin receptor by inflammatory and anti-inflammatory signals. *J Biol Chem*, 283(30): 20674-20686.

- Takeuchi I, Tomoda K, Hamano A & Makino K (2017). Effects of physicochemical properties of poly (lactide-co-glycolide) on drug release behavior of hydrophobic drug-loaded nanoparticles. *Colloids Surf Physicochem Eng Aspects*, 520: 771-778.
- Talaei F, Atyabi F, Azhdarzadeh M, Dinarvand R & Saadatzadeh A (2013). Overcoming therapeutic obstacles in inflammatory bowel diseases: a comprehensive review on novel drug delivery strategies. *Eur J Pharm Sci*, 49(4): 712-722.
- Texler B, Zollner A, Reinstadler V, Reider SJ, Macheiner S, Jelusic B, Pfister A, Watschinger C, Przysiecki N, Tilg H, Oberacher H & Moschen AR (2022). Tofacitinib-Induced Modulation of Intestinal Adaptive and Innate Immunity and Factors Driving Cellular and Systemic Pharmacokinetics. *Cell Mol Gastroenterol Hepatol*, 13(2): 383-404.
- Thakral S, Thakral NK & Majumdar DK (2013). Eudragit®: a technology evaluation. *Expert Opin Drug Deliv*, 10(1): 131-149.
- Thiesen A, Wild G, Tappenden K, Drozdowski L, Keelan M, Thomson B, McBurney M, Clandinin M & Thomson A (2003). The locally acting glucocorticosteroid budesonide enhances intestinal sugar uptake following intestinal resection in rats. *Gut*, 52(2): 252-259.
- Thoreson R & Cullen JJ (2007). Pathophysiology of inflammatory bowel disease: an overview. *Surg Clin North Am*, 87(3): 575-585.
- Tian B, Liu S, Lu W, Jin L, Li Q, Shi Y, Li C, Wang Z & Du Y (2016). Construction of pH-responsive and up-conversion luminescent NaYF₄: Yb³⁺/Er³⁺@ SiO₂@ PMAA nanocomposite for colon targeted drug delivery. *Sci Rep*, 6.
- Tirosh B, Khatib N, Barenholz Y, Nissan A & Rubinstein A (2009). Transferrin as a luminal target for negatively charged liposomes in the inflamed colonic mucosa. *Mol Pharm*, 6(4): 1083-1091.
- Tsikas D (2007). Analysis of nitrite and nitrate in biological fluids by assays based on the Griess reaction: appraisal of the Griess reaction in the L-arginine/nitric oxide area of research. *J Chromatogr B*, 851(1-2): 51-70.
- Uchiyama K, Kishi H, Komatsu W, Nagao M, Ohhira S & Kobashi G (2018). Lipid and Bile Acid Dysmetabolism in Crohn's Disease. *J Immunol Res*, 2018.

- Uronen-Hansson H, Persson E, Nilsson P & Agace W (2014). Isolation of cells from human intestinal tissue. *Bio Protoc*, 4(7): e1092.
- Van Citters GW & Lin HC (2006). Ileal brake: neuropeptidergic control of intestinal transit. *Curr Gastroenterol Rep*, 8(5): 367-373.
- van Kooyk Y, Ibarregui JM & van Vliet SJ (2015). Novel insights into the immunomodulatory role of the dendritic cell and macrophage-expressed C-type lectin MGL. *Immunobiology*, 220(2): 185-192.
- Varshosaz J, Emami J, Tavakoli N, Minaiyan M, Rahmani N, Dorkoosh F & Mahzouni P (2011). Development of novel budesonide pellets based on CODESTM technology: in vitro/in vivo evaluation in induced colitis in rats. *Daru*, 19(2): 107.
- Varshosaz J, Minaiyan M & Khaleghi N (2015). Eudragit nanoparticles loaded with silybin: a detailed study of preparation, freeze-drying condition and in vitro/in vivo evaluation. *J Microencapsul*, 32(3): 211-223.
- Varshosaz J, Riahi S, Ghassami E & Jahanian-Najafabadi A (2017). Transferrin-targeted poly(butylene adipate)/terephthalate nanoparticles for targeted delivery of 5-fluorouracil in HT29 colorectal cancer cell line. *J Bioact Comp Polym*, 32(5): 503-527.
- Venkatesan T, Choi Y-W, Lee J & Kim Y-K (2018). Falcarindiol inhibits LPS-induced inflammation via attenuating MAPK and JAK-STAT signaling pathways in murine macrophage RAW 264.7 cells. *Mol Cell Biochem*, 445(1): 169-178.
- Vindigni SM, Zisman TL, Suskind DL & Damman CJ (2016). The intestinal microbiome, barrier function, and immune system in inflammatory bowel disease: a tripartite pathophysiological circuit with implications for new therapeutic directions. *Therap Adv Gastroenterol*, 9(4): 606-625.
- Viscido A, Capannolo A, Latella G, Caprilli R & Frieri G (2014). Nanotechnology in the treatment of inflammatory bowel diseases. *J Crohns Colitis*, 8(9): 903-918.
- Waldner MJ & Neurath MF (2009). Chemically induced mouse models of colitis. *Curr Protoc Pharmacol*, 46(1): 5.55. 1-5.55. 15.
- Wang X-Q & Zhang Q (2012). pH-sensitive polymeric nanoparticles to improve oral bioavailability of peptide/protein drugs and poorly water-soluble drugs. *Eur J Pharm Biopharm*, 82(2): 219-229.

- Wang Y, Liu X, Liu G, Guo H, Li C, Zhang Y, Zhang F, Zhao Z & Cheng H (2016). Novel galactosylated biodegradable nanoparticles for hepatocyte-delivery of oridonin. *Int J Pharm*, 502(1-2): 47-60.
- Watts P & Smith A (2005). TARGIT™ technology: coated starch capsules for site-specific drug delivery into the lower gastrointestinal tract. *Expert Opin Drug Deliv*, 2(1): 159-167.
- Weigmann B & Neurath MF (2016). Oxazolone-induced colitis as a model of Th2 immune responses in the intestinal mucosa. *Gastrointestinal Physiology and Diseases*. Springer; 253-261.
- Wu B, Tong J & Ran Z (2020). Tacrolimus therapy in steroid-refractory ulcerative colitis: a review. *Inflamm Bowel Dis*, 26(1): 24-32.
- Xiao B, Chen Q, Zhang Z, Wang L, Kang Y, Denning T & Merlin D (2018). TNF α gene silencing mediated by orally targeted nanoparticles combined with interleukin-22 for synergistic combination therapy of ulcerative colitis. *J Control Release*, 287: 235-246.
- Xiao B & Merlin D (2012). Oral colon-specific therapeutic approaches toward treatment of inflammatory bowel disease. *Expert Opin Drug Deliv*, 9(11): 1393-1407.
- Xu Q, Zhang N, Qin W, Liu J, Jia Z & Liu H (2013). Preparation, in vitro and in vivo evaluation of budesonide loaded core/shell nanofibers as oral colonic drug delivery system. *J Nanosci Nanotechnol*, 13(1): 149-156.
- Yamamoto-Furusho JK, Mendivil-Rangel EJ & Fonseca-Camarillo G (2012). Differential expression of occludin in patients with ulcerative colitis and healthy controls. *Inflamm Bowel Dis*, 18(10): E1999-E1999.
- Yang C & Merlin D (2019). Nanoparticle-mediated drug delivery systems for the treatment of IBD: Current perspectives. *Int J Nanomedicine*, 14: 8875.
- Yang L (2008). Biorelevant dissolution testing of colon-specific delivery systems activated by colonic microflora. *J Control Release*, 125(2): 77-86.
- Yang M, Zhang Y, Ma Y, Yan X, Gong L, Zhang M & Zhang B (2020). Nanoparticle-based therapeutics of inflammatory bowel diseases: a narrative review of the current state and prospects. *J BioX Res*, 3(04): 157-173.

- Yin Y, Chen D, Qiao M, Lu Z & Hu H (2006). Preparation and evaluation of lectin-conjugated PLGA nanoparticles for oral delivery of thymopentin. *J Control Release*, 116(3): 337-345.
- Yoshida T, Lai TC, Kwon GS & Sako K (2013). pH-and ion-sensitive polymers for drug delivery. *Expert Opin Drug Deliv*, 10(11): 1497-1513.
- Zeeshan M, Ali H, Ain QU, Mukhtar M, Gul R, Sarwar A & Khan S (2021). A holistic QBD approach to design galactose conjugated PLGA polymer and nanoparticles to catch macrophages during intestinal inflammation. *Mater Sci Eng, C*, 126: 112183.
- Zeeshan M, Ali H, Khan S, Khan SA & Weigmann B (2019a). Advances in orally-delivered pH-sensitive nanocarrier systems; an optimistic approach for the treatment of inflammatory bowel disease. *Int J Pharm*, 558: 201-214.
- Zeeshan M, Ali H, Khan S, Mukhtar M, Khan MI & Arshad M (2019b). Glycyrrhizic acid-loaded pH-sensitive poly-(lactic-co-glycolic acid) nanoparticles for the amelioration of inflammatory bowel disease. *Nanomedicine*, 14(15): 1945-1969.
- Zembruski NC, Stache V, Haefeli WE & Weiss J (2012). 7-Aminoactinomycin D for apoptosis staining in flow cytometry. *Anal Biochem*, 429(1): 79-81.
- Zhang J, Tang C & Yin C (2013). Galactosylated trimethyl chitosan–cysteine nanoparticles loaded with Map4k4 siRNA for targeting activated macrophages. *Biomaterials*, 34(14): 3667-3677.
- Zhang X, Goncalves R & Mosser DM (2008). The isolation and characterization of murine macrophages. *Curr Protoc Immunol*, 83(1): 14.1. 1-14.1. 14.
- Zhang Y-Z & Li Y-Y (2014). Inflammatory bowel disease: pathogenesis. *World J Gastroenterol*, 20(1): 91.
- Zhang Y, Huo M, Zhou J, Zou A, Li W, Yao C & Xie S (2010). DDSolver: an add-in program for modeling and comparison of drug dissolution profiles. *AAPS Journal*, 12(3): 263-271.
- Zhou J, Li M, Lim WQ, Luo Z, Phua SZF, Huo R, Li L, Li K, Dai L & Liu J (2018). A transferrin-conjugated hollow nanoplatform for redox-controlled and targeted chemotherapy of tumor with reduced inflammatory reactions. *Theranostics*, 8(2): 518.

-
- Zhou Y & Zhi F (2016). Lower level of bacteroides in the gut microbiota is associated with inflammatory bowel disease: a meta-analysis. *Biomed Res Int*, 2016.
- Zizzari IG, Napoletano C, Battisti F, Rahimi H, Caponnetto S, Pierelli L, Nuti M & Rughetti A (2015). MGL receptor and immunity: when the ligand can make the difference. *J Immunol Res*, 2015.
- Zolnik BS & Burgess DJ (2007). Effect of acidic pH on PLGA microsphere degradation and release. *J Control Release*, 122(3): 338-344.
- Zu M, Ma Y, Cannup B, Xie D, Jung Y, Zhang J, Yang C, Gao F, Merlin D & Xiao B (2021). Oral delivery of natural active small molecules by polymeric nanoparticles for the treatment of inflammatory bowel diseases. *Adv Drug Del Rev*, 176: 113887.
- Zuo J, Gao Y, Bou-Chacra N & Löbenberg R (2014). Evaluation of the DDSolver software applications. *Biomed Res Int*, 2014: 204925-204925.
- Zuo L, Huang Z, Dong L, Xu L, Zhu Ya, Zeng K, Zhang C, Chen J & Zhang J (2010). Targeting delivery of anti-TNF α oligonucleotide into activated colonic macrophages protects against experimental colitis. *Gut*, 59(4): 470-479.

ANNEXURE

Annexure I: List of Publications

Published work from PhD Thesis:

1. Advances in orally-delivered pH-sensitive nanocarrier systems; an optimistic approach for the treatment of inflammatory bowel disease

Mahira Zeeshan, Hussain Ali, Salman Khan, Saeed Ahmad Khan, Benno Weigmann

Published in International Journal of Pharmaceutics 588(2019): p 201-214 (IF: 5.875)

2. A holistic QBD approach to design galactose conjugated PLGA polymer and nanoparticles to catch macrophages during intestinal inflammation

Mahira Zeeshan, Hussain Ali, Qurat Ul Ain, Mahwash Mukhtar, Rabia Gul, Atif Sarwar, Salman Khan

Published in Materials Science and Engineering: C, 126 (2021): 112183 (IF: 7.328)

Manuscripts Submitted to Journals:

1. Dual Stimuli-Sensitive ES100/Pullulan Coated Galactosylated Nanocargoes for Multi-Level Targeting to Combat Colitis
2. QbD-based fabrication of Tofacitinib citrate entrapped transferrin anchored polymeric nanocarriers for site-specific targeting of colon epithelial cells and macrophages to treat mucosal inflammation
3. pH-responsive lipid-PLGA/tfr nanoshells to target and treat ulcerative colitis via JAK/STAT blockade

To be submitted:

1. Double pH sensitive-L-Lysine-decorated tacrolimus loaded PLGA nanocargoes for the specific targeting and amelioration of intestinal inflammation via downregulation of pITK in the T-cells

Patent to be submitted:

Anti-ITK-siRNA based nanocarriers for IBD oral therapeutics

List of Other Publications

1. Small but powerful: Will nanoparticles be the future state-of-the-art therapy for IBD, *Expert Opinion on Drug Delivery* 558 (2022) 201–214 (IF=6.648)
 2. Glycyrrhizic acid-loaded pH-sensitive poly-(lactic-co-glycolic acid) nanoparticles for the amelioration of inflammatory bowel disease, *Journal: Nanomedicine* Vol. 14, No. 15 (2019), 1945-1969 (IF=5.307)
 3. Biomimetic hydroxyapatite as potential polymeric nanocarrier for the treatment of rheumatoid arthritis, *Journal: Journal of Biomedical Materials Research (Part A)* Vol. 107 (2019); 2595-2600 (IF=4.396)
 4. Fabrication and optimization of pH-sensitive mannose-anchored nano-vehicle as a promising approach for macrophage uptake. *Journal: Applied nanoscience*. Vol 10 (2020) 4013–4027 (IF= 3.674)
 5. Aerodynamic properties and in silico deposition of isoniazid loaded chitosan/thiolated chitosan and hyaluronic acid hybrid nanoplex DPIs as a potential TB treatment. *Journal: International Journal of Biological Macromolecules*. Vol 165, Part B (2020) 3007-3019 (IF: 6.953)
 6. Onco-Receptors Targeting in Lung Cancer via Application of Surface-Modified and Hybrid Nanoparticles: A Cross-Disciplinary Review, *Journal: Processes* (IF: 2.847)
 7. Topical delivery of curcumin-loaded transfersomes gel ameliorated rheumatoid arthritis by inhibiting NF- κ B pathway, *Journal: Nanomedicine* Vol. 16, No. 10 (2021), 1945-1969 (IF=5.307)
 8. DNA based and stimuli-responsive smart nanocarrier for diagnosis and treatment of cancer: Applications and challenges, *Journal: Cancers* (IF: 6.693)
 9. A holistic QBD approach to design galactose conjugated PLGA polymer and nanoparticles to catch macrophages during intestinal inflammation, *Journal: Materials Science and Engineering: C* (IF: 7.328)
 10. Evaluating the mucoprotective effects of glycyrrhizic acid-loaded polymeric nanoparticles in a murine model of 5-fluorouracil-induced intestinal mucositis via suppression of inflammatory mediators and oxidative stress, *Journal: Inflammopharmacology* (4.473)
 11. Simulation, In Vitro, and In Vivo Cytotoxicity Assessments of Methotrexate-Loaded pH-Responsive Nanocarriers, *Journal: Polymers* (IF: 4.329)
 12. Chitosan biopolymer, its derivatives and potential applications in nano-therapeutics: A comprehensive review, *Journal: European Polymer Journal* (IF: 4.598)
 13. Nanomaterials in the Management of Gram-Negative Bacterial Infections, *Journal: Nanomaterials* (IF: 5.076)
- BOOK CHAPTER: Nanopharmaceuticals: A Boon to the Brain-Targeted Drug Delivery, *Book: Pharmaceutical Formulation Design - Recent Practices (Chapter 7)* (IntechOpen)

List of Conferences and Seminars

- 2nd International Conference on Recent Innovations in Pharmaceutical Sciences (ICRIPS)-2017
- 3 Days National Workshop on Nanomedicine: Advancement & Challenges in Pakistan-2017
- 1st International Conference on Advances in Drug Discovery and Development (ICAD3)- 3-5th January, 2018
- First international conference on Nanoscience and nanotechnology (ICONN)- 1-2 November 2018 at NUST, Islamabad
- 3rd International conference on “Recent advancement in pharmaceutical research and drug delivery” at QAU, Islamabad (19-20th Feb, 2019)
- 4th International Conference (Virtual) on “Integrative multidisciplinary nanomedicine: a game-changing strategy for emerging infectious disease” at Quaid-i-Azam University, Islamabad (10th October, 2020)
- Online conference “First Anti-microbial resistance (AMR) Youth Summit” organized by world health students’ alliance (W.H.S.A) (20-22nd November, 2020)
- 6th CRC1811 symposium on “Th2 immunity mediated diseases” at University Hospital, Erlangen, Germany (18th November, 2021)
- Quarterly conference to present recent research findings at Medical Clinic 1, University Hospital, Erlangen, Germany (24th November, 2021)
- IV. Symposium of Young Researchers on Pharmaceutical Technology, Biotechnology and Regulatory Science at University of Szeged, Hungary (19-22nd January, 2022)

ORCID ID: 0000-0002-3539-7971

Cumulative Impact: 82.152

Total Citations (till Aug 2022): 230



Contents lists available at ScienceDirect

International Journal of Pharmaceutics

journal homepage: www.elsevier.com/locate/ijpharm

Review

Advances in orally-delivered pH-sensitive nanocarrier systems; an optimistic approach for the treatment of inflammatory bowel disease

Mahira Zeeshan^a, Hussain Ali^{a,*}, Salman Khan^a, Saeed Ahmad Khan^b, Benno Weigmann^c^a Department of Pharmacy, Quaid-i-Azam University Islamabad, 45320, Pakistan^b Department of Pharmacy, Kohat University of Science and Technology, KPK, Pakistan^c Medical Clinic I, University Hospital Erlangen, Research Campus, 91052 Erlangen, Germany

ARTICLE INFO

Keywords:

IBD
Drug delivery system
pH-sensitive nanocarriers
pH-dependent nanoparticles
pH-dependent microparticles
Colon targeting

ABSTRACT

Inflammatory bowel disease (IBD) is the inflammation of the gastrointestinal tract (GIT) affecting the colon and ileum in particular. Increasing IBD prevalence worldwide is alarming, and needs to be resolved. Due to the limited therapeutic efficacy, accompanying adverse effects, dependence, and pharmacokinetics issues of the available therapy, IBD patients have compromised quality of life. Meanwhile, conventional drug delivery systems (DDS) for IBD face many obstacles en-route to the colon, such as physiological and pathophysiological barriers, genetic variability, disease severity, and nutrition status. Therefore, the pH-dependent nanocarrier DDS is a recent advancement that fulfills the need for a more tolerable and effective remedy for IBD. It facilitates localized and targeted action, eliminating systemic adverse effects and unnecessary flushing of the drug from the inflamed colon tissues. The integration of a pH-sensitive polymer as a nanocarrier provides protection in drug transport to the lower region of the GIT. In this review, we will briefly explain IBD pathophysiology, the pros and cons of pH-dependent conventional DDS, and highlight a novel pH-dependent nanocarrier system for treating the disease.

1. Introduction

Inflammatory bowel disease (IBD) is a chronic, episodic mucosal inflammation of the gastrointestinal tract (GIT) mainly affecting the colon and ileum. Ulcerative colitis (UC) and Crohn's disease (CD) are the two most prevalent types of IBD (Abraham and Cho, 2009); the major point of differentiation between the two is the location and the depth to which the intestine is inflamed. In UC, inflammation afflicts the innermost mucosal layer and proceeds continuously from the rectum to the proximal colon. On the contrary, in CD, inflammation penetrates to the deeper tissues instead of being confined to the mucosal layer, and can appear in any GI section, often the colon and terminal ileum in a discontinuous manner (Abraham and Cho, 2009; Hua et al., 2015). The worldwide growing prevalence of IBD affected about 412–505/100,000 persons in Europe and 286/100,000 in North America and led to 51,000 deaths worldwide in 2013 (Kaplan, 2015; Naghavi et al., 2015; Ng et al., 2017). Although patients belong to any age group, the main target group is those aged 15–30 years (Hanauer, 2006). The etiology of IBD is still under investigation. However, genes, immune system dysfunction, environmental factors, and microbiome might contribute to it (Sartor, 2010). The underlying pathogenesis

involves one of the following: autoimmune response against a mucosal antigen, immune system dysfunction that attacks commensal microbes, or infection caused by pathogens, leading to a chronic inflammatory process (Hendrickson et al., 2002). Furthermore, genetic research investigations have suggested that chromosomes 1, 3, 6, 7, 12, 14, 16, and 19 play a role in the inflammatory process (Hanauer, 2006; Hendrickson et al., 2002). Genetic mutations in nucleotide-binding oligomerization domain 2 (NOD-2) probably provoke the innate immune response and susceptibility to CD (Hugot et al., 2001).

Patients with IBD alternate between two stages. One is the active disease period, where symptoms are obvious, and is termed the flare up/relapse state. This is followed by a silent period with negligible symptoms, known as the remission state. The general symptoms are abdominal pain, severe diarrhea, bloody stool, weight loss, fatigue, and fever. Other complications internal and external to the intestine, such as skin problems, liver inflammation, bone thinning, and anemia, might develop.

Multifarious etiology and disease complexity are the challenges for IBD therapeutics. Unfortunately, a permanent cure for IBD is not available to date, and patients have to rely on lifelong drug treatment. IBD therapy focuses on inducing and maintaining the remission state

* Corresponding author.

E-mail address: h.ali@qau.edu.pk (H. Ali).<https://doi.org/10.1016/j.ijpharm.2018.12.074>

Received 5 October 2018; Received in revised form 24 December 2018; Accepted 27 December 2018

Available online 04 January 2019

0378-5173/ © 2019 Elsevier B.V. All rights reserved.



Contents lists available at ScienceDirect

Materials Science & Engineering C

journal homepage: www.elsevier.com/locate/msec

A holistic QBD approach to design galactose conjugated PLGA polymer and nanoparticles to catch macrophages during intestinal inflammation

Mahira Zeeshan^a, Hussain Ali^{a,*}, Qurat Ul Ain^a, Mahwash Mukhtar^b, Rabia Gul^c, Atif Sarwar^c, Salman Khan^a

^a Department of Pharmacy, Faculty of Biological Sciences, Quaid-i-Azam University, Islamabad 45320, Pakistan

^b Faculty of Pharmacy, Institute of Pharmaceutical Technology and Regulatory Affairs, University of Szeged, Szeged 6720, Hungary

^c Shifa College of Pharmaceutical Sciences, Shifa Tameer-e-Millat University, Islamabad 44000, Pakistan

ARTICLE INFO

Keywords:

GAL-PLGA nanoparticles
Macrophage targeting
MGL-2 receptor
C-type lectins
Inflammation
Quality by design (QBD)

ABSTRACT

Recruited macrophages in inflammation attract various ligand-receptor drug delivery approaches. Galactose bound nanocarriers are promising to catch macrophages because of surface-expressed macrophage galactose type-lectin-C (MGL-2) receptor. The present study reported fabrication of galactose conjugated PLGA (GAL-PLGA) polymer and nanoparticles under quality by design (QBD) approach to investigate macrophages targeting potential at inflamed intestine. GAL-PLGA nanoparticles were fabricated through O/W emulsion-evaporation method under QBD approach and Box-Behnken design. Obtained GAL-PLGA nanoparticles have optimum particle size (~118 nm), drug entrapment (87%) and zeta potential (-9.5). TGA, XPRD and FTIR confirmed stability and negate drug-polymer interactions. Further, nanoparticles have considerable hemocompatibility, biocompatibility and cellular uptake; macrophage uptake was inhibited by D-galactose confirming involvement of MGL-2. Moreover, drug retention studies in the DSS-colitis model provide background for potential of nanoparticles to target and reside inflamed intestine. It is concluded that GAL-PLGA nanoparticles are suitable platform to target macrophages at the inflamed intestine through oral route.

1. Introduction

Inflammation is one of the protective mechanisms inside living bodies to encounter local irritants, foreign pathogens, and sometimes indigenous antigens. Our gastrointestinal tract (GIT) is naturally prone to inflammation because of various reasons including direct intake of pathogens, excitation of the body's self-defense mechanisms, and sometimes disturbance of natural resident microbes [1]. The most prone GIT regions to get inflamed are the intestines, both small and large. Major events during intestinal inflammation involve epithelial membrane damage, immune cell infiltration, mucous production, and ulceration [1]. Among immune cells, macrophages are the prototype cells in establishing intestinal homeostasis. However, in response to an inflammatory stimulus, naive and recruited monocytes acquired M1 macrophage phenotype with altered maturation which produces excessive proinflammatory cytokines and reactive oxygen species and impaired bacterial clearance that aggravates inflammation [2].

Both infiltrated and resident macrophages express various surface

receptors for cellular attachment, cytokines binding and production, ligand binding, etc. Since macrophage recruitment was increased in response to the inflammation, infection, and various diseases, therefore, macrophage-surface receptors serve as direct target for various drug delivery strategies via ligand attachment [3,4]. Further, macrophage targeting strategies delivered drugs, biological molecules, proteins, and genetic material inside the macrophages and interact with the pathways or various mechanisms to combat inflammation [3,5,6]. Therefore, focus has been laid to devise macrophage targeting strategies to invade inflamed tissues of intestine.

Meanwhile, nanoparticle-oriented drug delivery strategies with the size range of nanometers (10^{-9} m) are the focus of today's era. Perhaps, polymeric nanoparticles particularly PLGA based nanocarriers are widely developed because of their non-toxic, biodegradable, and biocompatible nature [7]. Moreover, characteristics like ease in size tuning, sustain drug release behavior, and capability to entrap both hydrophobic and hydrophilic drugs make PLGA a suitable and safe nanocarrier for the drug delivery and therapeutics in the inflammatory

* Corresponding author.

E-mail address: h.ali@qau.edu.pk (H. Ali).

<https://doi.org/10.1016/j.msec.2021.112183>

Received 10 October 2020; Received in revised form 2 May 2021; Accepted 7 May 2021

Available online 14 May 2021

0928-4931/© 2021 Elsevier B.V. All rights reserved.

Annexure II: Similarity Index Report

Turnitin Originality Report

Turnitin Originality Report

Bio-functionalized polymeric nanocarrier System for targeting inflamed intestinal mucosa
by Mahira Zeeshan
From CL QAU (DRSML)

Processed on 21-Feb-2022 12 01 PKT
ID: 1767383589
Word Count: 66733

Similarity Index
9%

Similarity by Source

Internet Sources
7%

Publications
5%

Student Papers
2%

**فائل
Focal Person (Turnitin)
Quaid-i-Azam University
Islamabad**

sources:

- 1 1% match (student papers from 25-Jan-2022)
[Submitted to Higher Education Commission Pakistan on 2022-01-25](#)
- 2 < 1% match (student papers from 10-Dec-2014)
[Submitted to Higher Education Commission Pakistan on 2014-12-10](#)
- 3 < 1% match (student papers from 22-Feb-2021)
[Submitted to Higher Education Commission Pakistan on 2021-02-22](#)
- 4 < 1% match (student papers from 01-Aug-2012)
[Submitted to Higher Education Commission Pakistan on 2012-08-01](#)
- 5 < 1% match (student papers from 06-Jul-2013)
[Submitted to Higher Education Commission Pakistan on 2013-07-06](#)
- 6 < 1% match (student papers from 29-Jan-2014)
[Submitted to Higher Education Commission Pakistan on 2014-01-29](#)
- 7 < 1% match (Internet from 18-Feb-2018)
<http://www.mdpi.com/2073-4360/19/2/159/html>
- 8 < 1% match (Internet from 10-Mar-2020)
<https://www.mdpi.com/2305-6320/7/3/11/htm>
- 9 < 1% match (Internet from 23-Dec-2019)
<https://www.mdpi.com/1422-0067/16/9/22711/html>
- 10 < 1% match (Internet from 07-Feb-2021)
<https://www.mdpi.com/1999-4923/12/8/597/html>
- 11 < 1% match (Internet from 30-Oct-2020)
<https://www.mdpi.com/1422-0067/21/11/4119/html>
- 12 < 1% match (Internet from 26-Sep-2020)
<https://www.mdpi.com/1420-3049/25/19/4400/html>
- 13 < 1% match (Internet from 19-Sep-2020)
<https://www.mdpi.com/1424-6247/13/3/44/html>
- 14 < 1% match (Internet from 22-May-2020)
<https://www.mdpi.com/1420-3049/19/11/17663/html>
- 15 < 1% match (Internet from 11-Nov-2020)
<https://www.mdpi.com/1420-3049/25/21/5139/html>
- 16 < 1% match (Internet from 06-Oct-2020)
<https://www.mdpi.com/1420-3049/25/19/4448/html>

21/2/22
ASSOCIATE PROFESSOR
Department of Pharmacy
Quaid-e-Azam University
Islamabad